Universidade do Minho
Escola de Engenharia

Bárbara Filipa Vasquez Vieira

Wave hydrodynamics in coastal stretches influenced by detached breakwaters

October 2014

Wave hydrodynamics in coastal stretches influenced by detached breakwaters
Bárbara Filipa Vasquez Vieira
UMinho | 2014

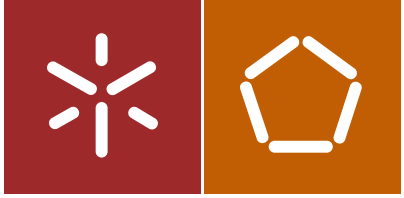

Universidade do Minho
Escola de Engenharia

Bárbara Filipa Vasquez Vieira

Wave hydrodynamics in coastal stretches influenced by detached breakwaters

MSc Thesis
Integrated Master in Civil Engineering

Supervised by:
Professor Doutor José Luís da Silva Pinho

October 2014

ACKNOWLEDGMENTS

The limited space of this section surely will not allow me to thank as I should to all the people who throughout my Master's degree in Civil Engineering helped me directly or indirectly to fulfil my goals and accomplish this stage of my academic training. This way, I leave a few words, but with a deep feeling of meaning and acknowledgement recognized.

To Professor José Luís da Silva Pinho, I express my deep gratitude for the guidance and unconditional support that much increased my scientific knowledge and undoubtedly that inspired me to always want to know more and the constant desire to want to do better. His wisdom, availability to guide me throughout this dissertation and share of knowledge were definitely crucial for this work come to an end with a huge feeling of satisfaction.

To my college António Pereira da Silva for the amazing person he is, for his friendship and all the help given not only in this final step but also throughout the past five years. I would also like to thank for his availability and will to collect the bathymetry data of the Ofir beach and for the sharing of this information that revealed to be important to this dissertation. I will never forget this gesture of friendship.

To all my friends, an unconditional thank for all the love, friendship, companionship, help, support and concern at moments of distress. These were very important factors in the realization of this dissertation and that allowed me to face each day with particular motivation. Also I would like to thank them for being available, for the sharing of the good and the less good moments, and for never giving up on cheering me up.

To my Father, my Mother, my Brothers and my Grandmother, an unconditional thank for always believing in me, for all the education given throughout my life, for making me who I am today, for always being available to give me advice and for all the trust and strength given whenever I needed. Without them this journey could never been possible and I really hope this final step in some way reciprocates and compensates for all the love, support and dedication that they constantly offer me. To them, I dedicate all this work.

(Page intentionally left blank)

WAVE HYDRODYNAMICS IN COASTAL STRETCHES INFLUENCED BY DETACHED BREAKWATERS

ABSTRACT

Coastal zones are highly dynamic systems directly influenced by natural driving forces and human induced impacts. Understanding the fundamentals of the physical, chemical, biological and anthropogenic phenomena related to these natural environments is of vital importance for coastal human life and property protection. Due to the predicted sea level rise over the next century and the increase in frequency and severity of storms, beaches and coastal defence structures are at risk. The worsening of erosion, with the consequent reduction of shorelines has great impact in the environment, in tourism and economy of regions affected by this problem. In order to protect coastal areas, defence structures reveal an important role in shielding urban areas. Many different engineering solutions can be used to reduce or to control coastal erosion, such as: breakwaters, groins, environmental-friendly structures and beach nourishment.

In this work the impact in hydrodynamics and sediment transport of a detached breakwater on the Portuguese Ofir beach was considered as a case study. The geometric parameters of a reference detached breakwater were obtained using UK Department of Environment Food and Rural Affairs methodology based on data of wave characteristics and bathymetry obtained from field measurements and from the Portuguese Hydrographic Institute monitoring stations. Ocean hydrodynamic data for a period between 1993 and 2007 obtained in the Leixões buoy were considered in the implementation of numerical models in order to understand the wave conditions in Ofir beach. The selected software for models construction were the COULWAVE (1D) for hydrodynamics (significant wave height and wave energy) and BOUSS-2D for 2DH hydrodynamics (significant wave height and water residual velocity). The input data needed depended on the characteristics of each one of those models. The combination of the parameters needed for the running of each model determined different simulation scenarios considering the situation of continuous and discontinuous detached breakwaters and the natural situation without detached breakwaters. In addition, a sensitivity analysis for comparing relative accuracy for significant wave height results between the two models was performed.

Keywords: coastal hydrodynamics, detached breakwater, mathematical modelling

(Page intentionally left blank)

HIDRODINÂMICA DAS ONDAS EM TRECHOS DE ZONAS COSTEIRAS INFLUENCIADOS POR QUEBRAMARES DESTACADOS

RESUMO

As zonas costeiras são sistemas altamente dinâmicos directamente influenciados por forças naturais e impactos antrópicos. A compreensão dos fundamentos físicos, químicos e biológicos e os fenómenos antrópicos relacionados a esses ambientes naturais é de vital importância para a protecção de pessoas e bens nas zonas costeiras. Atendendo à prevista elevação do nível médio do mar ao longo do próximo século e ao aumento da frequência e severidade das tempestades, as praias e as estruturas de defesa costeira estão sujeitas a riscos elevados. O agravamento da erosão, com a consequente redução de linhas de costa, tem grande impacto no meio ambiente, no turismo e na economia das regiões afectadas por este problema. As estruturas de defesa assumem um papel determinante na protecção das áreas urbanas localizadas em zonas costeiras. Diferentes soluções de engenharia têm sido adoptadas para reduzir ou controlar a erosão costeira, tais como: quebramares, esporões, estruturas ecológicas e alimentação de praias.

Neste trabalho, foi estudado o impacto de um quebramar destacado na hidrodinâmica e no transporte sedimentar na praia de Ofir, concelho de Esposende. Os parâmetros geométricos de um quebramar destacado de referência foram calculados com base na metodologia do Departamento de Ambiente, Alimentação e Assuntos Rurais do Reino Unido, utilizando dados de características de onda e de batimetria obtidos a partir de medições de campo e de estações de monitorização do Instituto Hidrográfico Português. Para implementar os modelos numéricos, foi necessário estudar a hidrodinâmica marítima na bóia de Leixões, considerando um conjunto de dados de agitação para um período entre 1993 e 2007. Os programas computacionais escolhidos para a construção dos modelos foram o COULWAVE (1D) para a hidrodinâmica 1D (altura significativa e energia das ondas) e o BOUSS-2D para a hidrodinâmica 2DH (altura significativa de onda e velocidade média do mar). Os dados de entrada foram os adequados às características de cada um dos modelos. A combinação dos parâmetros aplicados a cada modelo determinou diferentes cenários de simulação, considerando cenários com quebramares destacados contínuos e descontínuos e cenários sem quebramares destacados. Para os dois modelos, foi, ainda, realizada uma análise de sensibilidade à precisão dos resultados obtidos para alturas significativas de onda.

Palavras-chave: hidrodinâmica, modelação matemática, quebramar destacado

(Page intentionally left blank)

TABLE OF CONTENTS

(Page intentionally left blank)

LIST OF FIGURES

LIST OF TABLES

(Page intentionally left blank)

ACRONYMS

1D	One Dimensional
1DH	One Dimensional in the Horizontal plane
2DH	Two Dimensional in the Horizontal plane
3D	Three Dimensional
ADCIRC	Advanced Circulation
ADH	Adaptive Hydraulics Modelling System
ArcGIS	Aeronautical Reconnaissance Coverage Geographic Information System
ASCII	American Standard Code for Information Interchange
BOUSS-2D	Boussinesq wave model for coastal regions and harbours
CAD	Computer-Aided Design
CD	Chart Datum
CGWAVE	General-purpose wave prediction model for simulating the propagation and transformation of ocean waves
CMS-FLOW	Coastal Modelling System
CMS-WAVE	Coastal Modelling System. Formerly known as WABED (Wave-Action Balance Equation Diffraction)
COULWAVE	Cornell University Long and intermediate Wave
DEFRA	Department of Environment Food and Rural Affairs
DHI	Danish Hydraulic Institute
FESWMS	Finite Element Surface Water Modelling System
FVCOM	Finite- Volume Coastal Ocean Model
GenCade	GENESIS and Cascade combinational beach models
GENESIS	Generalized model for Simulating Shoreline charge
GIS	Geographic Information System
GPS	Global Positioning System
HAT	Highest Astronomical Tide
H	Significant wave height for a scenario
Hi	Significant wave height for Initial scenario
Hydro AS 2D	SMS model
IH	Portuguese Hydrographic Institute (Instituto Hidrográfico)
IPCC	Intergovernmental Panel on Climate Change

LAT	Lowest Astronomical Tide
MFAR	Multifunctional Artificial Reefs
MHWN	Mean High Water Neaps
MHWS	Mean High Water Springs
MIKE 21	DHI software
MLWN	Mean Low Water Neaps
MLWS	Mean Low Water Springs
MSL	Mean Sea Level
POOC	Plans for the management of coastal zone
PTM	Particle Tracking Model
RANS	Reynolds-averaged Navier Stokes
RiverFlo 2D	SMS model
RMA2	SMS model maintained by the Army Corp of Engineers Engineering Resource Development Center
RMA4	SMS model maintained by the Army Corp of Engineers Engineering Resource Development Center
SC	Scenario
SMC	Software Sistema Modelado Costero
SMS	Surface-water Modelling System
SRH-2D	Sedimentation and River Hydraulics- Two Dimensional model
STWAVE	Steady-State finite difference spectral model based on the Wave action balance equation
SWAN	Simulation Waves Nearshore
TMA	Shallow water spectrum
TUFLOW	SMS model
VBA	Visual Basic for Applications
WAM	Wave prediction Model
WINN	WaterInnovatiebron

CHAPTER 1

Introduction

‘The obstacle is the path.’

Zen Proverb

(Page intentionally left blank)

CHAPTER 1 INTRODUCTION

1.1 Motivation of the work

1.1.1 The importance of coastal defence

Estuarine and coastal zones are highly dynamic systems. Morphodynamic behaviour of these systems is directly influenced by natural driving forces (e.g., waves, tidal currents, wind, river discharges and sea level changes) and human-induced impacts (e.g., coastal physiography modifications and modifications in sediment supply) (Dias *et al*., 2011). Understanding the fundamentals of the physical, chemical, biologic and anthropogenic complex phenomena inherent to the integrated study of estuaries and beaches is of paramount importance for coastal, human life and property protection.

Projections presented by the Intergovernmental Panel on Climate Change (IPCC) indicate that global climate change may rise sea level as much as one meter over the next century (Figure 1.1) and, in some areas, increase the frequency and severity of storms (Gilbert and Vellinga, 1990). Consequences of this can result in the retreat of beaches as much as a few hundred metres and the rupture of protective structures. Flooding of hundreds of thousands of square kilometres of coastal wetlands and other lowlands would threaten lives, buildings, and infrastructures, as well as putting drinking water sources out of service due to salt intrusion in coastal aquifers. This way, functions and values of coastal zones are degraded with the related social and economic impacts. Consequently, populated coastal areas are becoming more and more vulnerable to sea level rise and other impacts of climate change.

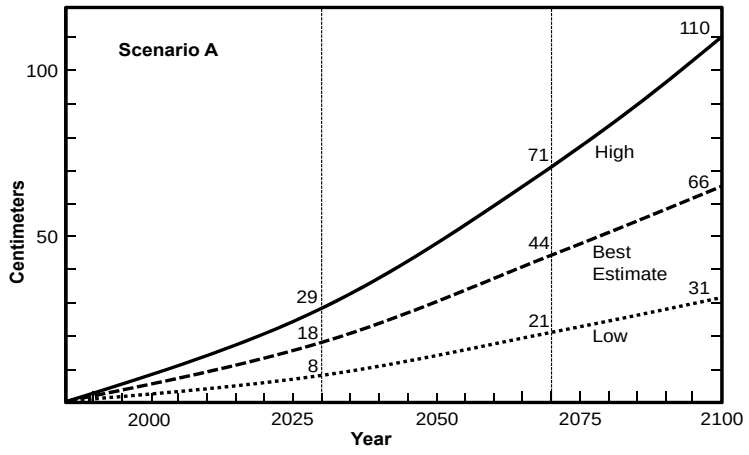

Figure 1.1: Global sea level rise, 1985-2100 for policy of no limitation of greenhouse gases (scenario A) (Adapted from Houghton *et al*., 1990).

Facing the effects of sea level rise requires adequate responses in order to minimize impacts. One vital element of a plan to manage this phenomenon is to formulate and implement effective integrated coastal management programs. This was one of the recommendations of the IPCC and the 1992 Earth Summit in Rio de Janeiro. The implementation of such a plan implies the consideration of responses that fall broadly into four categories: retreat, accommodation, protection, and do nothing (Granja and Pinho, 2012).

Retreat involves no effort to protect the land from the sea. The coastal zone is abandoned and ecosystems shift landward. This choice can be motivated by excessive economic or environmental impacts of protection, and can include demolitions, relocations and compensations. In the extreme case, an entire area may be abandoned.

Accommodation implies that people continue to use the land at risk but do not attempt to prevent the land from being flooded. This option includes erecting emergency flood houses, elevating buildings on piles, converting agriculture to fish farming, or beach nourishment to adapt the overall coastal marine dynamics.

Protection involves hard structures such as seawalls, groins, breakwaters, and dikes, as well as soft solutions such as dunes and vegetation, to protect coastal segments when social and economic interests are justified.

Do nothing option allows the natural evolution of coastal marine dynamics.

Cost-benefit analysis must be applied in order to decide the appropriate mechanism for implementation. Particular response must consider social, economic, and environmental aspects of the coastal zone considered.

Improving scientific and public understanding of the problem is also a critical component of any response strategy. Basic and applied research are needed for better projections of changes in the rate of sea level rise, precipitation, frequency and intensity of storms, and coastal dynamics. Finally, in most of the countries the available information has many uncertainties due to unreliable data from which to determine how much coastal zones are at risk.

1.1.2 Management of coastal zones in Portugal

The Atlantic coast of Portugal is exposed to rough wave climate conditions and frequently submitted to powerful storms, endangering waterfronts, infrastructures and natural landscapes (Pereira *et al.*, 2013). Main wave crest orientation is from the northwest, inducing a drift current

from north to south. However, this current is, in some areas, reversed due to the presence of some natural (bars, ebb tidal deltas, rocky outcrops) and artificial (breakwaters, jetties, groins) obstacles that promote local wave diffraction (Granja and Pinho, 2012).

Sandy coastlines, without headlands or rocky foreshores are the most vulnerable Portuguese coastal units to erosion. Figure 1.2 depicts some examples on the Portuguese coast of intense urban development on unstable and environmentally sensitive areas and the existent erosion problems (Veloso-Gomes and Taveira-Pinto, 1997).

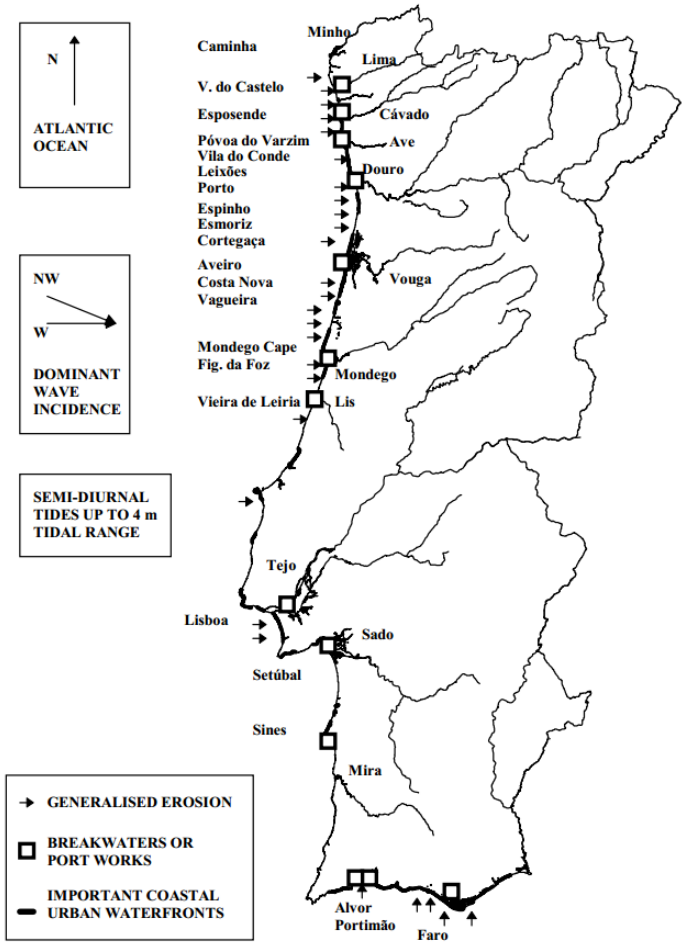

Figure 1.2: Portuguese coastal occupation and existent erosion problems. (Adapted from Veloso-Gomes and Taveira-Pinto, 1997)

The weaknesses of the coastal zone in Portugal are essentially due to the anthropogenic causes associated with urban and industrial occupation, river settlement interventions, dams, rise of the mean sea level and the frequency and intensity of storm events, as well as new accessibility (ports, motorways), traffic flows, and extraction of aggregates. These factors are the main responsible for reducing the amount of sediment transport along the coast, new hydrodynamic situations and major landscape changes.

Dunes have an important contribution not only in terms of slowing down the ocean's advance, because they can act as a sand reservoir for beaches, but also in terms of protecting and recovering other natural values. The continued destruction of dunes and vegetation by trampling and by building housing and improvised parking lots prevent the accumulation of sand, thus contributing greatly to the instability of natural defences (Veloso-Gomes and Taveira-Pinto, 2003).

These phenomena are observed in storm situations that cyclically occur mainly in winter time along the Portuguese coastal zone (Figures 1.3 and 1.4).

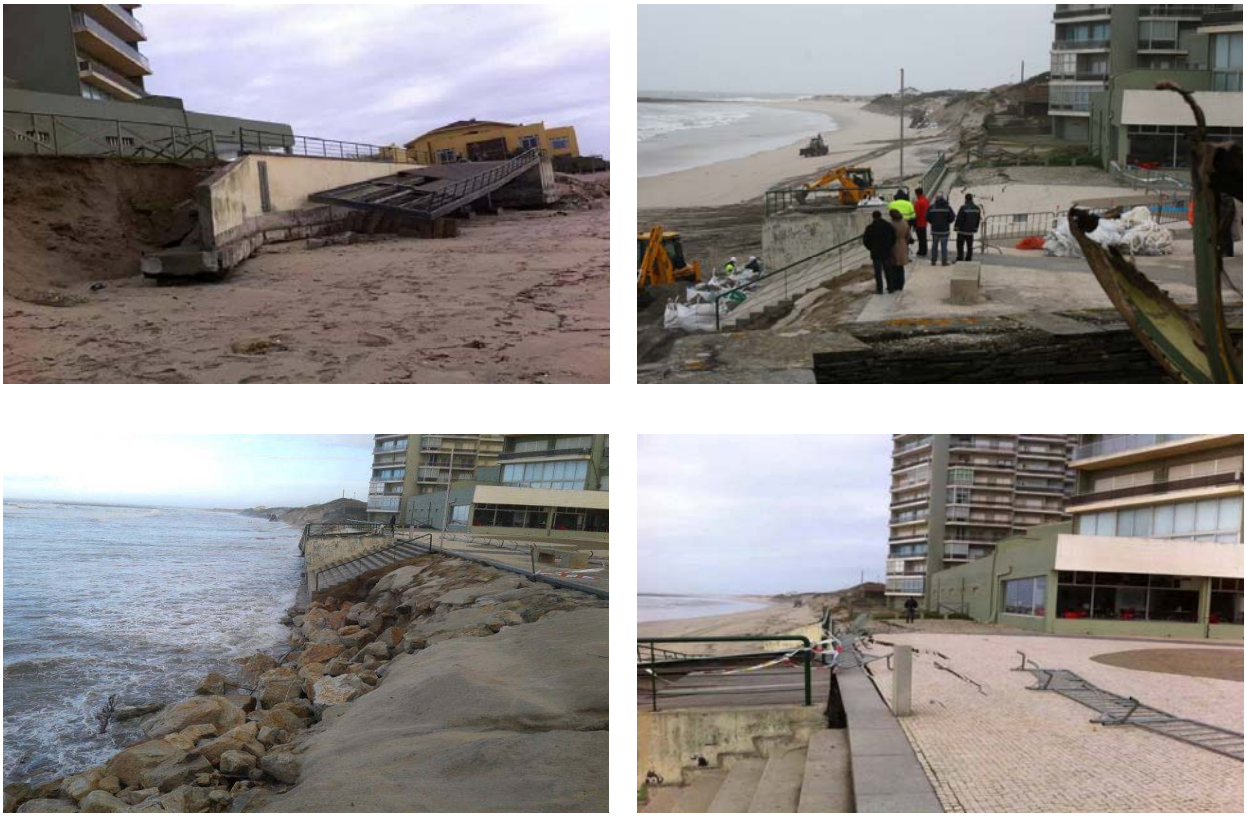

Figure 1.3: Erosion problems in Ofir beach (storm of 2014).

Figure 1.4: Flooding problems in the city of Póvoa de Varzim (storm of 2014).

In order to defend the urban areas and the land use, new solutions for coastal defence may be needed. However, these works may induce or anticipate other erosion problems southwards. The planning, design and construction processes of coastal structures must be based on information and knowledge of marine coastal dynamics and depend on the construction methods applied and on the characteristics of the available equipment.

Most people claim for coastal defences from the Government because they don't want to lose their homes due to erosion. Simões *et al* (2013) explain that currently, there is already a concern to reset sediments on the beaches, both by feeding artificially and by building defence structures (detached breakwaters and groins along the coast, multifunctional artificial reefs, for example).

The implementation and assessment of Plans for the Management of the Coastal Zone (POOC) should be a key instrument for effective integrated management of the Portuguese coastal zones.

1.2 Objectives

This research work aims to apply hydroinformatic tools to simulate the influence of detached breakwaters on coastal zones, considering different conditions of hydrodynamics (wave height and period) and detached breakwater geometrical parameters. Also, the prediction of sediment transport in the vicinity of these coastal defence structures was analysed, considering results obtained for residual velocities associated with wave propagation. Within this main objective the following specific issues were addressed:

- Comparative analysis of software solutions for coastal processes numerical simulation;
- Study of different types of detached breakwaters, materials and their impacts on the coastal zones;

- Assessment and identification of key variables in the design of detached breakwaters and their influence on sediment retention;
- Application of the developed methodology to the study site of Ofir beach, in the county of Esposende;
- Data analysis of the bathymetry and morphology of the study site;
- Construction of models and simulation of wave propagation scenarios to study the hydrodynamics and sediment transport patterns in the vicinity of detached breakwaters;
- Study of the variability of sediment transport and the significant wave height and wave energy for different wave regimes and types of detached breakwaters (submerged or emerged);
- Analysis of hydrodynamic patterns in the study site for different wave parameters (direction, significant height and period);
- Analysis of the influence of detached breakwater geometric parameters (crest level, distance from shore to the detached breakwater, number and length of detached breakwaters and spacing between them) in the resulting significant wave height and wave energy;
- Analysis of the wave residual velocities fields in order to predict the sediment transport patterns in the study site;

1.3 Methodology

To achieve the proposed objectives for this research work a Portuguese coastal stretch highly vulnerable to erosion (Ofir beach) was selected and the impact of a detached breakwater in the local hydrodynamics and sediment transport patterns was simulated for different scenarios.

The design of the simulated detached breakwater was obtained using UK Department of Environment Food and Rural Affairs (DEFRA, 2010) methodology based on bathymetric data obtained from field measurements and wave data collected at monitoring stations of the Portuguese Hydrographic Institute (IH).

To implement the numerical models it was studied the significant wave height extremes, as well as the determination of the depth of closure and the wave period associated considering a set of wave conditions data for a 14 year time period between 1993 and 2007.

COULWAVE (1DH) for hydrodynamics and BOUSS-2D for hydrodynamics and sediment transport were the selected software for models construction. Lynett and Liu (2014) demonstrated

that COULWAVE model is a very accurate tool for the analysis of significant wave heights in the presence of detached breakwater, comparing experimental with numerical wave height results. BOUSS-2D also revealed to be a suitable numerical model to analyse the significant wave heights in a 2DH domain. Although this model does not output directly the sediment transport, it can be predicted by analysing the residual velocity field through the study domain.

Input data depend on the characteristics of each one of those models. The variables for the COULWAVE model were: the significant have height and its period; the crest level; and the distance from shore to the detached breakwater. For the BOUSS-2D model the variables considered were: the significant have height and its period; the crest level of the detached breakwater; and the wave direction. The combination of these variables determined different simulation scenarios.

The simulation results were obtained considering different detached breakwaters scenarios. For 1DH model an Initial (without detached breakwater) condition and a situation with one continuous detached breakwater were simulated giving as output significant wave height and wave energy results. For 2D model an Initial (without detached breakwater) condition and two situations with one continuous and another discontinuous detached breakwater were simulated giving as output significant wave height and residual velocity fields results.

A sensitivity analysis for comparing relative accuracy between the two models was performed. Significant wave height results obtained with the 1DH and 2DH models were compared for the same wave height, domain and boundary conditions.

Figure 1.5 schematically explains the methodology adopted in the development of this dissertation.

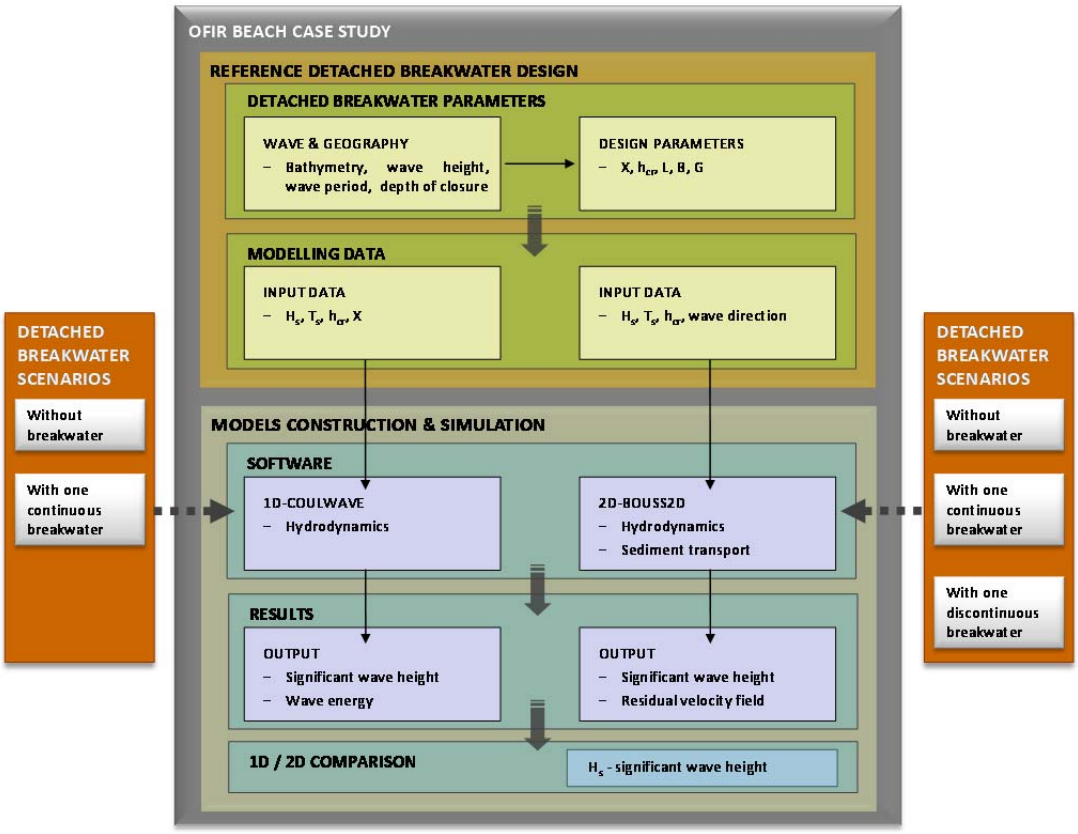

Figure 1.5: Scheme of the adopted methodology.

1.4 Organization of the dissertation

The contents of this dissertation are organized according to the following chapters.

Chapter 1 briefly describes the motivation and objectives of this research work. It also highlights the importance of the coastal defence as well as the management of the coastal zones in Portugal. This is followed by the presentation of the main objectives, the methodology adopted throughout the dissertation and its structure.

Chapter 2 indicates and describes some of the different types of technical solutions for coastal defence and the current coastal defence situation in Portugal. It also focus the general aspects and the design conditions for detached breakwaters, their geometry, the most widely used materials and the functional parameters that are crucial for the effectiveness of a detached breakwater. In addition, it is described the influence of the hydrodynamics and the mechanisms of sediment transport induced by the presence of a detached breakwater, its consequences and impacts, the global classification of the structural types of breakwaters and the description, application and limitations

of different hydroinformatics tools that can be used in coastal defence solutions modelling and analysis.

Chapter 3 presents a general description of the study area (Ofir beach) and the effects of a detached breakwater on coastal areas. Further, an analysis of the collected data for a period of 14 years by the Leixões buoy is made and the hydrological parameters needed to the design of a detached breakwater are highlighted and determined. This Chapter also includes a description of the tidal parameters used in this dissertation, the bathymetry and its slope and the calculations for determining the geometric parameters of a reference detached breakwater.

Chapter 4 describes in detail the implementation of the numerical models (COULWAVE and BOUSS-2D).

Chapter 5 presents results obtained with the 1DH COULWAVE model in a specific scenario. Also, the discussions of the results for significant wave heights and wave energy in scenarios with and without a detached breakwater are presented. The remaining results are included in Appendices 2 to 6.

Chapter 6 presents results obtained with the model implemented with BOUSS-2D. Also, the discussions of the results for significant wave height and residual velocity fields in different scenarios considering the presence or not of a detached breakwater are presented. The remaining results are included in Appendices 8 to 11.

Chapter 7 presents a comparison of the results obtained in a theoretical example for significant wave height with COULWAVE and BOUSS-2D at the same three locations of the domain for the same wave height and boundary conditions, and presents the conclusions of this work and the suggestions for future developments.

A list of the bibliographical references cited along the text is presented.

Appendices 1 to 11 contain simulation results, a programming code and details of software input data files.

(Page intentionally left blank)

CHAPTER 2

State of the art

‘Sometimes it's necessary to go a long distance out of the way in order to come back a short distance correctly.’

Edward Albee (1928 –)

(Page intentionally left blank)

CHAPTER 2 STATE OF THE ART

2.1 Technical solutions for coastal defence

In a zone prone to shoreline retreat due to high tide/wave energy action without natural defence and a high sediment transport deficit, many different solutions can be used to reduce or to control coastal erosion, namely: adherent works, transversal works, beach nourishment, sand bypassing and dunes rehabilitation, creating innovative and alternative breakwaters designs and, specially, 'environmental-friendly' structures (Taveira-Pinto and Neves, 2004).

It is important to highlight that the existence or the possible construction of defence structures should not be used as an excuse to allow building in areas of risk. These structures may locally reduce risks of exposure to sea action, but do not eliminate them. Each of these approaches has economic, aesthetic, environmental and human advantages and disadvantages and the choice of the solution will vary widely according to local, regional and national priorities (Veloso-Gomes and Taveira-Pinto, 1997).

A typical coastal urban area evolution is represented in Figure 2.1.

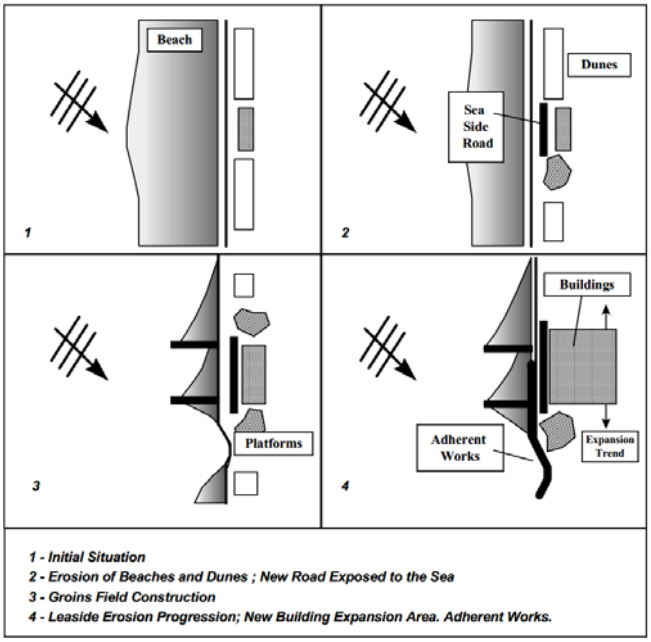

Figure 2.1: Coastal urban area: typical evolution (Veloso-Gomes and Taveira-Pinto, 1997).

In the next sections general characteristics of most usual coastal defence technical solutions (breakwaters, groins and eco-engineering solutions) will be briefly described.

2.1.1 Breakwaters

Breakwaters are constructed to provide a calm basin for ships and to protect harbour facilities. They are also sometimes used to protect the port area from the intrusion of littoral drift. In fact, for ports open to rough seas, breakwaters play a key role in port operations. Since sea waves have enormous power, the construction of structures to mitigate such power is not easily accomplished (Takahashi, 2002).

The breakwaters can take many forms and can be permanently submerged (reefs), permanently exposed or visible between tides. These structures can be adherent (rooted and/or located against the coast), detached (built away from the coast), or may have a one end anchored to the ground (acquiring usually a curved or an L shape: headland breakwaters). In all cases, the depth of the structure, its size and its position relative to the shoreline determine the level of protection provided (Antunes do Carmo *et al.*, 2011).

2.1.1.1 Headland breakwaters

A series of breakwaters constructed in an "attached" fashion to the shoreline and angled in the direction of predominant wave approach such that the shoreline behind the features evolves into a log spiral embayment (USACE, 2014a). Figure 2.2 depicts some examples of these kinds of structures.

Figure 2.2: Examples of headland breakwaters.

2.1.1.2 Detached breakwaters

Detached breakwaters are another example of coastal defence structures that are built offshore inside/near the surf zone, having an approximate orientation parallel to the coast built in shallow nearshore environments and that can be, according to their position relatively to the mean water level, emerged or submerged (Figure 2.3). Both constitute an obstacle to the normal wave propagation, allowing the dissipation of the incident wave energy and providing a "filter" shelter for the coast at their leeward side, reducing this way beach erosion. These structures also function well in areas where the cross-shore current, or shore-perpendicular transport of materials, is stronger as the structures will provide greater protection of original beach material while capturing new sediments entering the system.

As the waves approach the shore, the breakwaters reduce the energy of the waves, creating a calm environment on the leeward side of the structures. This environment is ideal for the deposition of sediment which in turn aids in retaining and enhancing beach width and thickness (ODNR, 2011). During the design process of these structures, it is important to consider the wave-structure interaction, defined by their functional parameters (e.g.: length, orientation and distance to the shoreline), that establish their efficiency.

The submerged breakwater is also a particularly attractive solution for the creation and preservation of beaches, due to its low environmental and visual impact (Figure 2.4). Inherent to the improvement of water quality, maintenance of fish habitats due to its lower impact of coastal development on aquatic habitat and a better integration of the coastal defence structure in the shore zone, are examples of the advantages of submerged breakwaters over the conventional structures (Taveira-Pinto and Neves, 2003).

The main technical characteristics of detached breakwaters are described in detail in Chapter 2.2.

Figure 2.3: Examples of detached breakwaters.

Figure 2.4: Examples of submerged breakwaters.

2.1.1.3 Artificial reefs

Across the world, certain types of artificial reefs generally built in mid to deep waters are seen as a management tool to sustain coastal fisheries to preserve marine life (Figure 2.5). In Portugal, the same types of artificial reefs are more used in the region of Algarve (one of the largest in Europe with an area of about 43 km^2) in order to avail the productive potential of surface currents because of their richness in nutrients and because it is a propitious area to natural coastal accidents (Whitmarsh *et al.*, 2008). Locations of these areas are shown in Figure 2.6.

Figure 2.5: Artificial reefs.

Figure 2.6: Artificial reefs in the Algarve (OR, 2014).

In California (United States) an artificial reef was built in 2001 at Dockweiler beach, which eventually was removed in 2008 for not complying with the intended goals. On the South coast of England, Boscombe area, in 2008, a reef was built in order to increase the number of visitors, to extend the tourist season and promote economic growth. However, after two years the construction of the reef has suffered significant damage, which derailed the effects of protection, particularly in terms of accumulation of sediments (Antunes do Carmo, 2013).

2.1.1.4 Multifunctional artificial reefs

The multifunctional artificial reefs (MFAR) is a particular case of artificial reefs and represent an innovative concept for coastal protection. In addition to have this function these artificial reefs create favourable conditions for the practice of surf, favouring other sporting activities such as diving and fishing, and enhance the environmental value of the area where they are located. MFAR provide a perfect visual amenity and can offer tourism and economic benefits to the region where they are installed (Antunes do Carmo *et al.*, 2011).

The construction of a MFAR may play an important role in different aspects of coastal protection, namely:

- Prevention of coastal erosion;
- Increase of sand deposition in combination with artificial nourishment, and increase of beach stability;
- Reduction of the wave load on the coast through a series of processes of transformation of wave occurring on the structure (reflection, refraction and energy dissipation);
- Use for control waves propagation, creating good surfable waves, due to refraction and diffraction effects.

More recently, MFAR have been proposed typically installed in shallow waters with coastal protection goals, particularly in protection of beaches and dunes, and in generating waves for surfing. In this context, arise as examples: the artificial reef in Cable Station (near Perth), built in 1999, and artificial reef at Narrowneck Beach (Gold Coast) built in 2000, both located in Australia.

In New Zealand, Maunganu Beach, was built in 2008 a MFAR using geotextile bags filled with sand with the main objective of improving local conditions for surfing.

In India, in 2010, the multifunctional reef Kovalam was built, which proved a case of great success to prevent coastal erosion and to generate great waves for surfing (Simioni and Esteves, 2010).

In Portugal there are still no MFAR, although the several studies for its implementation in some areas of the Atlantic coast, particularly in locations that require urgent protection measures and which are judged to be likely to benefit from good conditions for surfing. Examples are the coastal zones of São Pedro do Estoril (Mendonça *et al.*, 2010), Leirosa, south of Figueira da Foz (Voorde *et al*, 2009; Antunes do Carmo *et al*. 2011; Mendonça *et al.*, 2012) and Vagueira beach (Simões *et al.*, 2013; Di Bona *et al.*, 2013).

2.1.2 Groins

Groins are the oldest and most commonly beach stabilisation structure used on shore. They are structures that extend, fingerlike, perpendicularly to shoreline and that are relatively short when compared to navigation jetties. Usually constructed in groups called groin fields, their primary purpose is to trap and retain sand, nourishing the beach compartments between them.

Groins work as physical barriers to the alongshore transport of sand, that starts to accumulate up-drift (Figure 2.7). They are most effective where longshore transport is predominantly in one direction, and where their action will not cause unacceptable erosion of the downdrift shore. When a well-designed groin field fills to capacity with sand, longshore transport continues at about the same rate as before the groins were built, and a stable beach is maintained. Modern coastal engineering practice is to combine beach nourishment with groin construction allowing sand to immediately begin to bypass the groin field system, reducing transient erosion downdrift (USACE, 2014b).

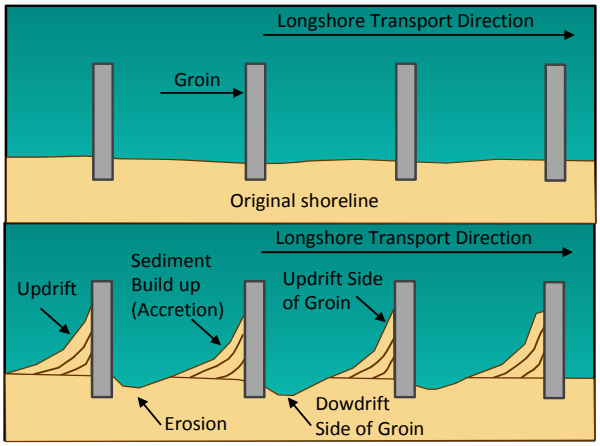

Figure 2.7: Schematic representation of the functioning of groins.

The volume of sediments accumulated updrift from the groin is a function of its dimensions, wave conditions and sediment grain size, being indicative of the erosion contention. If the limiting retention capacity of the groin is reached it stops blocking sediments, letting them pass through. The time elapsed to fill a groin depends on several factors, like wave conditions at the groin location, beach morphology, tide regime and even current pattern in the surrounding area (Silva *et al.*, 2007). Therefore, the filling time would be given by the ratio between the accumulated volume and the alongshore transport rate. It is important to be aware that although it may appear simple, both accumulated volume and alongshore transport are difficult to evaluate.

A very negative impact that would result from these works, if they had the capacity of inducing rip currents, would be the irreversible loss of sediments dragged to offshore. Short groins cannot jet material far offshore and permeable groins reduce the rip current effect. However, long impermeable jetties might produce large rips and jet material beyond the average surf zone width. Affirming that groins erode the offshore profile is questionable and doubtful. Under this perspective, groins should be permeable, allowing water and sand to move alongshore, and reduce rip current formation and cell circulation (Silva *et al.*, 2007). Examples of existing groins in Portugal are presented in Figure 2.8.

Figure 2.8: Groins in Portugal: a) Ofir; b) Lagos; c) Madeira; d) Espinho.

2.1.3 Eco-engineering solutions

Eco-engineering solutions improve traditional structures using natural resources to increase the structure functionality, or the use of natural materials (flora and fauna) to create structures. In the last decade, management and development of wet nature values of dikes has been incorporated in Dutch policies, and several concepts for 'green' dikes and submerged reefs have been developed. To further improve the ecological value of hard substrates, the Dutch Ministry of Public Works and Water Management WINN-project 'Diverse Dike' was initiated in 2007. The project aims for the

design of ecologically diverse coastal defence structures, dikes, dams, piers and groins, on a base of ecological functions. Safety against floods naturally plays a central role, but additionally the recreational value of the coastal environment can be improved as well. The concept has been developed in an intensive cooperation of ecologists and civil hydraulic engineers, and the designs are meant to be economically and practically feasible as part of existing or new designs for coastal infrastructure (Deltares, 2014a).

Eco-engineering is important because it creates a more natural environment, with a habitat for all kinds of organisms and possibilities.

Bio-Builders are organisms that naturally occur in the relatively shallow waters along the coast and in inland waters, and that are capable of changing their environment in a way favourable to themselves. Thus, as water levels vary due to climate change, the bio-builders can adapt to the variations and maintain their function of coastal protection. Furthermore, eco-engineers grow naturally, which means that construction costs can be limited, as are costs for maintenance and repair. By means of their activity, they play a crucial role in the cycle of all kinds of substances in the water: Some filter water so it becomes clearer, others assimilate substances so that these form a food source for other organisms. In this natural way, the water quality can be improved against much lower costs than what would be possible with chemical or mechanical purification.

Hard substrates are home to the most species diverse communities of all coastal systems in many world locations. Sea dikes and levees are a habitat to many, sometimes rare species and can contribute greatly to their dispersal. By enhancing the establishment possibilities for sea animals and plants like mussels, oysters, barnacles, algae and anemones, the ecological function of hard substrates can be significantly improved. (Deltares, 2014a).

2.1.3.1 Sand engine

Sand nourishment allows natural processes to maintain a sandy coast and ‘dynamically’ keep it in place (Figure 2.9). The sand for nourishment is dredged from deep waters (below the 20-metre depth contours). Water and wind distribute this sand naturally along the beach and across the dunes (Deltares, 2013).

Figure 2.9: Sand engine (Deltares, 2013).

2.1.3.2 Oyster and mussel reefs

Reefs of bivalves can function as stabilising or protecting agents because they reduce wave and current intensity, and because of their ability to alter properties of the sediment. Figure 2.10 shows an oyster and a mussel reefs (Deltares, 2014a).

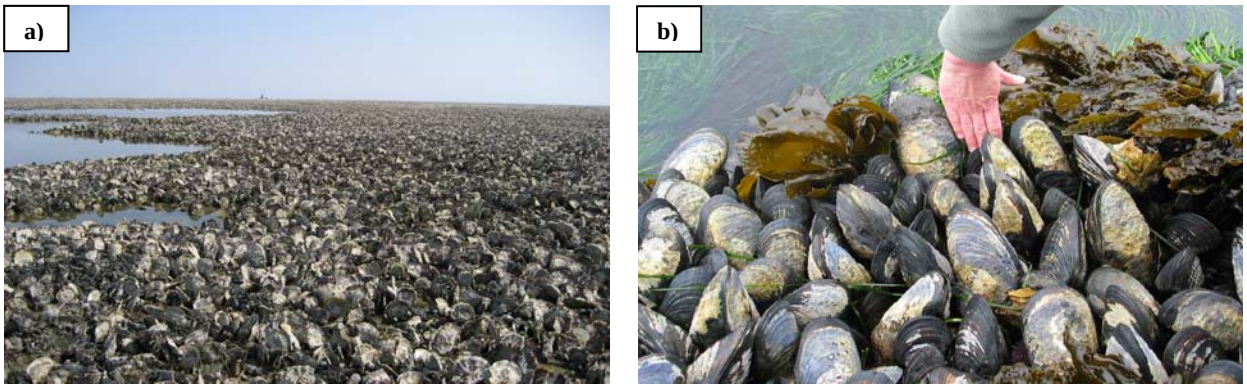

Figure 2.10: a) Oyster reef; b) Mussel reef.

2.1.3.3 Salt marshes, mangroves and osier-beds

Vegetated areas, such as salt marshes, mangroves and osier-beds (Figure 2.11), trap sediment by reducing flow velocities, by reducing hydrodynamic forces on the seabed and by improving consolidation of muddy soils by means of evaporation. Furthermore, they attenuate waves in front of coastal protection constructions, meaning that these require less height, enforcement and repair (Deltares, 2014a).

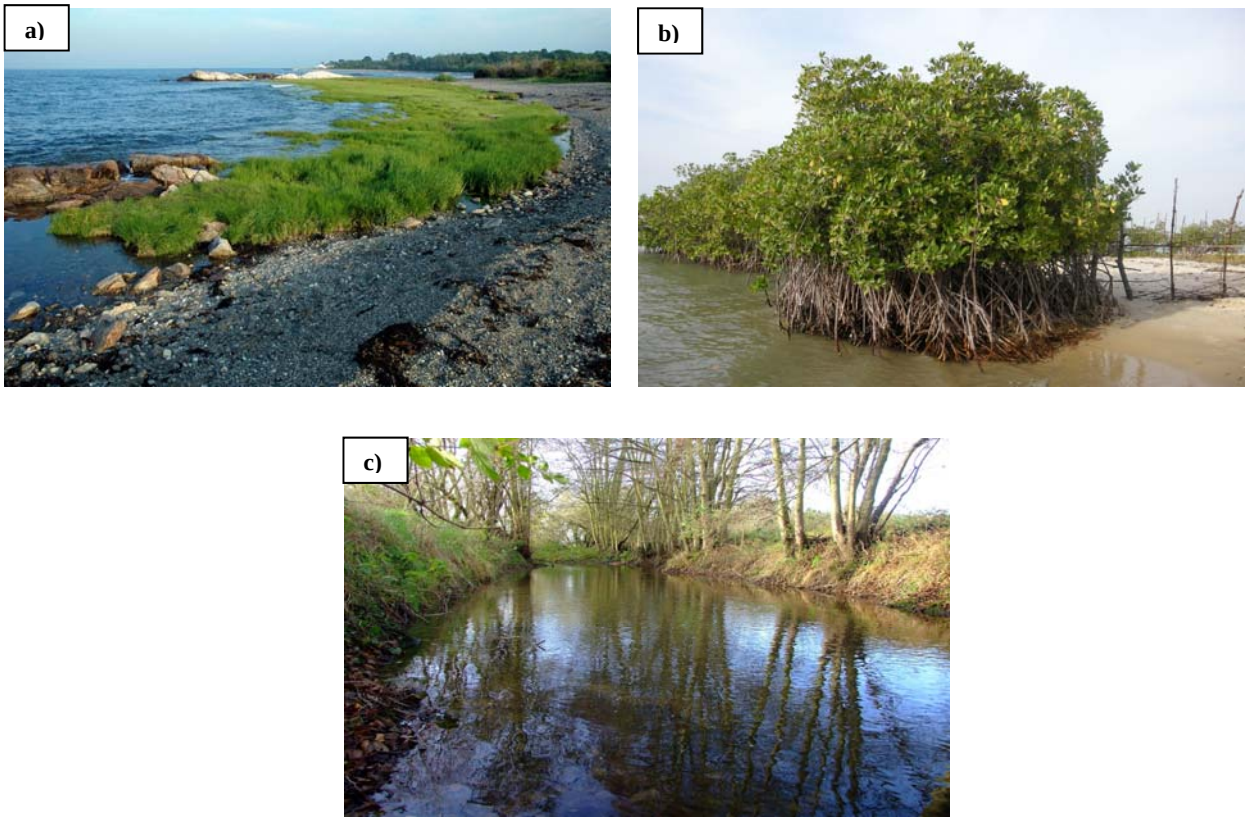

Figure 2.11: a) Salt marshes; b) Mangroves; c) Osier-beds.

2.1.3.4 Reed floats

In areas that are initially not suitable for bottom vegetation, for instance due to the lack of shallow shores or large variations in water levels, floating devices often are applicable (Deltares, 2013). Reeds do not affect the sediment stability directly, but do attenuate small waves and thereby protect nearby banks, prevent re-suspension of bed material and improve water clarity (Figure 2.12).

Figure 2.12: Reed floats (Deltares, 2013).

2.1.3.5 Eco concrete

Much marine life, such as mussels, barnacles and seaweed, need a hard surface to survive. Commonly, they find this surface on hydraulic engineering constructions, such as harbour piers and seawalls. But modern concrete is becoming increasingly smooth and therefore less suitable for these organisms to establish themselves. The use of special 'eco concrete' during the construction or renovation of hydraulic engineering structures appears to significantly speed up the process by which these species establish themselves and their diversity (Figure 2.13) (Deltares, 2013).

Figure 2.13: Eco concrete (Deltares, 2013).

2.1.3.6 Tidal pools

Solid constructions along the coast, such as dikes, harbour piers and dams, are the habitat of various marine species (Figure 2.14). Many of them live exclusively in places that are continuously underwater. By making simple and inexpensive adjustments to solid structures, water in higher parts of the intertidal zone will linger longer. This can be a huge boost to biodiversity and biomass and can be used as a mitigating measure for Natura 2000 objectives (Deltares, 2013).

Figure 2.14: Tidal pools (Deltares, 2013).

2.1.4 The Portuguese coastal defence situation

In Portugal, several different types of coastal defence structures have been built: frontal defences, groins, jetties, seawalls, breakwaters and cliff reinforcements. These structures are mainly concentrated in the Northwest coast due to the fact that this region is highly energetic with a wave regime typically from Northwest, characterised by a mean significant wave height of 2m and a mean period of 12s. Storms, occurring especially in the winter, come predominantly from Northwest with offshore significant wave heights that may reach 8m persisting for up to 5 days. The tide regime is semi-diurnal with a tidal range between 2m and 4m in spring tides. The potential alongshore transport mainly due to the wave action is approximately 1-2 million m^3/year (Oliveira, 1997).

The energetic Portuguese west coast wave climate requires a maintenance program that involves high investments throughout their life cycle. When these investments are not made, serious damage occurs to the structures, particularly during storm events. Artificial nourishment is not compatible with Portuguese west coast dynamics and nourished beach sediments are rapidly lost. But neither do groins nor revetments stabilize the coast or reduce erosion. On the contrary, they have contributed to the acceleration of erosion rates in several coastal stretches and their financial costs were very high (Granja and Pinho, 2012).

Detached breakwaters which have the potential to promote tombolo building seem to be a less harmful hard solution. While they might create local ‘solutions’, however, they contribute to downdrift erosion.

There are not many experiences with submerged or detached breakwaters in the Portuguese coast but it can be referred four cases, where these structures were used: in Leixões harbour as a submerged breakwater (protecting the main structure), in Caxinas-Vila do Conde beach, near Neiva’s river mouth, in Aguda beach and in Algarve region.

2.2 Detached breakwaters

2.2.1 General aspects

2.2.1.1 Emerged breakwaters

Emerged detached breakwaters are designed to attenuate the whole wave action and are submitted to the direct impact of wave breaking, resulting in larger structures that often eliminate water circulation at the leeward side (in the protected area). Consequently, degradation of water quality and of natural habitats in the leeward side is a frequent phenomenon (Taveira-Pinto and Neves, 2003).

A disadvantage of emerged breakwaters, in terms of environment, is the necessity of gaps between the barriers that often give rise to rip currents, bed irregularities and tombolos. Figure 2.15 depicts the format of a tombolo near an emerged breakwater.

Figure 2.15: Formation of a tombolo in the leeward side of an emerged breakwater due to the diffraction currents.

2.2.1.2 Submerged breakwaters

Submerged breakwaters could be constructed by several reasons, being the most common purposes the following (Taveira-Pinto and Neves, 2003):

- Beach protection caused by the wave dissipation/attenuation “shelter” effect;
- Creation of a calmer zone in an harbour, protecting them or preventing siltation in port access ways;
- Protection of a main structure by reducing the intensity of wave action on the principal coastal defence structure;

– Redistribution of sediment transport patterns, to create desirable beach features or alteration of the sediment deposition area in a navigation channel entrance.

Figure 2.16 demonstrates the main objective of a submerged breakwater: the capability for retaining or permitting sediment accumulation at its leeward side responsible for its important role in beach protection. This sediment accumulation is due to the attenuation of the wave height, caused by the energy dissipation and the formation of diffraction figures at the ends of the structure. Figure 2.17 illustrates the diffraction currents formed in the extremities of the submerged breakwater (Taveira-Pinto and Neves, 2003).

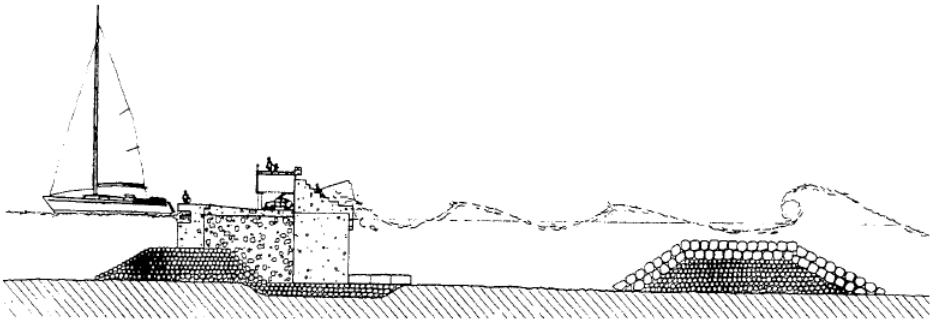

Figure 2.16: Schematic description of the effect of a submerged breakwater in the wave propagation, Olympic Port, Barcelona, Spain (Taveira-Pinto and Neves, 2003).

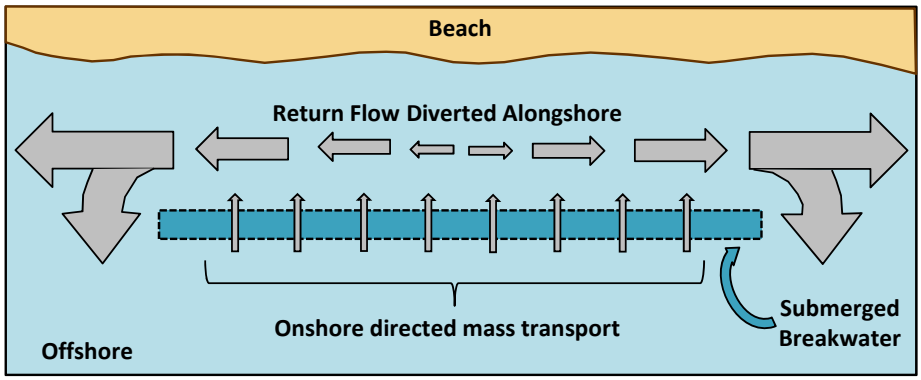

Figure 2.17: Schematics of rip currents generated in the leeward side of a submerged breakwater (Adapted from Browder, 1996).

The efficiency of a breakwater is influenced by many variables: bathymetry, wave climate, sedimentation, implantation depth, length, distance to the coast, gaps between structures, submergence level and length and submerged breakwaters structural configuration. Since there are many unknown processes and variables involved, the study of these kinds of structures is more complex than studying emerged breakwaters (Taveira-Pinto and Neves, 2003).

Chen and Chen (2001) found that as the length of breakwater increases, so does the reducing effect on wave height. They also verified that the wave height near the breakwater increased as the height of the submerged structure increased; when waves passed the breakwater, the wave height decreased as the height of the submerged breakwater increased.

Submerged breakwaters are less subjected to wave action because of their lower height and low visual and environmental impact. Besides that, the required volume of material is smaller than in similar emerged structures. However, it is important to be aware that submerged breakwaters have, obviously, a lower level of protection, since its efficiency in the formation of tombolos is lower. In some cases, however, it was concluded that the submerged structures dissipated wave energy more efficiently than the emerged ones (Taveira-Pinto and Neves, 2003).

2.2.2 Geometry of detached breakwaters

Figure 2.18 shows an example of a cross section of a possible detached breakwater scheme. In general, the section of a detached breakwater is not very different from a rubble mound breakwater, containing the following elements (Costa, 2009):

- **Resistant cloak**: exposed slope zone that receives the direct action of agitation, composed of two layers of artificial or natural blocks;
- **Intermediate cloak**: designed to prevent the escape of fine sediments from the core, comprises rows of decreasing diameters towards the inside of the breakwater. Geosynthetics like geotextile material type can be used to help accomplish this task;
- **Core**: inner zone of the breakwater;
- **Toe**: shot below the base of the cloak sturdy support and prevents infrastructure excavations.

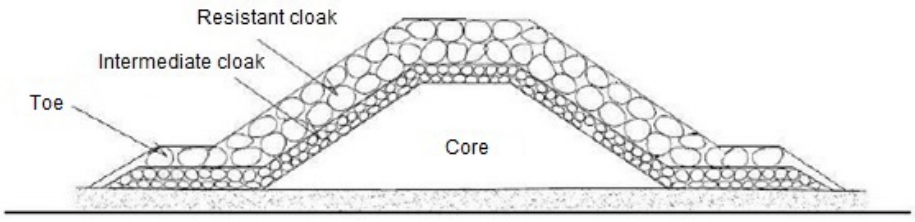

Figure 2.18: Cross section of a breakwater (Adapted from Costa, 2009).

2.2.3 Materials

The most used material in the construction of detached breakwaters is the rockfill. This happens mostly for its more affordable when compared with concrete blocks and because of their good quality and resistance against agitation (rockfill is more resistant than concrete to agitation and also lasts longer). Another important advantage of rockfill is the possibility of reducing the negative environmental impacts. It may allow attachment of marine species (Challinor and Hall, 2008), creating a new habitat on the breakwater if the rockfill is similar to geological characteristics of materials of the intervention zone (Figure 2.19 a)). In absence of rockfill material in the intervention zone, concrete solutions such as tetrapods, cubic blocks, or Antifer ™ blocks, among other patented blocks are also commonly used.

The use of geosynthetics is also important because it can serve to protect the base of the slope excavation infrastructure, as also applies to separate the various layers of the slope.

The blocks of rockfill are normally acquired in quarries, depending on the weight they need to resist to the actions that will be performed on them. The block of precast concrete feature patented several forms, varying the geometry, size and weight (C.E.M., 2008). The major differences between them are related to its permeability when the blocks are arranged together, and thus to its ability to dissipate energy. Another distinguishing factor among the various patents relates to stability of the blocks, as well as the entire structure.

Due to the scarcity of materials and/or the high price involved in this type of solutions, several alternative materials such as tires, carcasses of cars/buses, among others, were used in several places on the planet. However, the impacts for the environment and the requirements of structural stability are factors driving demand for viable alternative materials (CIRIA/CUR, 2007).

More recently, coastal defence works using geotextiles (Figure 2.19 b)) whether in the form of bags, containers or pipes have been built. These containers, ranging in size, are filled with sediment captured in rocks. Although there is still some reluctance in using these materials related to their long-term durability when exposed to ultraviolet, or radiation exposure to human action, there are already several cases where geotextiles were successfully used in coastal protection works or stabilization (Dubai and Australia as the most publicized cases). Because the durability of geotextiles decreases when exposed to ultraviolet radiation, the use of such material is best suited to underwater structures where the effect of such radiation is less intense. The fact that they are submerged is an advantage, decreasing exposure to wave action and the need to maintain the

detached breakwater. Another advantage is the fact that it is under water what makes this material less susceptible to damage by human actions (Nunes, 2012).

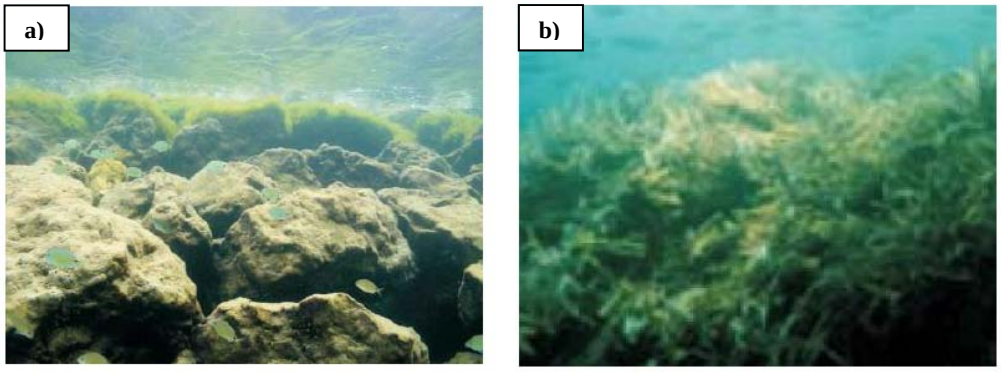

Figure 2.19: Type of organic growth associated with rockfill structures and geotextiles. a) Rockfill; b) Geotextiles.

Fauna and flora impacts, due to using geosynthetic as material in the construction of marine works have also been accompanied and studies have shown that this type of material contributes to the increase of biodiversity of species implantation sites, as well as for the proliferation of the species (Corbett *et al*., 2010).

In conclusion, the choice of material to use holds up much to their availability at the implantation site, with the cost associated with the material, and associated with the detached breakwater functionality.

2.2.4 Functional parameters

Along with the wave conditions of the site concerned, the functional parameters are crucial to the effectiveness of any coastal defence structure. The submergence of the breakwater and the transmission coefficient (related to the crest width, its submergence and wave climate) are two examples of these parameters.

The transmission coefficient is determined by the balance between the energy of the incident wave (immediately before the breakwater) and the energy of the transmitted wave (immediately after the breakwater), being the wave energy directly related to the wave height. In the case of submerged breakwaters, it is considered that the energy transfer is dominated by the dissipative effect of the surf wave and for emerged breakwaters, where overtopping is not admissible, the power transmission through the structure is what most affects the transmission coefficient (Nunes, 2012).

It is essential to evaluate the local physical characteristics such as bathymetry, the dimensions of foundation and depth of deployment, the dominant direction of sediment transport, their characteristics, the direction and intensity of prevailing winds and also the heights and wave periods.

The structure itself has structural parameters, the longitudinal length, the distance to the coast line, the spacing between breakwaters (if it is a system of detached breakwaters) and dimension and width of the crown (Costa, 2009).

The transmission coefficient has an undoubted importance in the design of submerged breakwaters (if we control this parameter, we can reduce the turbulence in the water landside). Reduced crest submergence, a sufficient height and width to reduce incident waves and a sufficient distance of the barrier from the shoreline to reduce the turbulence in the inner beach have an important role in the reduction of the wave transmitted inshore (Taveira-Pinto and Neves, 2003).

2.2.5 Hydrodynamics and sediment transport

Detached breakwaters may be of great interest to the local economy in terms of tourism, it could improve in several aspects the bathing area, whether increasing the area or improving the degree of protection against the action of the sea. Detached breakwaters provide a redistribution of sediment transport pattern in order to create the desired configuration beach (Taveira-Pinto and Neves, 2003). The current diffraction created at the ends of the breakwater promotes readjustment of sediments, spreading from the structure to the shoreline. The accumulation of sediments can be of two types: tombolo and salient.

When constructing a detached breakwater or series of detached breakwaters, consideration must be given to the proper placement of the structure(s). If a breakwater is placed too close to shore, or if the series of breakwaters are constructed too close together, an excess of sand may be captured on the leeward side of the project. The tombolo corresponds to a projection of sediment that extends from land to the breakwater, which, depending on the intended, may or may not be beneficial, because it may interrupt the longshore transport of sediment to nearby beaches. When the sediment does not extend completely to the breakwater, the area of sand is referred to as a salient. While this may seem ideal in creating a beach, the trapping of sand at the project site creates a loss of sand downdrift, potentially leading to increased erosion in the affected areas. To counter this, detached breakwater projects include the placement of sand, or pre-fill, during construction. The pre-fill volume of sand is equivalent to the amount that is estimated to be captured by the structure under

average water levels. While sand may naturally build up behind the breakwaters, pre-filling and periodic nourishment is beneficial typically required by regulatory agencies.

A correctly designed breakwater system will result in the formation of a salient which allows littoral drift to flow downdrift between the breakwater and the sand beach. An incorrectly designed breakwater system will result in the formation of a tombolo.

Schematic views of hydrodynamics and sand trapping near tombolo and salient generation are presented in Figure 2.20, Figure 2.21 and Figure 2.22.

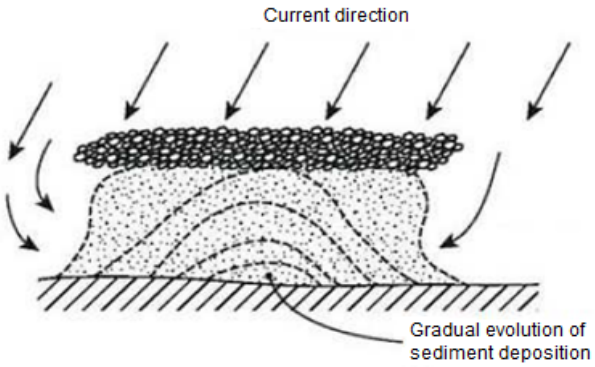

Figure 2.20: Scheme for formation of tombolo and action of refraction (French, 2002).

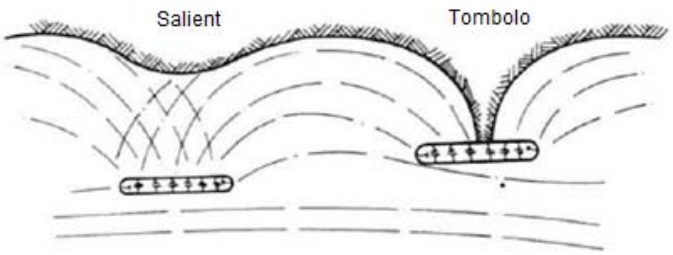

Figure 2.21: Scheme for a salient and tombolo generation (Abbott and Price, 1994).

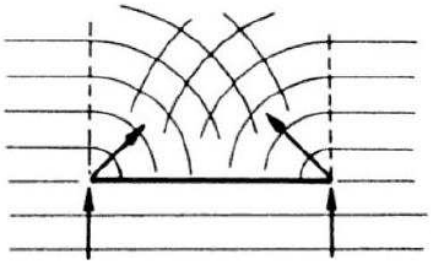

Figure 2.22: Scheme of diffraction caused by a detached breakwater (Silvester and Hsu, 1997).

Several studies on the ability to retain sediment by the breakwater are available in literature. In general these studies are related to the distance of the structure to the shoreline, the declivity of the

wave, the crowning above the mean water level and the length of the breakwater with its ability to retain sediment.

Studies show that the efficiency of a breakwater increases with wave steepness (H_s/L_m), with the growth of the crest elevation above the mean water level and with the length of the breakwater (between 60 and 120 m). In addition, it was also found that this efficiency remains constant for distances to the coastline between 90 and 120 m (Taveira-Pinto, 2007).

Cited by Herbich (2000), Toyoshima (1974) studied several high breakwaters in Japan, a country with a significant number of structures of this type, and concluded that to obtain a tombolo, the distance of the structure to the original shoreline divided by the total length of the detached breakwater shall not be less than 0,74. The same author has also found a relation between the wavelength and the length of the detached breakwater, and this should be two to six times the wavelength or be between 61 and 198 meters, while the distance between breakwaters should be at least a wavelength between 20 and 50 meters. Finally, Toyoshima (1974) also found that not only there is an increase in volume of the sediment in the leeward side of the breakwater but also in the direction opposite to the preferred transport of sediment moved by longshore currents.

2.2.6 Impacts caused by detached breakwaters

The construction of a detached breakwater causes many impacts on the surrounding area, ranging from hydrodynamic impacts and bio-morphological to the socio-economic and landscape.

With the implementation of detached breakwaters, the currents changes, wave conditions are affected, and the waves are mainly diffracted and refracted. Another important aspect regarding hydrodynamics is that if the breakwater is emerged it may occur stagnation of the water in the leeward side of the structure, which is negative for bathing. Detached breakwaters may also create new habitats, providing the fixing of marine species and seabirds. The issue of stagnant waters in the leeward side of the structure can promote the proliferation of algae species that may diminish the quality of beaches for bathing, due to the turbidity of the water and unpleasant odours. This problem is not so frequent if the breakwater is submerged, because the overtopping origins water recharge in the leeward side of the structure. It can also occur the formation of complex currents and eddies that can be dangerous for bathing. Mitigation of this problem is sometimes difficult, because even using scale models, and numerical prediction models of diffraction and refraction these phenomena have great complexity.

Despite a detached breakwater allows maintenance of sediment placed through artificial feeding and accumulate sediments, it can also cause erosions in the alongshore direction. However, this phenomenon is less shown than in the case of groins, which reduce more effectively the longitudinal sediment transport. The currents along the heads of detached breakwaters can create localized erosion and excavation at the bottom, which is most striking aspect in the case of a system of detached breakwaters, where the small gaps between them lead to higher speeds (Costa, 2009).

In terms of landscape, it is important to take into account at the design that featured breakwaters lead in general, a negative visual impact. This effect may be reduced if we consider higher submergence and natural materials as rockfill instead of concrete blocks, as mentioned before.

2.2.7 Structural types of breakwaters

General classification of breakwaters may be divided in two categories: rubble mound and composite breakwaters. Rubble mound breakwaters have a rubble mound and an armour layer that usually consists of shape-designed concrete blocks. Due to the development of these blocks, modern-day rubble mound breakwaters can strongly resist the destructive power of waves, even in deep waters. Composite breakwaters consist of a rubble foundation and vertical wall, and are therefore classified as vertical breakwaters. By using caissons as the vertical wall, composite breakwaters provide an extremely stable structure even in rough, deep seas. Such strength has led to their use throughout the world (Takahashi, 2002).

2.2.7.1 Global classification

Several structural types of breakwaters are used throughout the world. Table 2.1 describes three main structural types (Takahashi, 2002):

- Sloping or mound type;
- Vertical type which includes the basic (simple) vertical type, the composite and horizontally composite types;
- Special types.

Table 2.1: Structural types of breakwaters (Adapted from Takahashi, 2002).

Structural type	Characteristics
Sloping (mound)	Rubble mound breakwaters
	Rubble mound breakwaters (multi-layer)
	Rubble mound breakwaters armoured with blocks
	Concrete block breakwaters
	Reshaping rubble mound breakwaters (berm breakwaters)
	Reef breakwaters (submerged breakwaters)
Vertical (upright) Composite Horizontally composite	Monolith concrete breakwaters
	Block masonry breakwaters
	Cellular block breakwaters
	Concrete caisson breakwaters
	New caisson breakwaters
Special (non-gravity)	Curtain wall breakwaters
	Steel pile breakwaters
	Horizontal plate breakwaters
	Floating breakwaters
	Pneumatic breakwaters
	Hydraulic breakwaters

2.2.7.2 Sloping or mound type

The sloping or mound type of breakwaters basically consists of a rubble mound as shown in Figure 2.23. The most applied sloping type breakwater is one with randomly placed stones (a). To increase stability and decrease wave transmission, as well as to decrease material costs, the multi-layered rubble mound breakwater was developed having a core of quarry run (b). The stability of the armour layer can be strengthened using shape-designed concrete blocks, while wave transmission can be reduced using a superstructure (wave screen or wave wall), which can also function as an access road to the breakwater (c).

Breakwaters comprised of only concrete blocks (d) are also being constructed, especially for use as a detached breakwater providing coastal protection. Although wave transmission is not reduced so much for this breakwater type, its simple construction procedure and the relatively high permeability of the breakwater body are advantageous features. Recently, reef breakwaters or submerged breakwaters (e) have been constructed for coastal protection.

Reshaping breakwaters (f) utilize the basic concept of establishing equilibrium between the slope of the rubble stone and wave action, i.e., the rubble mound forms a Se-shape slope to stabilize itself

against wave actions. This breakwater has a large berm in front, which will ultimately be reshaped due to wave actions, and therefore it is called the berm breakwater or dynamically stable breakwater. It should be noted that this concept is not new, since ancient rubble mound breakwaters were all of this type, being naturally reshaped by damage and subsequent repairs (Takahashi, 2002).

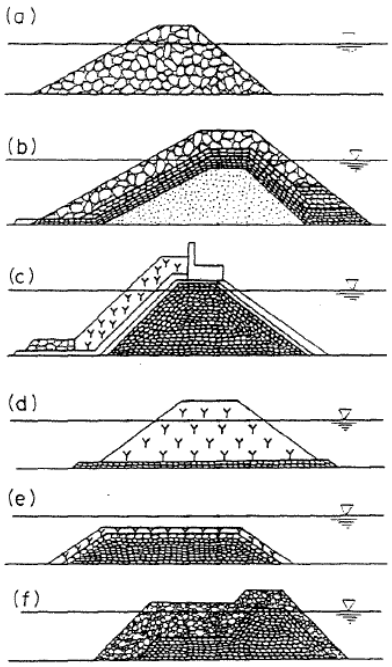

Figure 2.23: Examples of sloping type breakwaters (Takahashi, 2002).

2.2.7.3 Vertical type (composite and horizontally composite types)

The original concept of the vertical breakwater was to reflect waves, while that for the rubble mound breakwater was to break them. Figure 2.24 shows four vertical type breakwaters having different mound heights. The basic vertical wall breakwater is shown in (a), while the others are composite breakwaters with a rubble mound foundation, namely, the low-mound (b) and high-mound composite breakwaters (d). By convention, the high-mound composite breakwater has a mound that is higher than the low water level (L.W.L.). The former breakwater does not cause wave breaking on the mound, while the latter one does. Since the high-mound composite type is unstable due to wave-generated impulsive pressure and scouring caused by breaking waves, composite breakwaters with a low mound are more common. The composite breakwater with a relatively high mound (c) that is lower than L.W.L. occasionally generates impulsive wave pressure due to wave breaking. To reduce wave reflection and the breaking wave force on the vertical wall, concrete blocks are placed in front of it. This is called a composite breakwater covered with wave dissipating

concrete blocks, which is now called the horizontally composite breakwater. Such breakwaters are not new, however, since vertical wall breakwaters suffering damage to the vertical walls were often strengthened by placing large stones or concrete blocks in front of them so as to dissipate the wave energy and reduce the wave force, especially that from breaking waves. Modern horizontally composite breakwaters employ shape-designed concrete blocks such as tetrapods (Takahashi, 2002).

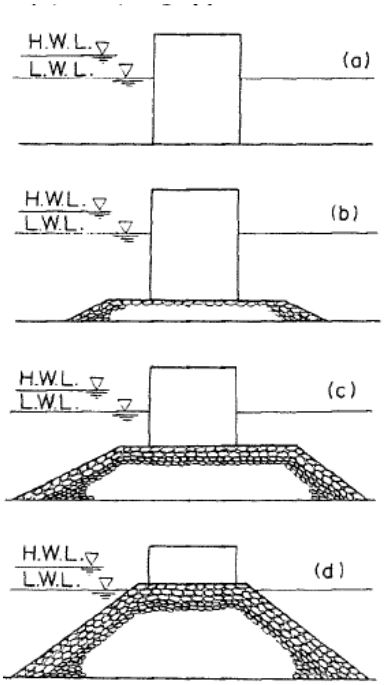

Figure 2.24: Examples of vertical type breakwaters (Takahashi, 2002).

The horizontally composite breakwater is very similar to a rubble mound breakwater armoured with concrete blocks. Figure 2.25 shows how its cross section varies with mound height, whereas the mound height increases, the breakwater becomes very similar to rubble mound breakwaters. In particular, a breakwater with core stones in front of the vertical wall (d) is nearly the same as the rubble mound breakwater. They are basically different, however, since the concrete blocks of the rubble mound breakwater act as the armour for the rubble foundation, while the concrete blocks of the horizontally composite breakwater function to reduce the wave force and size of the reflected waves. Thus, horizontally composite breakwaters are considered to be an improved version of the vertical types (Takahashi, 2002)

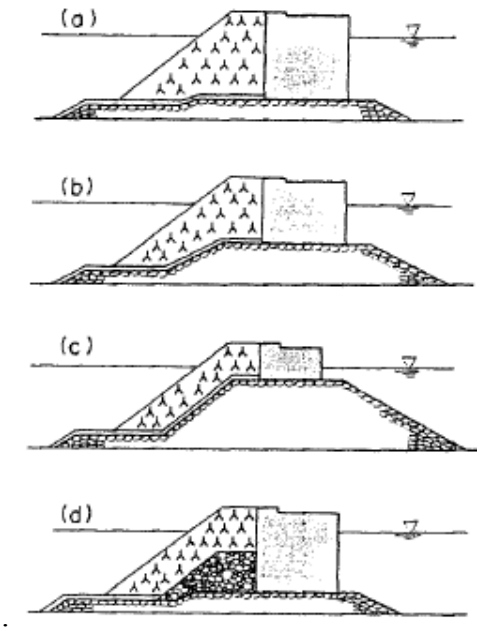

Figure 2.25: Examples of horizontally composite breakwaters (Takahashi, 2002).

Figure 2.26 shows several kinds of composite breakwaters having different upright sections. An upright wall with block masonry (b) was initially most popular, in which many different methods were applied to strengthen the interlocking between the blocks. Cellular blocks (c) have also been used to form the upright wall of vertical breakwaters. However, the invention of caissons (d) made these breakwaters more reliable, and many were subsequently constructed around the world. Caisson breakwaters have been improved using sloping top caissons (e) or perforated walls (f) (Takahashi, 2002).

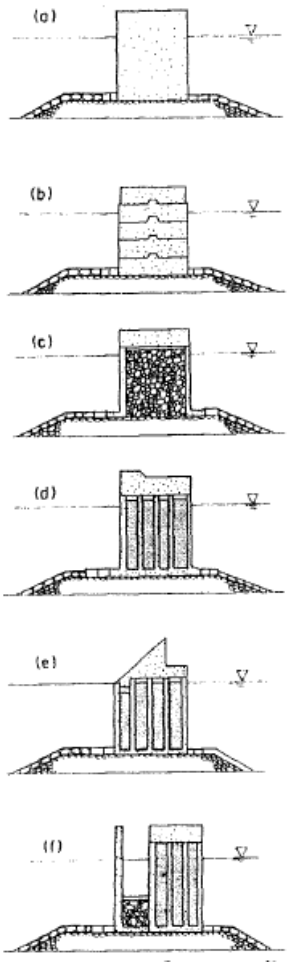

Figure 2.26: Examples of composite breakwaters (Takahashi, 2002).

It should be noted that the rubble mound/rubble foundation of composite breakwaters is vital to prevent the failure of the upright section by scouring, as well as stabilizing the foundation against the wave force and caisson weight (Takahashi, 2002).

2.2.7.4 Special types

Special type breakwaters are those employing some kind of special feature. Although they are not commonly used, their history is long, and in fact, some were constructed in ancient times. Special breakwaters, however, do not always remain special, because some of them later become a standard breakwater, e.g., the perforated caisson breakwater has become very popular in some countries and is now considered to be a standard breakwater there.

Common special type breakwaters are non-gravity type ones, such as the pile, floating, or pneumatic types. These breakwaters also have a long history, and some are still being currently

employed. Their uses though, are limited to special conditions. Figure 2.27 shows some special breakwaters. The curtain wall breakwater (a) is commonly used as a secondary breakwater to protect small craft harbours, and the vertical wall breakwater having sheet piles or continuous piles (b) is sometimes used to break relatively small waves. A horizontal plate breakwater (c) can reflect and break waves, and as shown, it is sometimes supported by a steel jacket. A floating breakwater (d) is very useful as a breakwater in deep waters, but its effect is limited to relatively short waves. The pneumatic breakwater (e) breaks the waves due to a water current induced by air bubble flow, and it is considered effective for improving nearby water quality, though only being effective for waves having a short length (Takahashi, 2002).

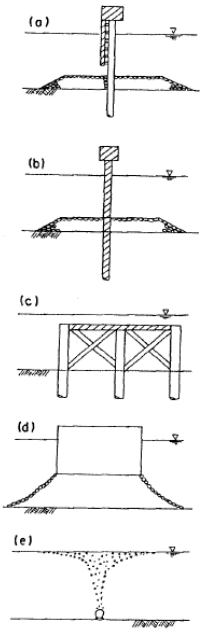

Figure 2.27: Examples of special breakwaters (Takahashi, 2002).

2.2.8 Detached breakwater design

Given the importance of coastal areas, both in terms economic or social, it becomes increasingly important to provide the decision-making entities of tools that they allow through certain scenarios, evaluate the evolution and the impact of measures on the coast. The sustainable management of coastal areas also involves predictive power of morphological evolution at medium and long term. This prediction is difficult and almost always accompanied by a great uncertainty, due to the high number and complexity of the processes involved, their interaction, and the scarcity of field data that usually characterize them. In this context, numerical modelling plays a paramount role in simulating the evolution of coastal morphology. In the last decades a number of powerful models

have been developed with many different capabilities/limitations and data requirements, although, in general, all of them of hard calibration and validation due to the large amount of parameters included in those models.

2.2.8.1 Introduction

The effect of a detached breakwater is to reduce the incident wave energy on a section of the coast in its leeward side. This reduction of wave energy in the leeward side of a breakwater scheme induces complex flow circulation patterns due to gradients in wave setup, wave-driven longshore flow and tidal flows, resulting in complex sediment transport patterns. In a meso or macro-tidal environment, the coastal zone is continually changing as the water level changes with the tide. Furthermore, the tidal currents also interact with the wave-driven currents, leading to more complex flow and sediment transport patterns. These complex sediment transport patterns result in morphological changes in the vicinity of the breakwater. These changes include: a) sediment deposition in the leeward side of the breakwater; b) erosion in the breakwater bays; and c) scour near the breakwater heads.

Thus, understanding the likely incident wave and water level conditions, how the breakwater influences the incident wave energy distribution and tidal flows on the beach and the beach's response to the new conditions are the three key elements for selecting an appropriate geometrical layout of a nearshore detached breakwater scheme.

2.2.8.2 Depth of closure and significant wave height

In a simplified form, in the case of sandy beaches dominated by sea waves, the depth of closure represents the limit in the direction of the sea, to which there is significant morphological variation of the beach profile, as a consequence of wave activity near the bottom.

The depth of closure was already defined in several ways (Kraus *et al.*, 1999): critical depth, depth of the active profile, depth of the active movement of sediments, maximum depth of beach erosion, limit towards the sea of erosion processes by wave action along the coast and limit towards the sea of construction processes by wave action. To all these definitions is associated some uncertainty.

The definition of Kraus et al. (1999) for the depth of closure in a characteristic time period is the closer land depth to beyond which, towards the sea, there is no significant variation of the bottom, neither occurs significant sedimentary exchanges between inland and outland area at this depth.

The depth of closure is one of the most relevant hydrological parameters, which its knowledge is important in several coastal engineering interventions, such as: artificial feeding projects of beaches; implementation location for coastal structures and its dimensioning; and shoreline evolution studies.

Ideally, the determination of the depth of closure should be done through the same surveying beach profile over a certain period of time. However, data are scarce, but even when are data available it may not have the necessary resolution to detect significant changes in the profile. For this reason, semi-empirical formulations are often used, allowing estimation of this morphological limit based on characteristic parameters of marine wave conditions and sediments.

The modelling of the transverse profile evolution, as well as the evolution of the coastline is significantly affected by the depth of closure.

The bottom variation depends on the location and timescale of interest, but also depends on the wave conditions, the sediments properties and form of the bottom profile.

Assuming an open coast dominated by wave action, sediment transport is induced by the littoral drift current and the orbital velocity of the wave currents.

There are several ways to determine this parameter. Hallermeier (1981) defined two critical depths in coastal zone, on the basis of interaction between waves and the bottom (Figure 2.28): d_i is the maximum depth for initial movement along the bottom by the action of medians conditions of waves; and d_l is the maximum depth of erosion by the action of extreme wave conditions.

The closest to land, d_l, limits a region called coastal zone while the region between the two called shoaling zone, where wave action results in a moderate effect of the transverse profiles over an annual cycle which corresponds to the transition zone between the coastal zone and the open sea.

The d_l depth corresponds to the limit value for the coastal zone, where occur the effects of wave activity near the bottom related to the surf processes and swash wave. Until this depth limit, longitudinal transport is significant and the transverse transport is intense. Between this depth and the outermost boundary towards the sea, d_i, transverse profiles show moderate variations over year.

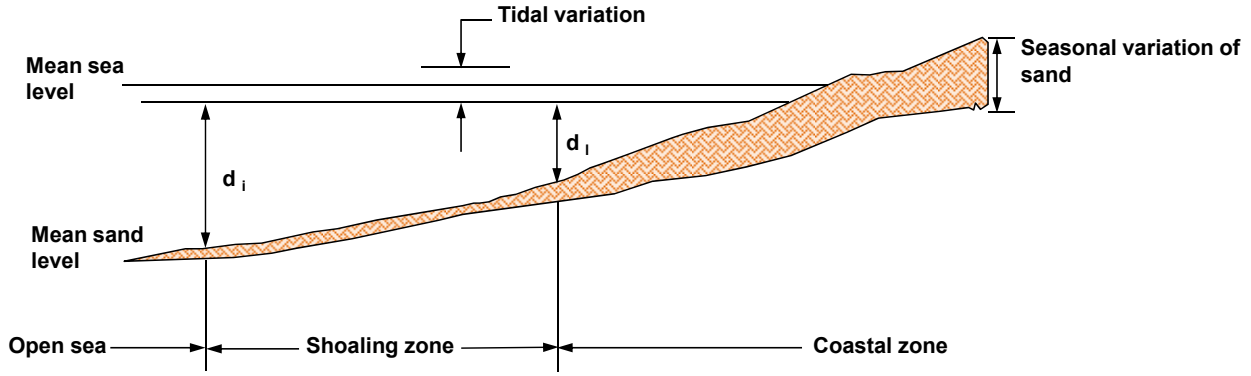

Figure 2.28: Annual zoning of the seasonal variation of beach profile (adapted by Hallermeier, 1981).

Thus, Hallermeier established relatively simple formulations (Equations (1) and (2)), which from wave characteristics and bottom sediments allow obtaining the limit depths, d_l and d_i, respectively.

Hallermeier (1978) developed analytical approaches that allow the estimation of d_i and d_l. Assuming that the bottom sediments are quartz sand in seawater (submerged relative density, $\gamma'(\rho_s/\rho_w - 1) = 1{,}6$), Hallermeier's depth of closure can be estimated by the following equations.

$$d_l = 2{,}28H_{s\,0{,}137} - 68{,}5\left(\frac{H_{s\,0{,}137}^2}{g\bar{T}_s^2}\right) \quad (1)$$

$$d_i = H_{s\,50}\bar{T}_s\left(\frac{g}{5000d_{50}}\right)^{0{,}5} \quad (2)$$

where: d_l (m) is the maximum depth of erosion by the action of extreme wave conditions; $H_{s\,0{,}137}$ (m) is the extreme significant wave height which is exceeded 12h in a year (i.e. with 0,137% probability of occurring); $\bar{T}_s$ (s) is the extreme wave period associated to the extreme wave; g (m/s^2) is the acceleration of gravity.

where: d_i (m) is the maximum depth for initial movement along the bottom by the action of medians conditions of waves; $H_{s\,50}$ (m) is the median annual significant wave height; $\bar{T}_s$ (s) is the extreme wave period associated to the extreme wave; g (m/s^2) is the acceleration of gravity; d_{50} (m) is the median diameter of sediments in the shoaling zone.

2.2.8.3 Tidal parameters

The gravitational forces of the Moon and Sun create areas of high and low water on the Earth's surface. As the Earth rotates the location of high and low tide changes. The Moon has the greatest effect on the water compared with the Sun due to its proximity to the Earth and the configuration of the Sun and Moon, whether aligned or offset, has an effect on the tidal range. The tides of increased

range occurring near the times of full Moon and new Moon are called spring tides. The gravitational forces of the Moon and the Sun act to reinforce each other. Since the combined tidal force is increased, the high tides are higher and the low tides are lower than average. The tides of decreased range occurring near the times of first and third quarter phases of the Moon are called neap tides. The gravitational forces of the Moon and the Sun counteract each other. Since the combined tidal force is decreased, the high tides are lower and the low tides are higher than average (PLA, 2014).

Tidal levels are presented in Figure 2.29.

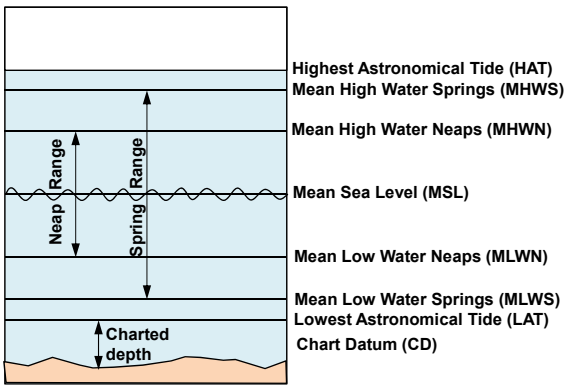

Figure 2.29: Diagram illustrating tidal terms (adapted from LINZ, 2014).

- **Highest Astronomical Tide (HAT) and Lowest Astronomical Tide (LAT)**

The highest and lowest levels, respectively, can be predicted to occur under average meteorological conditions and under any combination of astronomical conditions. These levels will not be reached every year. HAT and LAT are not the extreme levels, which can be reached as storm surges may cause considerably higher and lower levels to occur (PLA, 2014).

- **Mean High Water Springs (MHWS) and Mean Low Water Springs (MLWS)**

The height of mean high water springs is the average of the heights of two successive high waters during those periods of 24 hours (approximately once a fortnight) when the range of the tide is greatest. The height of mean low water springs is the average height obtained by the two successive low waters during the same period, i.e. (PLA, 2014): MHWS: The average height of the high waters of spring tides above Chart Datum; MLWS: The average height of all low waters of spring tides above Chart Datum.

- **Mean High Water Neaps (MHWN) and Mean Low Water Neaps (MLWN)**

The height of mean high water neaps is the average, throughout a year as defined above, of the heights of two successive high waters during those periods (approximately once a fortnight) when the range of the tide is least. The height of mean low water neaps is the average height obtained

from the two successive low waters during the same periods, i.e. (PLA, 2014): MHWN: The average height of the high waters of neap tides above Chart Datum; MLWN: The average height of the low waters of neap tides above Chart Datum.

– **Mean Sea Level (MSL)**

Mean Sea Level is the average level of the sea surface over a long period, normally 19 years, or the average level which would exist in the absence of tides (PLA, 2014).

2.2.8.4 Geometrical parameters. Outline design procedure

The first step in designing a nearshore detached breakwater scheme, or other infrastructural beach control option, is to consider what change is required to the existing shoreline.

The morphological changes (tombolo or salient) are controlled by the incident wave and water level conditions, the sediment characteristics and the geometrical layout of the breakwater scheme. Figure 2.30 illustrates the key variables specified in an outline design as proposed in DEFRA (2010).

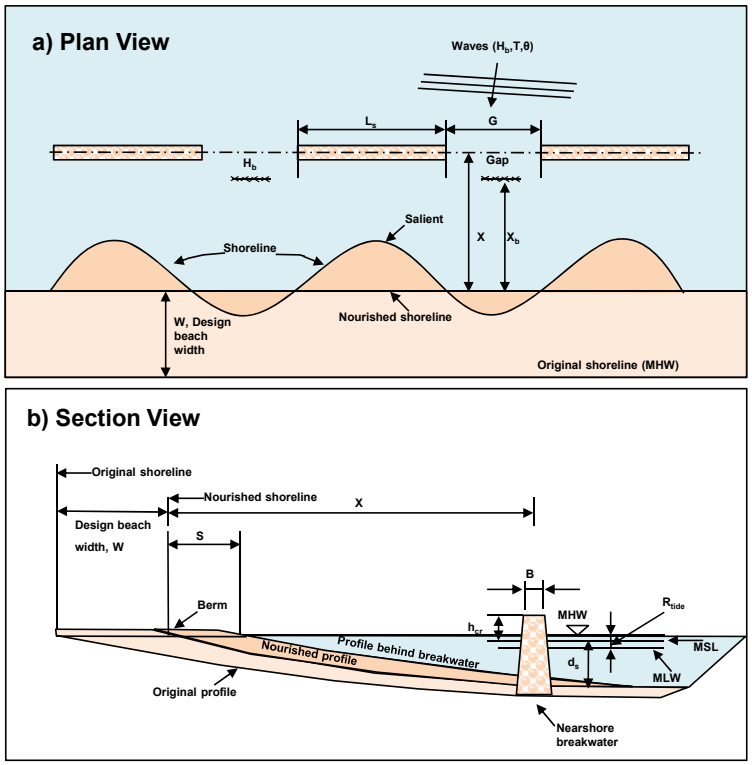

Figure 2.30: Definitions of key variables for nearshore breakwater scheme: a) plan view, b) section view (adapted from DEFRA, 2010).

The geometrical parameters of the breakwater scheme for the case study were determined according to the new outline design procedure proposed in DEFRA (2010). Although this guidance is recommended by the United Kingdom Environment Agency it had been assumed that this remains valid for the Portuguese coastline. This design guidance focus on the geometric layout of beach control breakwater systems rather than the structural design of breakwater structures.

Table 2.2 lists some characteristic parameters definitions used for determining the wave and tide conditions at a given site. These characteristic parameters are used in the design of curves for estimating the geometrical parameters of the breakwater scheme. A list of the parameters used is given in Table 2.3.

Table 2.2: Parameters for determining incident wave and tide conditions used in the design curves (DEFRA,2010).

Parameter	Suggestion	Further remarks
H_b	Determine H_b based on the H_{m0} exceeded 12hr/year at the site, calculated at the closure depth.	H_{m0} exceeded 12hr/year is the characteristic wave height used to determine the closure depth (limit of littoral drift movement) and can be considered as characteristic for determining the area affected by the littoral drift. H_b is used as the characteristic H_{m0} to determine the dimensionless tidal range (R_{Tide}/H_{m0}) and the submergence depth (d_{cr}/H_{m0}) in the design curves.
X_b	Determine X_b based on H_b determined as above and the average beach slope.	
R_{Tide}	Use the difference between the MHWS (mean high water spring) tide level and MLWS (mean low water spring) tide level.	A spring tidal cycle occurs every fortnight and thus it is likely that significant storms for sediment transport will occur during spring tides. Hence, this is considered as the appropriate parameter to use in outline design.
d_{cr}	This is defined as the submergence depth at high water during a typical annual residual surge level: d_{cr} = MHWS + $Surge_{1year}$ - h_{cr} $Surge_{1yr}$ = surge level with return period of one year; h_{cr} = elevation of breakwater crest level.	Although the numerical model simulations do not include the effect of residual surge level, it is expected that this will be important in practical situations, given that the numerical simulation results show significant impact on the submerged depth at the breakwater crest level.

Table 2.3: Parameters used for determining geometrical parameters of the breakwater (DEFRA, 2010).

Parameter	Units	Description
C_g	m/s	Wave group velocity
d_{cr}	m	Depth of water at the breakwater crest during high water
G	m	Gap width between breakwaters
h_{cr}	m	Height of breakwater above mean sea level
H_b	m	Characteristic significant wave height at the closure depth
H_{m0}	m	Significant wave height
L_s	m	Breakwater length
MSL	m	Mean sea level
R_{tide}	m	Tidal range
S	m	Salient length
T_p	s	Peak wave period associated with H_b
X	m	Distance from baseline to breakwater centre line
X_b	m	Distance from baseline to closure depth

According to DEFRA (2010), the beach response in the vicinity of nearshore breakwaters on macro-tidal sites is a function of some dimensionless parameters. The parameters that are used in this work are listed in Table 2.4.

Table 2.4: Dimensionless parameters that influence beach response in the vicinity of nearshore breakwaters.

Dimensionless parameter	Definition
L_s/X	is a measure of the breakwater blocking efficiency.
X/X_b	is the percentage of littoral drift affected by breakwaters (a measure of the relative location of the breakwaters in the surf zone).
d_{cr}/H_b	is a measure of wave energy dissipation rate over the breakwater.
R_{tide}/H_b	is a measure of the effect of tide range on the surf zone.

For a given L_s/X, the dimensionless salient length (S/X) increases for low values of X/X_b and thereafter decreases, as should be expected for breakwaters located far away from the surf zone.

The outline design of a nearshore detached breakwater scheme on a sandy coast consists of specifying the key geometrical parameters of the breakwater scheme in order to obtain a desired response under the prevailing wave and tidal conditions at the specified beach. The key geometrical parameters to be specified in outline design are (see Figure 2.30):

- the length of the breakwater, L_S, measured along the breakwater crest;

- the cross-shore distance of the breakwater relative to a characteristic initial shoreline (MSL shoreline), X;
- the gap distance between adjacent breakwaters, G, measured as the gap distance between the breakwater crests;
- the breakwater crest elevation, h_{cr}, measured relative to MSL and the breakwater crest width, B.

The procedure for the outline design of the detached breakwater scheme on sandy shoreline is organized according to the following stages (DEFRA, 2010) and it is used in Chapter 3:

- **Stage 1:** Fix the offshore distance by reference to the amount of longshore sediment transport that should be bypassed to downdrift beaches in order to minimize downdrift erosion. In general, the amount of transport bypassed to downdrift beaches (downdrift of the breakwater scheme) reduces as X/X_b increases;
- **Stage 2:** Once the optimum offshore distance of the breakwater has been determined, it is then straightforward to calculate X/X_b. Next, using the relationships determined in this study, calculate the breakwater length (L_s) for the desired beach response (in the leeward side of the breakwater), including the effect of tidal range, as shown in Figure 2.31.
  Decisions will need to be taken regarding the preferred beach response (limited response, salients or tombolos). Clearly, tombolos will be more disruptive than salients to the longshore movement of sediment, but will offer more protection during severe storms and offer a greater amenity area;

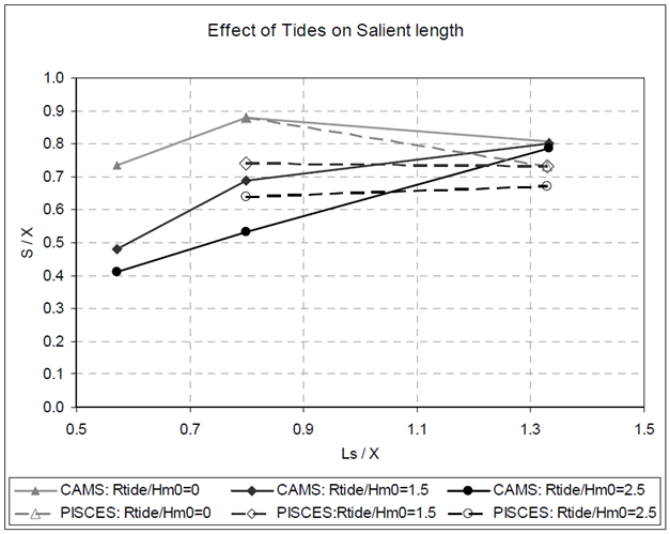

Figure 2.31: Effect of breakwater length for different dimensionless tidal ranges (R_{tidal}/H_{m0}; standing tides).

– **Stage 3:** Determine the breakwater crest level based on the desired salient length using the design graph shown in Figure 2.32. In general, the salient width (and also the beach level) reduces as the depth of water over the breakwater crest at high water increases;

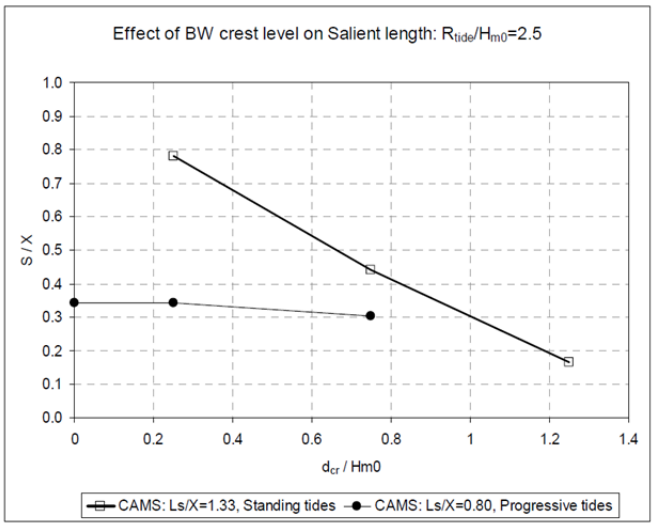

Figure 2.32: Effect of breakwater crest level (relative submerged depth at high water, d_{cr}/H_{m0}) for different breakwater length (R_{tide}/H_{m0} = 2,5).

– **Stage 4:** Lastly, estimate the gap width between the breakwaters based on the maximum shoreline erosion (MSL shoreline) allowed in the breakwater bays. This is done using the existing design curves (such as Figure 2.33).

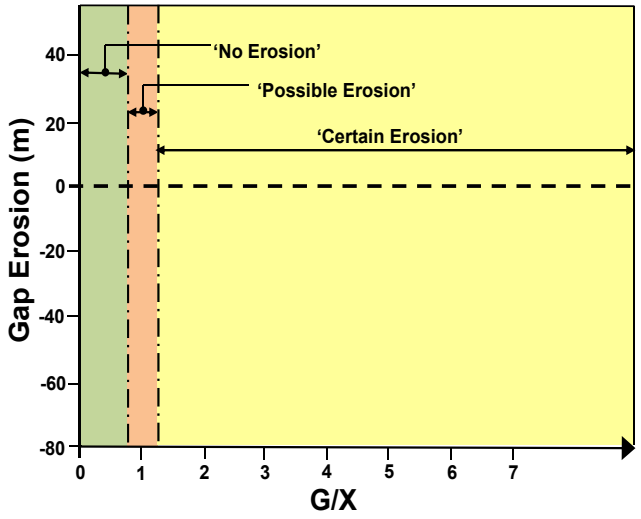

Figure 2.33: Existing design guidance for assessing possible shoreline erosion in the gaps between nearshore breakwaters.

Note: The effect of the breakwater gap width was not investigated in the present study. In general, the shoreline erosion is expected to increase as the gap width increases, until the

gap width is large enough that each breakwater can be considered to be independent of the adjacent one.

2.3 Numerical modelling applied in coastal zones

An important component of most coastal and ocean engineering projects is an accurate assessment of the wave climate at the project site. Typical applications include determination of siltation rates inside entrance channels and harbour basins, determination of safe conditions for the loading/offloading of ships, optimization of harbour layouts for both wind-generated and long-period waves, design of structures such as breakwaters, and the evaluation of the impact of coastal structures on adjacent shorelines.

A number of mathematical models have been developed to simulate the propagation and transformation of waves in coastal regions and harbours. The different models are based on different assumptions, which limit the types of problems to which they can be applied (Nwogu and Demirbilek, 2001).

The purpose of a model and the specific hydraulic questions a model is intended to address and define the necessary detail for various scalar and temporal components of a model's structure, its boundary conditions and key operational parameters. A numerical model is considered to be ready to produce reliable results only if the questions and problems to be addressed by the model are properly defined, all of the key input data have been thoroughly checked, and if model sensitivity, calibration and verification analyses have been carefully completed (NHC, 2012).

The next paragraphs describe and compare numerical models with wide application in hydrodynamics and sediment transport in coastal zones.

2.3.1 COULWAVE

COULWAVE (Cornell University Long and intermediate WAVE) is a free surface wave model. It solves various depth-integrated, long-wave based equation models, including the nonlinear shallow water wave equations and a number of the weakly dispersive Boussinesq-type equations. The primary applications for COULWAVE include landslide tsunami generation and propagation, nearshore tsunami evolution and inundation, and nearshore wind wave modelling. The numerical scheme uses a 4^{th} order finite difference scheme for the spatial derivatives, and a 4^{th} order iterative predictor-corrector scheme for the time integration. The unique features of COULWAVE, as well

as other phase-resolving, Boussinesq-type models, are that simulations can be relatively large scale (> 10 km^2) but contain spatial details on the order 1m. COULWAVE has been applied to a wide variety of topics, wave run-up, and wave generation by underwater landslides, among many others. Directional, random spectrums can readily be generated by the models, which capture near-shore evolution processes, such as shoaling, diffraction, refraction, and wave-wave interactions, with very high accuracy.

The COULWAVE allows simulating wave transformation phenomena in varying depth bottoms, since it includes refraction due to currents, run-ups and non-linear interactions of higher order (Teixeira *et al*., 2010).

The numerical model uses a predictor-corrector scheme to march forward in time, and uses finite differences to approximate spatial derivatives. The corrector segment of the procedure is implicit in time, and uses iteration to arrive at a solution.

For input, the model requires a specification of the incident wave condition, the bathymetry/topography, and boundary conditions. Input is facilitated through a set of Matlab scripts and a text-based user interface. As for output, the model outputs spatial snapshots of free surface elevation, mid-depth horizontal velocity, free surface velocity, eddy viscosity, and depth-averaged vorticity. The output frequency is user defined. Matlab scripts are provided for plotting the output. Output files are either ASCII or unformatted binary Fortran files (ISEC, 2014).

This model uses the concept of "multi-layer" approach for the integration of the primitive equations of motion (continuity and momentum equations) where the water column is divided into several layers. Each layer can tolerate a given velocity profile. With these velocity profiles matching at the boundary between layers is deduced a set of equations that allows to extend the applicability of the model to very deep waters. The accuracy of the model developed depends upon the number of layers that is considered, allowing its use in very deep waters. Thus, the model is good from the point of view of the linear dispersion characteristics. In addition, there were included additional terms associated with the time variation of the depth to take into account the sliding layers of emerged land and the occurrence of earthquakes that cause tsunamis.

For the one-layer model, the horizontal velocity vector is given as (Lynett and Liu, 2014):

$$U_1 = u_1 - \mu_0^2 \left\{ \frac{z_1^2 - k_1^2}{2} \nabla S_1 + (z_1 - k_1) \nabla T_1 \right\} + O(\mu_0^4) \quad (3)$$

where

$$S_1 = \nabla \cdot u_1, \qquad T_1 = \nabla \cdot (hu_1) + \frac{1}{\varepsilon_0}\frac{\partial h}{\partial t} \tag{4}$$

u_1 is the vector component of horizontal velocity to the depth defined in the layer, μ_0 is the frequency dispersion parameter ($\mu_0 = h_0/l_0$, where h_0 is the characteristic water depth or baseline water depth, function of space and l_0 is the characteristic horizontal lengthscale of the submarine slide), ∇ is the horizontal gradient vector, h is the water depth profile, function of space and time, ε_0 nonlinearity parameter ($\varepsilon_0 = a/h_0$, where a is the wave amplitude) and t is time.

The exact continuity equation can be rewritten approximately in terms of ζ and u_1 as (Lynett and Liu, 2014):

$$\frac{1}{\varepsilon_0}\frac{\partial h}{\partial t} + \frac{\partial \zeta}{\partial t} + \nabla \cdot [(\varepsilon_0 \zeta + h)u_1] - \mu_0^2 \nabla \cdot \left\{ \left[\frac{\varepsilon_0^3 \zeta^3 + h^3}{6} - \frac{(\varepsilon_0 \zeta + h)k_1^2}{2} \right] \nabla S_1 + \left[\frac{\varepsilon_0^2 \zeta^2 + h^2}{2} - (\varepsilon_0 \zeta + \right.\right.$$
$$\left.\left. + h)k_1 \right] \nabla T_1 \right\} = O(\mu_0^4) \tag{5}$$

where ζ is the free surface displacement.

Equation (5) is one of two governing equations for ζ and u_1. The momentum equation for u_1 is (Lynett and Liu, 2014):

$$\frac{\partial u_1}{\partial t} + \varepsilon_0 u_1 \cdot \nabla u_1 + \nabla \zeta + \mu_0^2 \frac{\partial}{\partial t} \left\{ \frac{k_1^2}{2} \nabla S_1 + k_1 \nabla T_1 \right\} + \varepsilon_0 \mu_0^2 \left[(u_1 \cdot \nabla k_1) \nabla T_1 + k_1 \nabla (u_1 \cdot \nabla T_1) + \right.$$
$$\left. + k_1 (u_1 \cdot \nabla k_1) \nabla S_1 + \frac{k_1^2}{2} \nabla (u_1 \cdot \nabla S_1) \right] + \varepsilon_0 \mu_0^2 \left[T_1 \nabla T_1 - \nabla \left(\zeta \frac{\partial T_1}{\partial t} \right) \right] + \varepsilon_0^2 \mu_0^2 \nabla \left(\zeta S_1 T_1 - \frac{\zeta^2}{2} \frac{\partial S_1}{\partial t} - \zeta u_1 \cdot \right.$$
$$\left. \nabla T_1 \right) + \varepsilon_0^3 \mu_0^2 \nabla \left[\frac{\zeta^2}{2} (S_1^2 - u_1 \cdot \nabla S_1) \right] = O(\mu_0^4) \tag{6}$$

The optimized model equations show good linear wave characteristics up to a kh of 8, while the second-order nonlinear behaviour is well-captured to kh of 6, being k the wave number and h the water depth.

The output of the model corresponds to the velocity values at a depth *0.531h* under the water surface, where h is the depth. The velocity at this depth is, by several authors, as Nwogu (1993), taken as the depth representative of the flow and was adopted by the authors of the COULWAVE model. The output velocity at a depth *0.531h* under the water surface can be used to determine the velocity cells near the shoreline that could give an indication of the sediment transport. Divergent cells indicate erosion nearby the shoreline and convergent cells indicate sedimentation (Mendonça *et al.*, 2012).

To enable the Boussinesq model to simulate surf zone hydrodynamics, energy dissipation due to wave breaking is treated by introducing an eddy viscosity term into the momentum equations, with

the viscosity strongly localized on the front face of the breaking waves. Wave run-up on the beach is simulated using a permeable seabed technique. Both wave breaking and run-up schemes follow the work of Kennedy *et al.,* (2000). Even though it has to be mentioned that, unlike 3D or quasi-3D Navier Stokes-type models, the overturning of the crest of the wave during breaking can never occur in a Boussinesq model (Mendonça *et al.*, 2012).

2.3.1.1 Breaker type

The shape of a breaking wave is of great importance for surfing. Battjes (1974) used the surf-similarity parameter, ξ_b (Equation (7)), to describe the breaker type on single slopes:

$$\xi_b = \frac{s}{\sqrt{H_b/L_0}} \quad (7)$$

where ξ_b is the inshore Iribarren number, s is the bottom slope, H_b is the wave height at breaking and L_0 is the deep water wave length. The values of the Iribarren number that correspond with each breaker type are presented in Table 2.5 (Mendonça *et al.*, 2012).

Table 2.5: Breaker type transition values for inshore Iribarren number.

Breaker type	Range
Surging/collapsing	$\xi_b > 2.0$
Plunging	$0.4 > \xi_b > 2.0$
Spilling	$\xi_b > 0.4$

2.3.1.2 Bottom friction and wave breaking

For the numerical exterior boundaries two types of conditions are applied: reflection and radiation. The reflective, or no-flux boundary condition follows the work of Wei and Kirby (1995) and for the radiation, or open boundary condition, a sponge-layer is applied, in the manner recommended by Kirby *et al.* (1998).

Lynett and Liu (2004) further introduced additional terms in the equations in order to account for bottom friction, wave breaking and wave generation inside the domain and added time-dependent water depth terms, in order to consider bottom-profile time variations induced by landslides and earthquakes.

Bottom friction $\overrightarrow{R_f}$ and wave breaking $\overrightarrow{R_b}$ are the two forms of physical dissipation considered, and modify the momentum equation according to Equation (8):

$$\frac{\partial \overrightarrow{u_1}}{\partial t} + \cdots + \overrightarrow{R_f} - \overrightarrow{R_b} = 0 \quad (8)$$

To solve the equations, a high-order predictor-corrector scheme is utilized, employing a third order in time explicit Adams-Bashforth predictor step and a fourth order in time Adams-Moulton implicit corrector step with an accuracy of Δt^4 (Press *et al.*, 1989). Finite differences are used to approximate spatial derivatives, with an accuracy of Δx^4 (Lima and Rocha, 2011).

2.3.1.3 Breaking scheme

The breaking scheme employed follows the scheme presented in Kennedy *et al.* (2000). The scheme is developed from an "eddy viscosity" approach, where a user-defined formulation for an eddy viscosity is developed based solely on agreement with experimental data. The eddy viscosity is part of a momentum conserving, ad-hoc dissipative term, $R_b = R_{bx}\mathrm{i} + R_{by}\mathrm{j}$, where:

$$R_{bx} = \frac{1}{H}\left\{[\nu(Hu_1)_x]_x + \frac{1}{2}[\nu(Hu_1)_y + \nu(Hv_1)_x]_y\right\} \quad (9)$$

$$R_{by} = \frac{1}{H}\left\{[\nu(Hv_1)_y]_y + \frac{1}{2}[\nu(Hv_1)_x + \nu(Hu_1)_y]_x\right\} \quad (10)$$

ν is the eddy viscosity, $\mathrm{H} = \mathrm{h} + \zeta$, the total water depth and u_1 and v_1 are the vector components of horizontal velocity to the depth defined in each layer. Eddy viscosity is calculated as:

$$\nu = BH\zeta_t \quad (11)$$

The purpose of the variable *B* is to ensure a smooth transition between breaking and nonbreaking states. The formulation developed and employed by Kennedy *et al.* is:

$$B = \begin{cases} \delta, & \zeta_t \geq 2\zeta_t^b \\ \delta(\zeta_t/\zeta_t^b - 1), & \zeta_t^b < \zeta_t \leq 2\zeta_t^b \\ 0, & \zeta_t \leq \zeta_t^b \end{cases} \quad (12)$$

where δ is some amplification factor and the parameter ζ_t^b determines the onset and stoppage of breaking. ζ_t^b is evaluated as:

$$\zeta_t^b = \begin{cases} \zeta_t^{(F)}, & t - t_0 \geq T^b \\ \zeta_t^{(I)} + \frac{t-t_0}{T^b}\left(\zeta_t^{(F)} - \zeta_t^{(I)}\right) & 0 \leq t - t_0 < T^b \end{cases} \quad (13)$$

where $\zeta_t^{(I)}$ is the initial free surface transient threshold that must be exceeded for a breaking event to initiate, $\zeta_t^{(F)}$ is the minimum transient required for a breaking event to continue, t is the local time, t_0 is the time breaking started, and T^b is a transition time. The beginning and the end of the surf wave are determined using the parameters $\zeta_t^{(I)}$ and $\zeta_t^{(F)}$ and the transition time T^b.

Through trial and error minimization of the difference between numerical and experimental results, the following set of free parameters is chosen (Lynett and Liu, 2014):

$$\delta = 6.5 \tag{14}$$

$$\zeta_t^{(I)} = 0.65\sqrt{gH}(m/s) \tag{15}$$

$$\zeta_t^{(F)} = 0.08\sqrt{gH}(m/s) \tag{16}$$

$$T^b = 8\sqrt{\frac{H}{g}}(s) \tag{17}$$

2.3.1.4 Spectrum in Matlab

The included Matlab scripts “spectrum 1D.m” and “spectrum 2D.m” can be used to create an input spectrum to be used in the numerical simulation. The “spectrum 1D.m” file will create a spectrum in one-horizontal dimension. This file creates a shallow-water based TMA spectrum. The first few lines of “spectrum 1D.m” must be edited to input the peak frequency, significant wave height, and the depth of these waves. The output from this script file will be a data file called “spectrum.dat”, which must be located in the same direction as the executable in order to be loaded by the simulation. The file “spectrum 2D.m” creates a two-horizontal dimension spectrum. The two-dimensionality is setup as (Lynett and Liu, 2014):

$$S(f,\theta) = S(f)h(\theta) \tag{18}$$

where the $h(\theta)$ directional function used in the Matlab file is a simple $\cos^2$ spreading function.

2.3.1.5 Files

The files included in the package are listed in Table 2.6.

Table 2.6: Files involved in COULWAVE (Lynett and Liu, 2014).

File name	Description
coulwave.f	the source code of the numerical program
plot_out.m	a Matlab script file that will load and plot the output of a numerical simulation
bath_ss.m	a Matlab script file that loads and saves bathymetry data from the Smith and Sandwell database. The saved data can then be used with a numerical simulation.
bath_loc.m	a Matlab script file that loads bathymetry data from specified local files, or creates a bathymetry based on user input, and saves that data in a form that the numerical program can read.
mygrid.m	a Matlab function file used by "bath_ss.m."
lat2m.m	a Matlab script file used by "bath_ss.m."
spectrum_1d.m	a Matlab script to create a 1DH input spectrum for COULWAVE
spectrum_2d.m	a Matlab script to create a 2DH input spectrum for COULWAVE

Figure 2.34 depicts a COULWAVE framework.

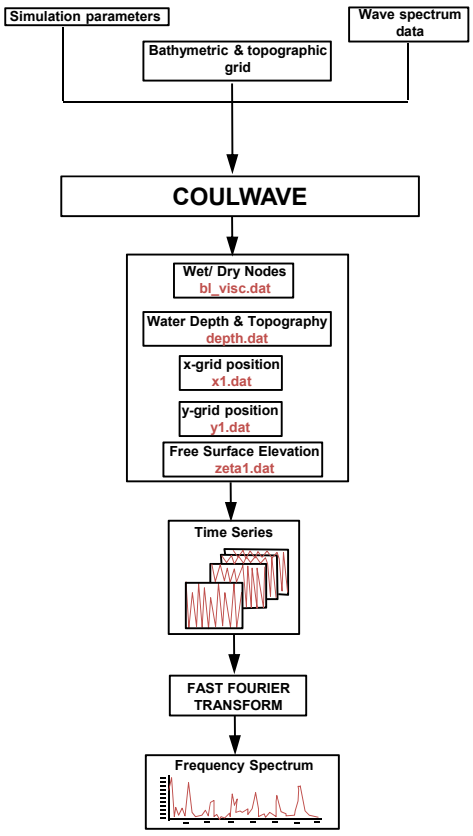

Figure 2.34: COULWAVE data framework (adapted from Douyère, 2003).

2.3.1.6 Limitations

The wave breaking is included by the inclusion of a term in turbulent viscosity in the momentum conservation equation, which is dependent on a number of parameters related to the beginning, end and duration of wave breaking that must be calibrated for each case study.

Because it is admitted a given velocity profile at a given point or layer, it is not possible to adequately describe the flow in areas where the depth effect is important (areas of abrupt variation of the depth, surf zones, run-up zones, for example).

Also this model is limited when requiring meshes with small cell sizes and with real complex bathymetries.

2.3.2 SWAN

SWAN (Simulation WAves Nearshore) is a third-generation wave model (formulations of the processes of wave generation, dissipation and wave-wave interactions in phase-average models) for obtaining realistic estimates of wave parameters in coastal areas, lakes and estuaries from given wind, bottom and current conditions. However, SWAN can be used on any scale relevant for wind-generated surface gravity waves. The model is based on the wave action balance equation with sources and sinks (SWAN, 2014).

SWAN is a high-resolution spectral numerical model that simulates and describes for the generation, propagation and dissipation of waves in coastal areas, based on the equation for the conservation of wave action for deep waters and the transition zone. This is a model of the public domain (freeware), in constant development by the Delft University of Technology in the Netherlands, which has one of the greatest advantages to maintaining the structure of the data files and results allowing for easy versioning more robust and complete model. From the knowledge of the boundary conditions, bathymetry, wind fields and currents, the model calculates the evolution of the directional spectrum, considering all relevant to an adequate description of waves in coastal waters as refractive procedures due to the depth variation, dissipation by bottom friction, the resonant nonlinear interactions and wave breaking (Booij *et al.*, 1999).

This model spreads the wave propagation from offshore to near shore considering the physical processes of refraction, diffraction and shoaling due to background variations and the presence of currents, wave growth by action of wind, wave breaking under the influence of background and

excess slope, power dissipation due to friction from the bottom, blocking and reflection by opposing currents and transmission through obstacles.

The wave field in the area is characterized by two-dimensional spectrum of the density of sea wave action. With this representation, it is possible to apply the model in areas where growth of waves by wind is remarkable or where sea states, or even waving, are present. The spread of wave propagation in stationary or non-stationary modes, in the geographical and spectral spaces is performed using implicit numerical schemes. The area under study can be described in spherical coordinates or Cartesian coordinates using a "rectangular" mesh.

An important question addressed is how to choose various grids in SWAN (resolution, orientation, etc.) including nesting. In general, it is considered two types of grids: structured and unstructured. Structured grids may be rectilinear and uniform or curvilinear. They always consist of quadrilaterals in which the number of grid cells that meet each other in an internal grid point is 4. In unstructured grids, this number can be arbitrarily (usually between 4 and 10). For this reason, the level of flexibility with respect to the grid point distribution of unstructured grids is far more optimal compared to structured grids. Unstructured grids may contain triangles or a combination of triangles and quadrilaterals (so-called hybrid grids).

Often, the characteristic spatial scales of the wind waves propagating from deep to shallow waters are very diverse and would require allowing local refinement of the mesh near the coast without incurring overhead associated with grid adaptation at some distance offshore. Traditionally, this can be achieved by employing a nesting approach.

The use of unstructured grids in SWAN offers a good alternative to nested models (a model in which the various factors are contained within one another in a specific hierarchical order) not only because of the ease of optimal adaption of mesh resolution but also the modest effort needed to generate grids about complicated geometries, e.g. islands and irregular shorelines. This type of flexible meshes is particularly useful in coastal regions where the water depth varies greatly. As a result, this variable spatial meshing gives the highest resolution where it is most needed. The use of unstructured grids facilitates to resolve the model area with a relative high accuracy but with a much fewer grid points than with regular grids (SWAN, 2014).

The data required for the implementation of SWAN are bathymetric mesh modelling area and wave conditions on the border of the input field, plus a host of other calculation parameters. Among the several results obtained by SWAN, these are the ones that stand out: significant wave height, peak

and average time periods, peak and average directions, directional dispersion, parameter of bandwidth and level of water anywhere in the computational domain (Capitão and Fortes, 2011).

Most applications of this model to the Portuguese coast has been carried out in operational forecasting systems of waves, Rusu and Guedes Soares (2008a, 2008b) and Silva *et al.* (2009), for example. There are several studies of performance analysis SWAN model when applied to the Portuguese coast, such as those resulting from its application to the maritime area of Pinheiro da Cruz, [Pires – Silva *et al.* (2002); Teles *et al.* (2009)], or the Alfeite beach [Santos *et al.* (2007); Capitão *et al.* (2009) and Rusu *et al.* (2009, 2011)], in which field measurements were made, or to situations in which they had data buoy such as the maritime area of the port of Sines and Faro Leixões [Capitão *et al.* (2006); Rusu *et al.* (2005a, 2005b, 2008b) and Silva *et al.* (2009)], or parts of the Madeira archipelago [Rusu *et al.* (2008a)], and the Azores archipelago, in the maritime area of the Port of Victoria Beach [Guilherme *et al*. (2009); Santos *et al.* (2009)]. In all these studies, the establishment of the conditions of application of the model as well as the calibration of its parameters is strongly conditioned by place of study, and hence the accuracy of the model depends on these conditions and other parameters.

2.3.2.1 Limitations

Most relevant limitations of SWAN can be listed as:

- The calibration of many of the parameters involved in the description of different physical phenomena in SWAN was based on data from the JONSWAP campaign undertaken in the North Sea (Hasselmann *et al.*, 1973). Such parameters may not be correct for areas with different climate characteristics of waves or with different characteristics of the seabed;
- The diffraction in SWAN is modelled simply as a directional dispersion, which may constitute the main limitation;
- The inclusion of the numerical calculations diffraction implies that the computational mesh spacing relative to the wavelength is such that ensures the convergence of the computations. This sometimes implies that the meshes are of such size that can derail the implementation of the calculations;
- It must be pointed out that the application of SWAN on ocean scales is not recommended from an efficiency point of view. The WAVEWATCH III model, which has been designed specifically for ocean applications, is probably one order of magnitude more efficient than

SWAN. SWAN can be run on large scales (much larger than coastal scales) but this option is mainly intended for the transition from ocean scales to coastal scales;

- SWAN does not calculate wave-induced currents. If relevant, such currents should be provided as input to SWAN, e.g. from a circulation model which can be driven by waves from SWAN in an iteration procedure;
- SWAN is not applicable to shallow waters (it is valid to deep waters and transition zones).

2.3.3 BOUSS-2D

BOUSS-2D is a comprehensive numerical model for simulating the propagation and transformation of waves in coastal regions and harbours based on a time-domain solution of Boussinesq-type equations. This model is included in the SMS-Surface-water Modelling System (XMS Wiki, 2014) that incorporates different modules (1D Grid, 1D River, Cartesian Grid, Curvilinear Grid, GIS, Map, Mesh, Particle, Raster and Scatter), general models (FVCOM, Generic Mesh, PTM and TUFLOW-FV), coastal models (ADCIRC, BOUSS-2D, CGWAVE, CMS-Flow, CMS-Wave, GENCade, STWAVE and WAM) and riverine/estuarine models (ADH, FESWMS, HYDRO AS-2D, RIVERFLO-2D, RMA2, RMA4, SRH-2D, Steering and TUFLOW).

The governing equations are uniformly valid from deep to shallow water and can simulate most of the phenomena of interest in the nearshore zone and harbour basins including shoaling/refraction over variable topography, reflection/diffraction near structures, energy dissipation due to wave breaking and bottom friction, cross-spectral energy transfer due to nonlinear wave-wave interactions, breaking-induced longshore and rip currents, wave-current interaction and wave interaction with porous structures. Many processes at inlets and harbours can be studied using BOUSS-2D.

BOUSS-2D can be applied to a wide variety of coastal and ocean engineering problems, including complex wave transformation over small coastal regions (1-5 km), wave agitation, wave breaking over submerged obstacles, breaking-induced nearshore circulation patterns, wave-current interaction near tidal inlets, infra-gravity wave generation by groups of short waves, and wave transformation around artificial islands (USACE, 2014c)

Phase resolving models based on either the mild-slope equation or Boussinesq-type equations are better suited for problems involving the reflection/diffraction of waves such as in coastal entrances and harbours. The mild-slope and Boussinesq equations are vertically integrated equations for wave

propagation in the two-dimensional horizontal plane with different assumptions made for the variation of fluid motion over the water depth. The mild-slope equation derivation assumes a hyperbolic cosine variation of the velocity potential over depth, consistent with linear monochromatic waves in water of arbitrary depth, while the Boussinesq equation derivation assumes a quadratic profile, valid for shallow-water waves with wavelengths much longer than the water depth. The classical form of the Boussinesq equations for wave propagation over water of variable depth was derived by Peregrine (1967). The equations were restricted to relatively shallow water depths, i.e., the water depth, h, had to be less than one-fifth of the wavelength, L, in order to keep errors in the phase velocity to less than 5 percent. Nwogu (1993) extended the range of applicability of Boussinesq-type equations to deeper water by recasting the equations in terms of the velocity at an arbitrary distance z_α from the still-water level, instead of the depth-averaged velocity. The elevation of the velocity variable z_α becomes a free parameter, which is chosen to optimize the linear dispersion characteristics of the equations. The optimized form of the equations has errors of less than 2 percent in the phase velocity from shallow-water depths up to the deep water limit (h/L = 0.5). Despite the improvement in the frequency dispersion characteristics, Nwogu's (1993) equations are based on the assumption that the wave heights were much smaller than the water depth. This limits the ability of the equations to describe highly nonlinear waves in shallow water and led Wei *et al*. (1995) to derive a fully nonlinear form of the equations. The fully nonlinear equations are particularly useful for simulating highly asymmetric waves in shallow water, wave-induced currents, wave setup close to the shoreline, and wave-current interaction (BOUSS-2D, 2001).

As ocean waves approach the shoreline, they steepen and ultimately break. The turbulence and currents generated by breaking waves are important driving mechanisms for the transport of sediments and pollutants. Nwogu (1996) extended the fully nonlinear form of the Boussinesq equations to the surf zone, by coupling the mass and momentum equations with a one-equation model for the temporal and spatial evolution of the turbulent kinetic energy produced by wave breaking. The equations have also been modified to include the effects of bottom friction and flow through porous structures. The modified equations can simulate most of the hydrodynamic phenomena of interest in coastal regions and harbour basins including:

a. Shoaling;

b. Refraction;

c. Diffraction;

d. Full/partial reflection and transmission;

e. Bottom friction;

f. Nonlinear wave-wave interactions;

g. Wave breaking and run-up;

h. Wave-induced currents;

i. Wave-current interaction.

The governing equations in BOUSS-2D are solved in time domain with a finite-difference method where the water-surface elevation and horizontal velocities are calculated at the grid nodes in a staggered manner. The area of interest is discretized as a rectangular grid, and time-histories of the velocities and fluxes corresponding to incident storm conditions are specified along wave generation boundaries.

Input wave may be periodic (regular) or nonperiodic (irregular), and either unidirectional or multidirectional sea states may be simulated. Waves propagating out of the computational domain are either absorbed in damping layers placed around the perimeter of the domain or allowed to leave the domain freely. Damping and porosity layers are used to simulate the reflection and transmission characteristics of jetties, breakwaters, and other structures existing in the modelling domain.

The BOUSS-2D interface allows users to interactively construct, evaluate, edit, and visualize finite-difference grids for the model. Users can define bathymetric conditions, model control parameters, and current, tidal and wave conditions to be simulated. The interface provides tools for visualizing model results in the form of graphical images, animations, and tabular output that may readily be ported into engineering study reports.

2.3.3.1 Governing Equations

BOUSS-2D is based on Boussinesq-type equations derived by Nwogu (1993, 1996). The equations are depth-integrated equations for the conservation of mass and momentum for nonlinear waves propagating in shallow and intermediate water depths. They can be considered to be a perturbation from the shallow-water equations, which are often used to simulate tidal flows in coastal regions. For short-period waves, the horizontal velocities are no longer uniform over depth and the pressure is non-hydrostatic. The vertical profile of the flow field is obtained by expanding the velocity

potential, O, as a Taylor series about an arbitrary elevation, z_α, in the water column. For waves with length, L, much longer than the water depth, h, the series is truncated at second order resulting in a quadratic variation of the velocity potential over depth:

$$\Phi(x,z,t) = \phi_\alpha + \mu^2(z_\alpha - z)[\nabla\phi_\alpha \cdot \nabla h] + \frac{\mu^2}{2}[(z_\alpha + h)^2 - (z+h)^2]\nabla^2\phi_\alpha + O(\mu^4) \quad (19)$$

where: $\phi_\alpha = \Phi(x, z_\alpha, t), \nabla = (\partial/\partial_x, \partial/\partial_y)$, and $\mu = h/L$ is a measure of frequency dispersion. The horizontal and vertical velocities are obtained from the velocity potential as:

$$u(x,z,t) = \nabla\phi = u_\alpha + (z_\alpha - z)[\nabla(u_\alpha \cdot \nabla h) + (\nabla \cdot u_\alpha)\nabla h] + \frac{1}{2}[(z_\alpha + h)^2 - (z+h)^2]\nabla(\nabla \cdot u_\alpha) \quad (20)$$

$$w(x,z,t) = \frac{\partial\Phi}{\partial z} = -[u_\alpha \cdot \nabla h + (z+h)\nabla \cdot u_\alpha] \quad (21)$$

where: $u_\alpha = \nabla\Phi|_{z_\alpha}$ is the horizontal velocity at $z = z_\alpha$. Given a vertical profile for the flow field, the continuity and Euler (momentum) equations can be integrated over depth, reducing the three-dimensional problem to two dimensions. For weakly nonlinear waves with height, H, much smaller than the water depth, h, the vertically integrated equations are written in terms of the water-surface elevation η(x, t) and velocity u_α(x, t) as (Nwogu, 1993):

$$\eta_t + \nabla \cdot u_f = 0 \quad (22)$$

$$u_{\alpha,t} + g\nabla\eta + (u_\alpha \cdot \nabla)u_\alpha + z_\alpha\left[\nabla\left(u_{\alpha,t} \cdot \nabla h\right) + \left(\nabla \cdot u_{\alpha,t}\right)\nabla h\right] + \frac{1}{2}[(z_\alpha + h)^2 - h^2]\nabla\left(\nabla \cdot u_{\alpha,t}\right) = 0 \quad (23)$$

where: g is the gravitation acceleration and u_f is the volume flux density given by:

$$u_f = \int_{-h}^{\eta} u\,dz = (h+\eta)u_\alpha + h\left(z_\alpha + \frac{h}{2}\right)[\nabla(u_\alpha \cdot \nabla h) + (\nabla \cdot u_\alpha)\nabla h] + h\left[\frac{(z_\alpha+h)^2}{2} - \frac{h^2}{6}\right]\nabla(\nabla \cdot u_\alpha) \quad (24)$$

The depth-integrated equations are able to describe the propagation and transformation of irregular multidirectional waves over water of variable depth. The elevation of the velocity variable z_α is a free parameter and is chosen to minimize the differences between the linear dispersion characteristics of the model and the exact dispersion relation for small amplitude waves. The optimal value, z_α = -0.535h, is close to mid depth.

For steep near-breaking waves in shallow water, the wave height becomes of the order of the water depth and the weakly nonlinear assumption made in deriving Equations (22) and (23) is no longer valid. Wei *et al.* (1995) derived a fully nonlinear form of the equations from the dynamic free

surface boundary condition by retaining all nonlinear terms, up to the order of truncation of the dispersive terms. Nwogu (1996) derived a more compact form of the equations by expressing some of the nonlinear terms as a function of the velocity at the free surface, u_η, instead of u_α. Additional changes have also been made to the equations to allow for weakly rotational flows in the horizontal plane and ensure that z_α remains in the water column for steep waves near the shoreline and during the wave run-up process. The revised form of the fully nonlinear equations can be written as:

$$\eta_t + \nabla \cdot u_f = 0 \tag{25}$$

$$u_{\alpha,t} + g\nabla\eta + (u_\eta \cdot \nabla)u_\eta + w_\eta \nabla w_\eta + (z_\alpha - \eta)\left[\nabla(u_{\alpha,t} \cdot \nabla h) + (\nabla \cdot u_{\alpha,t})\nabla h\right] + \frac{1}{2}[(z_\alpha + h)^2 - -(h+\eta)^2]\nabla(\nabla \cdot u_{\alpha,t}) - \left[(u_{\alpha,t} \cdot \nabla \mathrm{h}) + (h+\eta)\nabla \cdot u_{\alpha,t}\right]\nabla\eta + [\nabla(u_{\alpha,t} \cdot \nabla h + (\nabla \cdot u_{\alpha,t})\nabla h + +(z_\alpha + h)\nabla(\nabla \cdot u_\alpha)]z_{\alpha,t} = 0 \tag{26}$$

where: z_α is now a function of time and is given by $z_\alpha + h = 0{,}465(h+\eta)$. The volume flux density u_f is given by:

$$u_f = (h+\eta)\left\{\begin{array}{c} u_\alpha + \left[(z_\alpha + h) - \frac{(h+\eta)}{2}\right][\nabla(u_\alpha \cdot \nabla \mathrm{h}) + (\nabla \cdot u_\alpha)\nabla \mathrm{h}] \\ + \\ \left[\frac{(z_\alpha+h)^2}{2} - \frac{(h+\eta)^2}{6}\right]\nabla(\nabla \cdot u_\alpha) \end{array}\right\} \tag{27}$$

The fully nonlinear equations are able to implicitly model the effects of wave-current interaction. Currents can either be introduced through the boundaries or by explicitly specifying a current field, U.

2.3.3.2 Simulation of wave breaking

The turbulent and highly rotational flow field under breaking waves is extremely complex and difficult to model even with the Reynolds-averaged form of the Navier-Stokes equations (e.g., Lin and Liu, 1998; Bradford, 2000). BOUSS-2D simulates the effect of breaking-induced turbulence on the flow field rather than attempting to model details of the turbulent motion. It has been developed a generic model that can be applied to regular or irregular waves, unidirectional or multidirectional waves, and simple or complex bottom topography without having to recalibrate the model each time. The key assumptions made in developing the model are (see Nwogu 1996):

a. The breaking process is assumed to be "spilling";
b. Turbulence is produced in the near-surface region when the horizontal velocity at the free surface, u_η, exceeds the phase velocity, C;

c. The rate of production of turbulent kinetic energy is proportional to the vertical gradient of the horizontal velocity at the free surface, $\partial u/\partial z|_{z=\eta}$;
d. Breaking-induced turbulence is primarily converted in the near-surface region with the horizontal velocity at the free surface.

Considering a wave train consisting of two small amplitude periodic waves with amplitudes, a_1 and a_2, frequencies, ω_1 and ω_2, wave numbers, k_1 and k_2, and propagating in directions θ_1 and θ_2, respectively, the water-surface elevation can be written as:

$$\eta^{(1)}(x,t) = a_1 \cos(k_1 \cdot x - \omega_1 t) + a_2 \cos(k_2 \cdot x - \omega_2 t) \quad (28)$$

where: k=(kcosθ, ksinθ).

The effect of wave energy dissipation due to breaking is simulated in the Boussinesq model by introducing an eddy viscosity term to the right-hand side of the momentum equation (Equation (23) or (26)). Nwogu (1996) used a dissipative term of the following form:

$$F_{breaking} = -v_t \nabla(\nabla \cdot u_a) \quad (29)$$

where: v_t is the turbulent eddy viscosity. As pointed out by Kennedy *et al.* (2000), it is important for the dissipative term to dissipate energy but conserve momentum to accurately capture details of the mean flow field associated with breaking waves. A modified form of the dissipative term that ensures that momentum is conserved can be written as:

$$F_{breaking} = -\frac{1}{h+\eta} \nabla\{v_t(h+\eta)\nabla \cdot u_a\} \quad (30)$$

The eddy viscosity is determined from the amount of turbulent kinetic energy, k, produced by wave breaking, and a turbulence length scale, l_t, using:

$$v_t = \sqrt{k l_t} \quad (31)$$

A one-equation model is used to describe the production, advection, diffusion, and dissipation of the turbulent kinetic energy produced by wave breaking:

$$k_t = -u_\eta \cdot \nabla k + \sigma \nabla \cdot \nabla(v_t k) + B \frac{l_t^2}{\sqrt{C_D}} \left[\left(\frac{\partial u}{\partial z}\right)^2 + \left(\frac{\partial v}{\partial z}\right)^2 \right]_{z=\eta}^{3/2} - C_D \frac{k^{3/2}}{l_t} \quad (32)$$

The waves are assumed to start breaking when the horizontal component of the orbital velocity at the free surface, u_η, exceeds the phase velocity of the waves, *C*. The parameter *B* is introduced to ensure that production of turbulence occurs after the waves break, i.e.,

$$B = \begin{cases} 0 & |u_\eta| < c \\ 1 & |u_\eta| \geq c \end{cases} \quad (33)$$

The empirical constants C_D and σ have been chosen as 0.02 and 0.2 respectively. The turbulent length scale, l_t, remains the only free parameter in the turbulence model and is determined from comparisons of numerical model results with experimental data. Recommended values are the significant wave height ($l_t = H_{m0}$) for irregular waves, and the wave height ($l_t = H$) for regular waves.

2.3.3.3 Bottom friction

The bottom boundary layer in wave fields is typically confined to a tiny region above the seabed, unlike river and tidal flows where it extends all the way up to the free surface. There is, thus, very little wave energy attenuation due to bottom friction over typical wave propagation distances of O (1km) used in Boussinesq-type models. The bottom friction factor, however, plays a more important role in wave transformation close to the shoreline and nearshore circulation patterns. The effect of energy dissipation due to a turbulent boundary layer at the seabed has been modelled by adding a bottom shear stress term to the righthand side of the momentum equation (Equation (23) or (26)):

$$F_{bfriction} = -\frac{1}{h+\eta} f_w u_\alpha |u_\alpha| \quad (34)$$

where: f_w is the wave friction factor. The bottom friction term can also be written in terms of the Chezy coefficient, C_f, used in tidal flows by replacing f_w, with g/C_f^2

Equation 34 has been expressed in terms of u_α instead of the velocity at the seabed, u_b, to minimize the additional computational expense of evaluating u_b. The values of the friction factors specified in the model would thus be slightly different than those based on the bottom velocity.

2.3.3.4 Files

Two files are required for a BOUSS-2D simulation (Figure 2.35 and Table 2.7). These are the model parameters (*.par) and the bathymetry grid (*_bathy.grd). Other input files are optional (Demirbilek *et al.*, 2005). The name of a parameter file can be passed to the BOUSS-2D model as a command line argument or the program will prompt the user for this file.

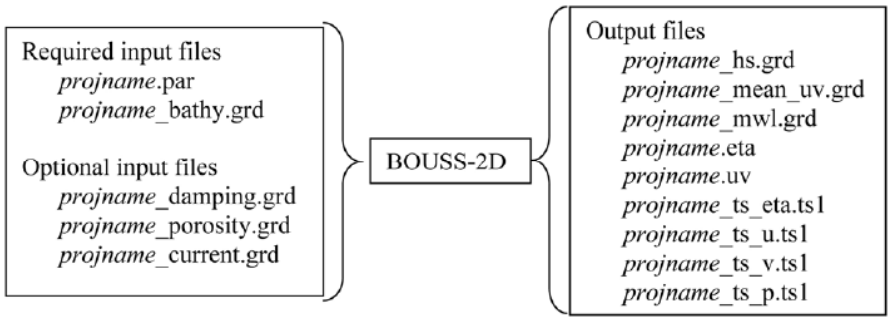

Figure 2.35: Files involved in a BOUSS-2D simulation.

Table 2.7: Files involved in BOUSS-2D Simulation (Adapted from Demirbilek *et al.*, 2005).

File name	Type	Description
projname.par	Input – required	Parameters, filenames, & boundary conditions
projname_bathy.par	Input – required	Elevation value at each node
projname_damping.grd	Input – optional	Damping value at each node
projname_porosity.grd	Input – optional	Porosity value at each node
projname_current.grd	Input – optional	Current vector at each node
projname_hs.grd	Output – ASCII grid	Significant wave height at each node
projname_mean_uv.grd	Output – ASCII grid	Mean current vector at each node
projname_mwl.grd	Output – ASCII grid	Mean water level at each node
projname.eta	Output – Binary grid	Transient water surface at each node
projname.uv	Output – Binary grid	Transient current vector at each node
projname_ts_eta.ts1	Output – ASCII time series	Transient water level at probes
projname_ts_u.ts1	Output – ASCII time series	Transient *u* component of current at probes
projname_ts_v.ts1	Output – ASCII time series	Transient *v* component of current at probes
projname_ts_p.ts1	Output – ASCII time series	Transient pressure at probes
projname.h5	Output –XMDF (hdf5)	Portable binary output file – all spatial output

2.3.4 SMC

The software *Sistema Modelado Costero* (SMC) is part of a project called *Modelo de Ayuda a la gestión del Litoral*, developed by the group of coastal and ocean engineering at the Universidade de Cantábria, for the Directorate of Coasts of the Spanish Environment Ministry (SMC, 2014). It constitutes a graphical user interface integrated in a set of numerical models developed by the project. This software provides a numerical tool within the coastal engineering that allows you performing various types of studies and projects, including:

- Create a working draft of a study area, from photos, nautical charts and bathymetric data;
- Access to *Baco*, a program that includes a database of nautical charts of the Spanish coast as well as its bathymetry, and from there can generate a draft study that can be completed and combined with other bathymetric data, allowing then to model different situations for the stretch of coast under study;
- Generate projects based on photos, charts, allowing then to predict the plant shape of the coast in long term conditions, comparing past, present and future situations;
- Create projects using bathymetric data in different times, in order to assess past and present situations, as well as predict future situations, due to several possible scenarios;
- Get the bathymetry of a coast line from a nautical chart or a referenced map;
- Access to a program with a wave conditions database of the Spanish coast, allowing then to generate the data required to perform the numerical models of the system;
- Accessing information on flooding heights in any region of the Spanish coast;
- Perform different numerical models to analyse the short, medium and long-term study area.

2.3.4.1 SMC global structure

The SMC is constituted by a series of numerical models organized according to the spatial and temporal scales of the processes being modelled. The model is divided into five main modules:

- Pre-processing;
- Short term *(Acordes)*;
- Medium and long term *(Arpa)*;
- Terrain model *(MMT)*;
- Tutor *(Tic)*.

The pre-process module allows the characterization and the processing of the input information for the different numerical models. The short term evolution beach analysis module *(Acordes)* uses numerical tools that allow analysing the morphodynamics of a coastal system in a temporal/spatial short-term scale. Likewise, the medium-long term *(Arpa)* analysis module contains morphodynamic tools that allow modelling the system in an appropriate temporal and spatial scale. The terrain model *(MMT)* allows modifying the contours of bathymetry, as well as groins, which is essential to study the different scenarios of the project under study. Finally there is the coastal engineering tutor module *(Tic)* which gives the theoretical and conceptual support for the different numerical models

of the system. These modules can be used from the central module, the project module. Figure 2.36 shows a schematic representation of SMC.

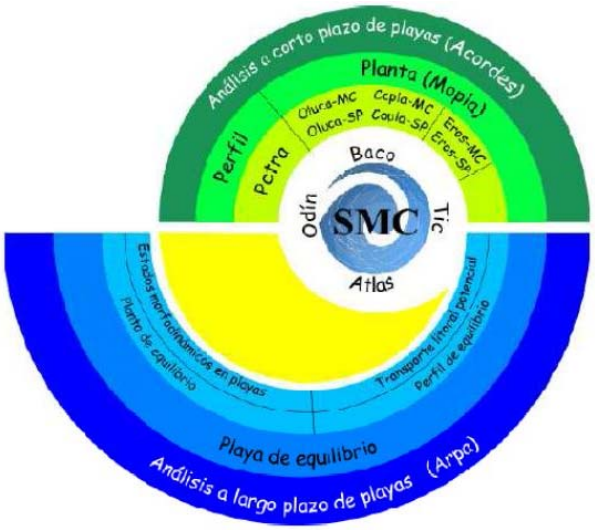

Figure 2.36: Schematic representation of SMC (SMC, 2014).

2.3.4.2 Limitations:

Most relevant limitations of SMC can be listed as:

- The pre-processing module that encompasses *Baco*, *Odín* and *Atlas* programs only have in the database, information relating to the Spanish coast;
- Avoid sudden changes in depth of the bathymetry (greater than 1:3);
- It is the first alignment that defines the initial wave conditions, where it is assumed that these are the same for all points (amplitude, period, and direction), so it is preferable that in this alignment there are no strong variations in the depths;
- Avoid side contours that alternate sea-land-sea because they could generate numerical errors when simulating the wave propagation (Figure 2.37);
- The model only propagates waves in depths higher than 0.30 m;
- The program limits land bathymetries to -7.0 meters, considering that the program assumes positive values for bathymetries in the direction of increasing sea depths;
- There are limitations to the size of the components of the calculation domain meshes.

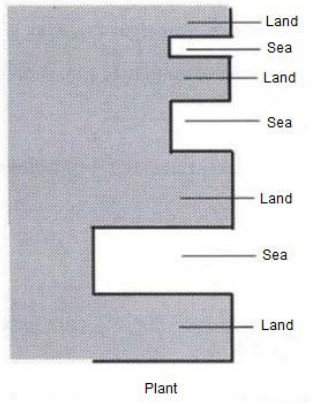

Figure 2.37: Contours to avoid (adapted from SMC, 2014).

2.3.5 MIKE 21

MIKE 21 is a modelling tool developed by the Danish Hydraulic Institute (DHI, 2013) which uses numerical algorithms to approximate flow properties under user-specified conditions. The level of accuracy of the results provided by MIKE 21 is strongly dependent upon the level of accuracy of the user-specified information. Such information includes the bathymetric and topographic data used to create the computational grid, the refinement of the grid itself, channel and floodplain roughness values used within the model, and the correct flow boundary conditions located at the correct locations throughout the model (NHC, 2012).

MIKE 21 is a depth-averaged two-dimensional (2D) numerical modelling tool designed to simulate water levels and flows in rivers, estuaries, bays and coastal areas. It can simulate both steady-state (constant) flow conditions or unsteady (time varying) flow conditions in the two horizontal dimensions.

Unlike one-dimensional models, two-dimensional models are intended to simulate more complex flow conditions (flow direction, depth and average velocity), which may vary laterally across the width of flow or include flows with variable directions. These models require the user to input a network of ground elevation points throughout the entire area to be modelled, not just at widely spaced cross sections. A network of computational cells (triangles or quadrilaterals) containing this information is then used by the model to determine the water surface elevation, average flow velocity, flow depth and flow direction at each computational point in the network of cells. There can be hundreds of thousands of computational points in a detailed 2D model, depending on the level of detail required to address a particular flow scenario.

MIKE 21 provides the last generation of modelling and resources in the simulation of physical processes, chemical or biological in sea or coastal areas. MIKE 21 can be considered as a 3 in 1 package. It comprehends three different simulation engines, single grid, multiple grids or a flexible mesh. The classic single grid is easy to setup rectilinear model which has a simple input/output platform. As well as single grid, the multiple grids consist in a rectilinear model but with dynamic grouping enabling the capacity to focus grid resolution. The flexible mesh performs the maximum flexibility grid resolution within the model which allows the user to specify small, closely spaced computational cells in areas where greater detail is needed to capture complex flow conditions.

With all these powerful engines, MIKE 21 is capable of numerous possible applications such as designing data assessments for coastal and offshore structures, optimization of port layout and coastal protection measures, do an analysis of recirculation, desalination and cooling water, evaluation of environmental impact assessment created by marine infrastructures in many other applications.

There are a vast number of modules designed for various applications. Focusing on the four major modules available (pre and post processing, hydrodynamics, advection-dispersion and sand transport) can be concluded that there is a variable potential in each one of this modules:

- Pre and post processing module provides an integrated environment offering convenient and compatible routines to facilitate the input and data analyses tasks and the presentation of the simulation results;
- The hydrodynamics module simulates the variation of flows and water level in response of forcing functions. With the advection-dispersion component, the dispersion and the decay of suspended or dissolved substances can be simulated;
- The sand transport module has several formulations for current or wave generated transport, including 3D description of sediment transport rates. This morphodynamics module is used in optimization of port layouts, stability of tidal inlets, impact of shore protection, as long with many other uses.

MIKE 21 is a highly respected modelling tool that comes with all of the standard hydrodynamic modelling capabilities needed to assess frequency and duration of flooding needs. However, as with all numerical models MIKE 21 is strongly dependent on user specified information including: inflow boundary conditions, tides, channel and floodplain roughness (including ground surface conditions, vegetation, cropping, cultivation patterns), floodplain topographic details, channel

bathymetry, characteristics of flow obstructions and other required model parameters such as eddy viscosity and bed friction.

2.3.5.1 Limitations

Based on a review of readily available reporting and discussions, the following is a list of limitations associated with the current version of MIKE-21 model (NHC, 2012):

- **Limitations related to topography and bathymetry:** The model results are controlled by the accuracy of the topography and bathymetric data sources; the mesh size and resolution; the accuracy and reliability of the boundary conditions (inflow hydrographs); the spatial, temporal and depth-dependent hydraulic roughness conditions; and the stability of the numerical (computational) scheme and its ability to handle wetting and drying;
- **Limitations related to hydrology and flow boundary conditions:** Reliability of west side tributary flows is questionable; Need to complete additional model sensitivity and calibration analyses;
- **Limitations related to Model Structure and Computational Assumptions:** Need to validate wetting and drying assumptions; Need to refine model to address questions related to impacts of flooding;
- **Model testing, calibration and verification:** Need additional sensitivity analyses;
- **MIKE 21 model availability:** MIKE 21 is a proprietary model.

MIKE 21 is a proprietary model and a model license must be purchased from DHI Water & Environment along with annual user support fees if one elects to receive annual technical support and model updates. Interested users can perform limited reviews (view only) of results files without a model license; however, a model license is required for users to develop input files and to open and work with output files to prepare graphics or perform additional model simulations. Therefore, independent evaluation of MIKE 21 modelling results by stakeholders may be difficult without owning a licensing agreement with DHI. Costs to purchase a license and pay for annual support fees can be significant.

2.3.6 GENESIS

The GENESIS (GENeralized model for Simulating Shoreline change) simulates the changes of the coast line in a given region, being able to determine the advances and retreats of it. This model allows the simulation of the change of the shoreline over a long period of months to years, mainly caused by wave action. The physical scale of the horizontal length of the model is between about one and ten kilometres. The model can be used to simulate changes in the coastline with a wide variety of settings and beach structures on the coast (transverse, longitudinal, emerged or submerged), specified by the user (Hanson, 1987).

The program GENESIS is part of the software package given in CEDAS (4.0) that encompasses several simulation modules related to coastal zone management problems such as wave propagation, river discharges, changes in coastal bathymetry associated with agitation and change of marine coastal setting near defence structures (Gomes, 2011).

GENESIS can be considered as two models into one (two-phase model), since a wave propagates from the surf zone to the coastline, and the other is responsible for calculating the longitudinal sediment transport and changes of the shoreline through evaluations of mass balances (Hanson and Kraus, 1991).

The breaking of the incident waves with a given angle causes a longitudinal transport along the line of study, and the gradients between the volumes entering and leaving a particular section can cause an advance or regress of the corresponding coastline.

Since GENESIS model considers sediment transport along and across the coast, it was designed to predict the trend of the position of the coast line in the long term, starting from an initial position. As a summary of the main features of the model, their capabilities, limitations and simplifications are listed hereafter (Hanson and Kraus, 1991).

2.3.6.1 Capabilities

- Wide and arbitrary combination between constructions that provide protection and marine shelter, as groins, breakwaters, detached breakwaters, walls and longitudinal adherent coatings, and nourishment of the beaches;
- Ability to create composite structures, for example T shaped or Y shaped;
- Diffraction forecast in marine structures;
- Simulations with geographic and temporal scales of considerable size;

- Insertion of arbitrary heights, periods and directions of waves;
- Insertion of multiple sets of waves series of independent origins;
- Transmission of waves through detached breakwaters.

2.3.6.2 Limitations

- The longitudinal transport is solely responsible for the movement of the shoreline, not being provided for situations where the perpendicular transport can be dominant, such as storm situations;
- The bottom profile does not change with time and moves parallel to itself;
- Beyond the depth of closure, h_c, it is assumed that the profile does not change and stops moving;
- While the immersed part of the profile moves perpendicularly to itself, the emerged part accompanies this movement, i.e. the height of the berm d_B accompanies the height h_c (depth of closure) (Figure 2.38);
- The longitudinal transport is caused solely by waves and currents induced by waves and it vary depending on the angle of incidence of the same. The fact that the model only considers currents generated by waves and do not take into account other types of currents such as tidal waves or induced by local winds, makes this is often insufficient for an accurate simulation;
- The model assumes the existence of a strong trend in the evolution of the coastline, where the longshore transport is the main cause of this trend. If there is no such trend in the evolution of the coastline, the model should not be applied.

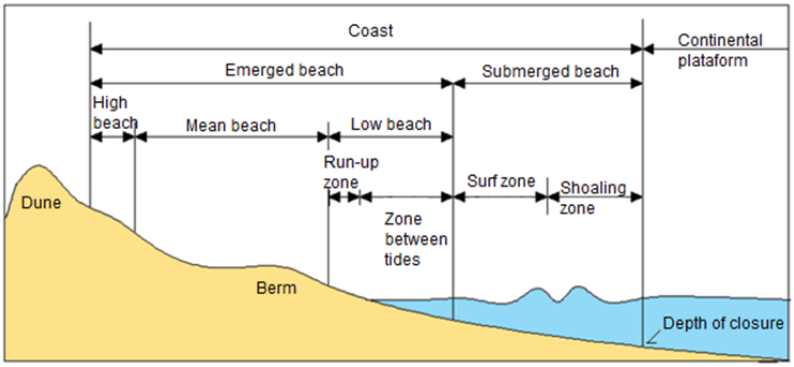

Figure 2.38: Representative scheme of the height of the berm, d_B, and the depth of closure, h_c (Adapted from Simões *et al.*, 2013).

2.3.6.3 Simplifications

- The program is only applicable to the sandy shores;
- The shape of the profile remains constant, the changes are given to moving this profile towards the sea or the opposite;
- The sand moves along the profile, by action of the surf, and the sediment transport along the coast takes place under the influence of surf height and direction of waves;
- The changes in the profiles are dependent on the boundary conditions and cyclic phenomena.

For the construction of models is necessary to introduce the following data (Mendes, 2009):

- Characteristics of maritime agitation along the segment (height, period, direction and depth where the wave records were made);
- Coordinates of the starting position of the shoreline;
- Conditions to be imposed on the lateral boundaries (streams of sand in the edges of the coastal segment);
- Location of structures and their characteristics (permeability and transmission coefficients);
- Characteristic dimension of sediments from coastal segment (D_{50});
- Geometric parameters of the beach and the coastal area (berm height and depth of closure);
- Values of the calibration parameters.

2.3.7 Delft3D

Delft3D (Deltares, 2014b) application is a numerical model used to simulate natural environments such as coastal areas, rivers, reservoirs and estuaries. This model allows two-dimensional horizontally and three dimensional applications. It is a high complexity mathematical model and it is applicable on analysing flows of tides, currents due to wind, river runoff simulations and lakes, the propagation of tsunamis, hydraulic rebounds, in coastal and fluvial morphodynamics and pollutant transportation analysis as well as in the water temperature changing panorama and salinity gradients.

Delft3D, which is Delft Hydraulics' fully-integrated program for the modelling of water flows, waves, water quality, particle tracking, ecology, sediment and chemical transports and morphology.

Delft3D is composed of several modules, where the FLOW module gets greater prominence.

The primary purpose of the computational model Delft3D-FLOW is to solve various one, two and three-dimensional, time-dependent, non-linear differential equations related to hydrostatic and non-hydrostatic free-surface flow problems on a structured orthogonal grid to cover problems with complicated geometry. The equations are formulated in orthogonal curvilinear co-ordinates on a plane or in spherical coordinates on the globe. In Delft3D-FLOW models with a rectangular or spherical grid (Cartesian frame of reference) are considered as a special form of a curvilinear grid (Kernkamp *et al.*, 2005; Willemse *et al.*, 1986).

The equations solved are mathematical descriptions of physical conservation laws for water volume (continuity equation), linear momentum (Reynolds-averaged Navier-Stokes (RANS) equations), and tracer mass (transport equation) and suspended sediments or passive pollutants. Furthermore, bed level changes are computed, which depend on the quantity of bottom sediments.

Delft3D-FLOW can be used in either hydrostatic or non-hydrostatic mode. In case of hydrostatic modelling the so-called shallow water equations are solved, whereas in non-hydrostatic mode the Navier-Stokes equations are taken into account by adding non-hydrostatic terms to the shallow water equations. A fine horizontal grid is needed to resolve non-hydrostatic flow phenomena.

This powerful computation model can be characterized in great distinguished properties. The grid alignment with complicated boundaries and local grid refinements to meet the needs of resolving finer spatial resolution in various numerical modelling tasks results in an accurate description of geometry. It has application for one and two-dimensional vertically averaged as well as hydrostatic or non-hydrostatic three-dimensional problems. Delft3D-FLOW is a solution technique that allows for solution based on accuracy considerations rather than stability (alternating direction implicit finite difference method). It is a computationally efficient and robust software that as a computational core and a separate user interface and its extremely efficient coupled with other physical processes via the other modules of the integrated Delft3D modelling system.

2.3.7.1 Delft3D Applications

This computational model can be used in a wide range of applications.

Delft3D can be used for an accurate prediction of the tidal dynamics (water elevation, currents) in estuaries or coastal seas, can be used for an accurate prediction of the density (salinity and/or temperature) driven flow and sediment concentrations can be taken into account with respect to density values. It also can be used for an accurate prediction of wind driven flow and storm surges and as an accurate prediction of horizontal transport of matter, both on large and small scales.

Other use of this software is the ability to investigate the hydrodynamic impact of engineering works, such as land reclamation, breakwaters, dikes and the impact of hydraulic structures such as gates, weirs and barriers.

Delft3D can be used for an accurate prediction of waste water dispersion from coastal outfalls, prediction of thermal stratification in seas, lakes and reservoirs and to describe and quantify the thermal recirculation between discharge and intake points.

Flows resulting from dam breaks can also be accurate predicted as well as small scale current patterns near harbour entrances.

(Page intentionally left blank)

CHAPTER 3

Case study

'The fishermen know that the sea is dangerous and the storm terrible, but they have never found these dangers sufficient reason for remaining ashore.'

Vincent Van Gogh (1853 – 1890)

(Page intentionally left blank)

CHAPTER 3 CASE STUDY

3.1 Study area: Ofir coastal zone

The Ofir Beach is located in the town of Fão, County of Esposende, Braga District, Portugal. It is a beach located on a coastal stretch delimitated at North by the Cávado river mouth and at South by the Ofir South groin. Also, this beach is nestled in the North Coast Natural Park (Figure 3.1).

Figure 3.1: Study area location.

The selected study area coincides with the stretch located between the North and South groins, where the Ofir towers (three residential buildings planted in the 70s) are located (Figure 3.2). Due to Hercules storm early 2014, the walkway that separates the Ofir towers and Ofir beach relented partially. The beach that had already yielded several weeks before this happened, during this storm, the sand height lowered two and a half meters putting at risk these buildings. Given these events and the vulnerability to erosion of this beach, it was considered relevant to study the potential influence of additional defence structures like detached breakwaters in this coastal segment.

Figure 3.2: North and South groins and Ofir towers location.

3.2 Reference detached breakwater design for Ofir beach

3.2.1 Depth of closure and significant wave height for Ofir beach

3.2.1.1 Extreme wave conditions off Leixões

Ofir beach is located in the North of Portugal. Because the nearest buoy located to Ofir beach is the Leixões buoy it was considered that the data recorded is valid for this beach.

Considering wave data recorded for the period between 1993 and 2007 (14 years) off Leixões, Silva *et al.* (2008) made an analysis of the significant wave heights to obtain the significant wave height that is exceeded 12h/year and the median significant wave height. From these values it is possible to estimate a value for the Hallermeier limit depths, d_l and d_i. In absence of other information, the estimated value of the depth of closure can be considered as a reference value on Portuguese northwest shore.

Silva *et al.* (2008) used the data resulted from compiling a wave data set acquired by the Leixões buoy station that belongs to the IH. When the station acquires normal mode, it performs records of 3 in 3 hours during 20 to 30 minutes. In case of a storm (wave height significantly exceeding 5 m) the acquisition is made in an almost continuously mode for periods of 20 minutes performing records of 30 in 30 minutes.

Figure 3.3 shows a time series of significant wave heights as well as the annual percentage of valid records. In this time series can be seen some gaps, in particular the low number of records in 1993 and 1995, and their absence over a period of time between 2000 and 2001. The results obtained from this time series where there are gaps must be viewed with some caution. However, gaps are common in wave data measured offshore, partly due to environmental conditions that jeopardize the proper functioning of the buoys.

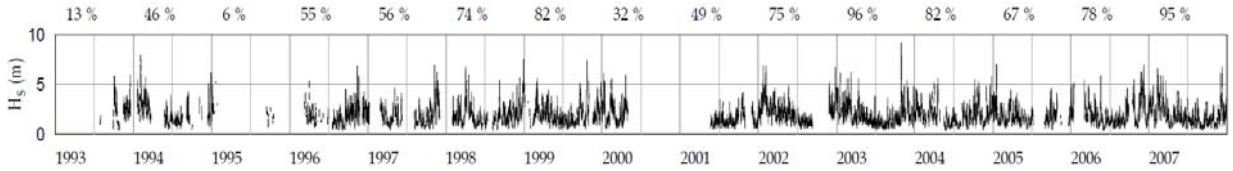

Figure 3.3: Time series of significant wave heights and annual percentage of valid records of 3 in 3 hours (Leixões 1993-2007) (Silva *et al.*, 2008).

Figure 3.4 depicts the relative frequency distribution of the significant wave heights for the set of data collected by the Leixões buoy station between 1993 and 2007 (excluding the years 1993, 1995 and 2001, with less than 40% of valid records in the winter).

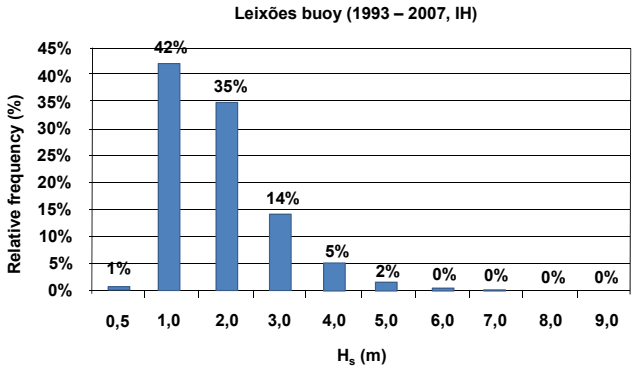

Figure 3.4: Relative frequency distribution of the significant wave height for the set of data collected by the Leixões buoy station between 1993 and 2007 (Silva *et al.*, 2008).

3.2.1.2 Characteristic significant wave heights and depth of closure

The technique of extremes analysis Silva *et al.* (2008) used consisted of setting a theoretical distribution function to the distribution function estimated for a sample of a random suitable variable. For this purpose, it was used a graphic method, where the axis system is graduated in order to ensure that the theoretical distribution function corresponds to a line, whatever their characteristic parameters are. The distribution function points of the sample were entered in the axis

system built. In order to find the line that best fits these points and which corresponds to the theoretical distribution function it was adopted the method of least squares. There are several proposals for the theoretical distribution functions (Carvalho *et al.*, 1990). The function that had been selected for this case was the Gumbel asymptotic distribution of the maximum.

The sample used for the determination of characteristic significant wave heights was the series of daily significant wave heights where the years with low percentage of valid records during winter (1993, 1995 and 2001) had been excluded. To estimate the sample distribution function it was used the graphical position that allowed the best quality adjustment of Gumbel distribution function to the sample of annual maximum significant wave heights.

As a result of this analysis, Silva *et al.* (2008) came to the extrapolated results and statistical parameters (mean significant wave height and period associated with significant average wave height shown in Table 3.1). Applying Hallermeier formulations, (Equations (1) and (2)) limit depths were estimated (Table 3.2).

Table 3.1: Results obtained using the Gumbel distribution.

Extrapolated results		**Statistical parameters**		
$H_{s\,50}$ (50% of probability of exceedance)	**$H_{s\,0,137}$ (0,137% of probability of exceedance)**	**Mean significant wave height**	**Standard deviation**	**Period associated with significant average wave height**
$H_{s\,50}$ = 1,20m	$H_{s\,0,137}$ = 6,64m	$\overline{H}_s$ = 1,89m	σ_s = 1,02m	$\overline{T}_s$ = 9,30s

Table 3.2: Estimated limit depths.

$\overline{T}_s$ **= 9,30s**	**Limit depths**
$H_{s\,50}$ = 1,20m	d_i = 28,5m (d_{50} = 0,3mm)
$H_{s\,0,137}$ = 6,64m	Depth closure (d_l) = 11,6m

3.2.1.3 Group velocity at deep water at the depth of closure

For these parameters a calculator provided by MetEd (2014a) had been used. Introducing the values of the significant wave height and its respective wave period the calculator automatically displays the values for the group velocity among other data (Figure 3.5). The Shallow-Water Wave Calculator can be used as an estimation tool for marine forecast operations. Output values should not be taken as certain, because of the calculator's built-in approximations and the sensitivity of

wave behaviour to nearshore bathymetry. Marine forecast offices are encouraged to validate output of this tool with actual observations (MetEd, 2014a).

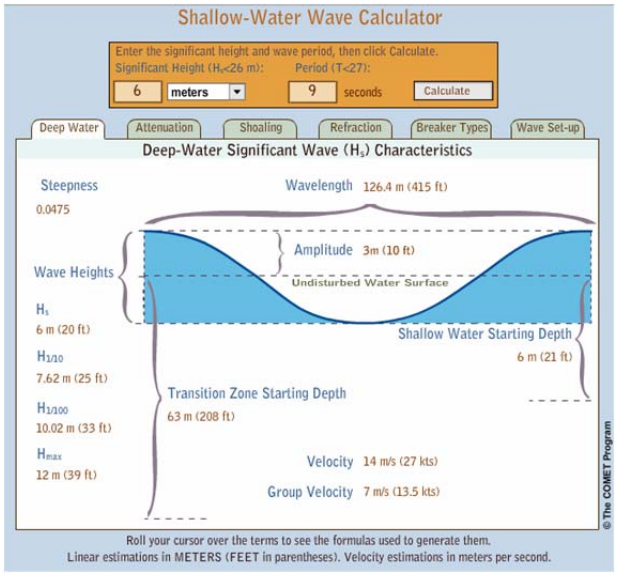

Figure 3.5: Shallow-Water Wave Calculator.

In the conditions of Figure 3.5 it had been assumed that the group velocity in the deep water-transition zone limit is 7 m/s and the group velocity at the depth of closure (d_l = 11,6 m) is 7 m/s as well.

3.2.2 Tidal parameters

For the main Portuguese ports, IH places available the forecast heights of tide (IH, 2014). Among other information, in this document lays the data for spring tidal range and mean high water spring (Volume I, Chapter III – Supplemental information about tides) which are going to be needed for the dimensioning of the detached breakwater proposed.

Once the closest buoy to Ofir beach is the Leixões buoy, it is going to be considered the data available for this port. Thus the spring tidal range is about 3,93m and the mean high water spring is about 3,52m.

Another important parameter that is going to be needed to the dimensioning of detached breakwaters is the 1 year surge which can be defined as the wave height with a return period of one year. This value can be determined by using the chart of Figure 3.6 that relates wave heights with return periods. From this chart it can be assumed that the 1 year surge is about 2m.

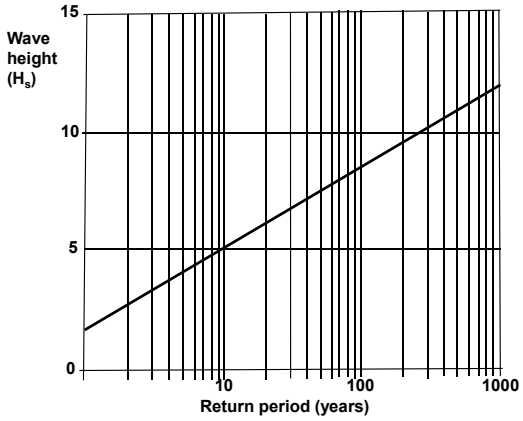

Figure 3.6: Wave heights as a function of return period (adapted from Taveira-Pinto, 1993).

3.2.3 Beach bathymetry

On 16th May 2014 a field survey was performed in order to characterize the topography of Ofir beach using DGPS equipment (Figure 3.7).

Figure 3.7: Trimble Geo XR-6000 equipment.

This fieldwork proved to be relevant to the real approximation of the beach profiles that will be further studied in the models used in COULWAVE. It was possible to present a real morphology of the study site, which will be reflected in more credible and accurate results. The surveys cover a longitudinal extension of approximately 1 km from the North to the South groins of the Ofir beach, and a transverse extension from the coast to the zone of low-water mark including the two groins.

Using ArcGIS the beach morphology and its contour lines (Figure 3.8) were analysed. From this information it was possible to represent beach profiles in order to be able to assess in detail 1DH cross sections.

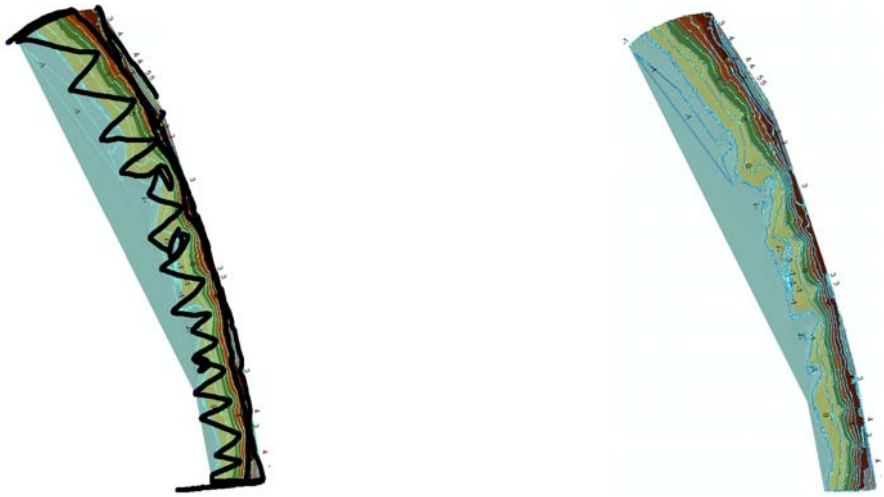

Figure 3.8: Representation of the survey path for collecting data of beach morphology (solid line) (on the left) and ArcGIS representation of the Ofir beach morphology and the contour lines (on the right).

Given this information it is also required to obtain the information about contour lines in submerged areas. Since there were not made any surveys in the sea, it was consulted a theme provided by IH that lays the data that is going to be needed.

The theme contains contour lines built on survey information from the hydrographic surveying in the Portuguese northern coastal zone area (in this case from Viana do Castelo to Leixões). These data can be read by ArcGIS. Once adding the collected field data information of the Ofir beach to the Viana do Castelo - Leixoes shapefile (Figure 3.9), the next step is to adjust both coordinates to the same coordinate system.

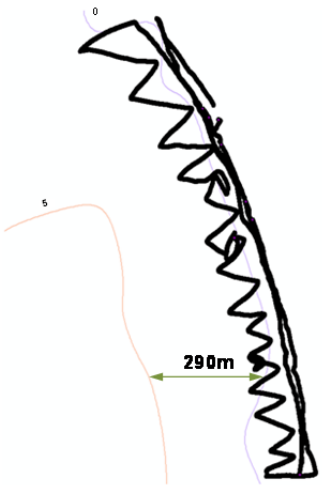

Figure 3.9: ArcGIS representation of the collected data of the Ofir beach and the Viana do Castelo to Leixões contour lines.

After having all information setup it is possible to determine the beach slope that is going to be needed for the subsequent calculation of the detached breakwaters. Assuming the location indicated in Figure 3.9 is the one that will be object of study for the subsequent profiles, it was horizontally measured the distance from this site to the -5 contour line. The distance measured was 290m. Taking into account that the data in the shapefile refers to the chart data and the information taken during the surveys is referenced to the GPS equipment coordinates (mean sea level), it was necessary to add -2m to the coordinate -5m (assuming the tide level reaches approximately this value). Thus the beach slope is (5+2) /290 = 0,024 ≈ 0,025 = 2,5%.

3.2.4 Breakwater geometrical parameters for Ofir beach

The design guidance as explained before was used to be applied to the outline design of nearshore detached breakwaters for Ofir beach erosion control considered as relatively straight sandy shoreline (initial condition) subject to tidal action up to macro-tidal range. It only provides advice on determining the parameters required to develop a preliminary geometrical layout.

Table 3.3 shows the basic data needed for determining the breakwater parameters (L_s, X, G, h_{cr}).

Table 3.3: Basic data for determining the breakwater design parameters.

Parameter	Basic data
H_{m0} exceeded 12hr/year in deep water	6,64m
Associated wave period, T_p	9,30s
Spring tidal range	3,93m
MHWS	3,52m relative to MSL
1 year surge	2,0m
Average beach slope	2,5%
Estimated depth of closure	11,6m relative to MSL
Percentage of incoming longshore transport.	50 per cent of incoming longshore transport is desired to be bypassed to downdrift beaches and a salient response is desired at the breakwater. This implies that the salient in the leeward side of the breakwater would be formed by the 50 per cent of the incoming longshore that is trapped in the leeward side of the breakwater
C_g deep water	7,0m/s
C_g depth of closure	7,0m/s

The calculations summarised in Table 3.4 were defined for a storm condition.

Table 3.4: Geometrical parameters of the breakwater (according to the calculation procedure proposed by DEFRA, 2010).

Calculations	Results
Stage 1: Breakwater location calculations	
1.1 Given H_{m0} exceeded 12hr/year in deep water, determine the corresponding H_{m0} at depth of closure (and water level at MSL).	
At MSL, the given water depth at the closure depth is: Depth = 11,6m Using conservation of energy equation for shore parallel contours and assuming shore normal waves (conservative assumption). $H_{m0}^2 C_g$ = constant $H_{m0;11,6} = H_{m0,deep\ water} \times \sqrt{C_{g,deep\ water}/C_{g;11,6m}}$ $H_{m0;11,6} = 6,64 \times \sqrt{7,0/7,0} = 6,64m$	
Check if H_{m0} is depth limited at closure depth during high water (HW)	
At HW, the water depth at the closure depth is: Depth = 11,6 + 3,52 + 2 = 17,12m Max H_{m0} = 0,5 × Depth = 0,5 × 17,12 = 8,56m Therefore, waves are not depth limited at closure depth.	
1.2 Estimate X_b as equal to the distance to closure depth	
X_b=closure depth /beach slope=11,6 /0,025 = 464m	X_b = 464m
1.3 Determine X based on percentage of longshore transport to be bypassed.	
Assuming that X/X_b = 0,5 gives 50 per cent bypassing: X = 0,5 × 464=232m. Use X = 235m. Therefore, depth at structure = 235 × 0,025 = 5,88m relative to MSL.	X = 235m
Max H_b at structure = 0,5 × depth at HW = 0,5 × (5,88 + 3,52 + 2) = 5,7m Therefore, waves at the structure are depth limited, as this wave height is less than the estimated incoming wave height at closure depth (H_{m0} = 6,64m at closure depth).	H_b = 5,7m
Stage 2: Breakwater length and accretion calculations	
2.1 Determine L_s for non-tidal beaches, given that tombolo response is desired.	
Depending on the relative location of the breakwater in the surf zone, tombolo formation can occur for L_s/X > 0,8. The limiting conditions for tombolo formation are postulated as: $L_s/X > 2,8 - 1,6 \times (X/X_b)$ $X/X_b \leq 1,25$ (36) $L_s/X > -10,2 + 8,8 \times (X/X_b)$ $1,25 < X/X_b \leq 2$ (37)	
Using Equation (36) (because it was assumed that X/X_b = 0,5)): L_s = 470m	L_s = 470m

Table 3.4: Geometrical parameters of the breakwater (according to the calculation procedure proposed by DEFRA, 2010) (continued).

Calculations	Results
2.2 Include effect of tidal range (assuming emergent breakwaters) on salient response using Figure 2.31. The effect of the tidal range on the salient in the leeward side of the breakwater is illustrated in Figure 2.31. Both models show a decrease in the salient length with increasing tidal range (the relative salient lengths (S/X) reduce as the tidal range increases for shore normal waves). However, for large values, L_s/X (>1,3), the influence of tidal range is smaller if the breakwater is emergent through the tidal cycle.	
From the calculation in step 2.1 above, $L_s/X = 2$, which is greater than 1,3. Thus, the effect of tidal range on the beach response is expected to be negligible (emergent breakwaters).	Tidal effect negligible for this case
Stage 3: Crest level calculations	
3.1 Determine crest level of breakwater. The numerical model simulations show that the relative salient length reduces as the breakwater crest level is reduced (Figure 2.32). The effect is more pronounced in cases where the breakwater is relatively close to the shoreline ($L_s/X \geq 1,3$). Using curve for $L_s/X = 1,33$ (Figure 2.32). (Note: $R/H_b = 3,93 / 5,7 = 0,69 < 2,5$; OK)) and taking $S/X = 0,6$ for salient → $d_{cr}/H_{m0} = 0,5$. Therefore, $d_{cr} = 0,5 \times H_{m0} = 0,5 \times H_b = 0,5 \times 5,7 = 2,85$m Breakwater crest level, h_{cr} = MHWS + 1 year surge $-$ $d_{cr} = 3,52 + 2 - 2,85 = 2,67$m $\approx h_{cr} = 2,70$m relative to MSL.	Breakwater crest level, h_{cr}=2,70m MSL.
Stage 4: Gap width and erosion calculations	
4.1 Determine G (gap width) based on erosion in breakwater bays. Using Figure 2.33 to determine G/X and knowing the X value, it can be determined G value. Assuming there is not going to have erosion in this site (G/X = 0,5) and that X = 235m → G = 117,5m ≈ G = 115m (conservative).	G = 115m

The crest width of a rubble mound breakwater, B, without a superstructure is a function of the overflowing and crest level relation and the allowable run-up. For run-up breakwaters the minimum value recommended relates to three characteristic dimensions of the crest blocks, i.e. (Taveira-Pinto, 1993):

$$B \geq 3K_{\Delta}\left(\frac{W}{\gamma_r}\right)^{1/3} \quad (35)$$

where: B is the crest width; K_Δ is the form coefficient; W is the unit weight of the blocks and γ_r is the specific weight of the material of the blocks.

Also in this case it may be relevant the minimum width required for the operation and movement of construction equipment and repair. The minimum value for this should be of 6m (Taveira-Pinto, 1993).

The form coefficient, K_Δ, depends on the material characteristics and breakwater slope. Table 3.5 presents different values for this coefficient assuming different breakwater materials, slopes and shapes. Tetrapods and cubic blocks are artificial blocks made of concrete because they require having a regular structure. Rockfill blocks, however, are natural blocks.

Table 3.5: Form coefficient, K_Δ, according to different breakwater materials, slopes and shapes (Taveira-Pinto, 1993).

Tetrapods - two layers	
Slope	K_Δ
3:2	1,13
2:1	1,14

Cubic blocks - two layers	
Slope	K_Δ
3:2	1,03
2:1	1,02

Rockfill blocks - two layers	
Type	K_Δ
Regular	1,02
Irregular	**1,15**

For this work was assumed the designed breakwater is constituted by two layers of irregular rockfill, so the form coefficient, K_Δ, is 1,15. The material considered was granite and its specific weight is 26 kN/m^3.

Like it was presented in Subchapter 2.2.3, the most used material in the construction of detached breakwaters is the rockfill because they are more affordable when compared with concrete blocks, have a good quality and resistance against agitation and they also have the possibility of reducing the negative environmental impacts. They may allow attachment of marine species (Challinor and Hall, 2008), creating a new habitat on the breakwater if the rockfill is similar to geological characteristics of materials of the intervention zone.

For the unit weight of the blocks, according to Taveira-Pinto, 1993 Waterways Experiment Station expressed the following equation to determine weight of blocks of resistant cloak:

$$W = \frac{\gamma_r \times H^3}{K_D \times (S-1)^3 \times \cot g(\alpha)} \quad (36)$$

where: K_D represents an empirical stability coefficient (Hudson's empirical coefficient); γ_r is the specific weight of the blocks material; H is the incident design wave height, S is the specific gravity of the blocks (γ_r/γ_w); γ_w is the specific weight of water and α is the slope angle with the horizontal.

The specific weight for seawater, γ_w, has been considered 10,25 kN/m^3. The stability coefficient K_D should be fixed according to the type, shape and location of block placement, roughness, angularity, fitting, permeability and number of rows per layer. Some values for this coefficient are presented in Table 3.6.

Table 3.6: Stability coefficient, K_D, according to different breakwater materials and shapes (Taveira-Pinto, 1993).

	K_D
Tetrapods	2 - 32
Cubes	2 - 15
Rockfill	**2 - 10**

Considering the detached breakwater of rockfill, the range for stability coefficient, K_D, goes from 2 to 10. For this work it has been assumed a K_D of 2 (conservative).

Table 3.7 presents valid slope angle with the horizontal, α, values for different breakwater materials.

Table 3.7: Slope angle with the horizontal, α, values for different breakwater materials (Taveira-Pinto, 1993).

	cotg(α)
Tetrapods	1,33
	1,50
	2,00
Cubic blocks	1,50
	2,00
	3,00
Rockfill	**2,00**
	3,00
	4,00

Slope angle values range from 2 to 4 for rockfill breakwaters. Because it is more conservative to use a smaller value, cotg(α) = 2 had been considered to this detached breakwater design.

Once having all coefficient values set it is possible to determine the crest width. Taking Equations (35) and (36):

$$B \geq 3 \times 1{,}5 \left(\frac{W}{26}\right)^{1/3} \tag{37}$$

$$W = \frac{26 \times 6{,}64^3}{2 \times \left(\frac{26}{10{,}25} - 1\right)^3 \times 2} = 524{,}50\ kN \tag{38}$$

$$B \geq 3 \times 1{,}5 \left(\frac{524{,}50}{26}\right)^{1/3} <=> B \geq 9{,}40\ m > 6\ m\ \textbf{OK!} \tag{39}$$

Thus, the crest width value used for this work had been considered B = 9,40 m.

(Page intentionally left blank)

CHAPTER 4

Models setup

‘As far as the laws of mathematics refer to reality, they are not certain, and as far as they are certain, they do not refer to reality.’

Albert Einstein (1879 – 1955)

(Page intentionally left blank)

CHAPTER 4 MODELS SETUP

4.1 1D Modelling. COULWAVE

In this section the COULWAVE model (version 2010) is applied to simulate the wave propagation in the Ofir beach. For determining the beach slope ArcGIS proved to be an important tool as demonstrated in Subchapter 3.2.4. Firstly it was necessary to choose the study site. Figure 4.1 shows the section view (profile graph) in the area of the Ofir towers that has been decided to analyse.

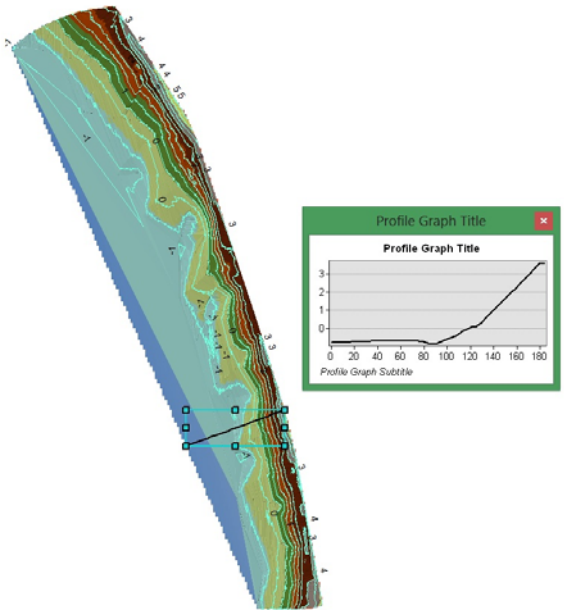

Figure 4.1: Profile graph shown in ArcGIS.

COULWAVE requires three input data sets. The first data set contains the bathymetry and topography of the area of interest. The second data set contains run-time and model parameters, which allow COULWAVE to generate the computational grid from the bathymetric and topographic input. The third data set contains the incident wave information. The input data sets and the generation of the computational grid are described in more detail.

The data contained in bathymetric and topographic data for 1DH simulations are organized in these 4 files (Douyère, 2003):

- x_topo.dat contains the locations of the grid points in meters along the x-coordinate from the point of origin to x_{max}. The increment between adjacent grid points should be kept constant;

- y_topo.dat contains the locations of the grid points in meters in the y-coordinate from the point of origin to y_{max}. The grid resolution should be the same as in x_topo.dat. For 1DH simulation first line= 0;
- size_topo.dat contains the number of points in x_topo.dat (first line) and y_topo.dat (second line);
- f_topo.dat contains the water surface and land elevations in meters at the grid points. Negative values represent water depth. The data is arranged by row in the x direction starting at the origin.

The total number of grid points is equal to the product of the numbers of grid points in the x and y directions.

The model-setup and run-up time parameters for COULWAVE are stored in the text file sim_set.dat shown in (APPENDIX 1). The parameters in the file define the computational grid and simulation conditions. The key parameters include grid resolution, time-step size, number of iterations per time-step, type of governing equations, sponge layer arrangement, wave maker location and simulation time. The program can generate regular or irregular waves. For irregular waves, the user needs to supply a directional spectrum as part of the input (Douyère, 2003).

For the study area for each incident wave condition defined by its significant height and significant period the COULWAVE model simulated different scenarios with duration of 200s and the results were written to file every 1s. Computational and time expenses made it difficult running all the simulations much longer.

Once the results listed in ArcGIS were presented every x= 4,17m, for the 1DH models had been considered a grid size Δx= 4,17m with 934,84m along the x-direction. This distance from the coastline to the offshore boundary is to provide sufficient time and distance for the waves to interact with each other. As for the depth it was fixed a maximum deepness of 12m in order to ensure a valid location of source wavemaker for the simulations and wave propagation. The steepness adopted was 2,5% as explained in Subchapter 3.2.4. To establish the underwater steepness, the original beach slope was prolonged to the maximum depth ensuring the 2,5% slope. As for the minimum number of grid points per wavelength it was set 35 in the simulations performed. The bathymetry considered corresponded to an approximation of the real bathymetry. Figure 4.2 represents the initial bathymetry (without any detached breakwater).

It was further added a constant depth zone to the domain where the referred incident waves were generated. The locations were set in the positions x= 60m, x= 20m, x= 25m, x= 31m, x= 35m for

H_s= 6,64m, H_s= 1m, H_s= 2m, H_s= 3m, H_s= 4m, respectively. (If position x is too short, the wave won't be able to propagate because its velocity is slower and it would have lower wave height peaks. A larger x position would promote higher wave heights.) In both left and right boundaries of domain were applied a solid-reflective wall and a sponge layer was added along the left boundary while the right boundary was considered with no absorption boundary. The sponge layer used here absorbs both mass and energy and has shown to be an excellent absorber of waves of all types with negligible reflection.

For all simulations, it was considered fully-nonlinear equations because allows for the simulation of waves with larger amplitudes (with arbitrary level approximation dispersive properties, because water depth/amplitude > 0,25), the finite difference scheme is accurate to the second order (Δx^2) in space, a bottom friction coefficient of 1.00E-03, a Courant number of 0,3 and a wave type defined by a spectrum of amplitudes generated by a Matlab file (spectrum_1D) where the user must introduce the frequency, the significant wave height and the depth at wave generation location (base depth). It was also considered a wave breaking model because if the wave transforms to a situation near breaking, and the breaking model is not turned on, the simulation will frequently overflow. The entire domain filtering was not activated once it does remove a small amount of long wave energy, and thus may affect the final solution. It is important to mention that the mean sea water level considered in COULWAVE is 0m.

The values of the parameters not mention herein were set as the default values suggested by the COULWAVE manual.

To optimize time simulation, it was activated the parallel processing. This information can be changed in the batch.dec file. In the first line of this file it is possible to determine whether to choose a parallel processing or a sequential processing by changing to number 1 or 0 option, respectively. The number of processors to be used should be based on the available computational resources. This information can be included in the s.dat file in the third column of the first line of the file.

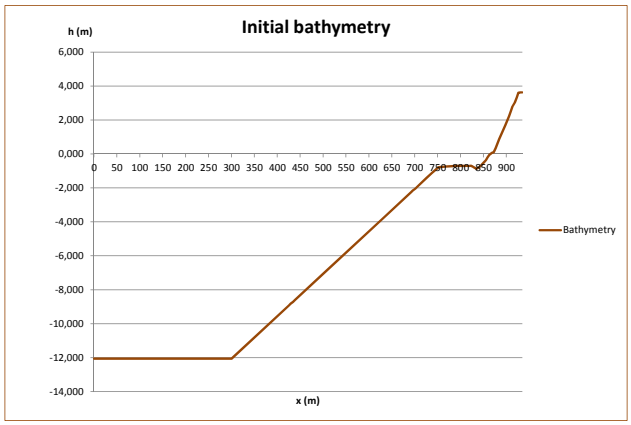

Figure 4.2: Representation of the domain bathymetry.

4.2 2D Modelling. BOUSS-2D

The SMS was applied to simulate residual velocities and the significant wave heights for different scenarios with and without detached breakwaters along the domain for different wave orientations. It is important to mention that this study is not directly related to the one done in COULWAVE, i.e. the analysis studied in BOUSS-2D will be focused on the residual velocities and the significant wave heights instead of comparing the COULWAVE significant wave heights and wave energy to the BOUSS-2D results. Although BOUSS-2D does not have a sediment transport module it is possible to antecipate sediment transport patterns by analysing the residual velocities results. It is not accurate to say these residual velocities are going to present the real sediment transport because the circumstances necessary to initiate movement of sediments are a function of sediment characteristics (density, size, shape), the fluid (density and viscosity) and flow conditions (average speed or intensity of the turbulent stress) (Miller *et al.*, 1977), but despite that, these residual velocities may draw the sediments possible path and it could be possible to assume the accumulation and erosion areas along the Ofir beach. Contrary to what was done with COULWAVE 1D model, this significant wave height analysis is going to focus all 2D domain instead of one only a cross section near the Ofir towers.

For this study it was used the BOUSS-2D model in order to simulate the propagation and transformation of waves in coastal regions based on a time-domain solution of Boussinesq-type equations.

SMS provides a custom interface to the BOUSS-2D model offering a simple way to set model parameters and a graphical user interface to run the model and visualize the results and also allows

gathering background data from a variety of sources from GIS to CAD (Aquaveo, 2014). The SMS version used was SMS 7.0.

The first step to define the model starts with adding the Viana do Castelo – Leixões and the Ofir beach topography information to the same file. It is very important to define both Viana do Castelo – Leixões and Ofir beach contour lines shape files with the same coordinate system. Because the Ofir beach shape file was in a different coordinate system, using the ArcToolbox in ArcGIS it was able to change it to ETRS_1989_Portugal_TM06 which was the Viana do Castelo – Leixões coordinate system. It was then exported to CAD and saved both shape files in a DXF_R2000 format, added to the SMS model and transformed both into a scatter mode (each scatter point contains elevation information). Once all information is set in a scatter mode, the Scatter Module is used to interpolate spatial data to other data types (in this case: grids). The module is also used to view and edit survey data. The actual bathymetry comes from the scattered data, BOUSS-2D interpolates this data to the created grid points.

Because the data taken from the IH shape file Viana do Castelo – Leixões is referenced to the chart datum (CD) and the Ofir beach data is referenced to the mean sea level (MSL) it was necessary to adjust the scatter data elevation. For this study it was decided to analyse the influence of a detached breakwater in the highest astronomical tide (HAT) situation. For Portugal the HAT and MSL situations are approximately 4m and 2m (IH, 2014) referenced to the CD, respectively (see Figure 4.3). Since Bouss-2D uses the reference level of the free surface (and this being = 0), for data compatibility all the elevation data (IH and Ofir beach) were referred to the HAT level.

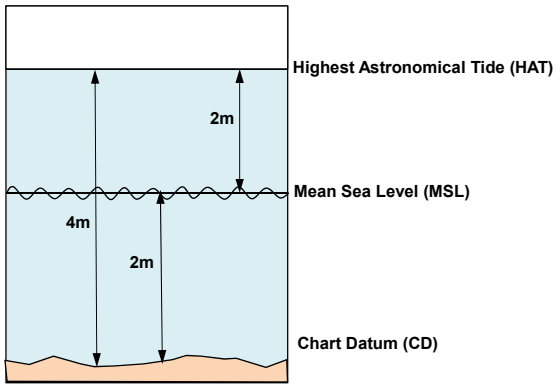

Figure 4.3: Scheme representing the HAT, MSL and CD values for the Portuguese coast.

Once these changes were set, the two scatter data files were merged into one (using Merge Scatter sets) and it was then created the grid using the Cartesian Grid module selecting the BOUSS-2D model. Figure 4.4 depicts the coordinate system assumed for the wave orientation angles.

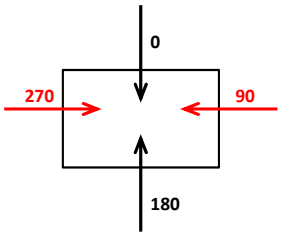

Figure 4.4: Coordinate system for wave orientation angles in degrees.

The wave reflection is avoided by using the appropriate coefficients at the boundaries. The grid domain exceeds the Ofir beach limits in order to avoid interference of values imposed at these limits. The grid domain is about 1150×1816m (x,y) and its angle is 0º. During the creation of the grid it was necessary to define the cell size so as the depth interpolation and extrapolation. In order to reduce some calculation time, and because it is a large domain, it was defined a 10 × 10m cell size. The interpolation was defined as linear and the extrapolation to a single value selected (land point: +4m). Some extrapolation points were created in the ocean domain, therefore because these points were defined as land points it was necessary to correct them by approaching the depth values to the surrounding ocean depths. Figure 4.5 depicts that issue.

Figure 4.5: "Islands" created by the depth extrapolation (brown lines between blue lines).

With all domain set and corrected, it was necessary to set the groins depth. According to the Ofir beach data, the North and the South groins have an average elevation (MSL) of 3,85m and 4,40m, respectively. Once it has been considered a HAT situation, those elevations were translated 2m down making the final elevation 1,85m for the North groin and 2,40m for the South groin.

BOUSS-2D can simulate a beater of regular or irregular waves (wave maker, represented by a green solid line in Figure 4.6) in a rectangular domain. It includes the option to add damping layers (represented by an orange solid line in Figure 4.6) in order to absorb the energy of the border area and porosity layers to simulate a partial reflection. In this study the porosity layers were considered 'impermeable', that is null the transmission coefficient. For this study and for all the scenarios the left boundary was set as a regular wave type because it eases the analysis of results process. The wave maker parameters set were the recommended by BOUSS-2D. The top and bottom boundaries were defined as damping layers with a width of 50m and a damping value of 1,0 to make the domain boundaries the least reflective. The damping value is a non-dimensional damping coefficient that is allowed to vary from 0,0 to 1,0. No damping will occur when a value of 0,0 is used. Waves will be damped when a value of 1,0 is used along the side boundaries. In the right boundary was not applied any boundary condition, so it simulates a reflective wall condition.

The wave height and the wave period as well as the wave maker orientation can be entered in the Wave Generator Properties by selecting the Boundary Conditions options and their values would depend on the scenarios considered.

Figure 4.6 (left) represents the initial grid (without any detached breakwater) and the entire domain that was considered for the models. Represented by the blue lines are the ocean cells and by the brown lines the land cells. Figure 4.6 (right) depicts the depth in meters along the domain (again, without any detached breakwater).

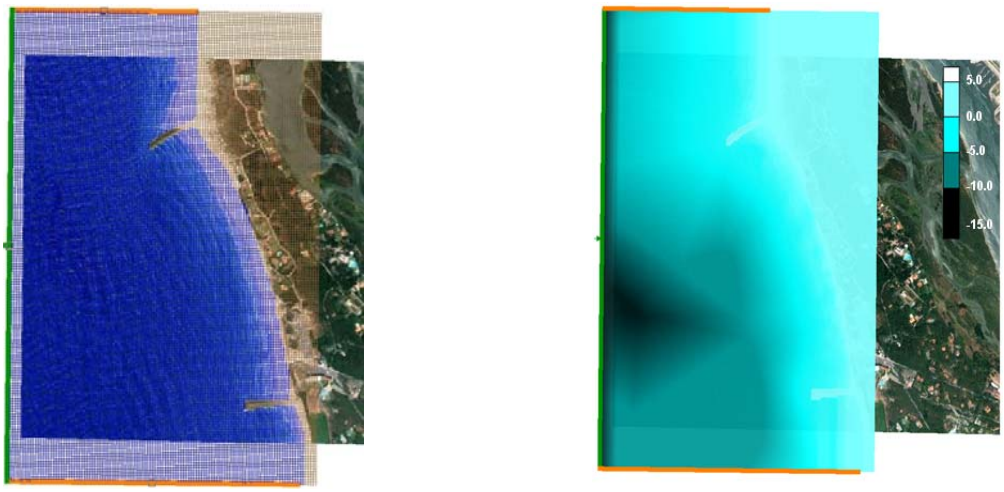

Figure 4.6: Initial grid without detached breakwater (left) and depth, in meters, along the domain without detached breakwater (right).

For all simulations, the time control and the time-step considered were the recommended values suggested by the BOUSS-2D in the Model Control options and it may vary a little depending on the

input wave height. So for the lowest wave height the simulation time and the time-step are 580s and 0,45s, respectively and for the highest wave height 572s and 0,41s, respectively. All the porosity friction factors and other parameters like the Courant number and the Chézy coefficient were set as the recommended suggested by the BOUSS-2D as well. It was considered a strong non-linear parameter option, and a Courant number of 0,6 and a Chézy coefficient of 30. It was also enabled a wave breaking model which allows dissipating wave energy. The wave run-up option was not considered though because there was no influence in the results.

As with many numerical models, BOUSS-2D can terminate or crash due to numerical instabilities. These are usually caused by problems related to the grid, the boundary conditions, or model parameters (XMS Wiki, 2014). During the modelling some instability issues needed to be corrected because simulations were not finishing successfully. Computation nodes surrounded on three or four sides by land were created during the grid creation process. These 'isolated' cells became unstable, so in order to modify the model, the cells needed to be converted to land cells. It is also important to be aware that wave makers have to be placed far enough from shore to avoid interaction between the wave maker and reflecting waves. This is because the external boundary behind the wave maker is treated as a vertical wall.

CHAPTER 5

1D modelling. Results and discussions

'It is better to know some of the questions than all of the answers.'

James Thurber (1894 – 1961)

(Page intentionally left blank)

CHAPTER 5 1D MODELLING. RESULTS AND DISCUSSIONS

The model was applied to study detached breakwater impact on significant wave height and wave energy near the shore. Different detached breakwater heights, distance from shore to the detached breakwater and different incident wave heights and periods were tested.

5.1 Scenarios

Sixty scenarios were considered, aiming the understanding of the influence of detached breakwater height and distance from shore to the detached breakwater and of incident wave height and periods, on the significant wave height and wave energy near the shore, considering the MSL as reference level. The characteristics of the scenarios correspond to the:

- Four detached breakwater crest levels: h_{cr}= 2,70m, h_{cr}= 1,50m, h_{cr}= -1,50m, h_{cr}= -0,50m;
- Three values for distance from shore to the detached breakwater: X= 235m, X= 170m, X= 300m;
- Five incident wave heights: H_s= 6,64m, H_s= 1,0m, H_s= 2,0m, H_s= 3,0m, H_s= 4,0m;
- Three wave periods: T= 9,30s, T= 7,00s, T= 11,00s.

Furthermore five additional scenarios (named Initial) were included considering identical situations referred before without the present of detached breakwater.

Tables 5.1 and 5.2 summarize the chosen scenarios for this study.

Table 5.1: Scenarios with the inclusion of detached breakwater.

Wave characteristics		Breakwater characteristics		Scenario
H_s (m)	T (s)	h_{cr} (m)	X (m)	
6,64	9,30	2,70	235,00	SC1
			170,00	SC2
			300,00	SC3
		1,50	235,00	SC4
			170,00	SC5
			300,00	SC6
		-1,50	235,00	SC7
			170,00	SC8
			300,00	SC9
		-0,50	235,00	SC10
			170,00	SC11
			300,00	SC12
1,00	7,00	2,70	235,00	SC13
			170,00	SC14
			300,00	SC15
		1,50	235,00	SC16
			170,00	SC17
			300,00	SC18
		-1,50	235,00	SC19
			170,00	SC20
			300,00	SC21
		-0,50	235,00	SC22
			170,00	SC23
			300,00	SC24
2,00	7,00	2,70	235,00	SC25
			170,00	SC26
			300,00	SC27
		1,50	235,00	SC28
			170,00	SC29
			300,00	SC30
		-1,50	235,00	SC31
			170,00	SC32
			300,00	SC33
		-0,50	235,00	SC34
			170,00	SC35
			300,00	SC36
3,00	7,00	2,70	235,00	SC37
			170,00	SC38
			300,00	SC39
		1,50	235,00	SC40
			170,00	SC41
			300,00	SC42
		-1,50	235,00	SC43
			170,00	SC44
			300,00	SC45
		-0,50	235,00	SC46
			170,00	SC47
			300,00	SC48
4,00	11,00	2,70	235,00	SC49
			170,00	SC50
			300,00	SC51
		1,50	235,00	SC52
			170,00	SC53
			300,00	SC54
		-1,50	235,00	SC55
			170,00	SC56
			300,00	SC57
		-0,50	235,00	SC58
			170,00	SC59
			300,00	SC60

Table 5.2: Scenarios without the inclusion of detached breakwater.

Wave characteristics		Scenario
H_s (m)	T (s)	
6,64	9,30	**Initial1**
1,00	7,00	**Initial2**
2,00	7,00	**Initial3**
3,00	7,00	**Initial4**
4,00	11,00	**Initial5**

This choice of scenarios intended to approach a wide range of possibilities often considered in real situations and to analyse the influence of four parameters considered when a detached breakwater is built. However, it was also constrained by model limitations, such as the difficulty of the model to simulate scenarios where bathymetry changes abruptly and where the number of grid points is large.

Also, when introducing the water depth value in the sim_set.dat file should be confirmed if this value is larger than the wave amplitude and if it is the same value as the maximum depth introduced in the f_topo.dat file. Otherwise, stack overflow error will pop up.

All the detached breakwaters were designed to have a crest width, B, of 9,40m and a side-slope of 2:1 (H:V).

In order to write time series of significant wave height at specific locations to file it was set 6 points (3 before the detached breakwater and 3 after the detached breakwater). The location of these points is assigned by ts_locations.dat file and the results can be seen in tmsr0001.dat, tmsr0002.dat, tmsr0003.dat, tmsr0004.dat, tmsr0005.dat, tmsr0006.dat files, each for every point defined. The x-coordinates set to file were:

- x= 90m;
- x= 360m;
- x= variable (first point of detached breakwater crest, depending on detached breakwater location);
- x= 650m;
- x= 800m;
- x= 870m.

Because it is a 1DH simulation the y-coordinates were set as 0m.

Every tmsr00.dat file presents the results of significant wave height (first column) and u and v (second and third columns, respectively) velocities. After gathering all the results the charts were generated using Microsoft Excel. After generating the charts and in order to make it easy to understand and comment the effect of different detached breakwater and hydrodynamic conditions, it was selected every maximum wave heights of each points of every scenarios. Besides analysing the results in conditions with a detached breakwater implemented, it was done the same with a situation without a detached breakwater (see Results) so that it was possible to assess the influence of a detached breakwater in different scenarios.

5.2 Results

For each scenario, the significant wave height and the wave energy were calculated for the 6 defined positions originating 65 different results. As an example, Figure 5.1 depicts the output of the simulation for scenario 1 (SC1). The remaining results for the scenarios left are presented in

APPENDIX 2 to 6. For all of these Appendices along with the scenario indications, the type of bathymetry is indicated at the top and by its side is shown the cumulative energy chart followed by the significant wave height and wave energy charts for the defined positions.

Although significant wave height results can be directly gathered from the tmsr00.dat files, in order to output the results of the wave energy an algorithm was created to separate every registered wave and then compute the wave energy for all the scenarios. With these results is now conceivable to represent the wave energy chart. After the calculation of wave energy in each position the results had been sum to generate the cumulative wave energy chart. APPENDIX 7 presents the algorithm written in VBA and depicts the code for every 6 positions for scenario 1 (SC1).

The total energy of waves is made up of half potential energy and half kinetic energy. Since gravity is nearly constant around the globe and water density changes very little, at least from the stand point of wave information, wave energy is directly proportional to wave height squared (MetEd, 2014b). Equation (43) represents the wave energy equation used for this study.

$$E = \frac{1}{8}(\rho g H^2) \quad (43)$$

where: E is the wave energy per unit area (J/m^2), ρ is the water density (kg/m^3), g is the gravity acceleration (m/s^2) and H is the wave height (m).

Considering $\rho_{seawater}$= 1025kg/m^3 and g= 9,81 m/s^2 the wave energy was calculated for all scenarios.

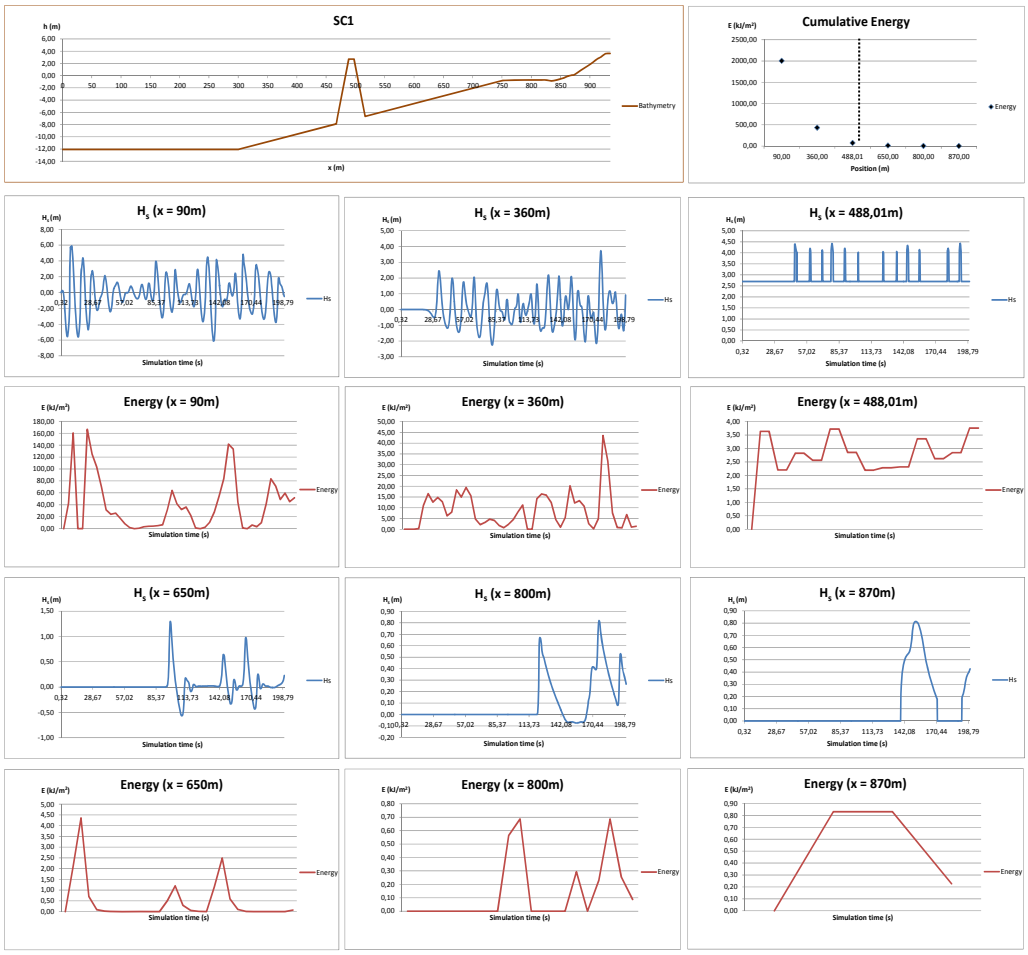

Figure 5.1: Output results for SC1.

5.3 Discussion of the results

In order to assess the influence of the magnitude of the significant wave height, H_s, the position, X, and the crest level, h_{cr}, of the detached breakwater in 6 predefined positions (x-coordinates) it was selected every maximum wave heights at each of those points for all the scenarios. Similar approach was developed to understand the influence of the significant wave height and the detached breakwater on the wave energy at those predefined positions. Firstly it will be displayed the results considering scenarios without a detached breakwater and then the results with a detached breakwater are presented.

5.3.1 Results for wave height in Initial scenarios

The Initial scenarios do not include a detached breakwater and simulate an initial condition. Figure 5.2 depicts the maximum significant wave heights in each point of every Initial scenarios.

Scenario	Position		Maximum H_s (m)
	Number	x (m)	
Initial1	1	90,00	**5,91**
	2	360,00	**3,93**
	3	500,00	**3,31**
	4	650,00	**2,65**
	5	800,00	**1,55**
	6	870,00	**1,37**
Initial2	1	90,00	**0,64**
	2	360,00	**0,53**
	3	500,00	**0,59**
	4	650,00	**0,68**
	5	800,00	**0,24**
	6	870,00	**0,28**
Initial3	1	90,00	**1,17**
	2	360,00	**0,96**
	3	500,00	**0,96**
	4	650,00	**1,11**
	5	800,00	**0,40**
	6	870,00	**0,54**
Initial4	1	90,00	**2,19**
	2	360,00	**1,76**
	3	500,00	**1,76**
	4	650,00	**1,91**
	5	800,00	**0,69**
	6	870,00	**1,01**
Initial5	1	90,00	**3,08**
	2	360,00	**2,45**
	3	500,00	**2,45**
	4	650,00	**2,54**
	5	800,00	**0,85**
	6	870,00	**1,37**

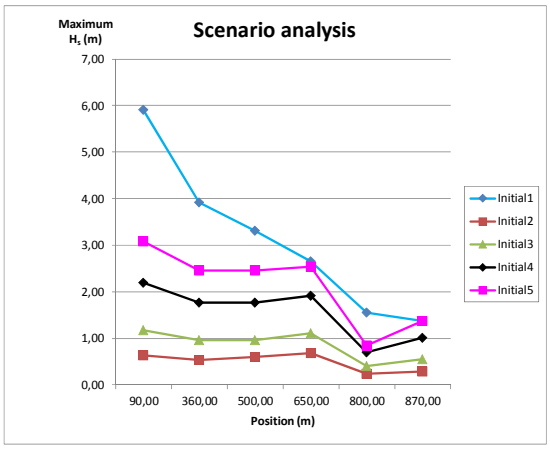

Figure 5.2: Results and analysis for Initial scenarios.

From the results shown in Figure 5.2 it is possible to establish the following comments:

- For the highest significant wave height, H_s= 6,64m, a very steep decrease in the maximum wave height at all the positions is verified. Moreover there is no influence of the bathymetry in the significant wave height near the shore (significant wave height in positions number 5 and 6 are similar);
- For smaller significant wave heights ($H_s \leq$ 4,00m) there is no significant decrease in the maximum wave height until the position number 4. After this point heading to the shore a significant effect of bathymetry is verified: a very steep decrease in the maximum wave height from the positions number 4 to 5 and a subsequent increase in the run-up zone (position number 6), probably due to wave breaking phenomena.

5.3.2 Results for wave height in scenarios with detached breakwater

Figures 5.3 to 5.7 show the maximum significant wave heights in each point of every scenario with a detached breakwater implemented.

Scenario	Position		Maximum H_s (m)
	Number	x (m)	
SC1	1	90,00	**5,91**
	2	360,00	**3,73**
	3	488,01	**4,43**
	4	650,00	**1,30**
	5	800,00	**0,82**
	6	870,00	**0,81**
SC2	1	90,00	**5,91**
	2	360,00	**5,06**
	3	556,31	**4,68**
	4	650,00	**1,48**
	5	800,00	**1,05**
	6	870,00	**0,73**
SC3	1	90,00	**5,91**
	2	360,00	**4,59**
	3	419,81	**4,76**
	4	650,00	**1,55**
	5	800,00	**1,34**
	6	870,00	**0,99**
SC4	1	90,00	**5,91**
	2	360,00	**2,88**
	3	490,21	**4,41**
	4	650,00	**1,88**
	5	800,00	**1,12**
	6	870,00	**1,13**
SC5	1	90,00	**5,91**
	2	360,00	**4,98**
	3	558,71	**4,11**
	4	650,00	**2,18**
	5	800,00	**1,39**
	6	870,00	**0,96**
SC6	1	90,00	**5,91**
	2	360,00	**3,78**
	3	422,21	**3,87**
	4	650,00	**2,15**
	5	800,00	**1,97**
	6	870,00	**1,53**

Scenario	Position		Maximum H_s (m)
	Number	x (m)	
SC7	1	90,00	**5,91**
	2	360,00	**3,49**
	3	496,41	**3,38**
	4	650,00	**1,72**
	5	800,00	**1,60**
	6	870,00	**1,45**
SC8	1	90,00	**5,91**
	2	360,00	**3,48**
	3	564,71	**3,19**
	4	650,00	**2,12**
	5	800,00	**2,13**
	6	870,00	**1,45**
SC9	1	90,00	**5,91**
	2	360,00	**2,65**
	3	428,21	**2,87**
	4	650,00	**2,00**
	5	800,00	**1,77**
	6	870,00	**1,62**
SC10	1	90,00	**5,91**
	2	360,00	**4,08**
	3	494,41	**3,67**
	4	650,00	**2,49**
	5	800,00	**1,54**
	6	870,00	**1,36**
SC11	1	90,00	**5,91**
	2	360,00	**4,12**
	3	562,71	**3,44**
	4	650,00	**3,37**
	5	800,00	**2,04**
	6	870,00	**1,47**
SC12	1	90,00	**5,91**
	2	360,00	**2,74**
	3	426,21	**2,63**
	4	650,00	**2,30**
	5	800,00	**1,66**
	6	870,00	**1,49**

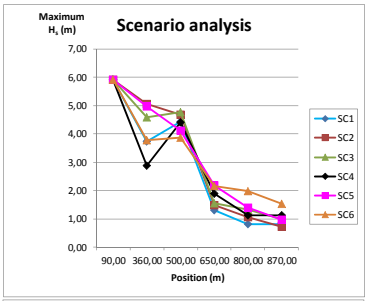

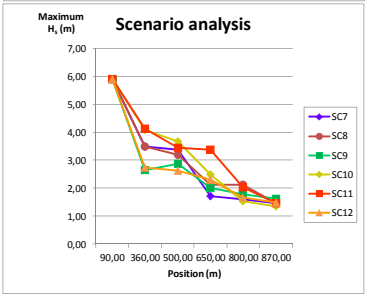

Figure 5.3: Results and analysis for scenarios 1 to 12.

Scenario	Position		Maximum H_s (m)
	Number	x (m)	
SC13	1	90,00	**0,64**
	2	360,00	**0,60**
	3	488,01	**2,70**
	4	650,00	**0,00**
	5	800,00	**0,00**
	6	870,00	**0,00**
SC14	1	90,00	**0,64**
	2	360,00	**0,53**
	3	556,31	**2,70**
	4	650,00	**0,00**
	5	800,00	**0,00**
	6	870,00	**0,00**
SC15	1	90,00	**0,64**
	2	360,00	**0,72**
	3	419,81	**2,65**
	4	650,00	**0,00**
	5	800,00	**0,00**
	6	870,00	**0,00**
SC16	1	90,00	**0,64**
	2	360,00	**0,61**
	3	490,21	**1,50**
	4	650,00	**0,00**
	5	800,00	**0,00**
	6	870,00	**0,00**
SC17	1	90,00	**0,64**
	2	360,00	**0,53**
	3	558,71	**1,50**
	4	650,00	**0,00**
	5	800,00	**0,00**
	6	870,00	**0,00**
SC18	1	90,00	**0,64**
	2	360,00	**0,61**
	3	422,21	**1,50**
	4	650,00	**0,00**
	5	800,00	**0,00**
	6	870,00	**0,00**

Scenario	Position		Maximum H_s (m)
	Number	x (m)	
SC19	1	90,00	**0,64**
	2	360,00	**0,53**
	3	496,41	**0,80**
	4	650,00	**0,55**
	5	800,00	**0,31**
	6	870,00	**0,43**
SC20	1	90,00	**0,64**
	2	360,00	**0,53**
	3	564,71	**0,82**
	4	650,00	**0,57**
	5	800,00	**0,27**
	6	870,00	**0,39**
SC21	1	90,00	**0,64**
	2	360,00	**0,47**
	3	428,21	**0,74**
	4	650,00	**0,49**
	5	800,00	**0,36**
	6	870,00	**0,49**
SC22	1	90,00	**0,64**
	2	360,00	**0,53**
	3	494,41	**0,92**
	4	650,00	**0,51**
	5	800,00	**0,36**
	6	870,00	**0,45**
SC23	1	90,00	**0,64**
	2	360,00	**0,53**
	3	562,71	**0,96**
	4	650,00	**0,48**
	5	800,00	**0,31**
	6	870,00	**0,37**
SC24	1	90,00	**0,64**
	2	360,00	**0,47**
	3	426,21	**0,84**
	4	650,00	**0,43**
	5	800,00	**0,27**
	6	870,00	**0,45**

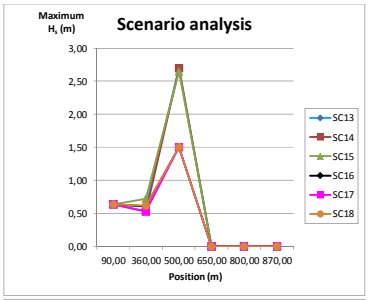

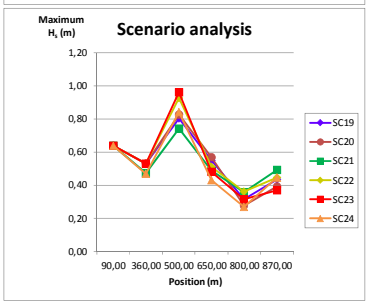

Figure 5.4: Results and analysis for scenarios 13 to 24.

Scenario	Position		Maximum H_s (m)
	Number	x (m)	
SC25	1	90,00	**1,17**
	2	360,00	**1,03**
	3	488,01	**2,70**
	4	650,00	**0,00**
	5	800,00	**0,00**
	6	870,00	**0,00**
SC26	1	90,00	**1,17**
	2	360,00	**0,96**
	3	556,31	**2,70**
	4	650,00	**0,00**
	5	800,00	**0,00**
	6	870,00	**0,00**
SC27	1	90,00	**1,17**
	2	360,00	**1,27**
	3	419,81	**2,65**
	4	650,00	**0,00**
	5	800,00	**0,00**
	6	870,00	**0,00**
SC28	1	90,00	**1,17**
	2	360,00	**1,10**
	3	490,21	**1,50**
	4	650,00	**0,00**
	5	800,00	**0,00**
	6	870,00	**0,00**
SC29	1	90,00	**1,18**
	2	360,00	**1,18**
	3	558,71	**1,50**
	4	650,00	**0,00**
	5	800,00	**0,00**
	6	870,00	**0,00**
SC30	1	90,00	**1,17**
	2	360,00	**1,12**
	3	422,21	**1,50**
	4	650,00	**0,00**
	5	800,00	**0,00**
	6	870,00	**0,00**

Scenario	Position		Maximum H_s (m)
	Number	x (m)	
SC31	1	90,00	**1,17**
	2	360,00	**0,96**
	3	496,41	**1,38**
	4	650,00	**0,94**
	5	800,00	**0,50**
	6	870,00	**0,68**
SC32	1	90,00	**1,17**
	2	360,00	**0,96**
	3	564,71	**1,40**
	4	650,00	**0,99**
	5	800,00	**0,49**
	6	870,00	**0,71**
SC33	1	90,00	**1,17**
	2	360,00	**0,86**
	3	428,21	**1,25**
	4	650,00	**0,86**
	5	800,00	**0,54**
	6	870,00	**0,78**
SC34	1	90,00	**1,17**
	2	360,00	**0,96**
	3	494,41	**1,42**
	4	650,00	**0,67**
	5	800,00	**0,42**
	6	870,00	**0,64**
SC35	1	90,00	**1,17**
	2	360,00	**0,96**
	3	562,71	**1,42**
	4	650,00	**0,85**
	5	800,00	**0,44**
	6	870,00	**0,62**
SC36	1	90,00	**1,17**
	2	360,00	**0,89**
	3	426,21	**1,43**
	4	650,00	**0,83**
	5	800,00	**0,42**
	6	870,00	**0,61**

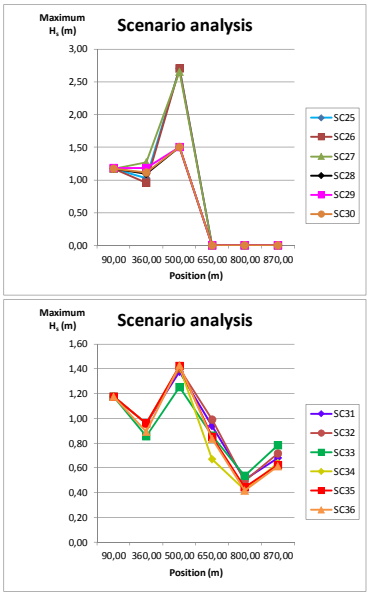

Figure 5.5: Results and analysis for scenarios 25 to 36.

Scenario	Position		Maximum H_s (m)
	Number	x (m)	
SC37	1	90,00	**2,19**
	2	360,00	**1,75**
	3	488,01	**4,20**
	4	650,00	**0,00**
	5	800,00	**0,00**
	6	870,00	**0,00**
SC38	1	90,00	**2,19**
	2	360,00	**1,76**
	3	556,31	**4,11**
	4	650,00	**0,00**
	5	800,00	**0,00**
	6	870,00	**0,00**
SC39	1	90,00	**2,19**
	2	360,00	**2,32**
	3	419,81	**4,29**
	4	650,00	**0,00**
	5	800,00	**0,00**
	6	870,00	**0,00**
SC40	1	90,00	**2,19**
	2	360,00	**1,75**
	3	490,21	**3,20**
	4	650,00	**0,68**
	5	800,00	**0,42**
	6	870,00	**0,50**
SC41	1	90,00	**2,19**
	2	360,00	**1,76**
	3	558,71	**3,05**
	4	650,00	**0,86**
	5	800,00	**0,45**
	6	870,00	**0,53**
SC42	1	90,00	**2,19**
	2	360,00	**2,09**
	3	422,21	**3,28**
	4	650,00	**0,46**
	5	800,00	**0,34**
	6	870,00	**0,43**

Scenario	Position		Maximum H_s (m)
	Number	x (m)	
SC43	1	90,00	**2,19**
	2	360,00	**1,76**
	3	496,41	**1,97**
	4	650,00	**1,58**
	5	800,00	**0,85**
	6	870,00	**1,30**
SC44	1	90,00	**2,19**
	2	360,00	**1,76**
	3	564,71	**2,01**
	4	650,00	**1,40**
	5	800,00	**0,87**
	6	870,00	**1,26**
SC45	1	90,00	**2,19**
	2	360,00	**1,64**
	3	428,21	**2,05**
	4	650,00	**1,51**
	5	800,00	**0,87**
	6	870,00	**1,21**
SC46	1	90,00	**2,19**
	2	360,00	**1,76**
	3	494,41	**1,98**
	4	650,00	**1,53**
	5	800,00	**0,85**
	6	870,00	**1,01**
SC47	1	90,00	**2,19**
	2	360,00	**1,76**
	3	562,71	**1,94**
	4	650,00	**1,61**
	5	800,00	**0,81**
	6	870,00	**1,03**
SC48	1	90,00	**2,19**
	2	360,00	**1,75**
	3	426,21	**2,07**
	4	650,00	**1,53**
	5	800,00	**0,82**
	6	870,00	**0,96**

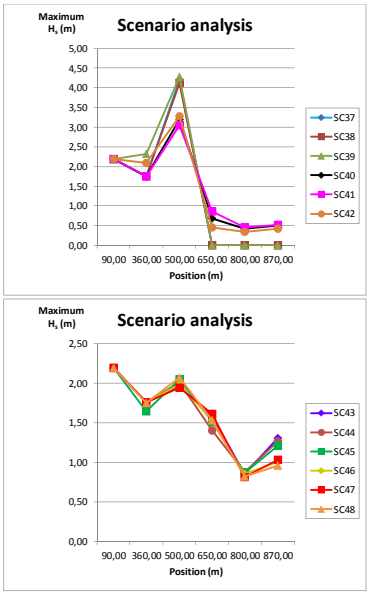

Figure 5.6: Results and analysis for scenarios 37 to 48.

Scenario	Position		Maximum H_s (m)
	Number	x (m)	
SC49	1	90,00	**3,08**
	2	360,00	**2,44**
	3	488,01	**4,54**
	4	650,00	**0,82**
	5	800,00	**0,48**
	6	870,00	**0,57**
SC50	1	90,00	**3,08**
	2	360,00	**2,45**
	3	556,31	**4,36**
	4	650,00	**1,19**
	5	800,00	**0,57**
	6	870,00	**0,63**
SC51	1	90,00	**3,08**
	2	360,00	**3,25**
	3	419,81	**4,69**
	4	650,00	**0,00**
	5	800,00	**0,00**
	6	870,00	**0,00**
SC52	1	90,00	**3,08**
	2	360,00	**2,45**
	3	490,21	**3,43**
	4	650,00	**1,30**
	5	800,00	**0,73**
	6	870,00	**0,87**
SC53	1	90,00	**3,08**
	2	360,00	**2,45**
	3	558,71	**3,33**
	4	650,00	**1,27**
	5	800,00	**0,66**
	6	870,00	**0,87**
SC54	1	90,00	**3,08**
	2	360,00	**2,97**
	3	422,21	**3,72**
	4	650,00	**1,03**
	5	800,00	**0,55**
	6	870,00	**0,84**

Scenario	Position		Maximum H_s (m)
	Number	x (m)	
SC55	1	90,00	**3,08**
	2	360,00	**2,45**
	3	496,41	**2,79**
	4	650,00	**1,50**
	5	800,00	**1,13**
	6	870,00	**1,56**
SC56	1	90,00	**3,08**
	2	360,00	**2,45**
	3	564,71	**2,55**
	4	650,00	**1,66**
	5	800,00	**1,04**
	6	870,00	**1,43**
SC57	1	90,00	**3,08**
	2	360,00	**2,41**
	3	428,21	**2,48**
	4	650,00	**2,16**
	5	800,00	**1,07**
	6	870,00	**1,39**
SC58	1	90,00	**3,08**
	2	360,00	**2,45**
	3	494,41	**2,48**
	4	650,00	**1,91**
	5	800,00	**1,07**
	6	870,00	**1,35**
SC59	1	90,00	**3,08**
	2	360,00	**2,45**
	3	562,71	**2,52**
	4	650,00	**1,89**
	5	800,00	**1,02**
	6	870,00	**1,31**
SC60	1	90,00	**3,08**
	2	360,00	**2,56**
	3	426,21	**2,48**
	4	650,00	**1,61**
	5	800,00	**1,01**
	6	870,00	**1,37**

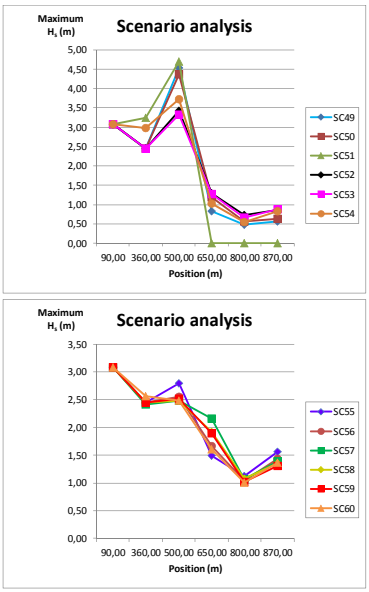

Figure 5.7: Results and analysis for scenarios 49 to 60.

The results obtained allow establishing the following comments:

- Emerged breakwaters:
  - Independently on the value of significant wave heights considered, h_{cr}= 2,70m induces a greater decrease of the maximum wave height in the leeward side of the detached breakwater than h_{cr}= 1,50m, as expected. For all of the detached breakwater positions, X, it is verified that the highest wave heights in the leeward side correspond to a crest level of h_{cr}= 1,50m. Conversely the smallest wave heights are verified for a crest level of h_{cr}= 2,70m;
  - For significant wave heights $H_s \leq$ 2,00m, the maximum wave height on the detached breakwater always reaches the crest level (Figures 5.4 and 5.5);
  - For significant wave heights $H_s \leq$ 3,00m and a specific h_{cr}, the position of the detached breakwater, X, is irrelevant to the maximum wave height on the detached breakwater (position number 3) (Figures 5.4, 5.5, and 5.6);
  - Considering the significant wave height H_s= 6,64m which determined the dimensioning of the detached breakwater is notable that the smallest wave height is in the position X= 235,00m (Figure 5.3);
  - For significant wave heights H_s= 3,00m and H_s= 4,00m it is apparent the effect of bathymetry on the maximum wave heights in the leeward side of the detached breakwater (Figures 5.3, 5.6, and 5.7;

- For every significant wave heights analysed, there is an increase in the maximum wave height between positions numbers 2 and 3 due to the addition of the incident and reflective waves in the windward side of the detached breakwater;
- The presence of the detached breakwater is responsible for the remarkable decrease in the maximum wave height between position numbers 3 and 4 for every significant wave heights analysed.

- Submerged breakwaters:
  - For significant wave heights $H_s \leq$ 3,00m, h_{cr}= -0,50m induces a greater decrease of the maximum wave height in the leeward side of the detached breakwater than h_{cr}= -1,50m, as expected (Figure 5.4, 5.5, and 5.6). For all of the detached breakwater positions, X, it is verified that the highest wave height in the leeward side corresponds to a crest level of h_{cr}= -1,50m. Conversely the smallest wave height is verified for a crest level of h_{cr}= -0,50m;
  - For a significant wave height of H_s= 3,00m and a specific h_{cr}, the position of the detached breakwater, X, is irrelevant to the maximum wave height at the detached breakwater (Figure 5.6);
  - Similarly to the Initial1 scenario, for the highest significant wave height, H_s= 6,64m, a very steep decrease in the maximum wave height at all the positions is verified. Moreover there is no influence of the bathymetry in the significant wave height near the shore (positions number 5 and 6) (Figure 5.3);
  - For significant wave heights $H_s \leq$ 4,00m it is apparent the effect of bathymetry on the maximum wave heights in the leeward side of the detached breakwater (positions number 5 and 6) (Figures 5.4, 5.5, 5.6, and 5.7);
  - For significant wave heights $H_s \leq$ 3,00m there is a substantial increase in the maximum wave height between position numbers 2 and 3 due to the addition of the incident and reflective waves in the windward side of the detached breakwater (Figures 5.4, 5.5, and 5.6);
  - For significant wave heights $H_s \geq$ 4,00m it doesn't verify any substantial increase in the maximum wave height between position numbers 2 and 3 meaning that, for these significant wave heights, there is no influence of the detached breakwater (Figures 5.3 and 5.7);

- The presence of the detached breakwater is responsible for the remarkable decrease in the maximum wave height between position numbers 3 and 4 for all significant wave heights.

In general:

- Submerged detached breakwaters have a smaller impact on significant wave heights compared to the emerged detached breakwaters;
- Comparing Initial conditions with all the 60 scenarios simulated it is evident that detached breakwaters (either submerged or emerged) have a relevant impact in decreasing the significant wave height;
- For all the wave conditions it is found that the most efficient solution is when the emerged detached breakwater is located at X= 235,00m and h_{cr}= 2,70m;
- For submerged detached breakwaters and significant wave heights $H_s \geq$ 4,00m the most efficient solution is found when h_{cr}= -1,50m and X= 235,00m (Figures 5.3 and 5.7);
- For submerged detached breakwaters and significant wave heights $H_s \leq$ 2,00m the most efficient solution is found when h_{cr}= -0,50m and X= 300,00m (Figures 5.4 and 5.5);
- When H_s= 3,00m the results are not so evident for determining the most efficient solution (Figure 5.6).

5.3.3 Results for wave energy in Initial scenarios

Figure 5.8 depicts the maximum wave energy in each point of every Initial scenarios.

Scenario	Position		Maximum E
	Number	x (m)	(kJ/m^2)
Initial1	1	90,00	**166,46**
	2	360,00	**49,81**
	3	500,00	**32,96**
	4	650,00	**9,48**
	5	800,00	**2,46**
	6	870,00	**2,35**
Initial2	1	90,00	**1,46**
	2	360,00	**1,26**
	3	500,00	**1,28**
	4	650,00	**1,42**
	5	800,00	**0,09**
	6	870,00	**0,10**
Initial3	1	90,00	**4,46**
	2	360,00	**3,76**
	3	500,00	**3,76**
	4	650,00	**3,45**
	5	800,00	**0,21**
	6	870,00	**0,37**
Initial4	1	90,00	**14,87**
	2	360,00	**11,08**
	3	500,00	**11,08**
	4	650,00	**7,35**
	5	800,00	**0,60**
	6	870,00	**0,75**
Initial5	1	90,00	**29,18**
	2	360,00	**19,70**
	3	500,00	**19,70**
	4	650,00	**10,93**
	5	800,00	**0,90**
	6	870,00	**2,37**

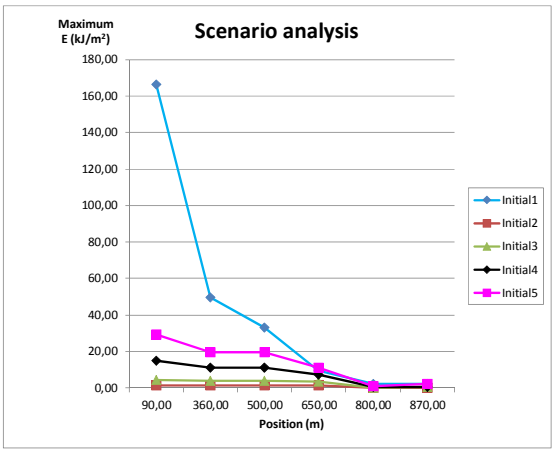

Figure 5.8: Results and analysis for Initial scenarios.

From the results shown in Figure 5.8 it is possible to establish the following comments:

- For significant wave height H_s= 6,64m, a very steep decrease in the maximum wave energy in all the positions considered is verified;
- For smaller significant wave heights ($H_s \leq$ 4,00m) there is no significant decrease in the maximum wave energy until the position number 4. After this point heading to the shore a significant effect of bathymetry is verified: a very steep decrease in the maximum wave energy from the positions number 4 to 5.

5.3.4 Results for wave energy in scenarios with detached breakwater

Figures 5.9 to 5.13 show the maximum wave energy in each point for all scenarios. From the results obtained it can be concluded that:

Scenario	Position		Maximum E
	Number	x (m)	(kJ/m²)
SC1	1	90,00	**166,46**
	2	360,00	**43,50**
	3	488,01	**3,76**
	4	650,00	**4,35**
	5	800,00	**0,69**
	6	870,00	**0,83**
SC2	1	90,00	**166,46**
	2	360,00	**90,34**
	3	556,31	**4,95**
	4	650,00	**4,94**
	5	800,00	**1,09**
	6	870,00	**0,67**
SC3	1	90,00	**166,46**
	2	360,00	**60,45**
	3	419,81	**5,59**
	4	650,00	**4,38**
	5	800,00	**1,55**
	6	870,00	**1,24**
SC4	1	90,00	**166,46**
	2	360,00	**28,74**
	3	490,21	**10,64**
	4	650,00	**4,87**
	5	800,00	**0,96**
	6	870,00	**0,83**
SC5	1	90,00	**166,46**
	2	360,00	**59,11**
	3	558,71	**8,54**
	4	650,00	**8,83**
	5	800,00	**1,59**
	6	870,00	**0,38**
SC6	1	90,00	**166,46**
	2	360,00	**45,04**
	3	422,21	**7,07**
	4	650,00	**9,84**
	5	800,00	**3,17**
	6	870,00	**2,06**

Scenario	Position		Maximum E
	Number	x (m)	(kJ/m²)
SC7	1	90,00	**166,46**
	2	360,00	**33,56**
	3	496,41	**29,89**
	4	650,00	**3,91**
	5	800,00	**1,26**
	6	870,00	**1,39**
SC8	1	90,00	**166,46**
	2	360,00	**37,70**
	3	564,71	**27,69**
	4	650,00	**5,04**
	5	800,00	**3,04**
	6	870,00	**1,45**
SC9	1	90,00	**166,46**
	2	360,00	**26,73**
	3	428,21	**23,95**
	4	650,00	**4,21**
	5	800,00	**1,10**
	6	870,00	**1,55**
SC10	1	90,00	**166,46**
	2	360,00	**50,89**
	3	494,41	**24,32**
	4	650,00	**6,07**
	5	800,00	**1,12**
	6	870,00	**2,11**
SC11	1	90,00	**166,46**
	2	360,00	**46,65**
	3	562,71	**20,66**
	4	650,00	**12,10**
	5	800,00	**3,01**
	6	870,00	**1,00**
SC12	1	90,00	**166,46**
	2	360,00	**27,45**
	3	426,21	**15,57**
	4	650,00	**5,75**
	5	800,00	**1,29**
	6	870,00	**2,30**

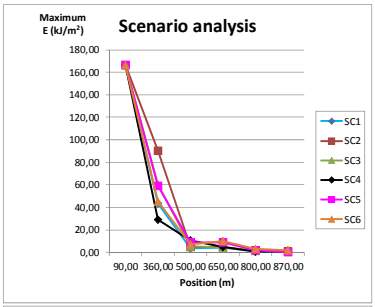

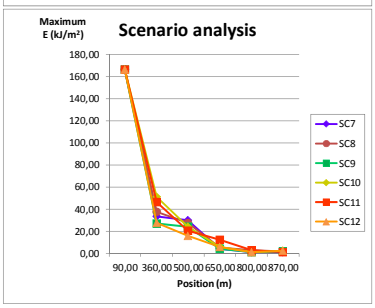

Figure 5.9: Results and analysis for scenarios 1 to 12.

Scenario	Position		Maximum E
	Number	x (m)	(kJ/m²)
SC13	1	90,00	**1,46**
	2	360,00	**1,58**
	3	488,01	**0,00**
	4	650,00	**0,00**
	5	800,00	**0,00**
	6	870,00	**0,00**
SC14	1	90,00	**1,73**
	2	360,00	**1,26**
	3	556,31	**0,00**
	4	650,00	**0,00**
	5	800,00	**0,00**
	6	870,00	**0,00**
SC15	1	90,00	**1,46**
	2	360,00	**2,19**
	3	419,81	**0,00**
	4	650,00	**0,00**
	5	800,00	**0,00**
	6	870,00	**0,00**
SC16	1	90,00	**1,46**
	2	360,00	**1,53**
	3	490,21	**0,00**
	4	650,00	**0,00**
	5	800,00	**0,00**
	6	870,00	**0,00**
SC17	1	90,00	**1,81**
	2	360,00	**1,26**
	3	558,71	**0,00**
	4	650,00	**0,00**
	5	800,00	**0,00**
	6	870,00	**0,00**
SC18	1	90,00	**1,46**
	2	360,00	**1,85**
	3	422,21	**0,00**
	4	650,00	**0,00**
	5	800,00	**0,00**
	6	870,00	**0,00**

Scenario	Position		Maximum E
	Number	x (m)	(kJ/m²)
SC19	1	90,00	**1,46**
	2	360,00	**1,26**
	3	496,41	**6,67**
	4	650,00	**0,59**
	5	800,00	**0,09**
	6	870,00	**0,24**
SC20	1	90,00	**1,46**
	2	360,00	**1,26**
	3	564,71	**6,79**
	4	650,00	**0,63**
	5	800,00	**0,08**
	6	870,00	**0,19**
SC21	1	90,00	**1,46**
	2	360,00	**1,28**
	3	428,21	**6,32**
	4	650,00	**0,49**
	5	800,00	**0,12**
	6	870,00	**0,31**
SC22	1	90,00	**1,46**
	2	360,00	**1,25**
	3	494,41	**3,44**
	4	650,00	**0,56**
	5	800,00	**0,26**
	6	870,00	**0,25**
SC23	1	90,00	**1,46**
	2	360,00	**1,26**
	3	562,71	**3,14**
	4	650,00	**0,43**
	5	800,00	**0,17**
	6	870,00	**0,17**
SC24	1	90,00	**1,46**
	2	360,00	**1,36**
	3	426,21	**3,78**
	4	650,00	**0,46**
	5	800,00	**0,13**
	6	870,00	**0,25**

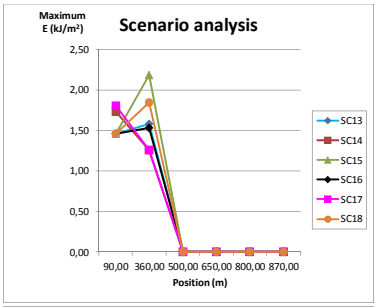

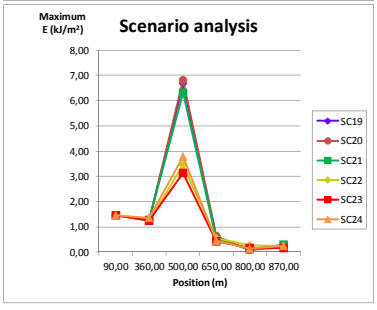

Figure 5.10: Results and analysis for scenarios 13 to 24.

Scenario	Position		Maximum E
	Number	x (m)	(kJ/m²)
SC25	1	90,00	**4,46**
	2	360,00	**4,55**
	3	488,01	**0,00**
	4	650,00	**0,00**
	5	800,00	**0,00**
	6	870,00	**0,00**
SC26	1	90,00	**5,28**
	2	360,00	**3,76**
	3	556,31	**0,00**
	4	650,00	**0,00**
	5	800,00	**0,00**
	6	870,00	**0,00**
SC27	1	90,00	**4,46**
	2	360,00	**6,19**
	3	419,81	**0,00**
	4	650,00	**0,00**
	5	800,00	**0,00**
	6	870,00	**0,00**
SC28	1	90,00	**4,46**
	2	360,00	**4,64**
	3	490,21	**0,00**
	4	650,00	**0,00**
	5	800,00	**0,00**
	6	870,00	**0,00**
SC29	1	90,00	**6,20**
	2	360,00	**6,20**
	3	558,71	**0,00**
	4	650,00	**0,00**
	5	800,00	**0,00**
	6	870,00	**0,00**
SC30	1	90,00	**4,46**
	2	360,00	**5,33**
	3	422,21	**0,00**
	4	650,00	**0,00**
	5	800,00	**0,00**
	6	870,00	**0,00**

Scenario	Position		Maximum E
	Number	x (m)	(kJ/m²)
SC31	1	90,00	**4,46**
	2	360,00	**3,76**
	3	496,41	**10,41**
	4	650,00	**1,47**
	5	800,00	**0,20**
	6	870,00	**0,18**
SC32	1	90,00	**4,46**
	2	360,00	**3,76**
	3	564,71	**10,58**
	4	650,00	**1,49**
	5	800,00	**0,22**
	6	870,00	**0,64**
SC33	1	90,00	**4,46**
	2	360,00	**3,75**
	3	428,21	**9,52**
	4	650,00	**1,37**
	5	800,00	**0,26**
	6	870,00	**0,77**
SC34	1	90,00	**4,46**
	2	360,00	**3,76**
	3	494,41	**5,81**
	4	650,00	**1,05**
	5	800,00	**0,16**
	6	870,00	**0,15**
SC35	1	90,00	**4,46**
	2	360,00	**3,76**
	3	562,71	**5,24**
	4	650,00	**1,35**
	5	800,00	**0,17**
	6	870,00	**0,21**
SC36	1	90,00	**4,46**
	2	360,00	**4,07**
	3	426,21	**6,78**
	4	650,00	**1,40**
	5	800,00	**0,17**
	6	870,00	**0,19**

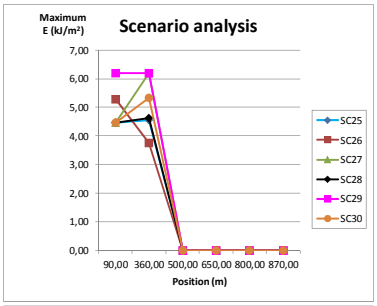

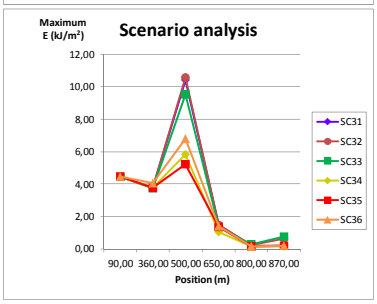

Figure 5.11: Results and analysis for scenarios 25 to 36.

Scenario	Position		Maximum E
	Number	x (m)	(kJ/m²)
SC37	1	90,00	**14,87**
	2	360,00	**12,66**
	3	488,01	**2,83**
	4	650,00	**0,00**
	5	800,00	**0,00**
	6	870,00	**0,00**
SC38	1	90,00	**18,01**
	2	360,00	**11,08**
	3	556,31	**2,51**
	4	650,00	**0,00**
	5	800,00	**0,00**
	6	870,00	**0,00**
SC39	1	90,00	**14,87**
	2	360,00	**17,44**
	3	419,81	**3,36**
	4	650,00	**0,00**
	5	800,00	**0,00**
	6	870,00	**0,00**
SC40	1	90,00	**14,87**
	2	360,00	**11,04**
	3	490,21	**3,61**
	4	650,00	**1,30**
	5	800,00	**0,39**
	6	870,00	**0,32**
SC41	1	90,00	**14,87**
	2	360,00	**11,08**
	3	558,71	**3,03**
	4	650,00	**1,66**
	5	800,00	**0,43**
	6	870,00	**0,35**
SC42	1	90,00	**14,87**
	2	360,00	**15,45**
	3	422,21	**3,98**
	4	650,00	**0,67**
	5	800,00	**0,27**
	6	870,00	**0,23**

Scenario	Position		Maximum E
	Number	x (m)	(kJ/m²)
SC43	1	90,00	**14,87**
	2	360,00	**11,07**
	3	496,41	**15,12**
	4	650,00	**3,59**
	5	800,00	**0,54**
	6	870,00	**1,41**
SC44	1	90,00	**14,87**
	2	360,00	**11,08**
	3	564,71	**15,48**
	4	650,00	**2,44**
	5	800,00	**0,49**
	6	870,00	**1,52**
SC45	1	90,00	**14,87**
	2	360,00	**11,18**
	3	428,21	**15,83**
	4	650,00	**3,42**
	5	800,00	**0,59**
	6	870,00	**1,64**
SC46	1	90,00	**14,87**
	2	360,00	**11,07**
	3	494,41	**9,23**
	4	650,00	**4,29**
	5	800,00	**0,44**
	6	870,00	**1,27**
SC47	1	90,00	**14,87**
	2	360,00	**11,08**
	3	562,71	**8,22**
	4	650,00	**4,75**
	5	800,00	**0,40**
	6	870,00	**1,21**
SC48	1	90,00	**14,87**
	2	360,00	**12,27**
	3	426,21	**11,03**
	4	650,00	**4,11**
	5	800,00	**0,44**
	6	870,00	**1,15**

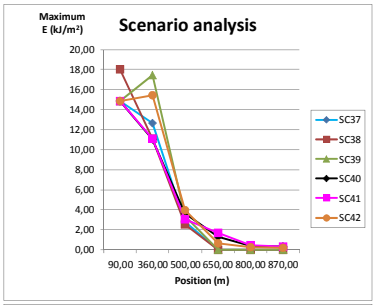

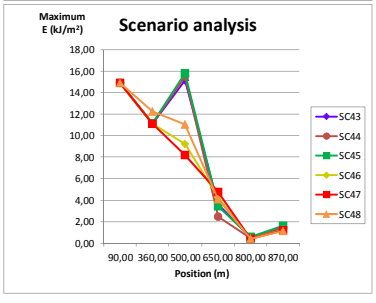

Figure 5.12: Results and analysis for scenarios 37 to 48.

Scenario	Position		Maximum E
	Number	x (m)	(kJ/m²)
SC49	1	90,00	**29,18**
	2	360,00	**19,62**
	3	488,01	**4,24**
	4	650,00	**1,83**
	5	800,00	**0,46**
	6	870,00	**0,40**
SC50	1	90,00	**29,41**
	2	360,00	**19,70**
	3	556,31	**3,46**
	4	650,00	**3,11**
	5	800,00	**0,60**
	6	870,00	**0,50**
SC51	1	90,00	**29,18**
	2	360,00	**34,24**
	3	419,81	**5,22**
	4	650,00	**0,00**
	5	800,00	**0,00**
	6	870,00	**0,00**
SC52	1	90,00	**29,18**
	2	360,00	**19,66**
	3	490,21	**4,69**
	4	650,00	**3,80**
	5	800,00	**0,67**
	6	870,00	**0,95**
SC53	1	90,00	**29,18**
	2	360,00	**19,70**
	3	558,71	**4,20**
	4	650,00	**3,93**
	5	800,00	**0,28**
	6	870,00	**0,88**
SC54	1	90,00	**29,18**
	2	360,00	**27,41**
	3	422,21	**6,20**
	4	650,00	**2,05**
	5	800,00	**0,37**
	6	870,00	**0,88**

Scenario	Position		Maximum E
	Number	x (m)	(kJ/m²)
SC55	1	90,00	**29,18**
	2	360,00	**19,70**
	3	496,41	**23,11**
	4	650,00	**3,15**
	5	800,00	**0,71**
	6	870,00	**2,19**
SC56	1	90,00	**29,18**
	2	360,00	**19,70**
	3	564,71	**20,60**
	4	650,00	**3,51**
	5	800,00	**0,76**
	6	870,00	**2,38**
SC57	1	90,00	**29,18**
	2	360,00	**20,64**
	3	428,21	**19,93**
	4	650,00	**6,53**
	5	800,00	**0,81**
	6	870,00	**2,42**
SC58	1	90,00	**29,18**
	2	360,00	**19,69**
	3	494,41	**12,97**
	4	650,00	**6,31**
	5	800,00	**0,63**
	6	870,00	**1,10**
SC59	1	90,00	**29,18**
	2	360,00	**19,70**
	3	562,71	**12,36**
	4	650,00	**6,28**
	5	800,00	**0,63**
	6	870,00	**1,77**
SC60	1	90,00	**29,18**
	2	360,00	**22,60**
	3	426,21	**14,31**
	4	650,00	**4,11**
	5	800,00	**0,70**
	6	870,00	**1,95**

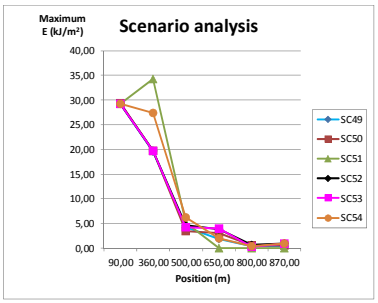

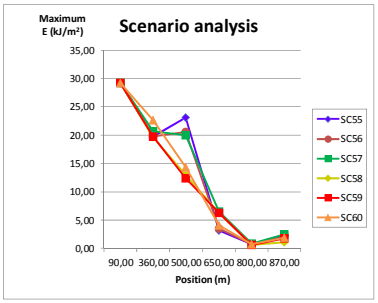

Figure 5.13: Results and analysis for scenarios 49 to 60.

- Emerged breakwaters:
  - For significant wave height H_s= 6,64m and up to position number 3, the maximum wave energy follows the same pattern observed in the Initial scenarios, that is, a very steep decrease in wave energy in the windward side of the detached breakwater. From this position to the shore negligible energy variations are verified (Figure 5.9). This fact is justified by the detached breakwater influence in wave height;
  - As the significant wave height decreases there is an increasing maximum wave energy in position number 2 certainly due to the addition of the incident and reflective waves in the windward side of the detached breakwater;
  - For significant wave heights $H_s \leq$ 2,00m, the detached breakwater has a great influence in the decrease of the maximum wave energy due to the fact that there is no overtopping on the detached breakwater (Figure 5.10 and 5.11);
  - For each of all significant wave heights it is observed that in position number 3 the values of the maximum wave energy converge to the same value;
  - For significant wave heights $H_s \geq$ 3,00m the bathymetry near the shore slightly influences maximum wave energy (Figures 5.9, 5.12, and 5.13).

- Submerged breakwaters:
  - For all significant wave heights the maximum wave energy in position number 3 is always higher when the crest level h_{cr}= -1,50m comparing to the values obtained when h_{cr}= -0,50m;
  - For each crest level (h_{cr}= -1,50m and h_{cr}= -0,50m) it is verified that the maximum wave energy in position number 3 is independent from the distance of the detached breakwater to the shore, X;
  - For all significant wave heights there is a substantial increase of the maximum wave energy from position numbers 2 to 3 when the crest level is h_{cr}= -1,50m. The same findings are apparent when the crest level is h_{cr}= -0,50m only for significant wave heights $H_s \leq$ 2,00m (Figures 5.10 and 5.11);
  - For all the scenarios, a decreasing wave energy is observed due to a significant bathymetric effect from position number 4 to the shore.

In general:

- In all the studied scenarios the maximum wave energy over the detached breakwater (position number 3) is always higher in submerged than in emerged detached breakwaters, as expected;
- Comparing the results obtained for the maximum wave energy in position number 3 it is observed that in emerged detached breakwaters there is a decrease in the maximum wave energy converging to a same value whereas in submerged detached breakwaters the maximum wave energy at the same location increase reaching 2 different values, one for crest level h_{cr}= -1,50m and other for crest level h_{cr}= -0,50m. This means that in emerged detached breakwaters there is a total energy dissipation while in submerged detached breakwaters a partial energy dissipation is verified.

CHAPTER 6

2D modelling. Results and discussions

'The mind that opens to a new idea never returns to its original size.'

Albert Einstein (1879 – 1955)

(Page intentionally left blank)

CHAPTER 6 2D MODELLING. RESULTS AND DISCUSSIONS

The models herein presented were created to study the influence of detached breakwaters and wave orientations on the significant wave heights and residual velocities near the shore and the detached breakwaters. Different detached breakwater heights, different incident wave heights, periods and orientation, and number and length of detached breakwaters were analysed in this study.

6.1 Scenarios

For this model a set of twenty four scenarios was considered. The smaller number of simulations in BOUSS-2D, compared to those simulated in COULWAVE, was due to the need to simplify and benefit from conclusions drawn from that model. It was found that during the models simulation in COULWAVE the wave heights generally decreased significantly when the detached breakwater was 235m away from the coast, while for other distances this reduction was not so significant. Therefore, for models to be created in BOUSS-2D it was only considered this distance from the shore to the detached breakwater. Regarding the detached breakwater crest levels two alternatives were considered: one for emerged detached breakwaters with h_{cr}= 2,70m (the most efficient solution for all the scenarios obtained in COULWAVE); and another for submerged detached breakwaters with h_{cr}= -0,50m (the most efficient solution obtained in COULWAVE when dealing with the most frequent wave heights). Relatively to the incident wave heights were chosen only two of the initial set analysed in COULWAVE. The choice had to consider the storm situation (H_s= 6,64m) and a frequent wave height that is verified throughout the year (H_s= 2,0m).

In this study were analysed the influence of different wave and detached breakwater conditions on significant wave heights and residual velocities near the shore and the detached breakwaters. The characteristics of the scenarios correspond to the:

- Two detached breakwater crest levels: h_{cr}= 2,70m, h_{cr}= -0,50m;
- One value for distance from shore to the detached breakwater: X= 235m;
- Two incident wave heights: H_s= 6,64m, H_s= 2,0m;
- Two wave periods: T= 9,30s, T= 7,00s;
- Three wave orientations: 270º, 315º, 225º;
- One or two number of detached breakwater per scenario;
- Two detached breakwater lengths: L= 470m; L= 235m;

– Gap between two detached breakwaters: G= 115m.

The detached breakwater length and gap assumed were calculated in Chapter 3. In the situations where two breakwaters are introduced, the length of each equals to half the length of the detached breakwater calculated in the same Chapter.

Similar to what was done in COULWAVE all the detached breakwaters were designed to have a crest width, B, of 9,40m. Because the grid spacing is 10m, in order to represent the detached breakwater in the model it was considered only one cell.

Since Bouss-2D uses the reference level of the free surface, the elevation of the detached breakwater were compatibilized with the HAT level (h_{cr}= 0,70m, h_{cr}= -2,50m).

Furthermore six additional scenarios (named Initial) were included considering identical situations referred before without the presence of the detached breakwater.

Tables 6.1 and 6.2 summarize the chosen scenarios for this study.

Table 6.1: Scenarios with the inclusion of detached breakwater.

Wave characteristics				Breakwater characteristics					Scenario
H_s (m)	T (s)	Direction (°)		X (m)	h_{cr} (m)	Number	G (m)	L (m)	
2,00	7,00	270,00	→	235,00	2,70	1	---	470,00	SC1
						2	115,00	235,00	SC2
					-0,50	1	---	470,00	SC3
						2	115,00	235,00	SC4
		315,00	↘		2,70	1	---	470,00	SC5
						2	115,00	235,00	SC6
					-0,50	1	---	470,00	SC7
						2	115,00	235,00	SC8
		225,00	↗		2,70	1	---	470,00	SC9
						2	115,00	235,00	SC10
					-0,50	1	---	470,00	SC11
						2	115,00	235,00	SC12
6,64	9,30	270,00	→	235,00	2,70	1	---	470,00	SC13
						2	115,00	235,00	SC14
					-0,50	1	---	470,00	SC15
						2	115,00	235,00	SC16
		315,00	↘		2,70	1	---	470,00	SC17
						2	115,00	235,00	SC18
					-0,50	1	---	470,00	SC19
						2	115,00	235,00	SC20
		225,00	↗		2,70	1	---	470,00	SC21
						2	115,00	235,00	SC22
					-0,50	1	---	470,00	SC23
						2	115,00	235,00	SC24

Table 6.2: Scenarios without the inclusion of detached breakwater.

Wave characteristics					Scenario
H_s (m)	T (s)	X (m)	Direction (°)		
2,00	7,00	235,00	270,00	→	Initial1
			315,00	↘	Initial2
			225,00	↗	Initial3
6,64	9,30	235,00	270,00	→	Initial4
			315,00	↘	Initial5
			225,00	↗	Initial6

As mentioned before and unlike what was done in the COULWAVE model, the analysis is going to be made along the beach and the vicinity of the detached breakwater domain instead of taking observations at a specific point.

Before proceeding with the analysis of the scenarios, it is important to underline that a study for the possibility of inclusion of a boundary condition (porosity type) in the vicinity of a detached breakwater was carried out. Similarly to the damping boundary condition, the porosity value also varies from 0,0 to 1,0. A value of 0,0 corresponds to an impermeable structure, while a value of near 1,0 would correspond to a highly porous structure. Typical porosity for stone type breakwaters is 0,4. Taking into account this, it was studied the influence of this type of boundary near the detached breakwater on the significant wave height results. It was then considered a porosity value of 0,4 and a width of 5 meters for two different scenarios: one with an emerged and other with a submerged detached breakwater. For this study were selected the scenarios SC1 and SC3. In Figure 6.1 the yellow line near the detached breakwater represents the porosity boundary. Figure 6.1 (left) depicts the difference in results between scenario SC1 with the porosity boundary and without the porosity boundary. Similarly, Figure 6.1 (right) represents the difference in results between scenario SC3 with the porosity boundary and without the porosity boundary.

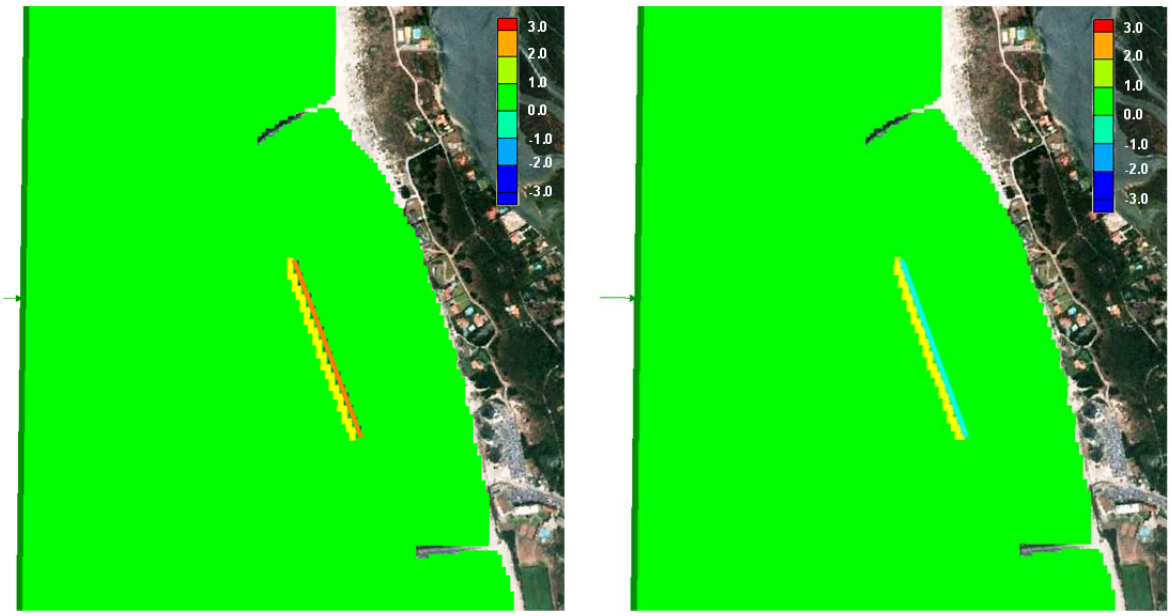

Figure 6.1: Difference in significant wave heights results with and without a porosity boundary (SC1 on the left and SC3 on the right).

Considering the results presented for both situations it is possible to state that there is no influence of this porosity boundary in the vicinity of the detached breakwater: all domain is represented in green which reveals that the difference in results is between 0 and 1m.

This study was concentrated in results of residual velocities near the vicinity of the detached breakwater and near the beach and groins. Also comparisons of significant wave heights obtained for initial conditions scenarios and scenarios that include breakwaters are presented. The analysis proceeds with the comparison of the submerged and emerged detached breakwaters situations and finalises with a comparison between the existence of two detached breakwaters and one detached breakwater. In order to briefly present which scenarios were analysed and how the study was done, Table 6.3 organizes a list of comparisons taken for the BOUSS-2D models. This table is divided in two major columns: residual velocity and significant wave height. In the first major column is observed that the residual velocity analysis was performed in Initial conditions and in the remaining twenty-four scenarios, whereas in the second major column an analysis of the significant wave height using the scenario comparison was made. In the first case the comparison is made between conditions without detached breakwater (Initial) and with detached breakwater (SC) for the same height, period and orientation conditions. In the second case a comparison is made between conditions with submerged detached breakwater and emerged detached breakwater for the same conditions of height, period and orientation of the wave, and same detached breakwater length conditions. Lastly, in the third case a comparison is made between conditions with two detached

breakwater (Duo) and one detached breakwater (Solo) for the same conditions of height, period and orientation of the wave, and same detached breakwater crest height conditions.

As an example of the meaning of the acronyms presented in the Table 6.3, Hi1 stands for significant wave height in Initial1 situation, whereas H1 stands for significant wave height for SC1

Table 6.3: Scenario analysis considered.

Residual Velocities	Relative Significant Wave Height		
	Initial – SC	**Submerged – Emerged**	**Duo – Solo**
Initial1	Hi1 – H1	H3 – H1	H2 – H1
Initial2	Hi1 – H2	H4 – H2	H4 – H3
Initial3	Hi1 – H3	H7 – H5	H6 – H5
Initial4	Hi1 – H4	H8 – H6	H8 – H7
Initial5	Hi2 – H5	H11 – H9	H10 – H9
Initial6	Hi2 – H6	H12 – H10	H12 – H11
SC1	Hi2 – H7	H15 – H13	H14 – H13
SC2	Hi2 – H8	H16 – H14	H16 – H15
SC3	Hi3 – H9	H19 – H17	H18 – H17
SC4	Hi3 – H10	H20 – H18	H20 – H19
SC5	Hi3 – H11	H23 – H21	H22 – H21
SC6	Hi3 – H12	H24 – H22	H24 – H23
SC7	Hi4 – H13	---	---
SC8	Hi4 – H14	---	---
SC9	Hi4 – H15	---	---
SC10	Hi4 – H16	---	---
SC11	Hi5 – H17	---	---
SC12	Hi5 – H18	---	---
SC13	Hi5 – H19	---	---
SC14	Hi5 – H20	---	---
SC15	Hi6 – H21	---	---
SC16	Hi6 – H22	---	---
SC17	Hi6 – H23	---	---
SC18	Hi6 – H24	---	---
SC19	---	---	---
SC20	---	---	---
SC21	---	---	---
SC22	---	---	---
SC23	---	---	---
SC24	---	---	---

6.2 Results

For each scenario, the residual velocity was calculated for the all beach domain between groins originating 30 different results. Also, it was studied the difference in significant wave height results between scenarios Initial and scenarios with detached breakwater (Initial – SC), submerged and emerged (Submerged – Emerged), and duo and solo (Duo – Solo) detached breakwater situations. The total number of scenarios for the Initial – SC comparison is 24, for the Submerged – Emerged is 12 and for the Duo – Solo is also 12.

As an example, Figure 6.2 depicts the output of the residual velocity simulation for scenario 1 (SC1), Figure 6.3 the output of the difference in significant wave height results between scenario Initial and scenario with detached breakwater (Initial1 – SC1), Figure 6.4 the output of the difference in significant wave height results between submerged and emerged detached breakwater scenario (SC3 – SC1) and finally, Figure 6.5 the output of the difference in significant wave height results between duo and solo detached breakwater scenario (SC2 – SC1). The results for significant wave heights and residual velocities are calculated for a recommended simulation period as well as the differences between significant wave heights for different scenarios. The remaining results for the scenarios left are presented in APPENDIX 8 (residual velocity), APPENDIX 9 (significant wave height: Initial – SC), APPENDIX 10 (significant wave height: Submerged – Emerged) and APPENDIX 11 (significant wave height: Duo breakwater – Solo breakwater).

SC1

Figure 6.2: Residual velocity in all beach domain (SC1).

Hi1 – H1

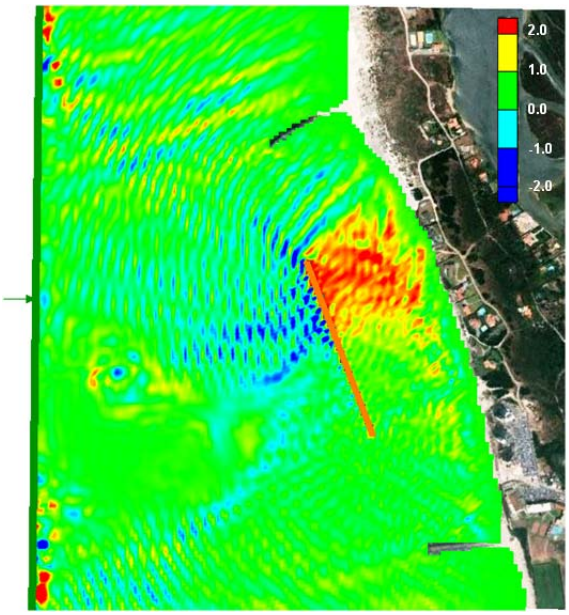

Figure 6.3: Difference in significant wave height results between scenario Initial and scenario with detached breakwater (Initial1 – SC1).

H3 – H1

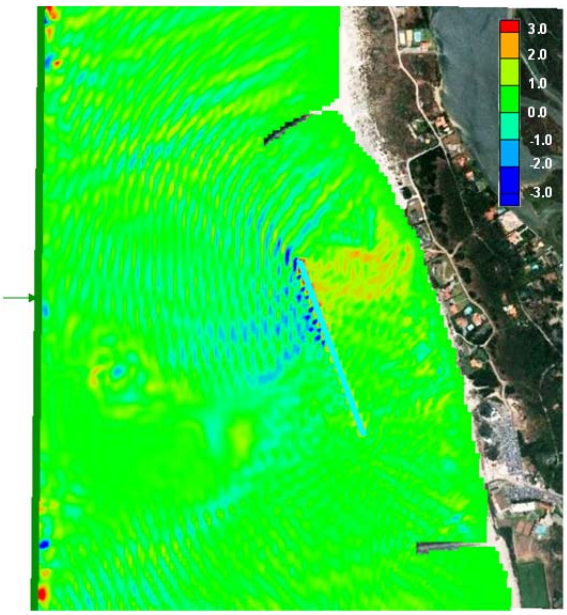

Figure 6.4: Difference in significant wave height results between submerged and emerged detached breakwater scenario (SC3 – SC1).

H2 – H1

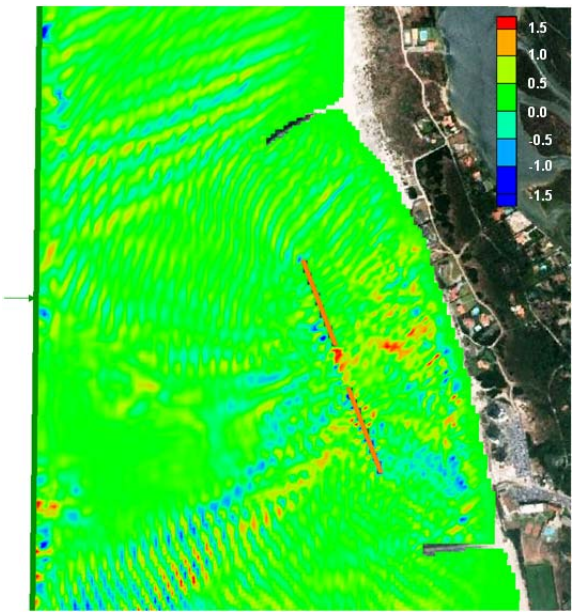

Figure 6.5: Difference in significant wave height results between duo and solo detached breakwater scenario (SC2 – SC1).

6.3 Discussion of the results

The magnitude and the direction of the significant wave height, H_s, as well as the crest level, h_{cr}, and the number of detached breakwaters were the parameters selected for understanding the variability of the water residual velocity and consequently the sediment transport behaviour. Also situations with and without detached breakwaters were used to predict the influence of these structures on the significant wave height, H_s.

6.3.1 Results for residual velocity in Initial scenarios

In Appendix 8 the results obtained for residual velocity in Initial scenarios (Initial1 to Initial6) simulate the water dynamics with different significant wave height and direction from where the following comments can be observed:

- For the same significant wave direction it is noted that for lower waves the residual velocity is lower in the scenarios Initial1 to Intial3 (noticeable by low or null velocities) and for higher significant waves (scenarios Initial4 to Initial6) occurs the formation of localized vortices depending on the significant wave direction;
- The significant wave direction determines the residual velocity orientation as can be observed comparing Initial1, Initial2, Initial3 and Initial4, Initial5, Initial6. This effect is more evident when comparing Initial5 with Initial6 where a reverse direction of the residual velocity is perceived;
- It is apparent that the presence of the groins could originate erosive fluxes in the coastal zone at the full length between groins being more significant for NW significant wave direction (Initial 2 and Initial5);
- The vortices formation and location is highly dependent on the bathymetry and the significant wave direction;
- For all the scenarios a significant erosion effect could be observed at the leeward side of both groins. Conversely a significant accretion effect could be observed at the windward side of the South groin (except for the Initial1 scenario) and of the North groin (except for the Initial1, Initial2 and Initial5 scenarios).

6.3.2 Results for residual velocity in scenarios with detached breakwater

In Appendix 8 the results obtained for residual velocity in scenarios with duo and solo, submerged and emerged detached breakwaters (SC1 to SC12 for significant wave height of 2,00m and SC13 to SC24 for significant wave height of 6,64m) simulate the water dynamics with different significant direction. Comments on results obtained are the following:

- For significant wave height of 2,00m:
  - Direction 270º: comparing the residual velocities verified in Intial1 scenario, it is verified that the maximum residual velocities in scenarios SC3 and SC4 (submerged detached breakwaters) are similar and in SC1 and SC2 (emerged detached breakwaters) are greater. In addition, it is verified that the residual velocities are higher for SC2 (duo detached breakwater) than for SC1 (solo detached breakwater). Also, a high circular movement is verified in submerged detached breakwaters, different from the emerged detached breakwaters;
  - Direction 270º: the salient/tombolo formation is more evident for emerged detached breakwaters than for submerged detached breakwaters where this phenomenon is hard to predict. The accretion process (lower velocities) is more apparent in the situations of duo detached breakwaters probably due to their largest occupation;
  - Direction 315º: the results obtained in the scenarios with this wave direction (Initial2, SC5 to SC8) are similar to those obtained with direction 270º. However in SC8 a very unstable situation is observed in the leeward side of the detached breakwater;
  - Direction 225º: the overall behaviour of water circulation is similar to those observed for the other two directions. In this case, the effect of the detached breakwaters is more effective, mainly in SC9 and SC10. Observing the submerged detached breakwaters, it can be emphasized that the detached breakwater in SC11 appears to be more efficient in sediment retention.

- For significant wave height of 6,64m:
  - A generalised erosion in the coastal zone between groins due to high residual velocities is observed in all the scenarios (SC13 to SC24). This is probably justified by the formation of a channel between the detached breakwater and the coastline;

- Due to this significant wave height the breakwaters behave as submerged detached breakwaters independently of its crest level. This justifies the slight difference verified in the residual velocities in all scenarios;
- In these scenarios the groins effect in accretion appears to be more significant than the presence of detached breakwaters.

6.3.3 Results for significant wave height comparing Initial scenarios with scenarios with detached breakwaters

In Appendix 9 the results of the effect of detached breakwaters on the significant wave height are presented. These results were obtained by means of the difference between the significant wave height in Initial scenarios and the correspondent significant wave height in scenarios with detached breakwaters. Comments on results obtained are the following:

- For significant wave height of 2,00m:
  - Direction 270º: the effect in wave height reduction of emerged detached breakwaters is higher than that of the submerged ones. In addition it can be observed that this effect is slightly higher in the Hi1-H1 than in the Hi1-H2 scenarios. Also it is verified that the southern part of the detached breakwaters (solo and duo) has no influence in wave height reduction. Negative difference of wave heights is registered in the windward side of the emerged detached breakwaters (Hi1– H1 to Hi1– H4);
  - Direction 315º: the difference between significant wave heights is highly dependent on the wave direction. In this case the wave height reduction is apparent through the entire detached breakwater length. Also it is verified that the southern part of the duo detached breakwaters causes higher wave height differences than the correspondent part of the solo detached breakwaters (Hi2– H5 to Hi2– H8);
  - Direction 225º: the difference between significant wave heights is highly dependent on the wave direction determining that only the southern part of the detached breakwaters is effective. Also, duo detached breakwaters causes higher wave height differences than the correspondent part of the solo detached breakwaters (Hi3– H9 to Hi3– H12);
  - For all wave directions it is observed that in the windward side of the submerged detached breakwaters there is no differences in wave heights;
  - The results obtained for the scenarios considering wave direction of 315º are always higher than those obtained for the correspondent scenarios in directions 270º and 225º.

- For significant wave height of 6,64m:
  - Direction 270º: it is observed that the negative wave height differences are higher for the windward side of the submerged than for the emerged detached breakwaters. Also, the detached breakwater is effective in wave height reduction in its total length (Hi4− H13 to Hi4− H16);
  - Direction 315º: a negative wave height difference is verified in the windward side of the detached breakwaters being more evident in the submerged detached breakwaters. A positive difference of wave heights is observed in the northern part of the submerged detached breakwaters. Also, the detached breakwater is effective in wave height reduction in its total length (Hi5− H17 to Hi5− H20);
  - Direction 225º: the higher positive differences in wave height are observed in the southern part of the detached breakwaters. For all the scenarios it is observed that there is not a negative difference in wave height in the windward side of the detached breakwaters. Also, it is verified a high influence of the wave direction in the difference between significant wave heights (Hi6− H21 to Hi6− H24).

6.3.4 Results for significant wave height comparing scenarios with submerged and emerged detached breakwaters

In Appendix 10 the results of the effect of detached breakwaters on the significant wave height are presented. These results were obtained by means of the difference between the significant wave height in submerged detached breakwater scenarios and the significant wave height in scenarios with emerged detached breakwaters. Comments on results obtained are the following:

- For direction 270º: for significant wave height of 2,00m there is a slight positive difference in the leeward side of the detached breakwater whereas a slight negative difference is verified in the windward side of the detached breakwater. For significant wave height of 6,64m there is no significant influence of the type of detached breakwater in its leeward side whereas a significant positive difference in wave height is observed in the windward side of the detached breakwater (H3−H1, H4−H2, H15−H13, H16−H14);
- For direction 315º: for significant wave height of 2,00m there is a positive difference in the leeward side of the detached breakwater whereas a negative difference is verified in the windward side of the detached breakwater. For significant wave height of 6,64m there is significant influence of the type of detached breakwater in its leeward side whereas

significant positive and negative differences in wave height are observed in the windward side of the detached breakwater (H7−H5, H8−H6, H19−H17, H20−H18);

- For direction 225º: for significant wave height of 2,00m there is a positive difference in the leeward side of the detached breakwater whereas a negative difference is verified in the windward side of the detached breakwater. For significant wave height of 6,64m there is significant influence of the type of detached breakwater in its leeward side whereas significant positive and negative differences in wave height are observed in the windward side of the detached breakwater (H11−H9, H12−H10, H23−H21, H24−H22).

6.3.5 Results for significant wave height comparing scenarios with duo and solo detached breakwaters

In Appendix 11 the results of the effect of detached breakwaters on the significant wave height are presented. These results were obtained by means of the difference between the significant wave height in duo detached breakwater scenarios and the significant wave height in scenarios with a solo detached breakwater. Comments on results obtained are the following:

- For significant wave height of 2,00m:
  - It is observed that for all the wave directions a positive difference in significant wave height at the detached breakwater gap location and a slight negative and positive difference near the shoreline (H2− H1 to H12− H11).

- For significant wave height of 6,64m:
  - It is observed that for most of the wave directions a positive difference in significant wave height at the detached breakwater gap location and for the wave directions 270º (H14− H13, H16− H15) and 315º (H18− H17, H20− H19) there is no influence of the type of the detached breakwater in its leeward side. For the wave direction 225º (H22− H21, H24− H23) it is observed a negative difference in wave height in the leeward side of the detached breakwaters and for the submerged detached breakwaters it is also verified a negative difference in its windward side.

CHAPTER 7

Discussion, conclusions and future works

'The important thing is not to stop questioning. Curiosity has its own reason for existing.'

Albert Einstein (1879 – 1955)

(Page intentionally left blank)

CHAPTER 7 DISCUSSION, CONCLUSIONS AND FUTURE WORK

7.1 Discussion. 1D modelling *versus* 2D modelling

This Subchapter aims to compare and make some comments about the results obtained from the analysis of two different numerical models in the same wave, domain and boundary conditions. One of these models was developed in COULWAVE (1D) and the other in BOUSS-2D. In order to make it easier to understand, Table 7.1 specifies all considerations taken for each model.

Table 7.1: Modelling conditions for COULWAVE and BOUSS-2D models.

MODELLING CONDITIONS		COULWAVE	BOUSS-2D
Wave height (m)		0,5	0,5
Wave period (s)		7,0	7,0
Depth (m)		Fixed: -4,0	Fixed: -4,0
Wave type		Wave spectrum (Irregular)	Irregular (unidirectional)
Spectrum type		TMA (shallow water)	TMA (shallow water)
Wave parameters		Gamma: 3,0 (default)	Min. wave period: 7s Max. wave period: 25s (default) Gamma: 3,3 (default)
Wave maker location (m)		60,0	100,0
xx domain (m)		260,0	200,0
yy domain (m)		---	100,0
Simulation time (s)		200,0	200,0
Observation points location (m)	First point	110,0	150,0
	Second point	160,0	200,0
	Third point	210,0	250,0
Boundaries	Left	Without sponge layer (reflective)	Wave maker
	Right	Without sponge layer (reflective)	Reflective
	Top	---	Porosity Width: 5,0m Value: 1,0
	Bottom	---	Porosity Width: 5,0m Value: 1,0
Courant number		0,3	0,6
Spacing/Cell dimension (m)		1,0	2,5 × 2,5

COULWAVE and BOUSS-2D have the same wave conditions (incident wave height, period and type) and fixed depth. Even though the x-domains are 260m and 200m, respectively, both models have the same x-domain because the wave source in the COULWAVE model was set at position 60m (260-60= 200m). Also for both models were placed observation points at equivalent positions and separated 50m from each point.

BOUSS-2D grid has its origin at (x,y)= (100,100) m while COULWAVE model has its origin at (x,y)= (0,0) m.

The choice of the boundary conditions in BOUSS-2D was imperative to allow the model to match the best way COULWAVE (1D) conditions. For this study the left boundary was set as irregular (unidirectional) wave type and the spectrum type selected was the TMA, which is the same as the COULWAVE's and is recommended for shallow waters. The wave maker parameters set were the recommended by BOUSS-2D. The top and bottom boundaries were defined as porosity layers with a width of 5m and a porosity value of 1 to make the domain boundaries the least reflective. In the right boundary was not applied any boundary condition, so it simulates a reflective wall condition (the same as in COULWAVE). In this model, as well as in the COULWAVE, was enabled the wave breaking option which allows dissipating wave energy. The wave run-up option was not considered though because there was no influence in the results.

For the COULWAVE model, the values of all the other parameters not mentioned here were the ones used in the COULWAVE models in Subchapter 4.1.

For both models had been observed the significant wave height recorded in a time simulation of 200 seconds at three observation points. Figure 7.1 depicts the BOUSS-2D model domain where the three observation points are represented thoroughly located at the centre of the grid. This way the results would be less influenced by possible reflection due to boundaries.

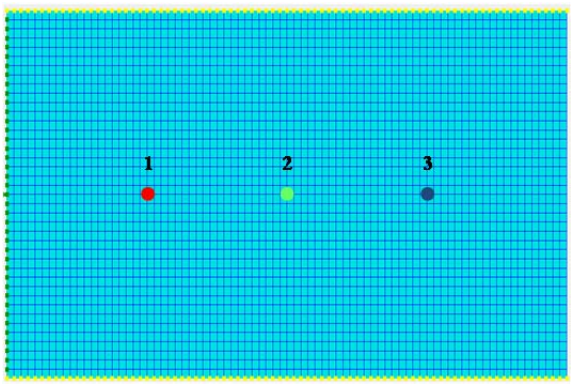

Figure 7.1: Observation points location for BOUSS-2D model.

From each observation point it is possible to observe the significant wave height registered throughout the 200s simulation. Figure 7.2 shows the COULWAVE results, whereas Figure 7.3 displays the BOUSS-2D results.

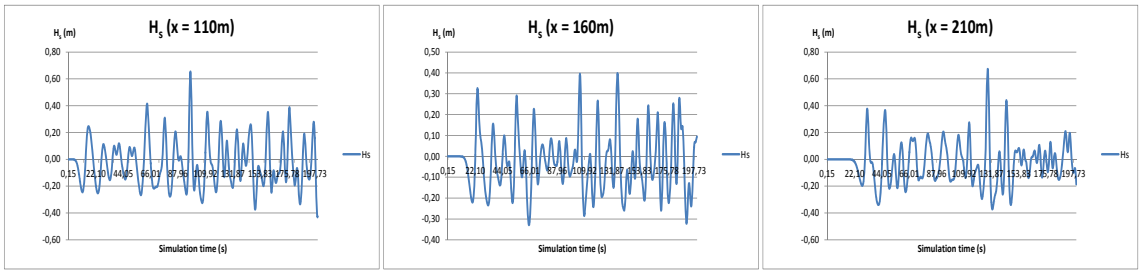

Figure 7.2: Significant wave height results at three observation points in COULWAVE.

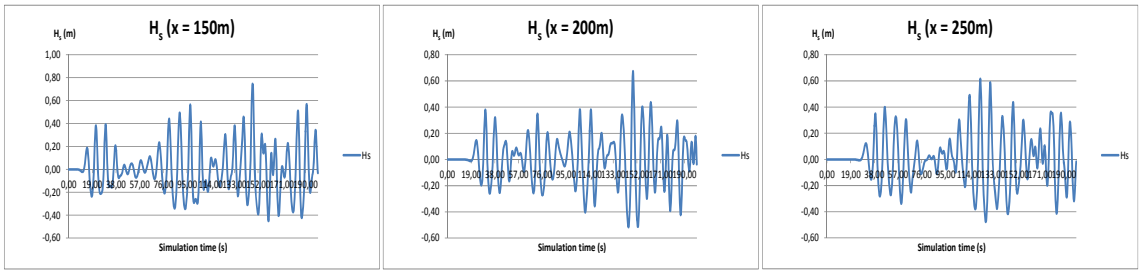

Figure 7.3: Significant wave height results at three observation points in BOUSS-2D.

It is slightly obvious the difference between the results of both models. At a first glance, the COULWAVE model appears to provide significant wave heights of a longer period relatively to the BOUSS-2D model: its results appear to be more widely spaced. In order to simplify the comparison of the results presented in Figures 7.2 and 7.3, Table 7.2 provides the maximum and minimum significant wave heights as well as the standard deviation at each observation point.

Table 7.2: Model results.

COULWAVE				BOUSS-2D			
Observation Point	**1st Point**	**2nd Point**	**3rd Point**	**Observation Point**	**1st Point**	**2nd Point**	**3rd Point**
Maximum H_s (m)	0,65	0,40	0,67	Maximum H_s (m)	0,75	0,67	0,62
Minimum H_s (m)	-0,43	-0,33	-0,37	Minimum H_s (m)	-0,45	-0,52	-0,48
Standard deviation	0,17	0,14	0,16	Standard deviation	0,21	0,19	0,20

The slight difference of results may be explained by differences in other parameters applied in each model. Regarding to the maximum significant wave height (H_s) analysis is visible that the largest difference is at the second observation point (0,27m). At the first observation point there is small difference of 0,10m, whereas at the third point the difference is negligibly of 0,05m.

Similarly to the maximum value differences, the largest difference in minimum significant wave height (H_s) is observed at the second observation point (0,19m). At the first observation point the difference is negligible (0,02m) and at the third point the difference is of 0,11m.

By examining the standard deviation obtained for each model it is evident a smaller value at all observation points in the COULWAVE model, which indicates that the data points tend to be closer to the mean comparing to the BOUSS-2D.

In conclusion, slight differences in maximum and minimum significant wave heights are observed with COULWAVE which could mean that this model appears to be more accurate than BOUSS-2D due to smaller values for standard deviation and because of its more complete mathematical model.

7.2 Conclusions

Coastal zone protection is a very crucial issue in order to protect populations and infrastructures as well as to environment conservation. Adequate tools must be tested and implemented for supporting engineering solutions to face its challenges.

In this research work, an inventory of existing modelling software to simulate hydrodynamics and sediment transport in coastal zones was presented. The applicability of these tools was tested in a real case study of a very vulnerable sandy beach. For this purpose 1D and 2D models were implemented considering both the presence of detached breakwaters or natural conditions aiming the study of the impact of these structures as protective measures in Ofir beach.

Good results were obtained applying COULWAVE 1D model in the analysis of detached breakwater effects on the significant wave height and wave energy considering its different types (submerged or emerged) and positioning relatively to the shoreline. For a significant wave height analysis it is evident that either submerged or emerged detached breakwaters have a substantial impact in decreasing the significant wave height. Conversely, submerged detached breakwaters have a smaller impact on significant wave heights when compared to the emerged detached breakwaters. In respect to wave energy it was verified that the maximum wave energy over the crest of the detached breakwater is higher in submerged (where partial energy dissipation is verified) than in emerged (with total energy dissipation) detached breakwaters.

2D model BOUSS-2D was applied in a HAT situation to assess the effect of two types of detached breakwaters (one continuous and other discontinuous) on the sediment transport pattern, analysing the water residual velocity fields and the significant wave height. From the obtained results it was

concluded that the water residual velocity is greatly influenced by the incident wave direction, the significant wave height, the crest level and the type of the detached breakwater. For low significant wave height the accretion process (lower velocities) is more apparent in the situations of duo detached breakwaters probably due to their largest occupation. Also, the salient/tombolo formation is more evident for emerged detached breakwaters than for submerged detached. For high significant wave height a generalised erosion in the coastal zone is observed probably justified by the formation of a channel between the detached breakwater and the coastline, situation in which the two types of detached breakwaters behave as submerged.

Comparing the performance of the two types of models (1D/2D) it can be concluded that the results obtained with the two are similar when the significant wave height is simulated, and only the 2D model is adequate to analyse residual velocity fields in the vicinity of the structures.

The methodology adopted in this research work where a generalised way of model application was used allows its replication to other coastal stretches being this application dependant on different local bathymetry.

7.3 Future works

Based on the results obtained in this study future developments can be made in the following research lines:

- Inclusion of different tidal conditions in hydrodynamic simulation for 1D modelling;
- Application of the COULWAVE 2D model and comparing hydrodynamics results with BOUSS-2D;
- Consideration of different distance and orientation of the detached breakwater relatively to the shoreline in 2D modelling;
- Use of the results obtained for water residual velocities as input for software able to simulate sediment transport dynamics;
- Extensive monitoring of the sea water hydrodynamics of Ofir beach for modelling calibration;
- Investment cost analysis for evaluation assessment of the different alternatives adopted for the detached breakwaters;
- Consideration of 3D hydrodynamic modelling together with wave-currents models for further analysis of hydrodynamics at Ofir beach.

(Page intentionally left blank)

REFERENCES

‘Do not go where the path may lead, go instead where there is no path and leave a trail.’

Ralph Waldo Emerson (1803 – 1882)

(Page intentionally left blank)

REFERENCES

Abbott, M. B.; Price, A.W. (1994) Coastal, estuarial, and harbour engineers' reference book. Taylor & Francis.

Antunes do Carmo, J.S. (2013) Experiência de recuperação de um sistema dunar e proposta de instrumentos complementares de proteção, atração e valorização ambiental. Revista de Gestão Costeira Integrada 13(3): 317-328.

Antunes do Carmo, J.S.; Neves, M.; Voorde, M. (2011) Designing a multifunctional artificial reef: studies on the influence of parameters with most influence in the vertical plane. Journal of Coastal Conservation 15(1): 99-112.

Aquaveo (2014). Aquaveo. BOUSS-2D. http://www.aquaveo.com/software/sms-bouss2d (last visited 21-09-2014).

Battjes, J.A. (1974). Surf similarity. Proc. 14th International conference on coastal engineering, pp 466–479.

Booij, N.; Ris, R.C.; Holthuijsen, L.H. (1999). A third-generation wave model for coastal regions, Part I, Model description and validation. Journal of Geophysical Research, 104(C4): 7649-7666.

BOUSS-2D (2001). BOUSS-2D: A Boussinesq wave model for coastal regions and harbors. Report 1, Theoretical background and user's manual. US Army Corps of Engineers, Engineer Research and Development Center.

Bradford, S. F. (2000). Numerical simulation of surf zone dynamics. Journal of Waterway, Port, Coastal and Ocean Engineering, ASCE, 126(1), 1-13.

Browder, A.E., Dean, R.G., Chen, R. (1996) Performance of a submerged breakwater for shore protection, ASCE, Vol. 2. Proceedings of the 25th International Conference Coastal Engineering, pp. 2312-2323, Orlando, Florida, USA .

Capitão, R.; Fortes, C. (2011). Análise comparativa entre estimativas do modelo SWAN e medições de agitação marítima efectuadas na Praia da Amoreira, Portugal. Revista da Gestão Costeira Integrada 11(3) :283-296.

Capitão, R.; Fortes, C.J.E.M.; Carvalho, F.; Coli, A.B.; Pinheiro, L.V. (2006). Wave regime characterization on the Portuguese coast using hindcast and wave propagation models. Coastal Engineering 2006: Proceedings of the 30th International Conference on Coastal Engineering, 1: 603-615.

Capitão, R.; Fortes, C.J.E.M.; Santos, J.A.; Pinheiro, L.V. (2009). In-situ and model wave characterization at the Alfeite beach. Journal of Coastal Research, SI56 (Proceedings of the 10th International Coastal Symposium): 168-172.

Carvalho, M.M.; Capitão, R.P.; Abreu, F.V.; Sobral, J.T. (1990). Ajustamento gráfico de distribuições. Nato PO-WAVES, Sub-projecto A, Instituto Hidrográfico. Laboratório Nacional de Engenharia Civil, Lisboa, Portugal 67 pp.

C.E.M. (2008) Shore protection projects. Coastal engineering manual. Vol. 1100. U.S. Army Corps of Engineers.

Challinor, S.; Hall, H. (2008). Multi-functional artificial reefs scoping study, CIRIA.

Chen, B.F.; Chen, P.H. (2001) Fully nonlinear waves past submerged and floating breakwater, Proceedings of the XXIX IAHR Congress, Beijing, China.

CIRIA/CUR (2007) CIRIA. CIRIA, 773–908.

Corbett, B.; Jackson, L.A.; Evans, T.; Restall, S. (2010) Comparison of geosynthetic materials as substrates on coastal structures – Gold Coast (Australia) and Arabian Gulf: 1-7.

Costa, G.M.S. (2009). Modelação de Quebramares Destacados. Departamento de Engenharia Civil, Faculdade de Engenharia da Universidade do Porto, Portugal.

DEFRA (2010). Department for Environment Food and Rural Affairs. Guidance for outline design of nearshore detached breakwaters on sandy macro-tidal coasts. Environment Agency of United Kingdom.

Deltares (2013). Eco-engineering in the Netherlands. Soft interventions with a solid impact. Rijkswaterstaat Ministry of Infrastructure and the Environment, the Nertherlands.

Deltares (2014a) Eco-engineering. http://www.innoverenmetwater.nl/upload/documents/Eco%20engineering%20(brochure).pdf (last visited 25-02-2014).

Deltares (2014b). Delft 3D. http://oss.deltares.nl/web/delft3d (last visited 22-02-2014).

Demirbilek, Z.; Zundel, A.; Nwogu, O. (2005). BOUSS-2D Wave Model in the SMS: 1. Graphical Interface. US Army Corps of Engineers.

DHI (2013). MIKE21. Danish Hydraulic Institute. http://www.dhisoftware.com (last visited 22-02-2014).

Di Bona, S.; Trigo-Teixeira, A.; Ruol, P. (2013) Costaline change – Longterm simulation in the Vagueira region. 2ª Conferência sobre Morfodinâmica Estuarina e Costeira. Universidade de Aveiro.

Dias, J.A.; Klein, A.; Freire, P.; Silva, P.; Freitas, C. (2011). The importance of estuarine and coastal morphodynamics in littoral management. Journal of Integrated Coastal Zone Management 11(3): 271-272.

Douyère, Y.M.J. (2003). Analysis of Harbor Oscillation with a Boussinesq Model. University of Hawaii.

French, P.W. (2002) Coastal Defences: Processes Problems and Solutions. Routledge.

Gilbert, J.; Vellinga, P. (1990). IPCC response strategies working group coastal zone management Report 05.

Gomes, G.D.M.L. (2011). Previsão das configurações da costa na proximidade. Departamento de Engenharia Civil da Universidade do Minho, Portugal.

Guilherme, L.; Santos, J.A.; Fortes, C.J.E.M.; Simões, A. (2009). Validação da metodologia utilizada para a previsão da agitação marítima implementada no projecto MOIA. Congreso de Métodos Numéricos en Ingeniería 2009, pp 435 (CDRom). Barcelona, Spain.

Granja, H.; Pinho, J.L.S. (2012). Coastal defense in NW Portugal: the improbable victory. The Pitfalls of Shoreline Stabilization, Springer, USA: 251-266.

Hallermeier, R.J. (1978). Uses for a calculated limit depth to beach erosion. Proceedings of 16th Coastal Engineering Conference, ASCE, Hamburg, Germany, pp. 1493-1512.

Hallemeier, R.J. (1981). A profile zonation for seasonal sand beaches from wave climate. Coastal Engineering, Vol. 4, pp. 253-277.

Hanson, H. (1987). GENESIS – A generalized shoreline change numerical model for engineering use . Report No. 1007. Department of Water Resources Engineering, University of Lund, Lund, Sweden.

Hanson, H.; Kraus, N.C. (1991). GENESIS – Generalized model for simulating shoreline change". Vol. 2: Reference Manual and Users Guide, US Army Corps of Engineers, pp 431.

Hasselmann, K.; Barnett, T.P.; Bouws, E.; Carlson, H.; Cartwright, D.E.; Enke, K.; Ewing, J.A.; Gienapp, H.; Hasselmann, D.E.; Kruseman, P.; Meerburg, A.; Mller, P.; Olbers, D.J.; Richter, K.; Sell, W.; Walden, H. (1973). Measurements of wind-wave growth and swell decay during the joing NorthSea Wave Project (JONSWAP), Deutsche Hydrographische Zeitschrift, A8(12).

Herbich, J.B. (2000) Offshore (detached) breakwaters. In Handbook of Coastal Engineering. McGraw-Hill Handbooks,pp 5.2-5.97. Texas, EUA.

Houghton, J.T.; Jenkins, G.J.; Ephraums, J.J. (1990). Climate change. The IPCC scientific assessment. Cambridge University Press. Cambridge, UK.

IH (2014) Instituto Hidrográfico. Hydrographic Institute. http://www.hidrografico.pt/download-tabelas-mare.php (last visited 01-07-2014).

ISEC (2014). Inundation Science & Engineering Cooperative. ISEC model respository. Contributed models. http://isec.nacse.org/models (last visited 22-02-2014).

Kennedy, A.B.; Chen, Q.; Kirby, J.T.; Dalrymple, R. A. (2000). Boussinesq modeling of wave transformation, breaking, and runup. I: 1D. Journal of Waterway, Port, Coastal, and Ocean Engineering, pp 39–47.

Kernkamp, H.W.J.; Petit, H.A.H.; Gerritsen and de Goede, E.D. (2005). A unified formulation for the three-dimensional shallow water equations using orthogonal co-ordinates: theory and application. Ocean Dynamics. Vol. 55. pp. 351-369.

Kirby, J.; Wei, G.; Chen, Q.; Kennedy, A.; Dalrymple, R. (1998). FUNWAVE 1.0: Fully nonlinear Boussinesq wave model documentation and user's manual. Center for Applied EngiCoastal Research, University of Delaware. 80 pp.

Kraus, N.C.; Larson, M.; Wise, R.A. (1999). Depth of Closure in Beach-fill Design. Proceedings of the 12th Conference on Beach Preservation Technology, FSBPA, Tallahassee, Florida, pp. 271-286.

Lima, M.V.; Rocha, M. (2011). Numerical modelling of groin impact on nearshore hydrodynamics. Universidade de Aveiro, Departamento de Física.

Lin, P.; Liu, P. L. -F. (1998). A numerical study of breaking waves in the surf zone. Journal of Fluid Mechanics 359, 239-264.

LINZ (2014). Land information New Zealand. http://www.linz.govt.nz/hydro/tidal-info/tidal-intro/definitions (last visited 01-07-2014).

Lynett, P.J.; Liu, P.L.-F. (2014). Modeling wave generation, evolution, and interaction with depth-integrated, dispersive wave equations. COULWAVE Code Manual. Cornell University Long and Intermediate Wave. Modeling Package. USA.

Mendes, J.N.V. (2009). Aplicação de modelos matemáticos para a previsão da morfodinâmica e transporte sedimentar em faixas costeiras. Departamento de Engenharia Civil da Universidade do Minho, Portugal.

Mendonça, A.; Fortes, C.J.; Capitão, R.; Neves, M.G.; Moura, T.; Antunes do Carmo, J.S. (2012). Wave hydrodynamics around a multi-functional artificial reef at Leirosa. Journal of Coastal Conservation 16(4): 543-553.

Mendonça, A.; Proença, B.; Fortes, C.; Neves, A. (2010) Estudo da hidrodinâmica em torno do recife artificial para a prática do surf a construir em São Pedro do Estoril, Cascais. Aplicação dos Modelos de Boussinesq: COULWAVE e FUNWAVE. Revista da Gestão Costeira Integrada 10 (1): 95-125.

MetEd (2014a). Wind and wave forecasting distance learning course, shallow water waves.

https://www.meted.ucar.edu/marine/SWW/navmenu.php?tab=1&page=6.0.0&type=flash (last visited 01-07-2014).

MetEd (2014b). Wave types and characteristics.

https://www.meted.ucar.edu/marine/mod1_wv_type_char/print.htm#page_4.6.2 (last visited 22-07-2014)

Miller, M.C.; McCave, I.N.; Komar, P.D. (1977). Threshold of sediment motion under unidirectional currents. Sedimentology, 24: 507-527.

NHC (2012). Yolo Bypass MIKE-21 Model review: strengths, limitations and recommendations for refinement. Northwest Hydraulic Consultants with Yolo County and cbec eco engineering.

Nunes, B.A.F. (2012) Comportamento de quebramares destacados no litoral noroeste Português. Departamento de Engenharia Civil, Universidade de Aveiro, Portugal.

Nwogu, O. (1993). Alternative form of Boussinesq equations for nearshore wave propagation. J Waterw Port Coast Ocean Eng 119 (6):618–638.

Nwogu, O. (1996). Numerical prediction of breaking waves and currents with a Boussinesq model. Paper presented at the 25th International Conference on Coastal Engineering, ICCE '96, Orlando, FL.

Nwogu, O.G.; Demirbilek, Z. (2001). BOUSS-2D: A Boussinesq wave model for coastal regions and harbors. Theoretical Background and User's Manual. U.S. Army Corps of Engineers. Washington, DC, USA.

OR (2014). Artificial reefs. Ocean revival. http://www.oceanrevival.pt/en/projecto/recifes-artificias.html (last visited 25-02-2014).

ODNR (2011). Ohio Lake Erie shore erosion management plan - Appendix: Erosion control methods detached, breakwaters. Ohio Department of Natural Resources. Office of Coastal Management, Ohio.

Oliveira, I.B.M. (1997) Proteger ou não proteger ou sobre a viabilidade de diferentes opções face à erosão da costa oeste Portuguesa, In: Carvalho, G.S. (ed.), Colectânea de ideias sobre a zona costeira de Portugal, Associação Eurocoast-Portugal, pp. 205-227.

Peregrine, D. H. (1967). Long waves on a beach. Journal of Fluid Mechanics 27, 815-827.

Pereira, R.C.; Taveira-Pinto, F.; Silva, R.; Neves, L. (2013). Avaliação experimental da influência de diferentes configurações da cabeça de quebramares destacados no comportamento morfológico da praia adjacente. Revista da Gestão Costeira Integrada 13 (3): 301-316.

Pires-Silva, A.A.; Makararynskyy, O.; Monbaliu, J.; Ventura-Soares, C.; Coelho, E. (2002). WAM/SWAN simulations in an open coast: comparisons with ADCP measurements. Proc. of the 6th Int. Symposium Littoral 2002, pp.169-173. Porto, Portugal.

PLA (2014) Port of London Authority. http://www.pla.co.uk/Safety/Tides-Definitions-and-Notes (last visited 01-07-2014).

Press, W., Flannery, B. and Teukolsky, S. (1989). Numerical recipes. Cambridge University Press, 569-572.

Rusu, L.; Bernardino, M.; Guedes Soares, C. (2011). Modelling the influence of currents on wave propagation at the entrance of the Tagus estuary. Ocean Engineering, 38(10): 1174-1183.

Rusu, L.; Pilar, P.; Guedes Soares, C. (2005a). Reanalysis of the wave conditions in the approaches to the Portuguese port of Sines. In: C. Guedes Soares, Y. Garbatov & N Fonseca (eds.), Maritime Transportation and Exploitation of Ocean and Coastal Resources, Vol. 2, pp. 1137-1142. Francis & Taylor Group. Lisbon, Portugal.

Rusu, L.; Pilar, P.; Guedes Soares, C. (2005b). Hindcasts of the wave conditions in approaches to ports of the north of Portugal. Proceedings Fifth International Symposium on Ocean Wave Measurement and Analysis (WAVES 2005), CD edition, 9p. Madrid, Spain.

Rusu, L.; Pilar, P.; Guedes Soares, C. (2008a). Evaluation of the wave conditions in Madeira Archipelago with spectral models. Ocean Engineering, 35(13): 1357-1371.

Rusu, L.; Pilar, P.; Guedes Soares, C. (2008b). Hindcast of the wave conditions along the west Iberian coast. Coastal Engineering, 55(11): 906-919.

Rusu, L.; Pilar, P.; Guedes Soares, C. (2009). Influence of wind resolution on the prediction of waves generated in an estuary. Journal of Coastal Research, SI56 (Proceedings of the 10th International Coastal Symposium): 1419-1423.

Santos, J.A.; Coli, A.B.; Capitão, R.; Fortes, C.J.E.M. (2007). Wave forecast at the Tagus estuary by using the SWAN model. Proceedings of the Seventeenth (2007) International Offshore and Polar Engineering Conference. ISOPE, 2007. pp. 2348-2355. Cupertino, CA, U.S.A.

Santos, J.A.; Guilherme, L.; Fortes, C.J.E.M.; Pinheiro, L.V.; Simões, A. (2009). Coupling numerical models for wave propagation in the MOIA Package. Journal of Coastal Research, SI56 (Proceedings of the 10th International Coastal Symposium): 544-548.

Silva, F.; Pinto, J.P.; Almeida, S. (2009). Operational wave forecast system for the Portuguese Coast. Journal of Coastal Research, SI56 (Proceedings of the 10th International Coastal Symposium): 1055-1059.

Silva, R.; Coelho, C.; Veloso-Gomes F.; Taveira-Pinto, F. (2007). Dynamic numerical simulation of medium-term coastal evolution of the West coast of Portugal. Journal of Coastal Research, SI 50 (Proceedings of the 9th International Coastal Symposium), pp. 263-267.

Silva, R.; Coelho, C.; Veloso-Gomes, F.; Taveira-Pinto, F. (2008). A importância de alguns parâmetros hidromorfológicos em estudos de modelação das zonas costeiras. 3ªs Jornadas de Hidráulica, Recursos Hídricos e Ambiente, FEUP, ISBN 978-989-95557-2-3.

Silvester, R.; Hsu, J.R.C. (1997) Coastal stabilization. World Scientific.

Simioni, B.; Esteves, L. (2010) Avaliação qualitativa do desempenho dos recifes artificiais multifuncionais (RAM). Revista da Gestão Costeira Integrada 10(1): 127-145.

Simões, S.C.; Pereira, C.A.; Coelho, C.D.B.; Antunes do Carmo, J.S. (2013). Quebramares destacados: análises comparativas de eficiências de proteção na praia da Vagueira. Recursos Hídricos. Associação Portuguesa dos Recursos Hídricos 34 (02): 25-40.

SMC (2014). User manual SMC 2.5. English. IH Cantabria. Instituto de Hidráulica Ambiental.

SWAN (2014). SWAN manual. http://swanmodel.sourceforge.net/online_doc/swanuse/node3.html (last visited 22-02-2014).

Takahashi, S. (2002) Design of vertical breakwaters. Revised Version of Reference Document No.34, PHRI. Port and Airport Research Institute, Japan.

Taveira-Pinto, F. (2007) Análise da concepção e dimensionamento hidráulico-estrutural de quebramares destacados. Lição de Síntese, Faculdade de Engenharia da Universidade do Porto.

Taveira-Pinto, F. (1993). Quebramar de taludes. Dimensionamento hidráulico. Universidade do Porto, Faculdade de Engenharia, Laboratório de Hidráulica.

Taveira-Pinto, F.; Neves, C.V. (2003). Environmental aspects of using detached breakwaters for coastal protection purposes. Environmental 2010: Situation and perspectives for the European Union, 6-10 May 2003. Porto, Portugal.

Taveira-Pinto, F.; Neves, C.V. (2004) Environmental aspects of using detached breakwaters for coastal protection purposes. Management of Environmental Quality An International 15(1):62-71.

Teixeira, P.R.F.; Fortes, C.J.; Pinheiro, L.; Okamoto, T. (2010). Análise comparativa dos modelos não-lineares COULWAVE e BOUSS3W aplicados à simulação da rebentação. Revista da Gestão Costeira Integrada 11(3):283-296.

Teles, M.J.; Pires-Silva, A.A.; Belo-Pereira, M.; Fortes, C.J. (2009). O Modelo SWAN em regime não estacionário: sensibilidade à resolução do campo de ventos e às condições fronteira de mar. Actas das 6as Jornadas Portuguesas de Engenharia Costeira e Portuária, CD-ROM. Funchal, Madeira, Portugal.

Toyoshima, O. (1974). Design of a detached breakwater system. Proceedings, 14th International Conference on Coastal Engineering. American Society of Civil Engineers, Copenhagen, Denmark, pp 1419-31.

USACE (2014a) Coastal & Hydraulics Laboratory. US Army Corps of Engineers, Breakwaters. http://chl.erdc.usace.army.mil/chl.aspx?p=s&a=Articles;187&g=41 (last visited 25-02-2014).

USACE (2014b) Coastal & Hydraulics Laboratory. US Army Corps of Engineers, Groins. http://chl.erdc.usace.army.mil/chl.aspx?p=s&a=Articles;188&g=41 (last visited 25-02-2014).

USACE (2014c). Coastal & Hydraulics Laboratory. US Army Corps of Engineers. http://chl.erdc.usace.army.mil/chl.aspx?p=s&a=Software;23 (last visited 22-02-2014).

Veloso-Gomes, F.; Taveira-Pinto, F. (1997). Portuguese urban waterfronts expansion near coastal areas. Environmental Challenges In An expanding urban world and the role of emerging information technologies conference, Lisbon, Portugal.

Veloso-Gomes, F.; Taveira-Pinto, F. (2003). Portuguese coastal zones and the new coastal management plans. Journal of Coastal Conservation 9: 25-34.

Voorde, M.; Antunes do Carmo, J.S.; Neves, M. (2009) Designing a preliminar multifunctional artificial reef to protect the Portuguese coast. Journal of Coastal Research 25(1): 69-79.

Wei, G.; Kirby, J. (1995). A time-dependent numerical code for extended Boussinesq equations. Journal of Waterway, Port, Coastal and Ocean Engineering, 120: 251-261.

Wei, G.; Kirby, J. T.; Grilli, S. T.; Subramanya, R. (1995). A fully nonlinear Boussinesq model for surface waves, Part 1, highly nonlinear unsteady waves. Journal of Fluid Mechanics 294, 71-92.

Whitmarsh, D.; Santos, M.; Ramos, J.; Monteiro, C. (2008) Marine habitat modification trough artificial reefs off the Algarve (Southern Portugal): an economic analysis of the fisheries and the prospects for management. Ocean & Management 51(6): 463-468.

Willemse, J.B.T.M.; Stelling, G.S.; Verboom, G.K. (1986). Solving the shallow water equations with anorthogonal coordinate transformation. Delft Hydraulics Communication No. 356.

XMS Wiki (2014). SMS: BOUSS-2D. http://www.xmswiki.com/xms/SMS:BOUSS-2D (last visited 21-09-2014).

(Page intentionally left blank)

APPENDICES

‘The starting point of all achievement is desire.’

Napoleon Hill (1883 – 1970)

(Page intentionally left blank)

TABLE OF APPENDICES

(Page intentionally left blank)

APPENDIX 1

COULWAVE.

Sim_set.dat file

(Page intentionally left blank)

Line	Code	Meaning	Options	Comments
1	sim_opt	Type of simulation	1 - Surface wave evolution 2 - Wave generation by submarine landslide	Choosing "1" will create a simulation examining surface wave evolution (solitary, cnoidal, or sine) with a water depth profile to be created later. Choosing "2" will create a simulation examining surface waves created by movement of the sea floor bottom. This option is not ready for general use.
2	dim	# of dimensions	1 - 1D 2 - 2D	Choosing "1" creates a simulation with only one horizontal dimension. Choosing "2" creates a simulation with two horizontal dimensions.
3	deriv_order_ind	Order to which higher-order dispersive terms are finite-differenced	1 - All terms to at least O(dx**4) 2 - All terms to at least O(dx**2) recommended	
4	nonlin_ind	Include full nonlinear effects	0 - Linear simulation 1 - Weakly nonlinear simulation 2 - Fully nonlinear simulation	Choosing "0" will make use of a linear, dispersive set of governing equations. The linear assumption implies that wave amplitude/water depth $\ll 0.1$. Choosing "1" will make use of a weakly nonlinear, dispersive set of governing equations. The weakly nonlinear assumption implies that wave amplitude/water depth $\ll 1$. This approximation will significantly reduce CPU time, but may lead to large errors in the prediction of large amplitude waves. For example, if prediction of wave shoaling - wave height grows as water depth decreases - is desired, especially over mild slopes (< 1/20) the weakly nonlinear assumption should not be used as it tends to overestimate the wave height. Choosing "2" will make use of a fully nonlinear, dispersive set of governing equations. The fully nonlinear assumption implies that wave amplitude/water depth = O(1)
5	disp_prop	Dispersion properties	1 -Use arbitrary level approximation 2 - Use depth averaged approximation (only for weakly nonlinear case) 3 - Shallow water equations	Choosing "1" will make use of a set of governing equations based on evaluation of horizontal velocity at an arbitrary depth, given as $z = -\beta h$, where the optimum $\beta = 0.531$ for the one-layer (Boussinesq) model. The advantage of using the $z\beta$ method is that the wave and group velocities of higher wave numbers ($h/\lambda > 0.25$) are more accurately described. The disadvantage is increased computational cost. When using more than one-layer, this option must be chosen. Choosing "2" will make use of a set of depth-averaged governing equations. This option will have decreased CPU time, as compared to using option "1", but intermediate-depth waves may have significant phase and group speed errors. Therefore, a depth-averaged simulation should be utilized if the user is fairly certain that all wave numbers will be small, i.e $h/\lambda < 0.2$, or if computational speed is important (typically 5-15 % less for 2D). Choosing "3" will employ the shallow water wave equations. These equations are nondispersive, and are only accurate for very long waves. Note that there are numerical packages in existence that will solve the shallow water equations many times faster than this program.
6	conv	Convenction type	1 - 'Proper' convenction 2 - Wei & Kirby's convenction	
7	wave_type	Wave type	1 - Solitary Wave 2 - Solitary Wave with a/h=0.58 3 - Solitary Wave with a/h=0.42 4 - Cnoidal Waves 5 - Sine Waves 6 - Wave Spectrum	Choosing "1" will input a solitary wave (a positive elevation wave of permanent form). This profile is the analytic solution to the weakly nonlinear equations. Therefore, larger amplitude waves will not initially be of permanent form when using this option. Choosing "2" will input a highly nonlinear solitary wave. This solitary wave is the numerically permanent solution to the fully nonlinear equations. This wave will only work with a water depth of h=0.45 m, and the program will force this water depth to be used. Choosing "3" will input a highly nonlinear solitary wave. This solitary wave is the numerically permanent solution to the fully nonlinear equations. This wave will only work with a water depth of h=0.45 m, and the program will force this water depth to be used. Choosing "4" will input a cnoidal wave (oscillatory wave of permanent form) train. Choosing "5" will input a simple sine wave train consisting of up to two frequencies. Sine waves can be created using an internal source function. The option to use the internal source will be given a little later. Choosing "6" will input a spectrum of amplitudes. The input data files when implementing a spectrum must be generated by the "spectrum.m" Matlab file included.
8	depth	Water depth in meter		This is the water depth at the initial location of the wave or the location of the internal source
9	wave_hgt	Amplitude of landslide displacement		
10	depth	Water depth in meter		This is the water depth at the initial location of the wave or the location of the internal source
11	x0	Location of source wavemaker		Length from the left side boundary to the crest of the solitary wave
12	mk2	Square of the modulus of the elliptic integal of the first kind	This value theoretically varies from 0 (sine waves) to 1 (solitary waves) but realistically can only be varied from 0.4-1	Enter the modulus of the elliptic integral of the first kind'
13	ramp	# of waves to ramp		Enter total number of wavelengths to be ramped to eliminate free surface discontinuity
14	dom_wave	# of full (non-ramped) waves in initial domain	2-3 Recommended	Enter number of wavelengths to be in initial domain - must be at least one (the user can have as many waves in the initial domain as is desired)
15	end_wave	# of waves to be created		Enter total number of wavelengths to be created during entire simulation
16	inc_ang	Oblique angle of inicident wave	0 - Waves traveling in positive x-direction	Enter incident angle of waves (degrees)
17	slide_type	Type of landslide	Only for sim_opt = 2	
18	ts	Start time of landslide		Must be > 0
19	per	Time scale of landslide		
20	te	End time of landslide		
21	filt	Filter	1 - Filter entire domain at using 9-point filter 2 - Do not filter entire domain	The 9-point filter that can be used is an effective approach to eliminating short wave instabilities. Note that although this filter has a steep response function (i.e. it totally eliminates the $2\Delta x$ waves, and removes very little energy from the longer wavelengths) it should be used sparingly. The reason for this is that it does remove a small amount of long wave energy, and thus may affect the final solution in a non-physical manner. If filtering is chosen, the user will be prompted:
22	filt_int	# of time steps between filtering	Values less than 3 are recommended	Number of times to filter entire domain per wave period: (lower values will effect the solution less - values less than 3 are recommended if filtering is needed)
23	filtsld_int	# of time steps between filtering over landslide area	Only for sim_opt = 2	
24	screen_output	Screen output	1 - Display output data to screen 2 - Do not display	Choosing "1" will have the program print program information to screen. The information to be displayed is: Current time step out of total time steps, and number of iterations required for convergence in the corrector loop of the last time step. Choosing "2" will have the program display no information while it is running. If the user has chosen to display data to screen, the following prompt will be given: Time step interval to print select information to screen (i.e. if 10 is inputted, information will be displayed on screen every tenth time step)
25	display	Increment to display information on screen		Time step interval to print select information to screen
26	itr	Maximum # of iterations for Corrector Loop	20 - Default	
27	min_itr	Minimum # of iterations for Corrector Loop	5 - Default	
28	itr_or	Iteration after which over-relaxtion should be used	15 - Default	
29	o	Over-relaxtion coefficient	0.5 - Default	Using over relaxtion will sometimes make the corrector loop converge more rapidly

Line	Code	Meaning	Options	Comments
30	bc_1	Left side domain boundary condition	1 - Solid-reflective wall 2 - Input wave- sending a wave through boundary	The user will be prompted to specify a value for each of the boundaries (there are 2 for a 1D simulation (left and right), and 4 for a 2D simulation (left, right, top and bottom)). Choosing "1" will enforce a solid, completely reflecting Wall. Choosing "2" will allow for waves to be sent through the boundary. This is not a radiation boundary condition, and will not allow for waves for arbitrary shape to exit the numerical domain. This boundary is required along the left wall when using cnoidal or sine waves.
31	bc_2	Right side domain boundary condition	1 - Solid-reflective wall 2 - Input wave- sending a wave through boundary	
32	bc_3	Bottom side domain boundary condition	1 - Solid-reflective wall 2 - Input wave- sending a wave through boundary	
33	bc_4	Top side domain boundary condition	1 - Solid-reflective wall 2 - Input wave- sending a wave through boundary	
34	spng_1	Sponge layer on left side boundary	0 - Do not use sponge layer 1 - Use sponge layer on left side boundary	Adding a sponge layer along any boundary will add a length in the normal direction equal to one wavelength. The sponge layer used here absorbs both mass and energy, and has shown to be an excellent absorber of waves of all types, with negligible reflection.
35	spng_2	Sponge layer on right side boundary	0 - Do not use sponge layer 1 - Use sponge layer on right side boundary	
36	spng_3	Sponge layer on bottom side boundary	0 - Do not use sponge layer 1 - Use sponge layer on bottom side boundary	
37	spng_4	Sponge layer on top side boundary	0 - Do not use sponge layer 1 - Use sponge layer on tp side boundary	
38	load_topo	Load topography	1 - Specify profile by giving location/ depth nodes 2 - Use bathymetry data files created	Choosing "1" will allow the user to input nodes describing the water depth profile. A node represents the location where the slope of water depth changes. This option does not create a 2HD variable bathymetry. Choosing "2" will tell the program to load topography data from files. These topography files must be created using the included Matlab files. The Matlab script "bath ss" will create topography data from the Smith and Sandwell 2-minute database (see the file "bath ss.m" for details). The Matlab script "bath loc" will create topography data from local files (again, see the file "bath loc.m" for details). The files created by these scripts are: "x topo.dat, y topo.dat, f topo.dat, size topo.dat", and must be located in the same directory as the executable when running the program. For more information on how to create a topography using the Matlab scripts, see the later section "Creating a Bathymetry in Matlab."
39	num_nodes	Number of nodes required to create bottom profile, incuding first and last		Enter the number of nodes required to create bottom profile, including first and last
40	x_1	xx Coordinate	0 - xx location of first node is forced to 0	
41	h_1	yy Coordinate		Enter depth of first node
42	x_2	xx Coordinate		Enter xx location of second node
43	h_2	yy Coordinate		Enter depth of second node
44	x_3	xx Coordinate		Enter xx location of third node
45	h_3	yy Coordinate		Enter depth of third node
46	x_4	xx Coordinate		Enter xx location of fourth node
47	h_4	yy Coordinate		Enter depth of fourth node
48	x_5	xx Coordinate		Enter xx location of fifth node
49	h_5	yy Coordinate		Enter depth of fifth node
50	x_6	xx Coordinate		Enter xx location of sixth node
51	h_6	yy Coordinate		Enter depth of sixth node
52	x_7	xx Coordinate		Enter xx location of seventh node
53	h_7	yy Coordinate		Enter depth of seventh node
54	x_8	xx Coordinate		Enter xx location of eighth node
55	h_8	yy Coordinate		Enter depth of eighth node
56	x_9	xx Coordinate		Enter xx location of ninth node
57	h_9	yy Coordinate		Enter depth of ninth node
58	chan_width	Width in meter of channel	Ignore for 1D simulation	Ignore for 1D simulation. If 2D enter domain width (yy direction)

Line	Code	Meaning	Options	Comments
59	end_t	Time in seconds to run simulation		Enter the physical simulation time in seconds (total physical time ofnumerical simulation)
60	writ_inc	Time increment		Enter the time increment at which spatial snapshots of free surface should be written to file (the time increment to write free surface, depth and velocity to file). (If you choose to write time series to file, you will next be prompted to input the locations of each time series)
61	pts_xvl	# of grid points per wavelength		Enter the number of grid points per wavelength (this is the resolution, a value of 30-50 is typically enough to ensure numerical convergence)
62	courant	Courant number		Enter the courant number = dx/(dt*co): (this will determine the time step used in the model, for weakly nonlinear simulations, and value of 0.5 will typically yield stability and convergence, but for simulations with highly nonlinear waves, a value as low as 0.1 may be required for stability - this is unfortunately trial and error at this point. However, for nearly all cases a value of 0.5 will be stable)
63	slide_node			
64	load_topo	Wave length		If wave type = 6 this information is not necessary
65	per_sld			
66	slope_reg			
67	sponge_width	Width of the sponge layer in wavelengths	1 - Default	From numerical tests, it was found that using a sponge layer width of one wavelength yielded excellent results for most waves. For highly nonlinear waves, one may want to increase this value
68	cdamp1	First sponge layer coefficient		
69	cdamp2	Second sponge layer coefficient		
70	rotate			
71	smooth	Smooth depth profile using four-point filter	0 - Do not use smooth depth profile using four point filter 1 - Smooth depth profile using four point filter	
72	y1			
73	y2			
74	depth_top			
75	depth_bottom			
76	smooth_top			
77	radius_coef			
78	amp_top			
79	int_src	Internal source wavemaker	0 - Do not use internal source wavemaker 1 - Use internal source wavemaker	Sine waves can be effectively modeled using an internal source wavemaker. With this option, waves are created inside the numerical domain. Internal source generation, coupled with sponge layer absorbers along the outer domain boundaries allow for the development of a quasi-steady state wave field. Entering "1" will create an internal source function. If the user has chosen to use the internal source, next will be a prompt to enter the location of the centerline of the internal source. For 1D simulations, this is simply the x-coordinate of the internal source centerline. For 2D cases, this the normal distance from the origin. It recommended to always use the internal source wavemaker when generating sine waves.
80	wave_hgt_2			
81	bottom_fric	Bottom friction	0 - Do not include bottom friction 1 - Include bottom friction	For real coastline problems, the bottom friction model should be used. This is especially the case with breaking waves, where, if the bottom friction model is not used, the thin film rundown can reach extremely large velocities, causing numerical stability problems. If you select to use the Bottom Friction model, you will be prompted: The bottom friction model is partly empirical, and a bottom friction coefficient must be inputted. This value is typically in the 10-4 to 10-2 range. Enter coefficient: (For real shoreline problems, where the coefficient is not well known, a value of 0.005-0.01 is recommended)
82	f_BF	Bottom friction coefficient		
83	wave_breaking	Wave breaking	0 - Do not use wave breaking model 1 - Use wave breaking model	For practical simulations, the model should always be used. If the wave transforms to a situation near breaking, and the breaking model is not turned on, the simulation will frequently overflow.
84	ep	Corrector stage convergence error		
85	ep2	Corrector stage convergence error		
86	L_2			
87	swash_filt			

Line	Code	Meaning	Options	Comments
88	smooth_bathy			
89	use_av			
90	spec_type			
91	slope_ang			
92	gamma			
93	Cd			
94	Cm			
95	Frd			
96	num_ts	Time series output	0 - Not write time series of zeta, u and v at specific locations to file Enter the number of locations you would like time series for (60 max.)	The time series output form the model can be loaded with the Matlab file "load ts.m". Write time series of zeta,u, and v at specific locations to file? Enter 0 for no, or enter the number of locations you would like time series for (60 max.))
97	current	Uniform wave current	0 - No 1 - Yes	
98	FR_cur			
99	bf_ratio			
100	sh_mov			
101	cutoff			
102	num_levels			
103	aspects_ratio			
104	is_oreint			
105	upwind_baseline			
106	visc_coef	Coefficient for subgrid horizontal eddy viscosity	0.08 - 0.2 = Smag form	
107	rotationality	Rotational model	0 - Use irrotational (potencial) model 1 - Use rotational (vertical) model	
108	decomp_type			
109	dims(1)			
110	dims(2)			
111	spec_pp			
112	spec_ts			
113	numerical_scheme			
114	limiter_on			
115	breaker_type			
116	bf_type			
117	Ch	Coefficient for vertical eddy viscosity	0.0667 - Elders model	
118	backscatter	Backscatter model	0 - No using backscatter model	

Line	Code	Meaning	Options	Comments
119	CB			
120	ihvor			
121	elder_length			
122	Ch_length			
123	c int_scr		c int_src= 2	
124	do i		do i= 1.20	
125	0.0			Dummy space for future parameter additions
126	enddo			
127	close			

(Page intentionally left blank)

APPENDIX 2

COULWAVE.

Scenario Initial1

Scenarios 1 to 12

(Page intentionally left blank)

Scenarios Initial and scenarios with detached breakwater

Wave characteristics		Scenario
Hs (m)	T (s)	
6,64	9,30	**Initial1**
1,00	7,00	**Initial2**
2,00	7,00	**Initial3**
3,00	7,00	**Initial4**
4,00	11,00	**Initial5**

Wave characteristics		Breakwater characteristics		Scenario
H (m)	T (s)	hcr (m)	X (m)	
6,64	9,30	2,70	235,00	SC1
			170,00	SC2
			300,00	SC3
		1,50	235,00	SC4
			170,00	SC5
			300,00	SC6
		-1,50	235,00	SC7
			170,00	SC8
			300,00	SC9
		-0,50	235,00	SC10
			170,00	SC11
			300,00	SC12
1,00	7,00	2,70	235,00	SC13
			170,00	SC14
			300,00	SC15
		1,50	235,00	SC16
			170,00	SC17
			300,00	SC18
		-1,50	235,00	SC19
			170,00	SC20
			300,00	SC21
		-0,50	235,00	SC22
			170,00	SC23
			300,00	SC24
2,00	7,00	2,70	235,00	SC25
			170,00	SC26
			300,00	SC27
		1,50	235,00	SC28
			170,00	SC29
			300,00	SC30
		-1,50	235,00	SC31
			170,00	SC32
			300,00	SC33
		-0,50	235,00	SC34
			170,00	SC35
			300,00	SC36
3,00	7,00	2,70	235,00	SC37
			170,00	SC38
			300,00	SC39
		1,50	235,00	SC40
			170,00	SC41
			300,00	SC42
		-1,50	235,00	SC43
			170,00	SC44
			300,00	SC45
		-0,50	235,00	SC46
			170,00	SC47
			300,00	SC48
4,00	11,00	2,70	235,00	SC49
			170,00	SC50
			300,00	SC51
		1,50	235,00	SC52
			170,00	SC53
			300,00	SC54
		-1,50	235,00	SC55
			170,00	SC56
			300,00	SC57
		-0,50	235,00	SC58
			170,00	SC59
			300,00	SC60

Initial1	Hs (m)	T (s)
	6,64	9,30

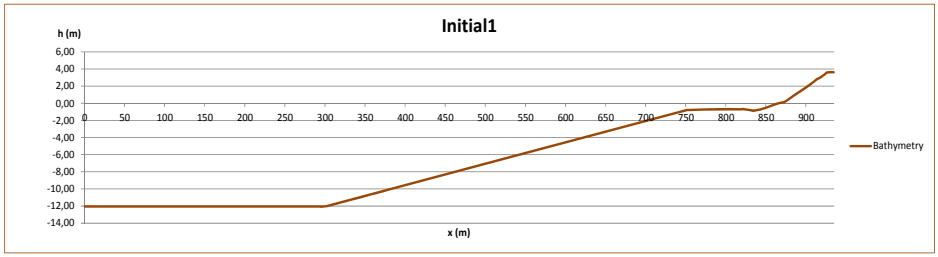

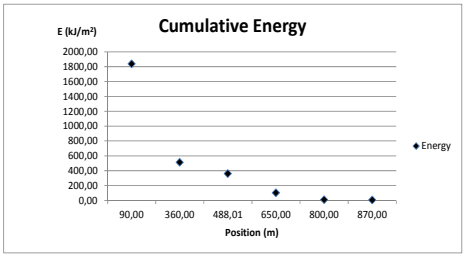

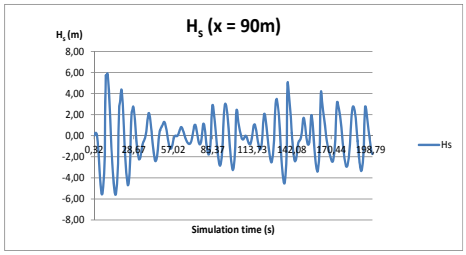

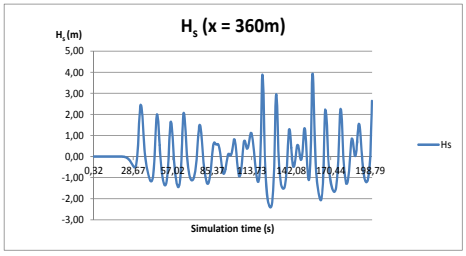

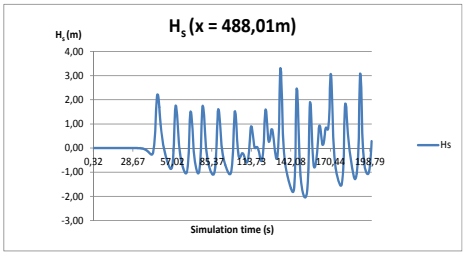

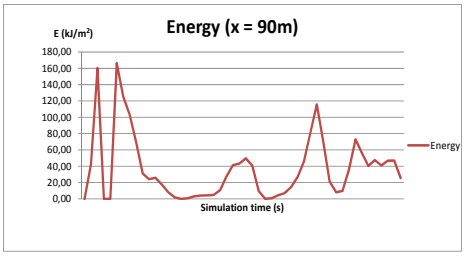

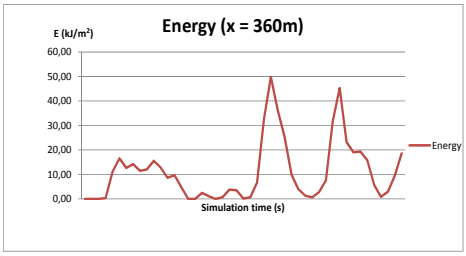

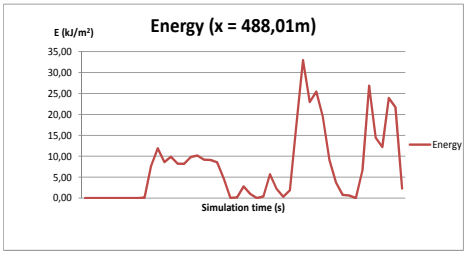

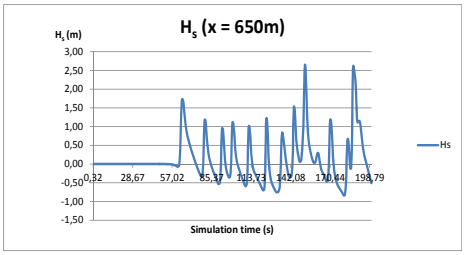

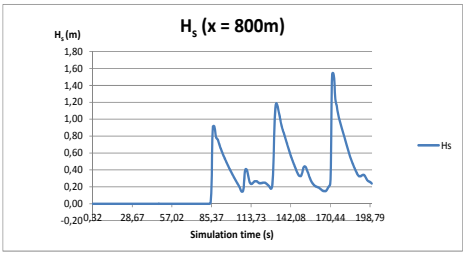

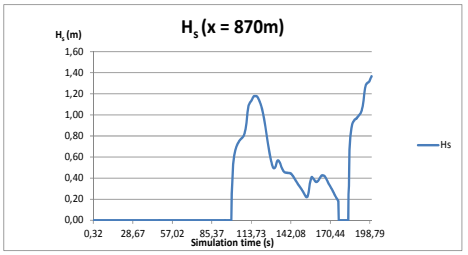

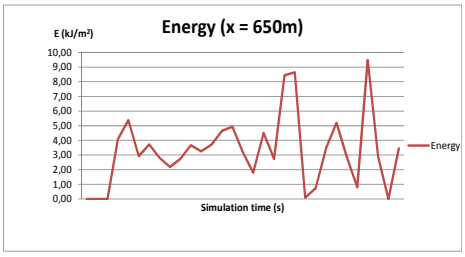

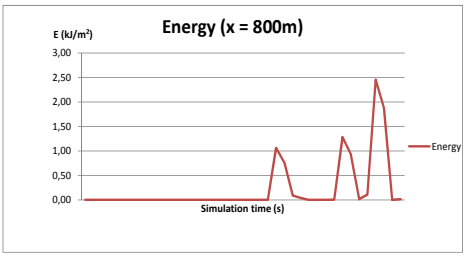

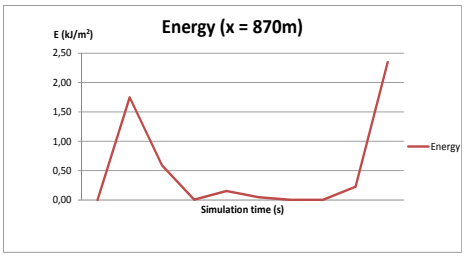

SC1	H_s (m)	T (s)	h_{cr} (m)	X (m)
	6,64	9,30	2,70	235,00

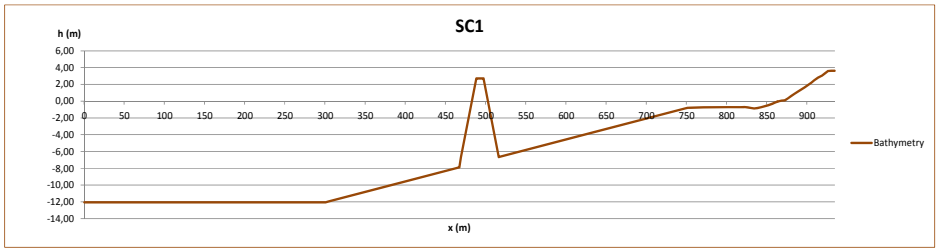

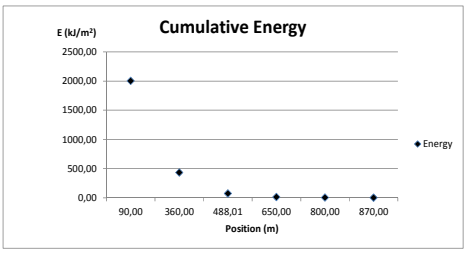

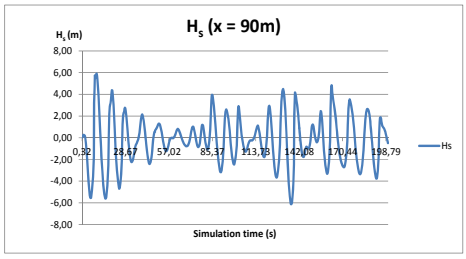

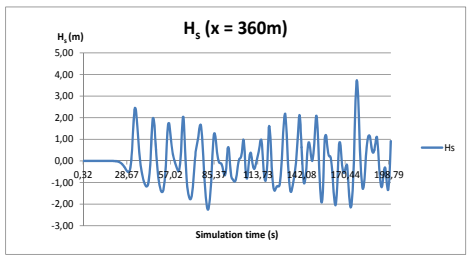

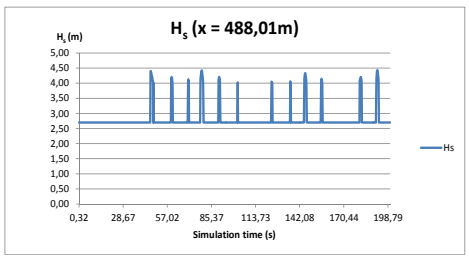

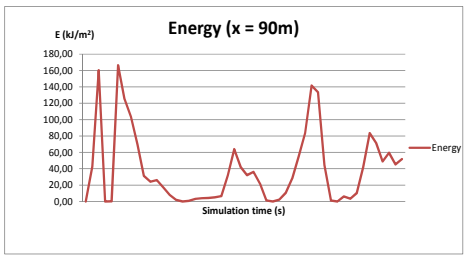

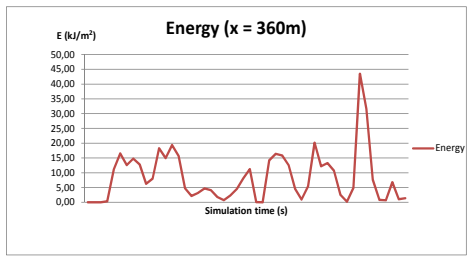

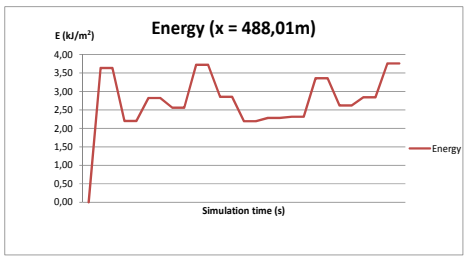

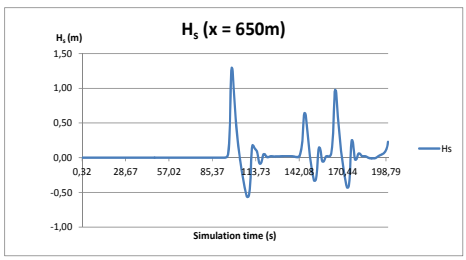

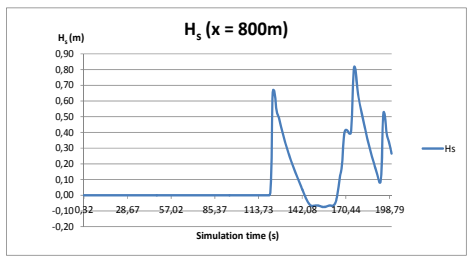

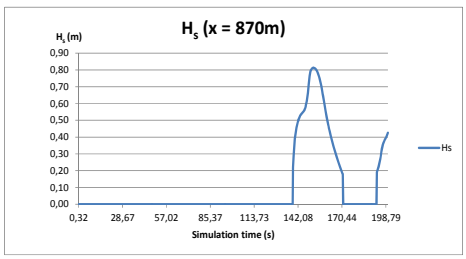

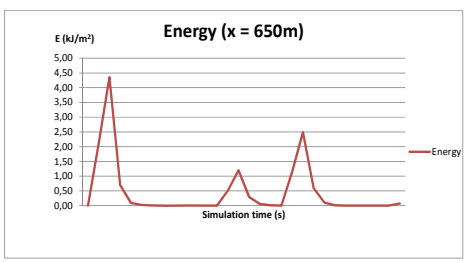

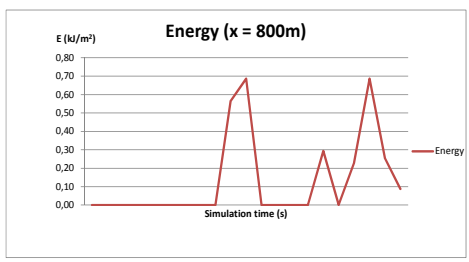

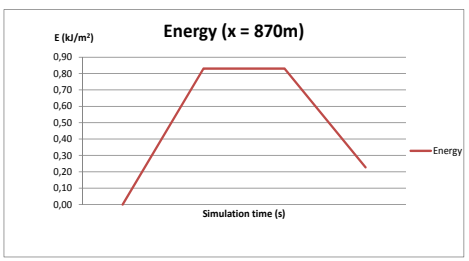

SC2	H_s (m)	T (s)	h_{cr} (m)	X (m)
	6,64	9,30	2,70	170,00

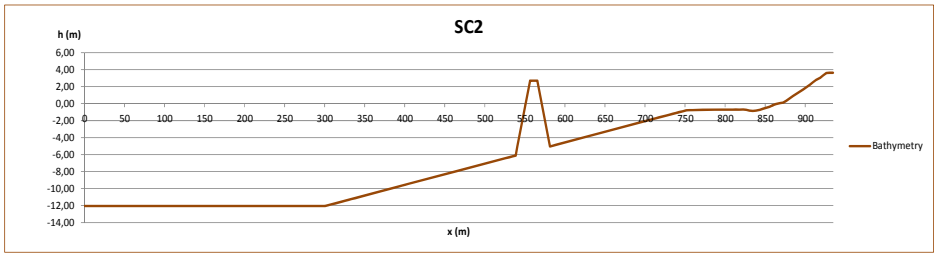

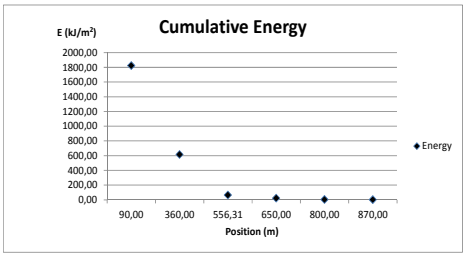

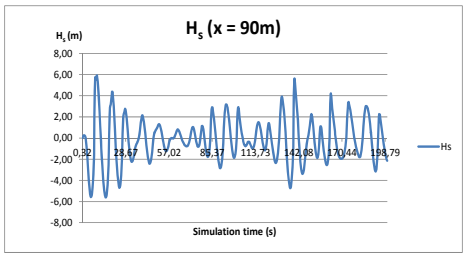

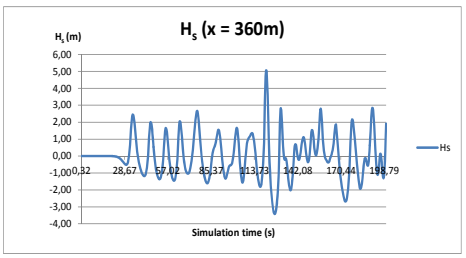

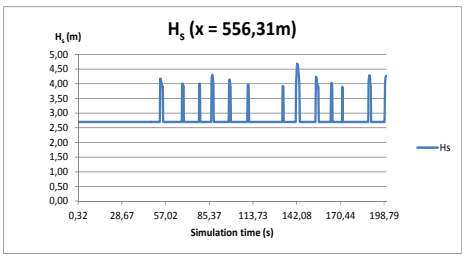

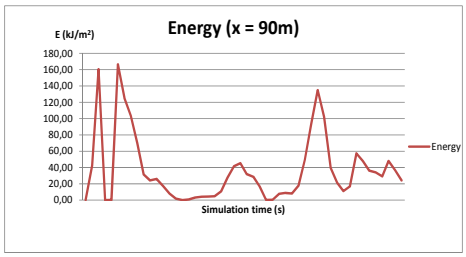

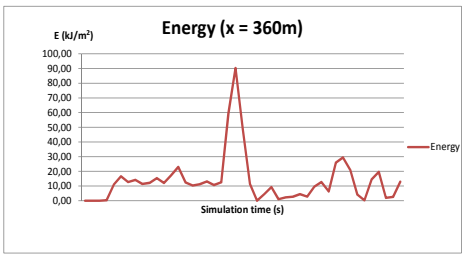

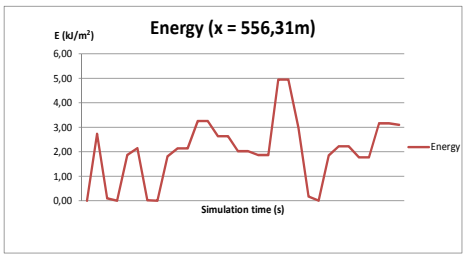

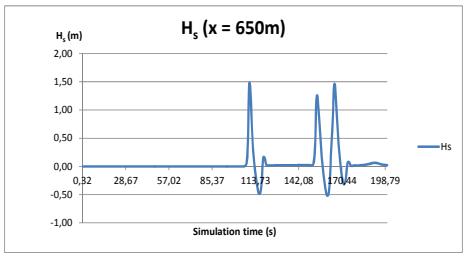

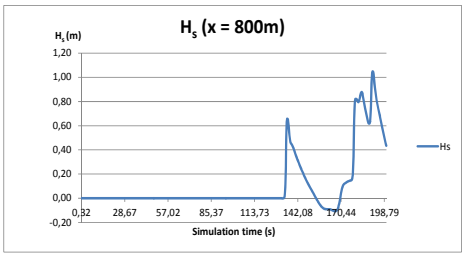

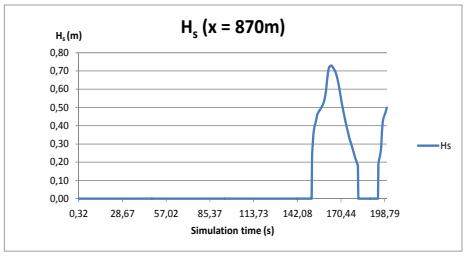

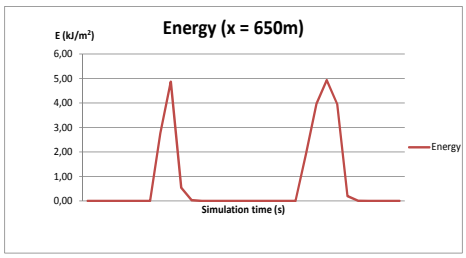

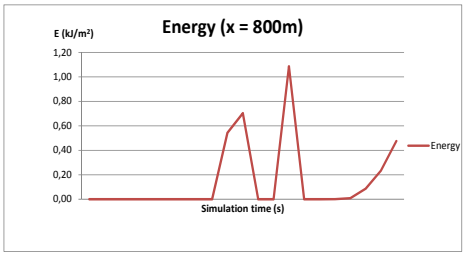

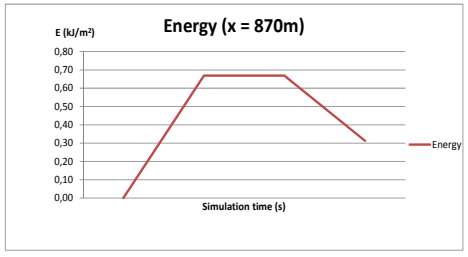

SC3	H_s (m)	T (s)	h_{cr} (m)	X (m)
	6,64	9,30	2,70	300,00

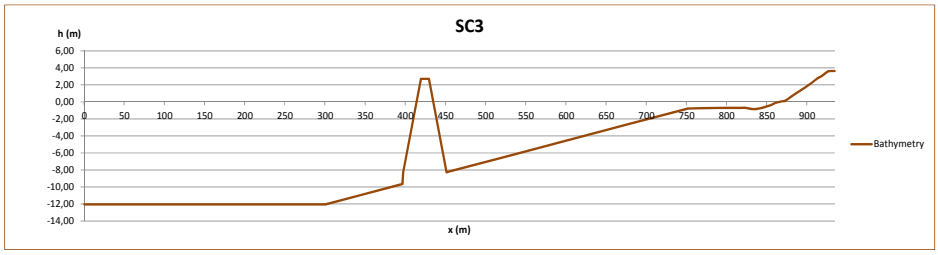

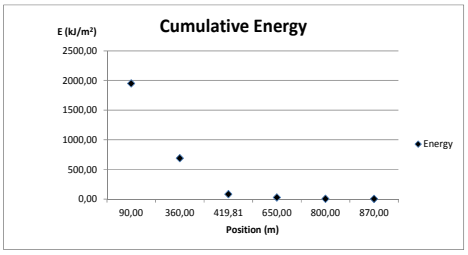

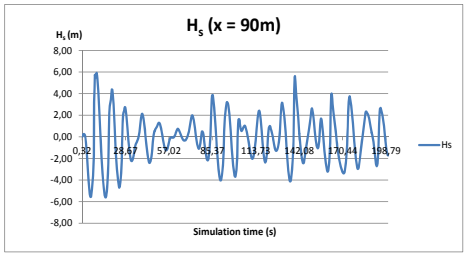

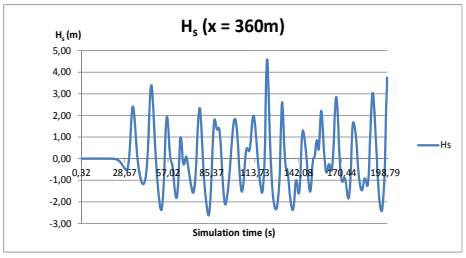

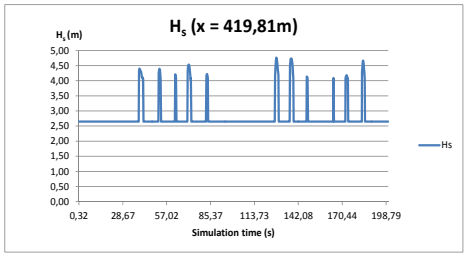

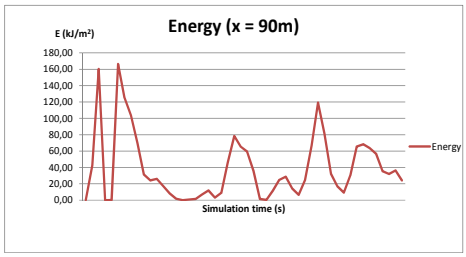

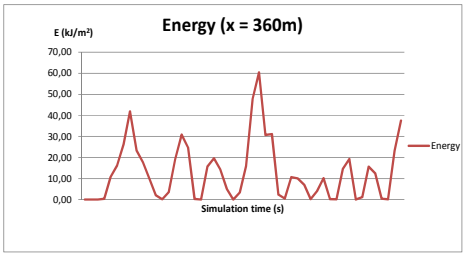

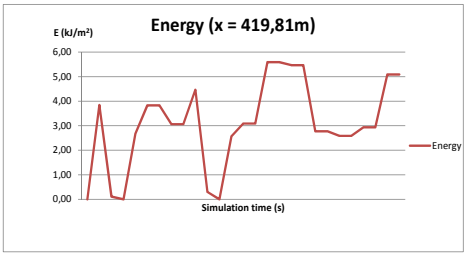

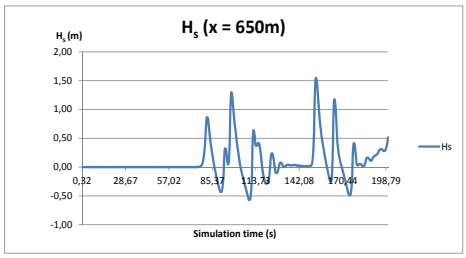

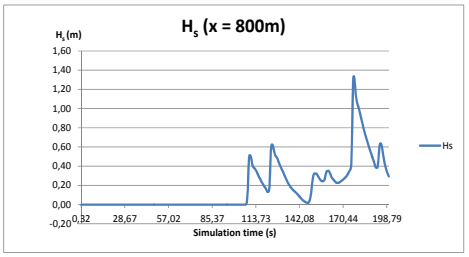

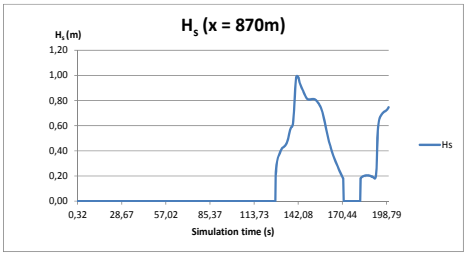

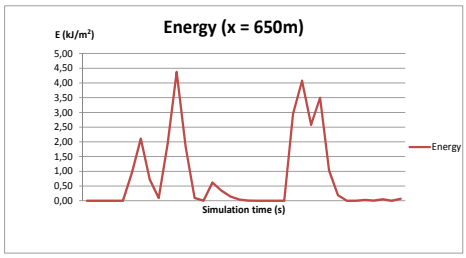

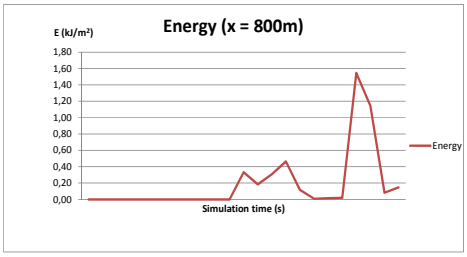

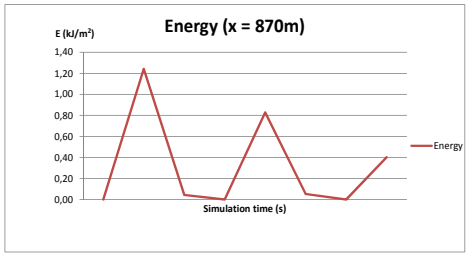

SC4	H_s (m)	T (s)	h_{cr} (m)	X (m)
	6,64	9,30	1,50	235,00

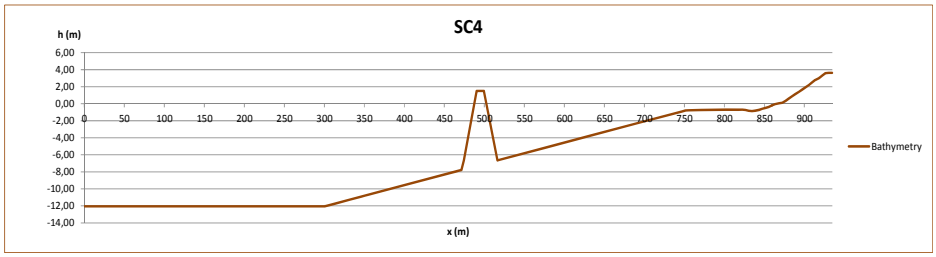

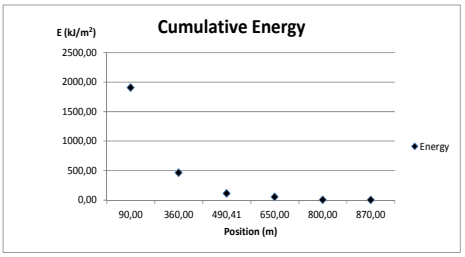

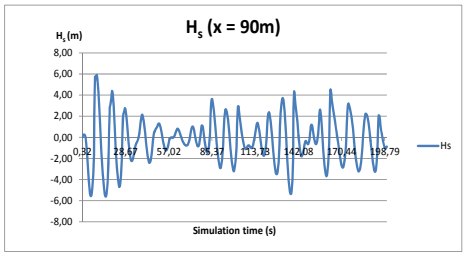

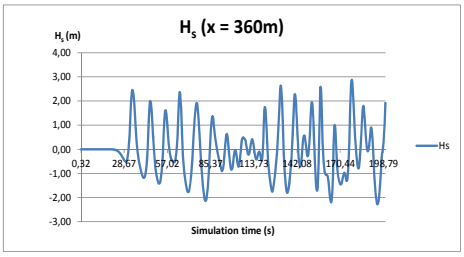

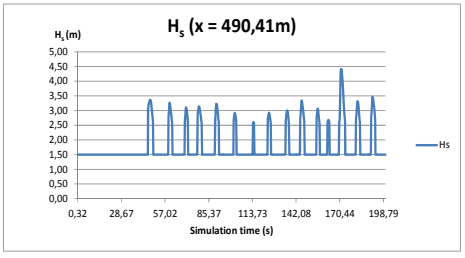

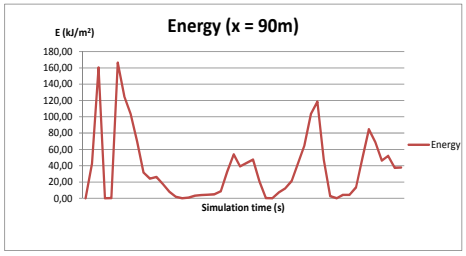

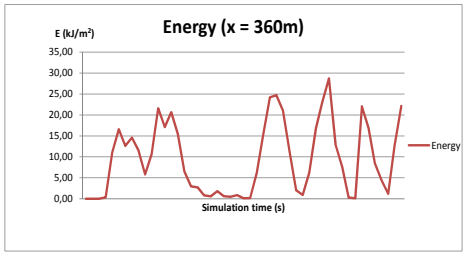

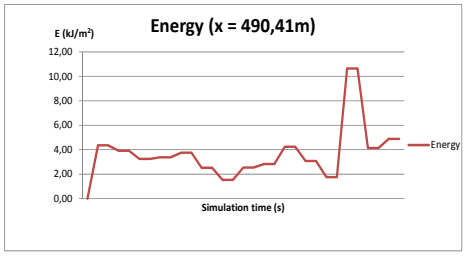

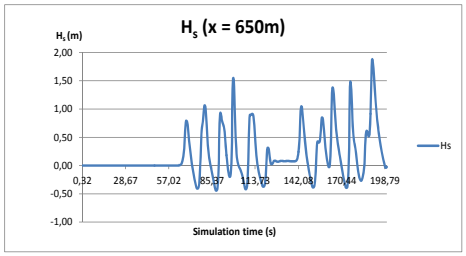

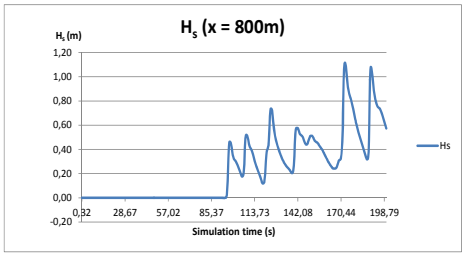

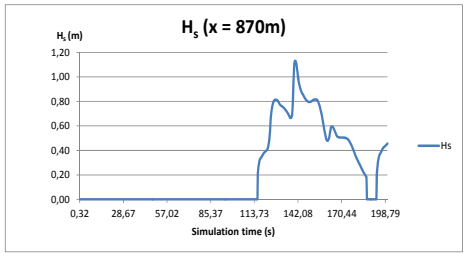

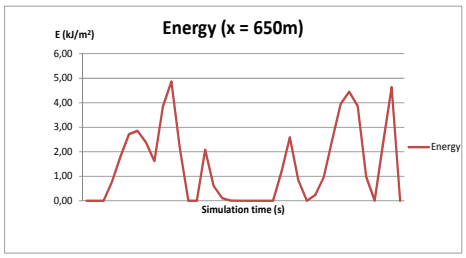

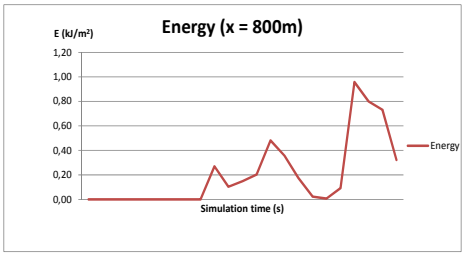

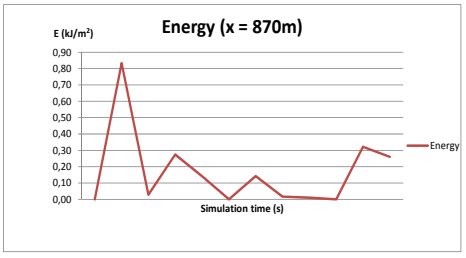

SC5	H_s (m)	T (s)	h_{cr} (m)	X (m)
	6,64	9,30	1,50	170,00

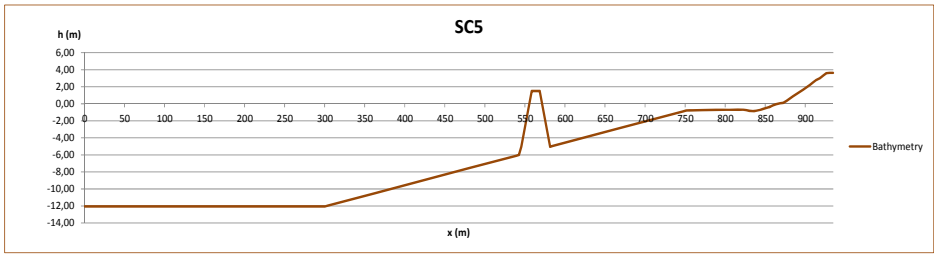

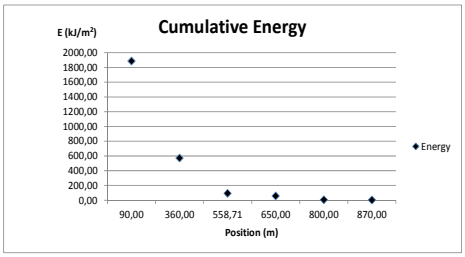

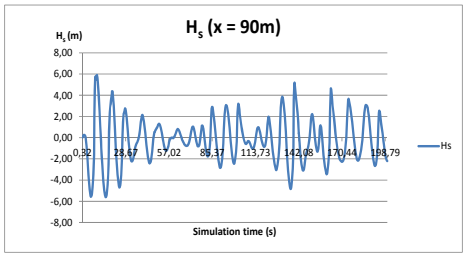

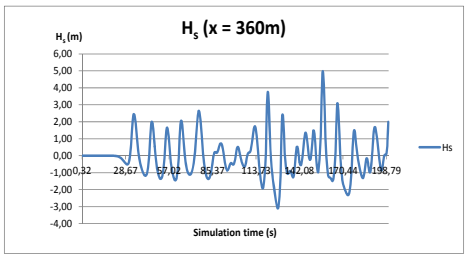

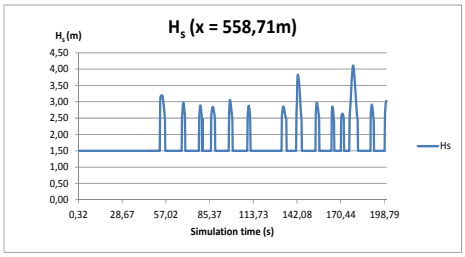

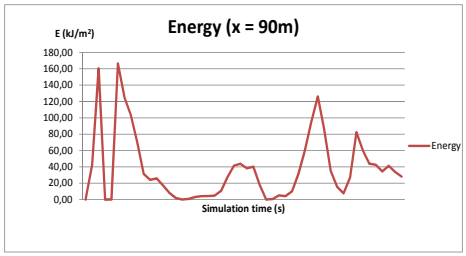

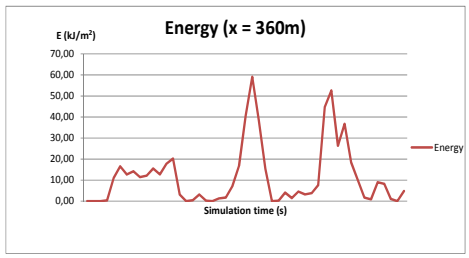

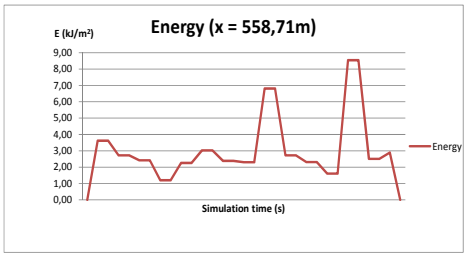

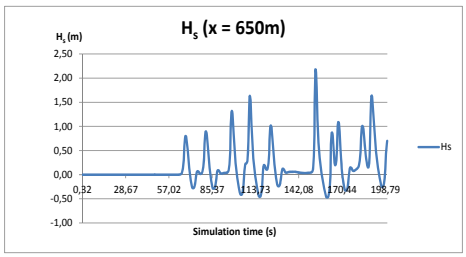

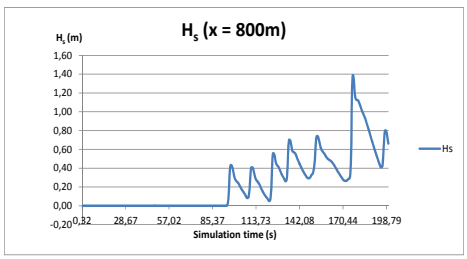

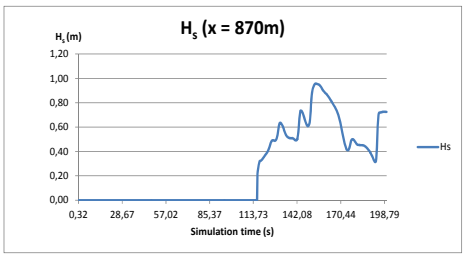

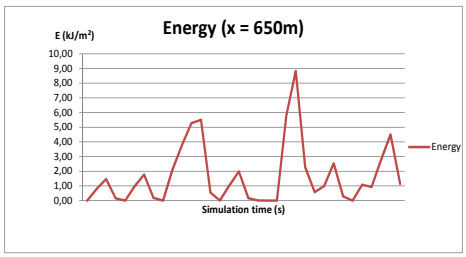

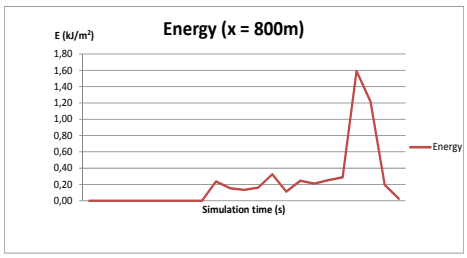

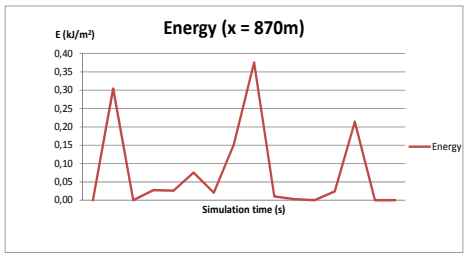

SC6	H_s (m)	T (s)	h_{cr} (m)	X (m)
	6,64	9,30	1,50	300,00

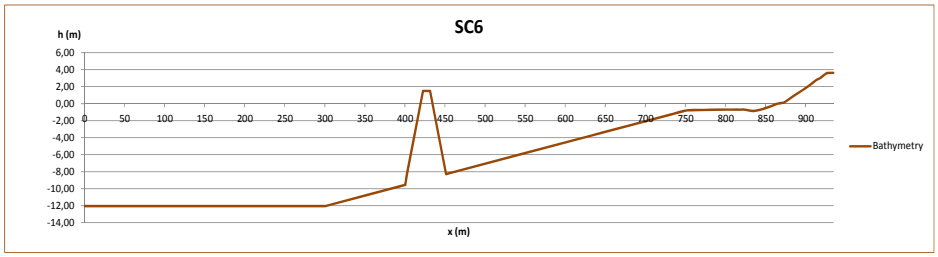

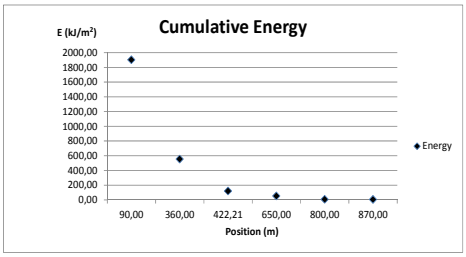

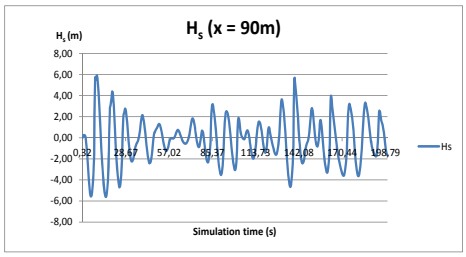

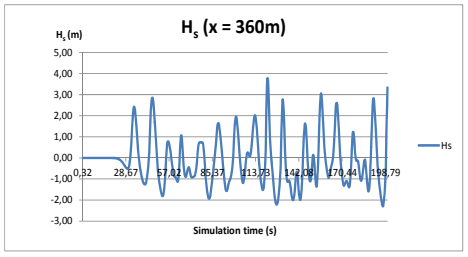

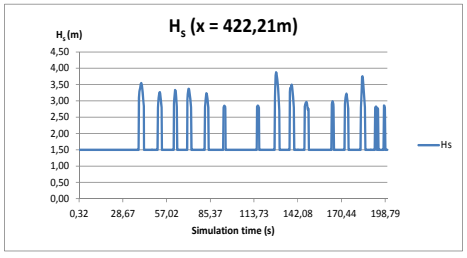

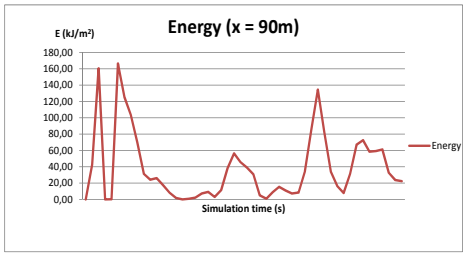

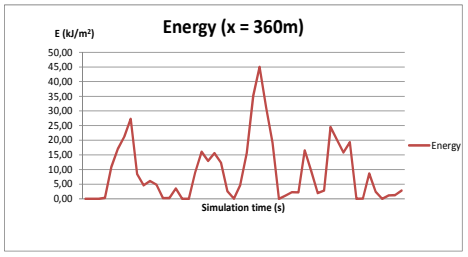

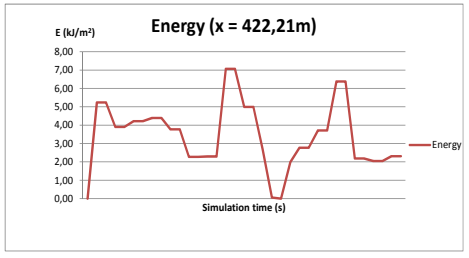

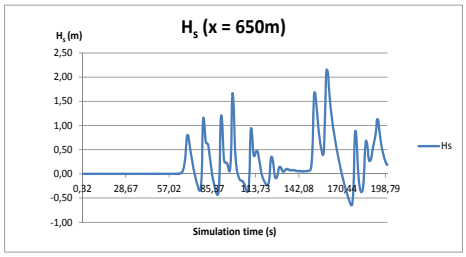

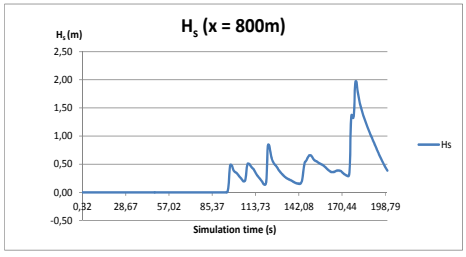

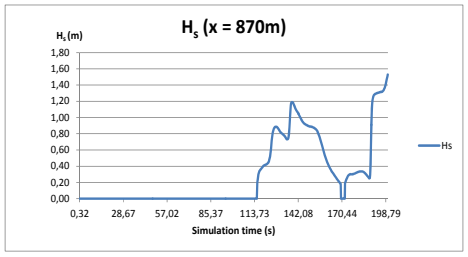

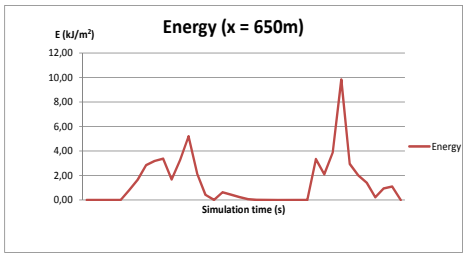

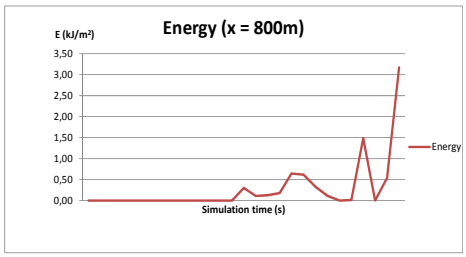

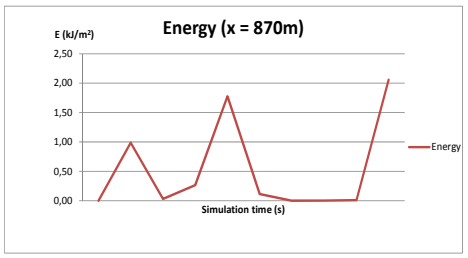

SC7	H_s (m)	T (s)	h_{cr} (m)	X (m)
	6,64	9,30	-1,50	235,00

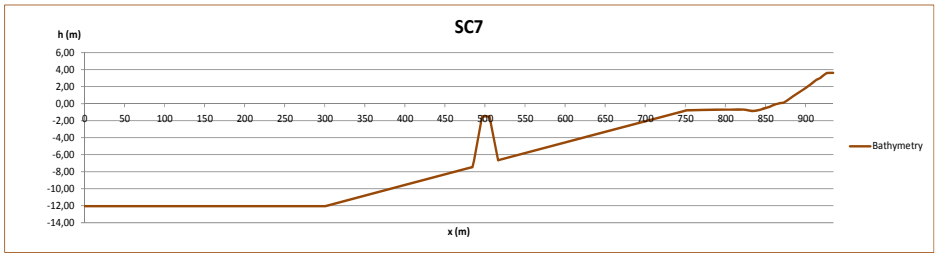

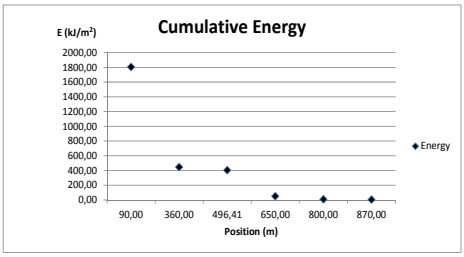

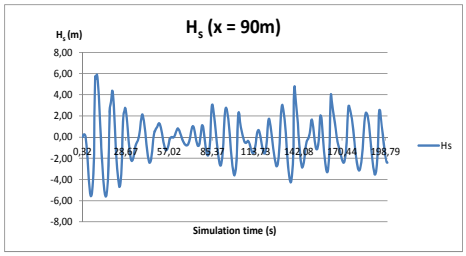

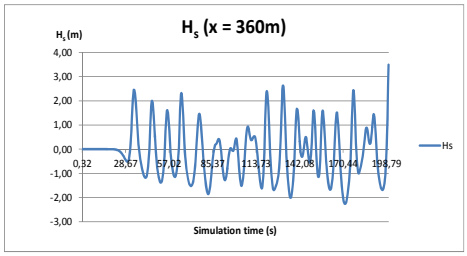

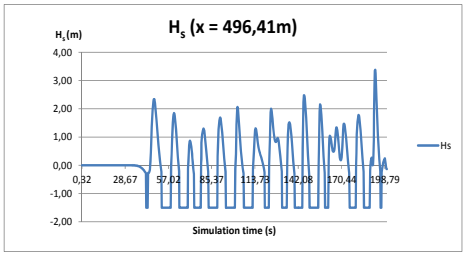

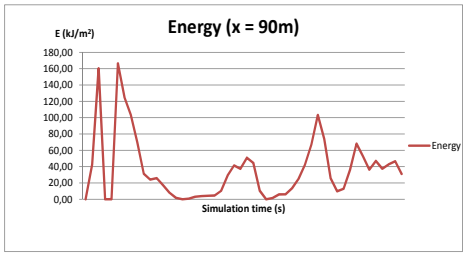

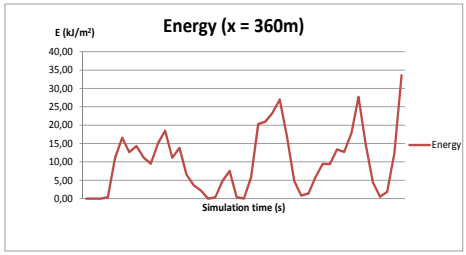

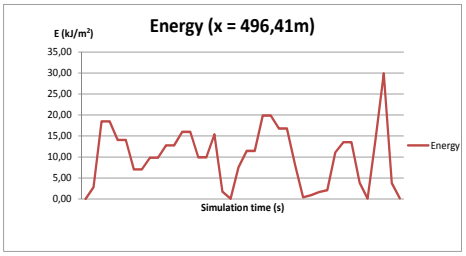

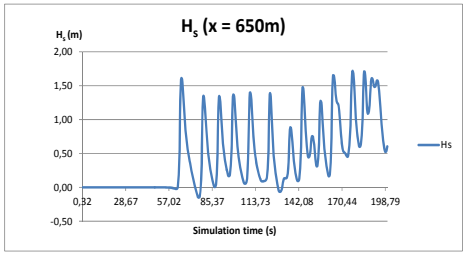

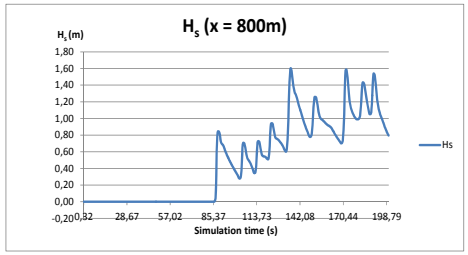

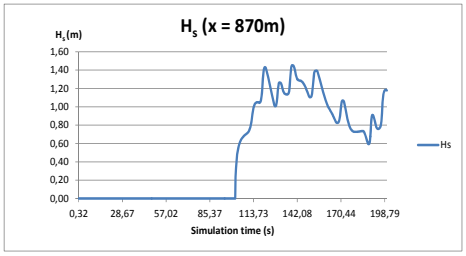

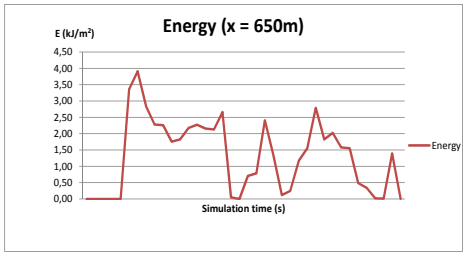

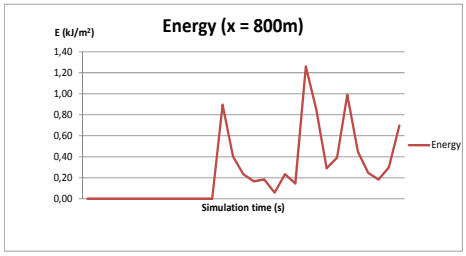

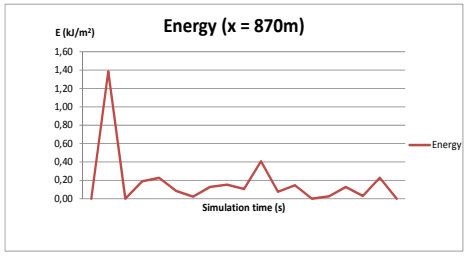

SC8	H_s (m)	T (s)	h_{cr} (m)	X (m)
	6,64	9,30	-1,50	170,00

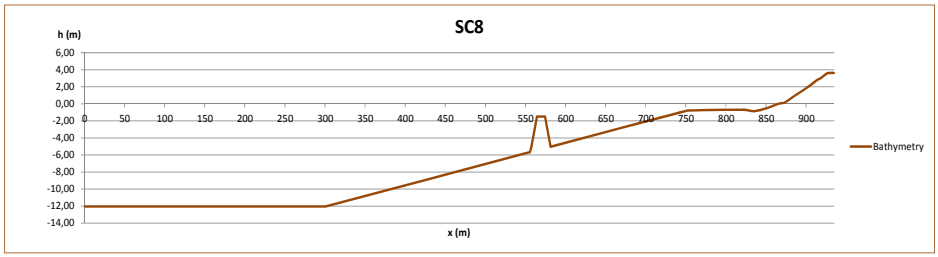

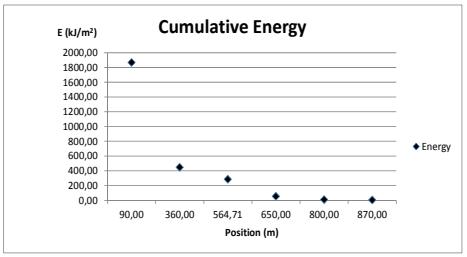

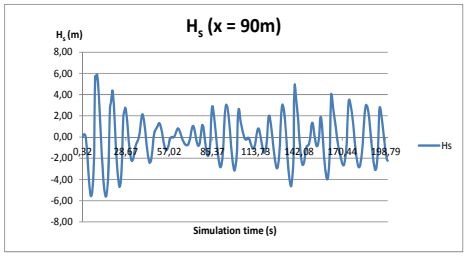

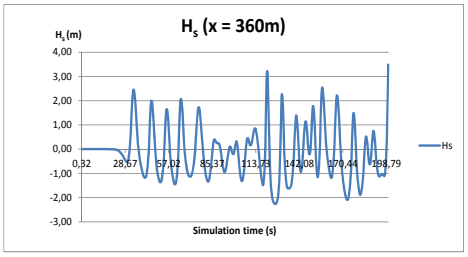

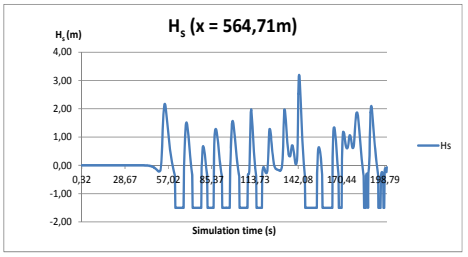

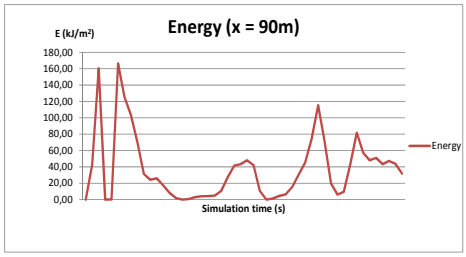

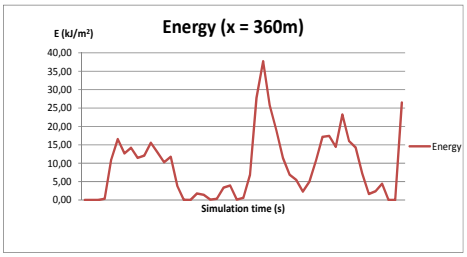

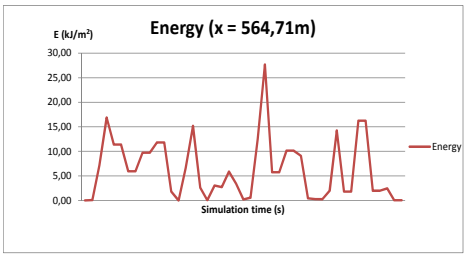

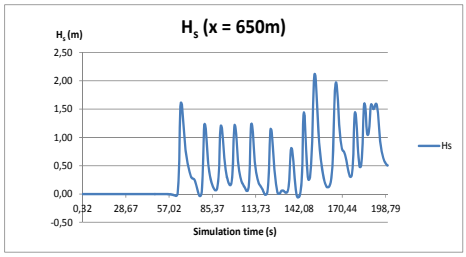

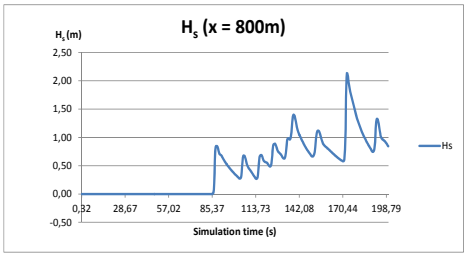

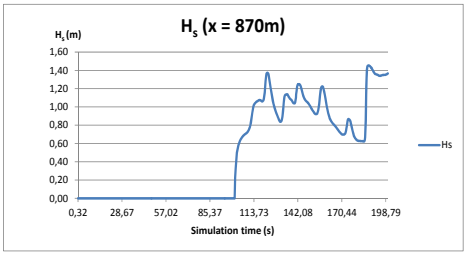

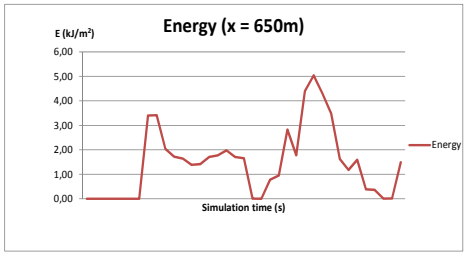

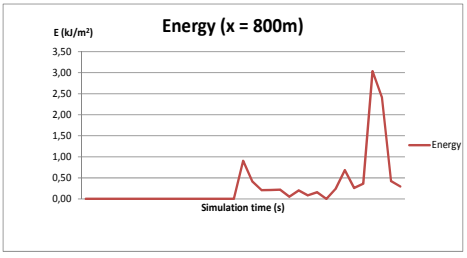

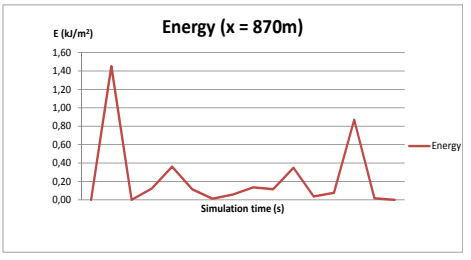

SC9	H_s (m)	T (s)	h_{cr} (m)	X (m)
	6,64	9,30	-1,50	300,00

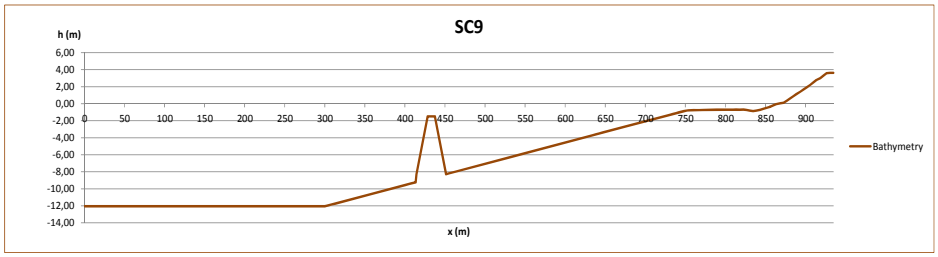

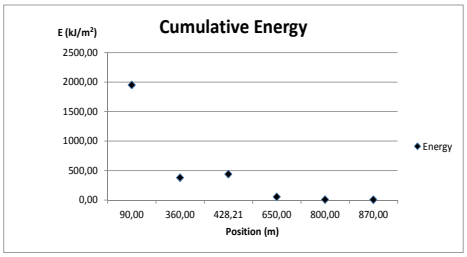

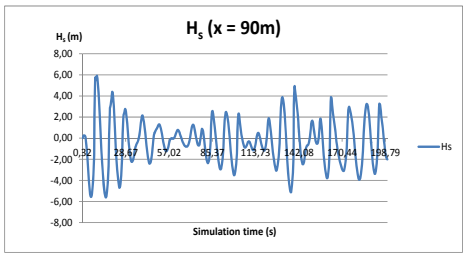

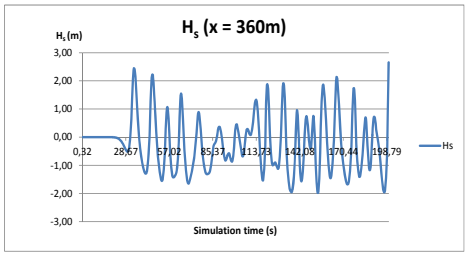

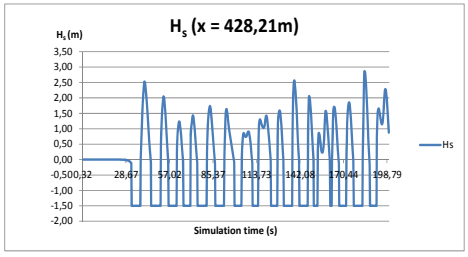

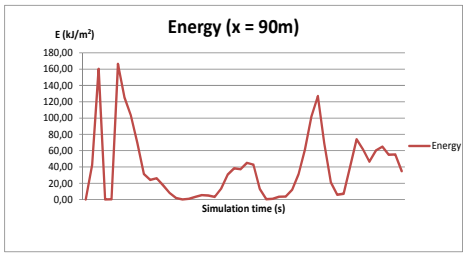

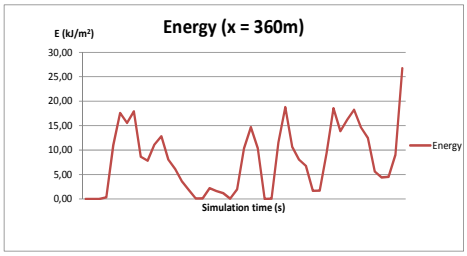

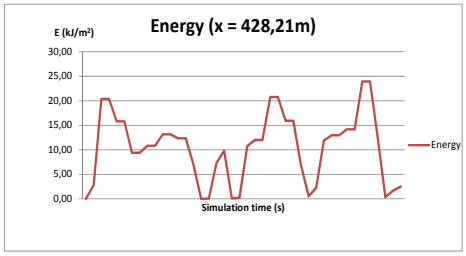

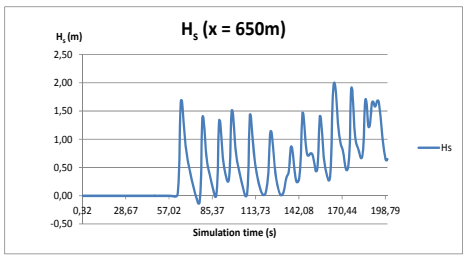

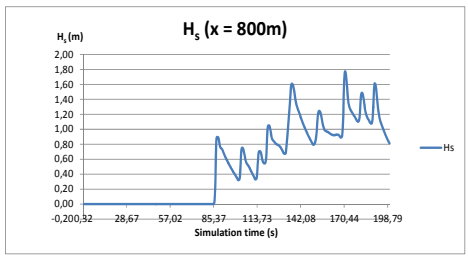

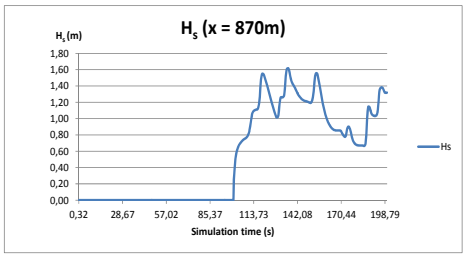

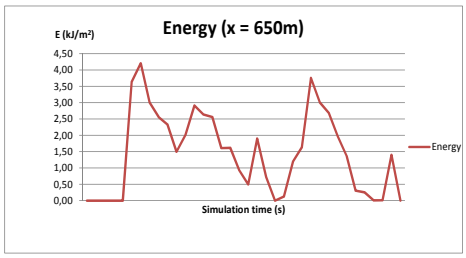

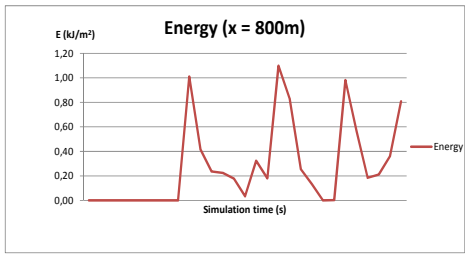

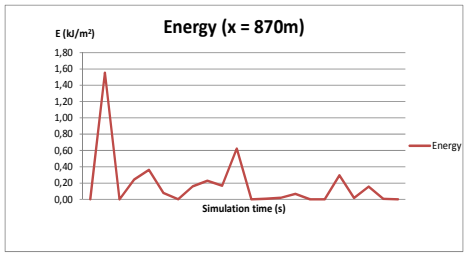

SC10	H_s (m)	T (s)	h_{cr} (m)	X (m)
	6,64	9,30	-0,50	235,00

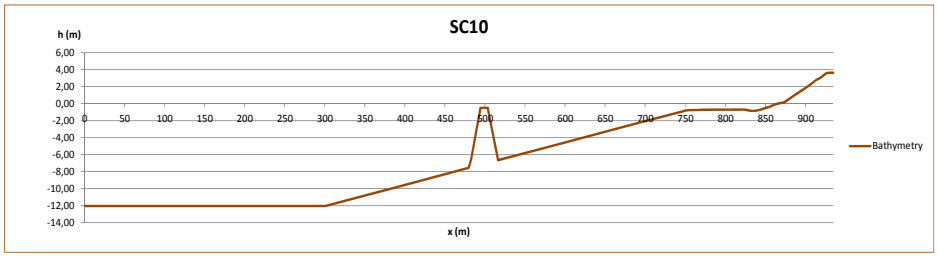

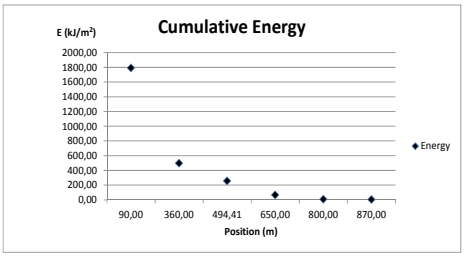

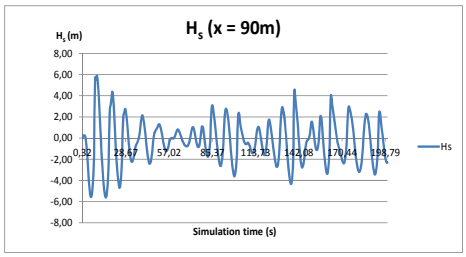

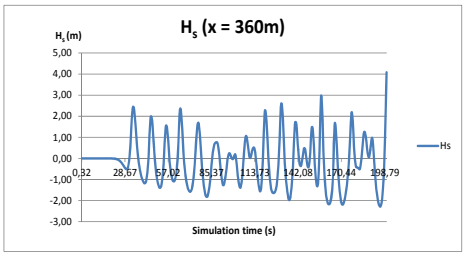

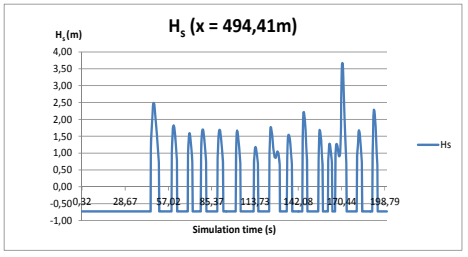

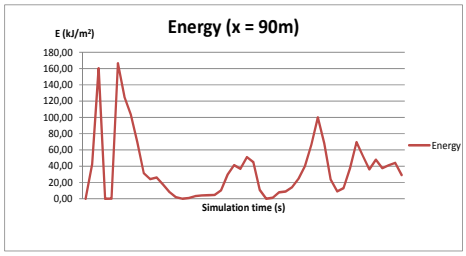

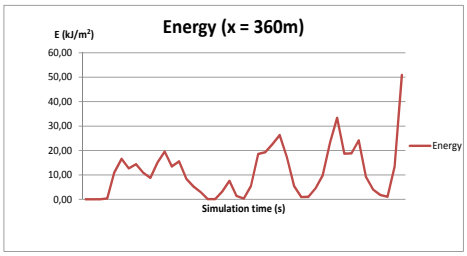

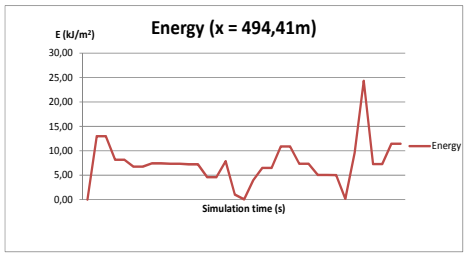

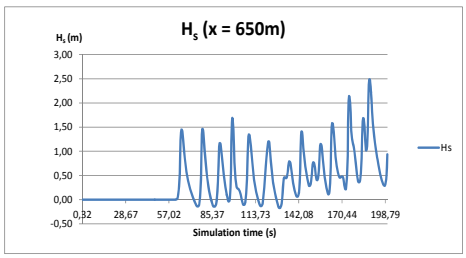

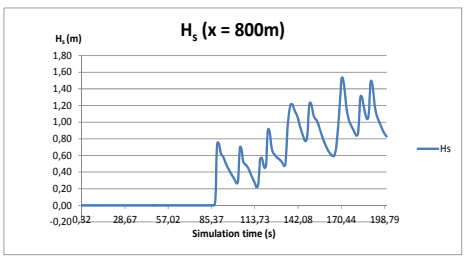

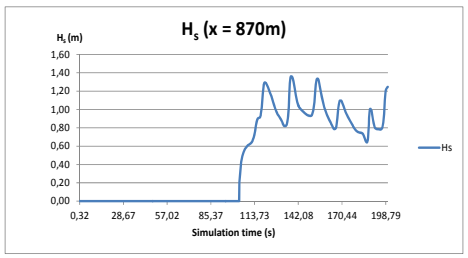

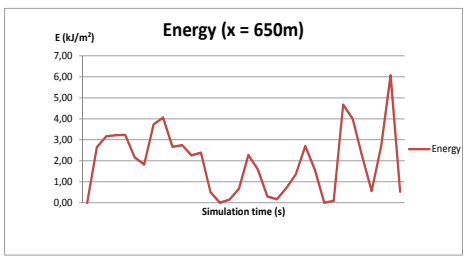

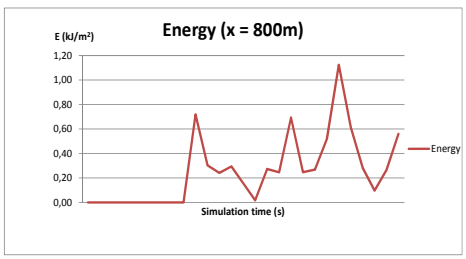

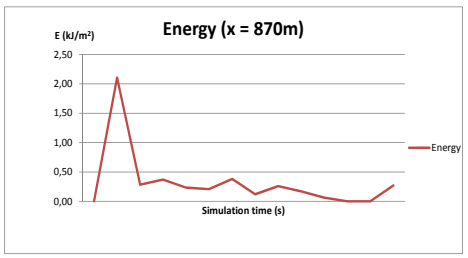

SC11	H_s (m)	T (s)	h_{cr} (m)	X (m)
	6,64	9,30	-0,50	170,00

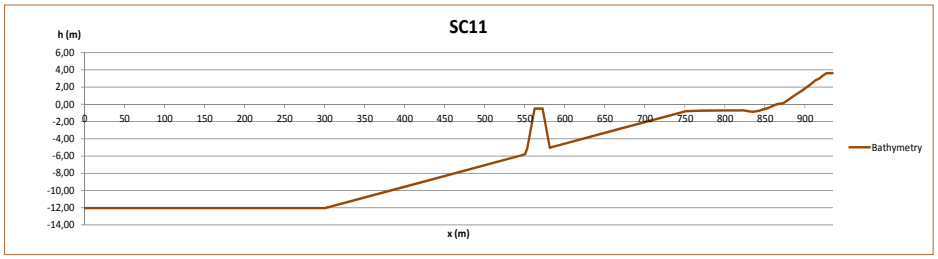

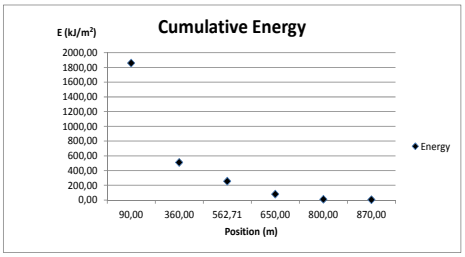

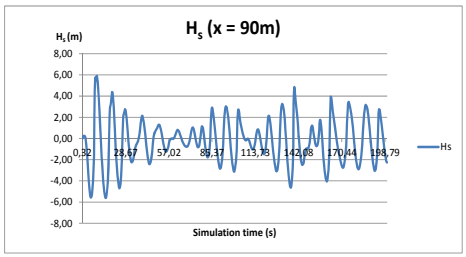

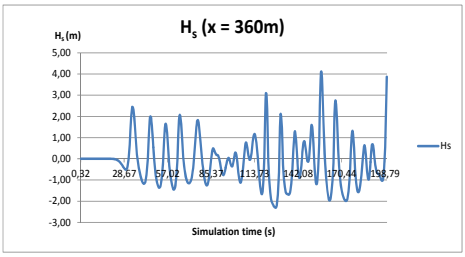

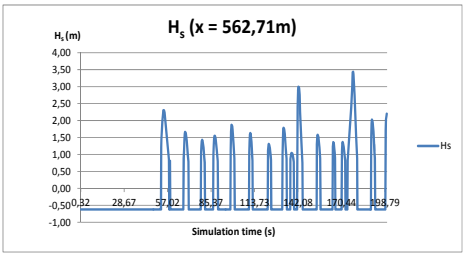

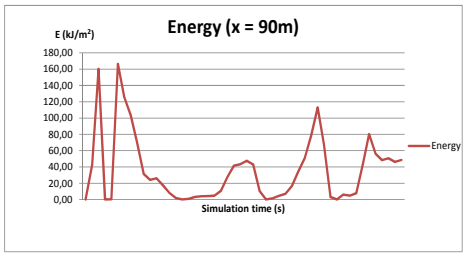

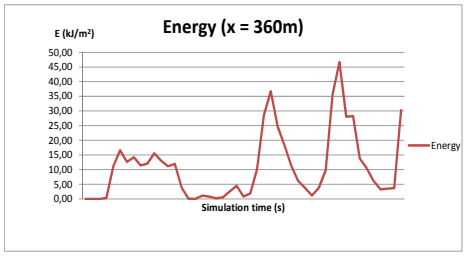

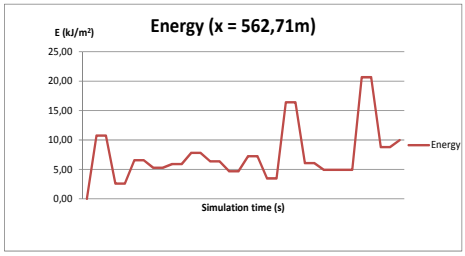

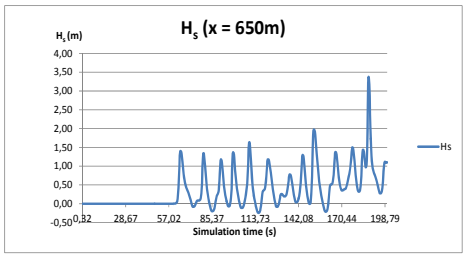

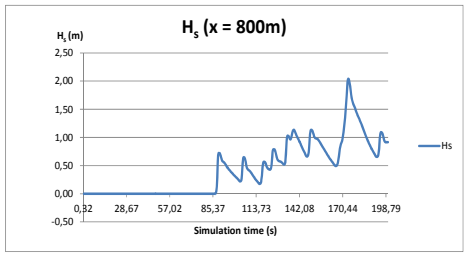

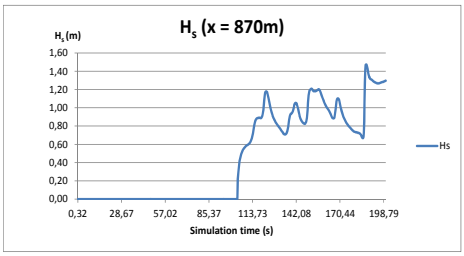

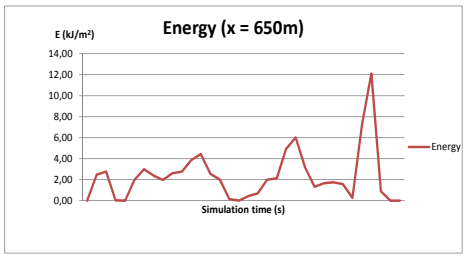

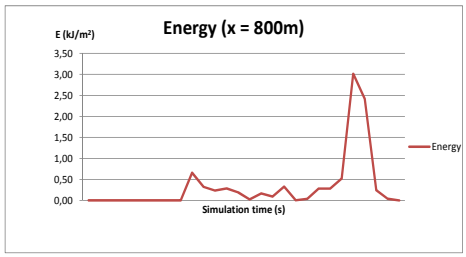

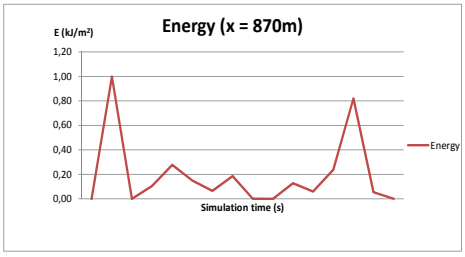

SC12	H_s (m)	T (s)	h_{cr} (m)	X (m)
	6,64	9,30	-0,50	300,00

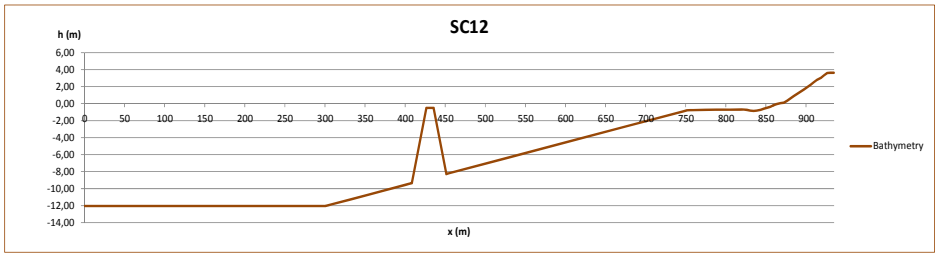

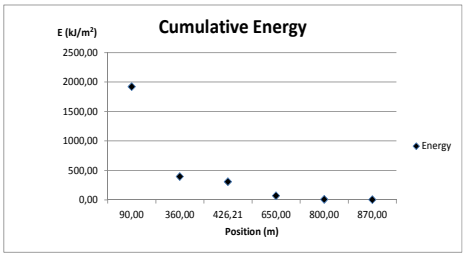

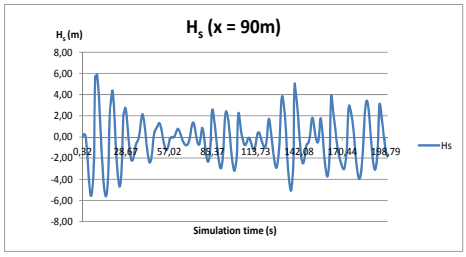

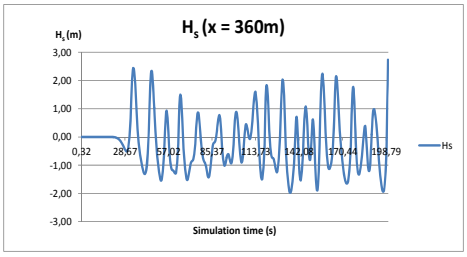

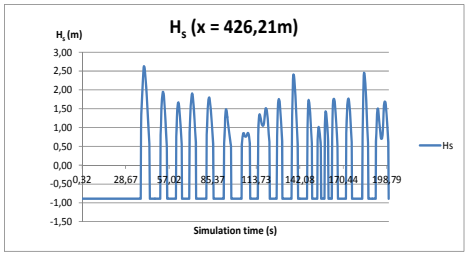

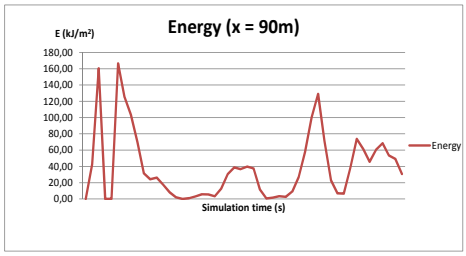

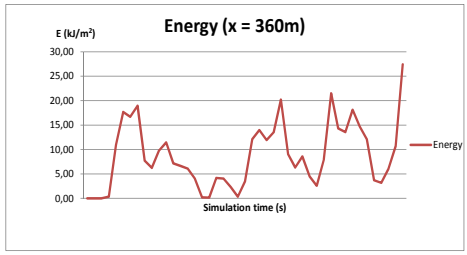

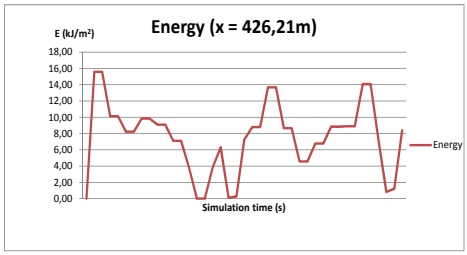

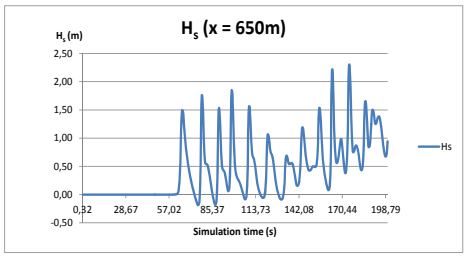

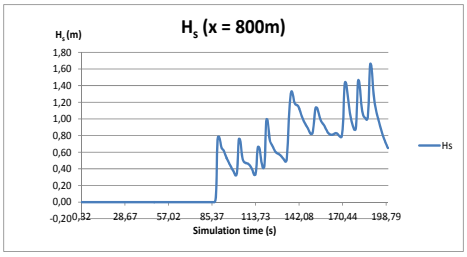

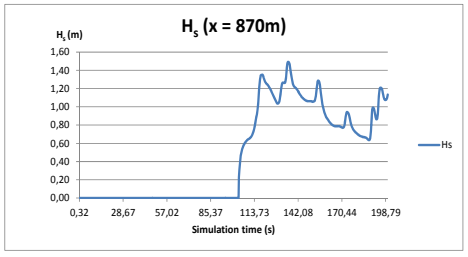

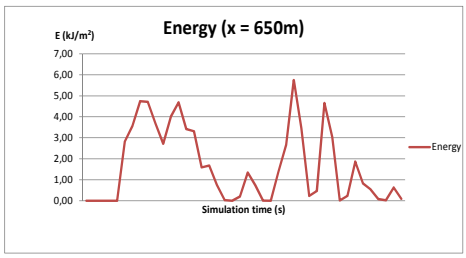

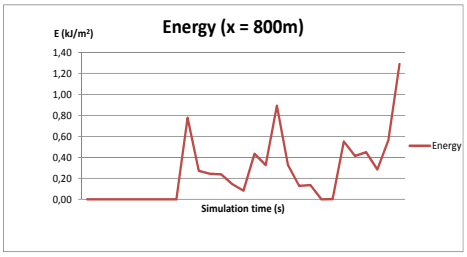

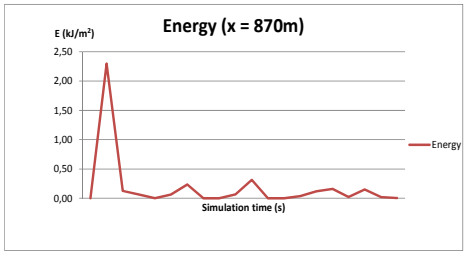

APPENDIX 3

COULWAVE.

Scenario Initial2

Scenarios 13 to 24

(Page intentionally left blank)

Scenarios Initial and scenarios with detached breakwater

Wave characteristics		Scenario
Hs (m)	T (s)	
6,64	9,30	**Initial1**
1,00	7,00	**Initial2**
2,00	7,00	**Initial3**
3,00	7,00	**Initial4**
4,00	11,00	**Initial5**

Wave characteristics		Breakwater characteristics		Scenario
H (m)	T (s)	hcr (m)	X (m)	
6,64	9,30	2,70	235,00	SC1
			170,00	SC2
			300,00	SC3
		1,50	235,00	SC4
			170,00	SC5
			300,00	SC6
		-1,50	235,00	SC7
			170,00	SC8
			300,00	SC9
		-0,50	235,00	SC10
			170,00	SC11
			300,00	SC12
1,00	7,00	2,70	235,00	SC13
			170,00	SC14
			300,00	SC15
		1,50	235,00	SC16
			170,00	SC17
			300,00	SC18
		-1,50	235,00	SC19
			170,00	SC20
			300,00	SC21
		-0,50	235,00	SC22
			170,00	SC23
			300,00	SC24
2,00	7,00	2,70	235,00	SC25
			170,00	SC26
			300,00	SC27
		1,50	235,00	SC28
			170,00	SC29
			300,00	SC30
		-1,50	235,00	SC31
			170,00	SC32
			300,00	SC33
		-0,50	235,00	SC34
			170,00	SC35
			300,00	SC36
3,00	7,00	2,70	235,00	SC37
			170,00	SC38
			300,00	SC39
		1,50	235,00	SC40
			170,00	SC41
			300,00	SC42
		-1,50	235,00	SC43
			170,00	SC44
			300,00	SC45
		-0,50	235,00	SC46
			170,00	SC47
			300,00	SC48
4,00	11,00	2,70	235,00	SC49
			170,00	SC50
			300,00	SC51
		1,50	235,00	SC52
			170,00	SC53
			300,00	SC54
		-1,50	235,00	SC55
			170,00	SC56
			300,00	SC57
		-0,50	235,00	SC58
			170,00	SC59
			300,00	SC60

Initial2	Hs (m)	T (s)
	1,00	7,00

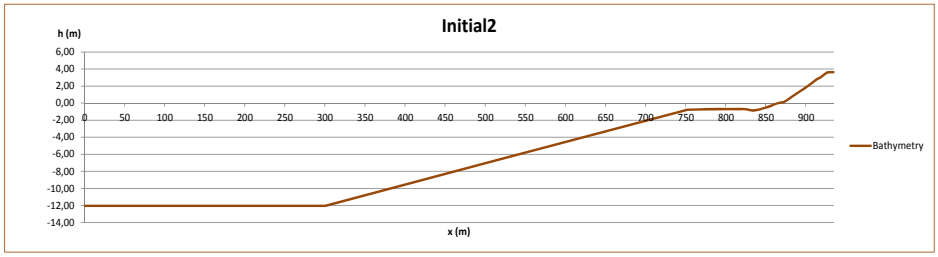

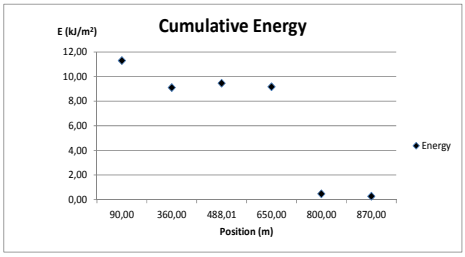

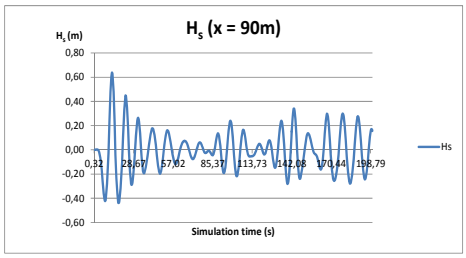

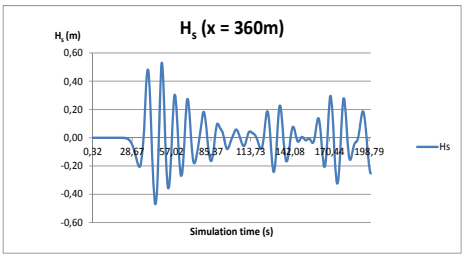

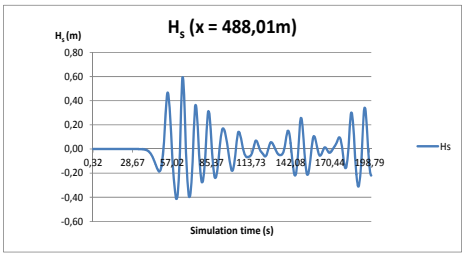

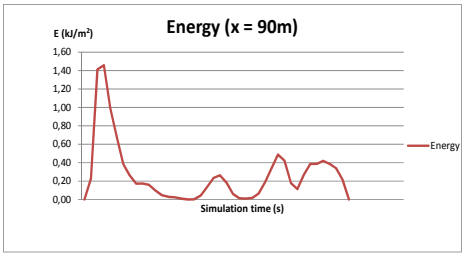

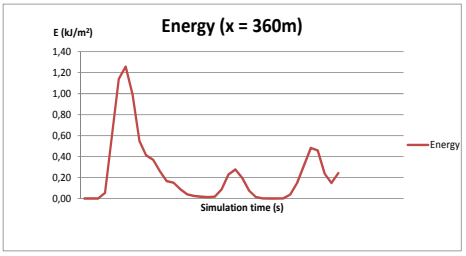

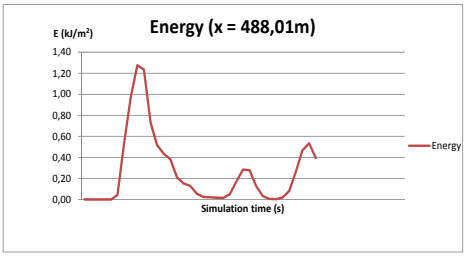

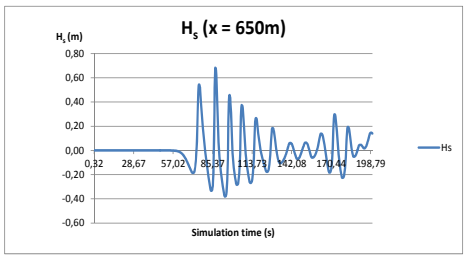

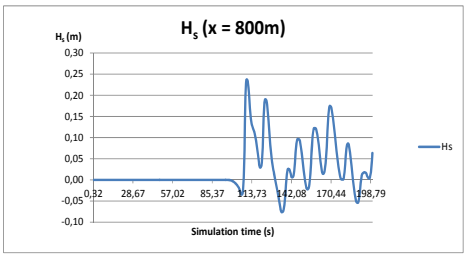

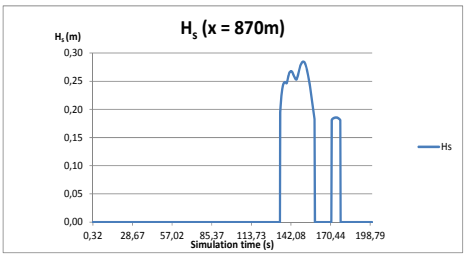

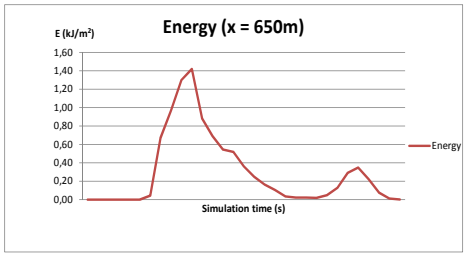

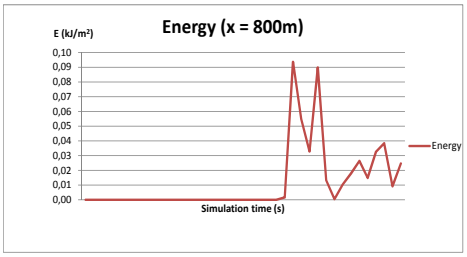

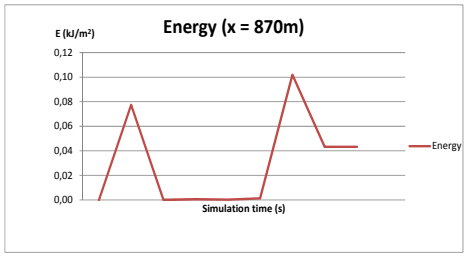

SC13	H_s (m)	T (s)	h_{cr} (m)	X (m)
	1,00	7,00	2,70	235,00

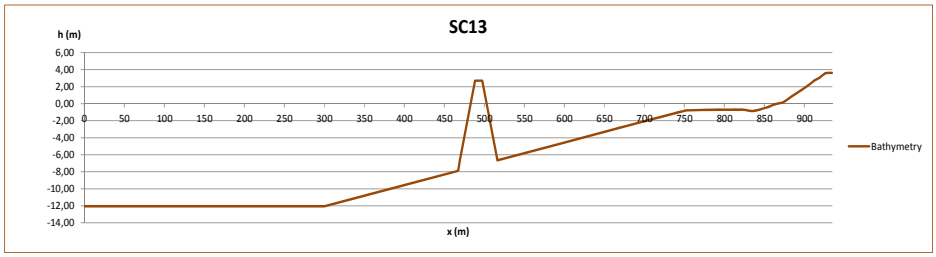

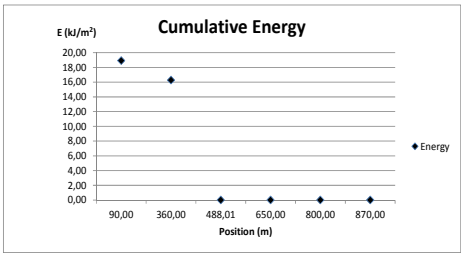

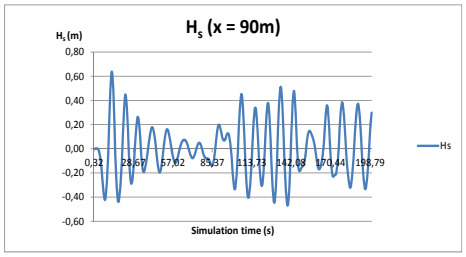

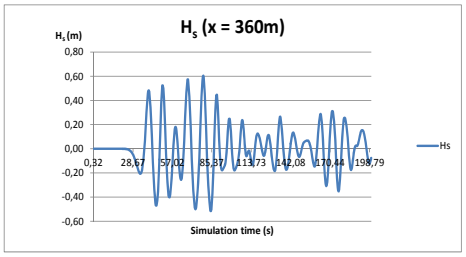

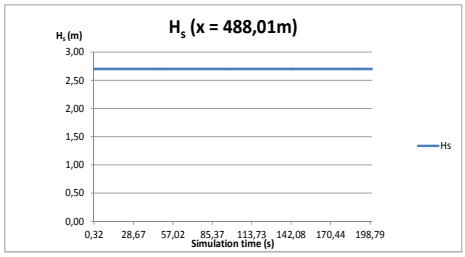

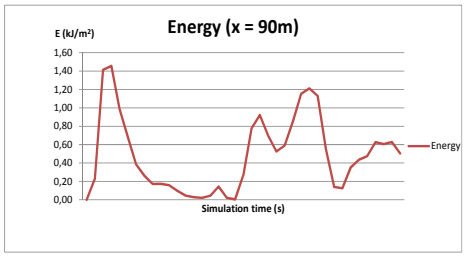

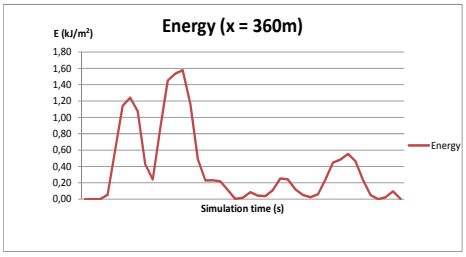

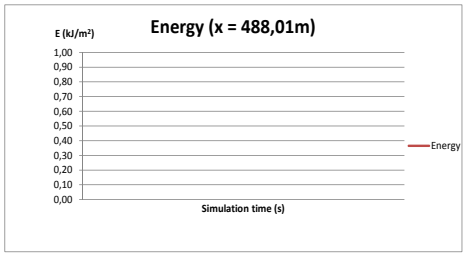

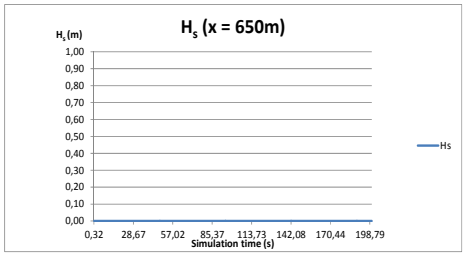

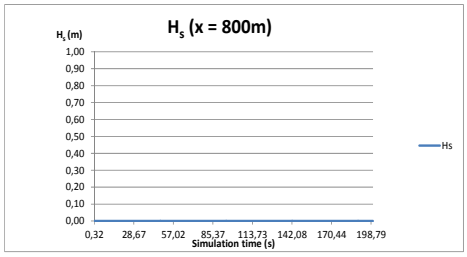

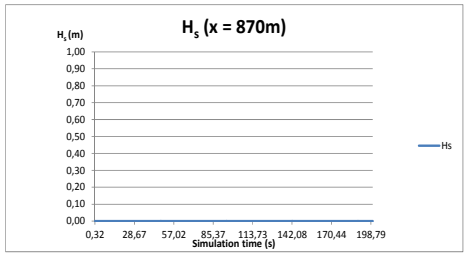

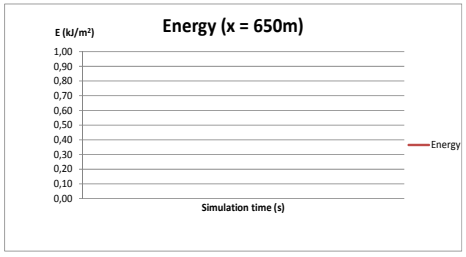

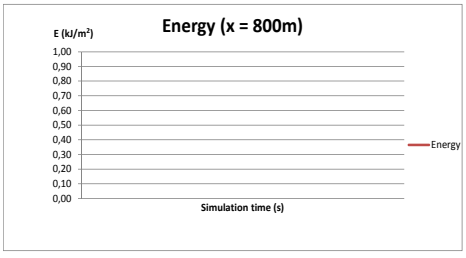

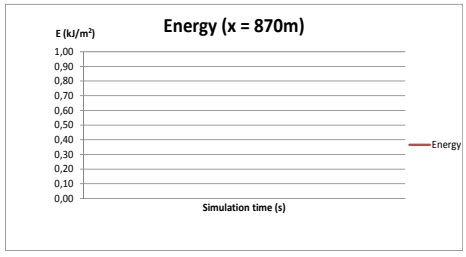

SC14	H_s (m)	T (s)	h_{cr} (m)	X (m)
	1,00	7,00	2,70	170,00

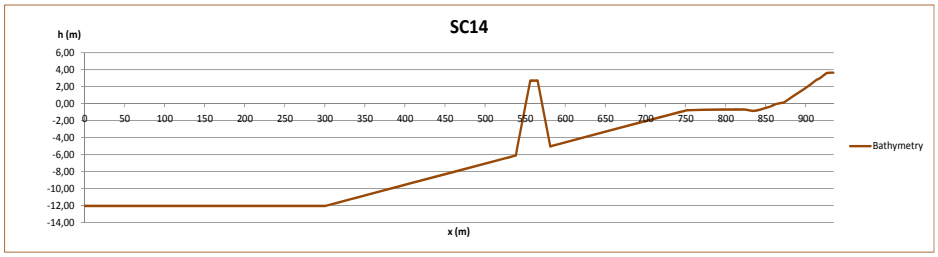

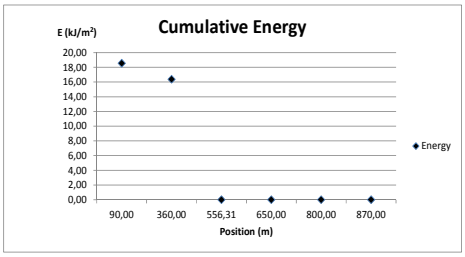

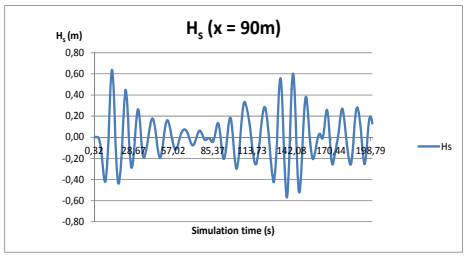

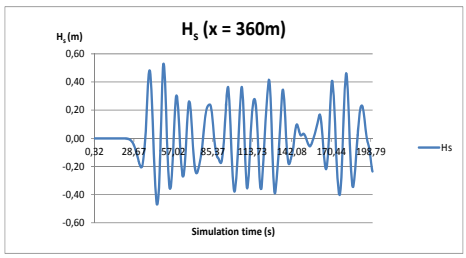

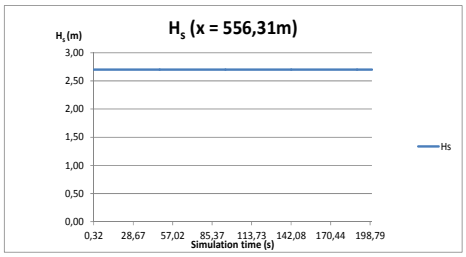

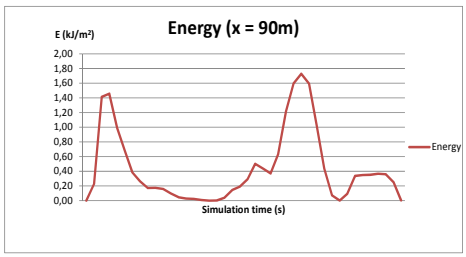

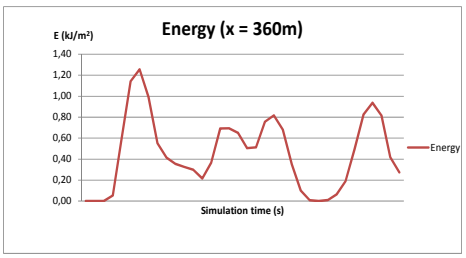

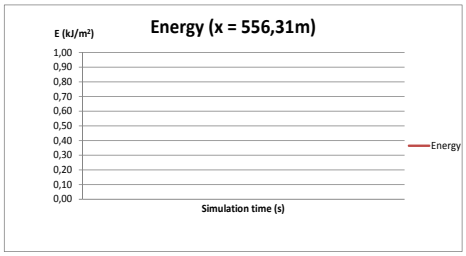

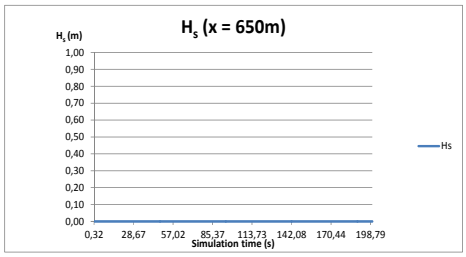

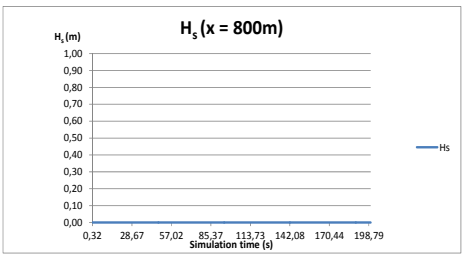

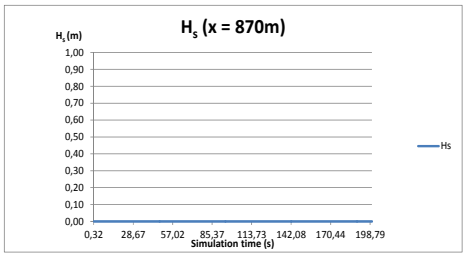

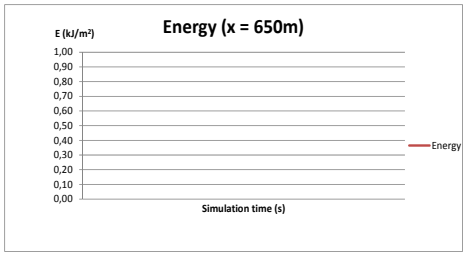

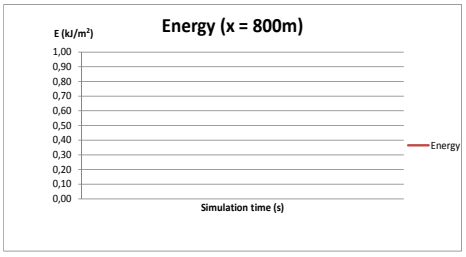

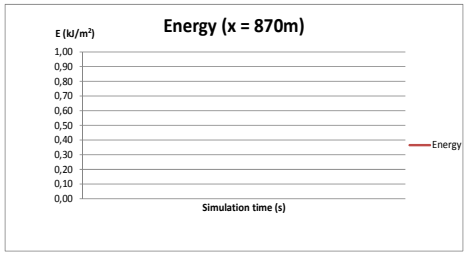

SC15	H_s (m)	T (s)	h_{cr} (m)	X (m)
	1,00	7,00	2,70	300,00

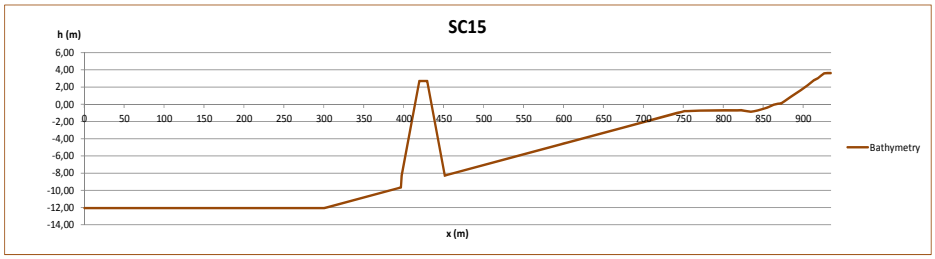

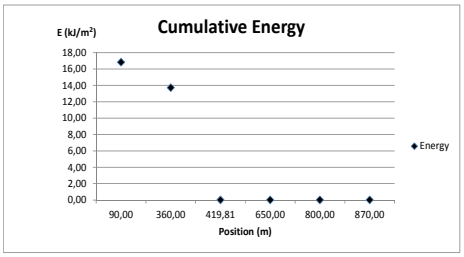

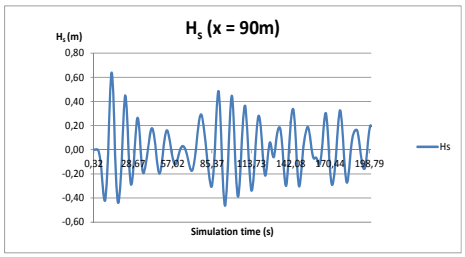

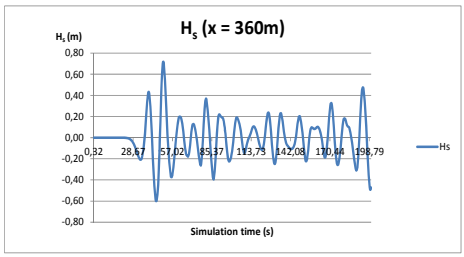

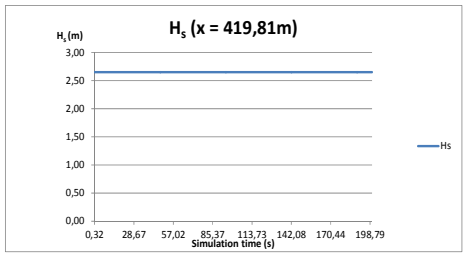

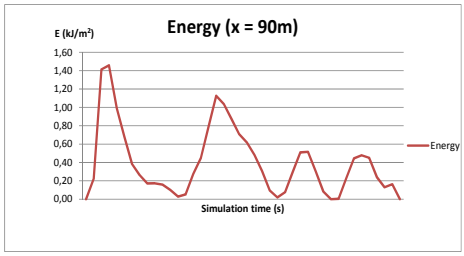

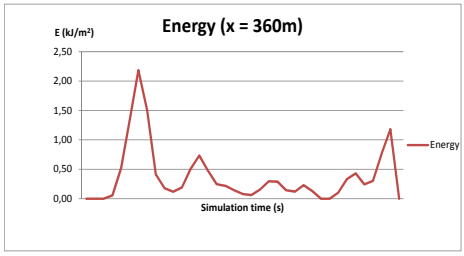

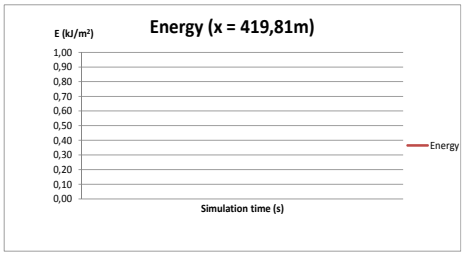

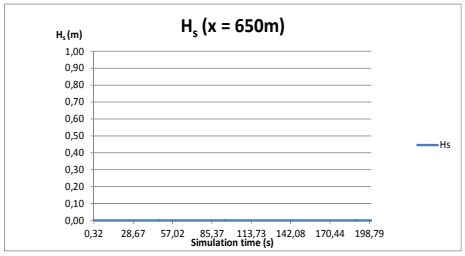

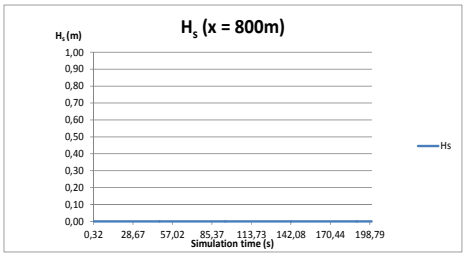

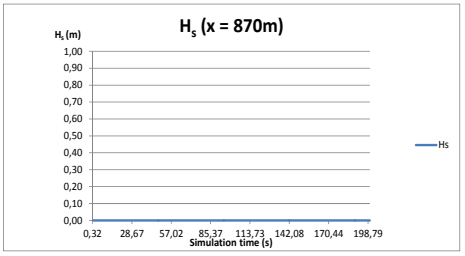

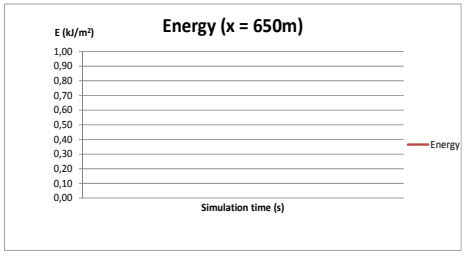

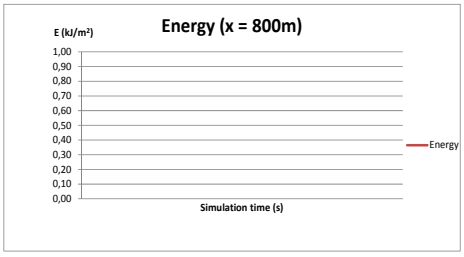

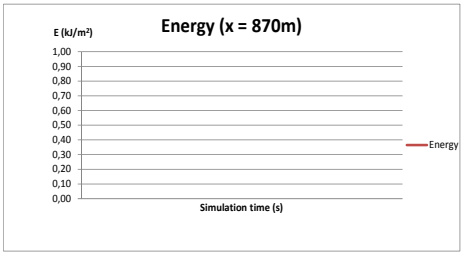

SC16	H_s (m)	T (s)	h_{cr} (m)	X (m)
	1,00	7,00	1,50	235,00

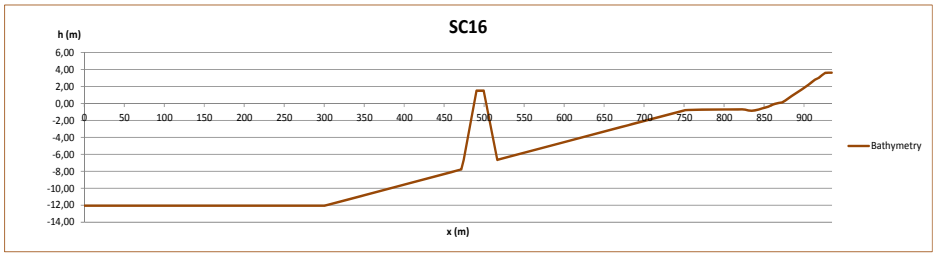

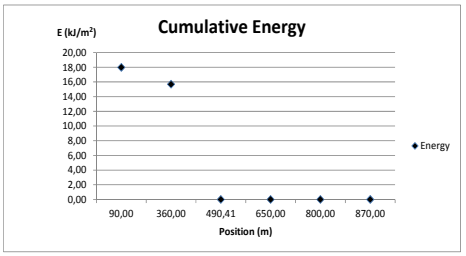

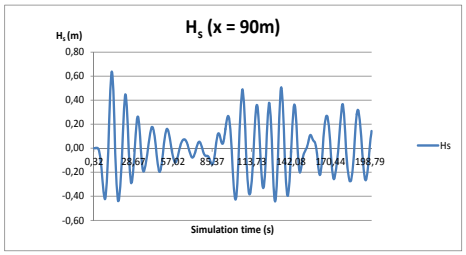

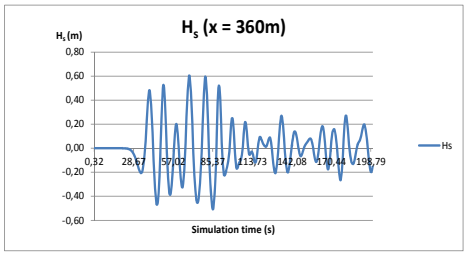

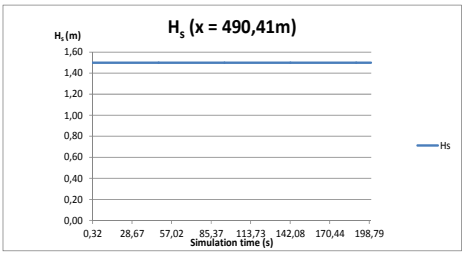

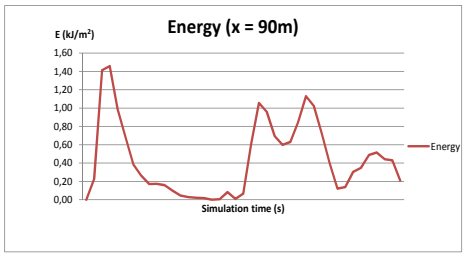

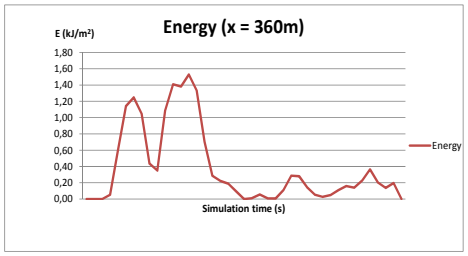

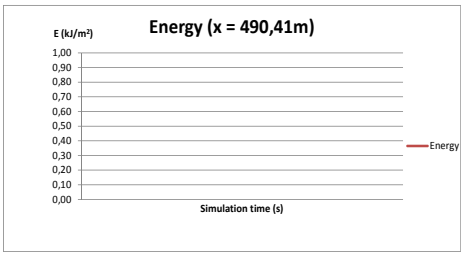

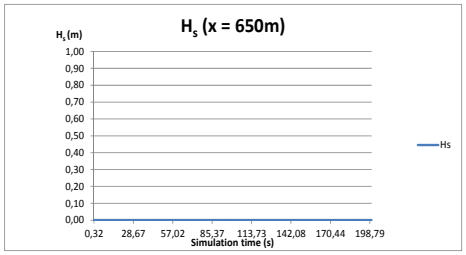

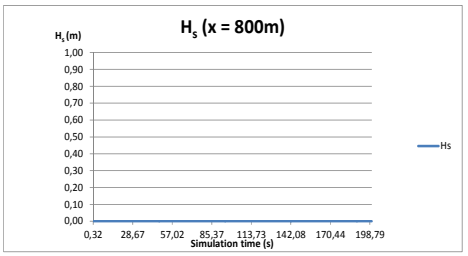

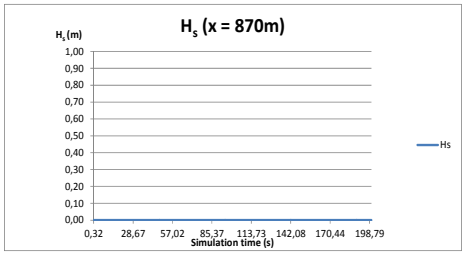

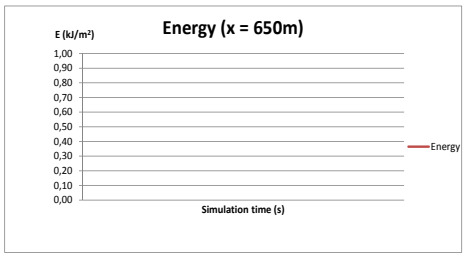

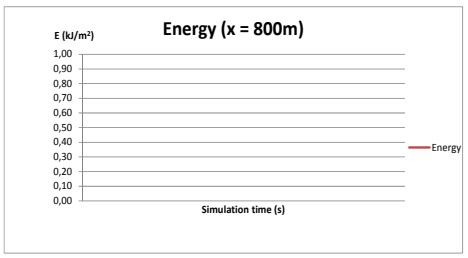

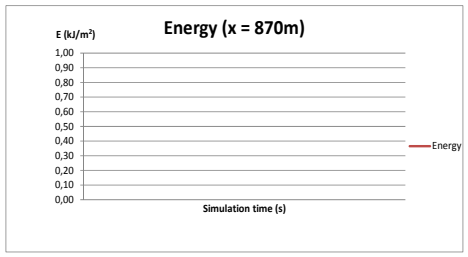

SC17	H_s (m)	T (s)	h_{cr} (m)	X (m)
	1,00	7,00	1,50	170,00

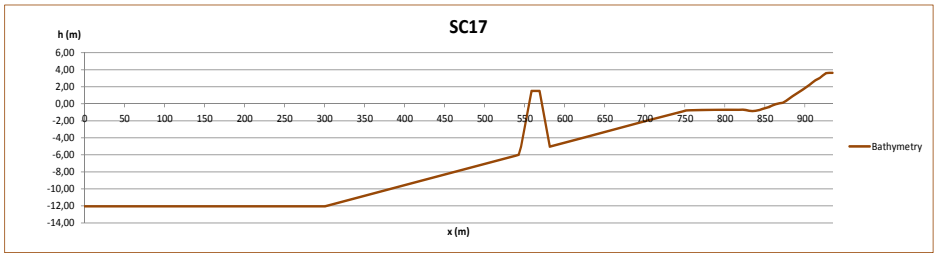

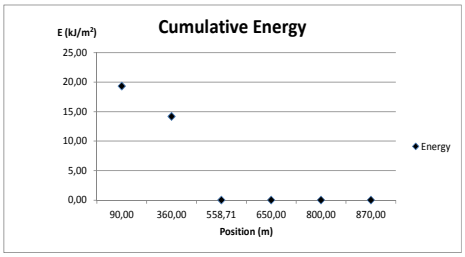

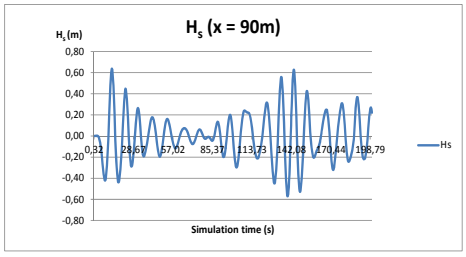

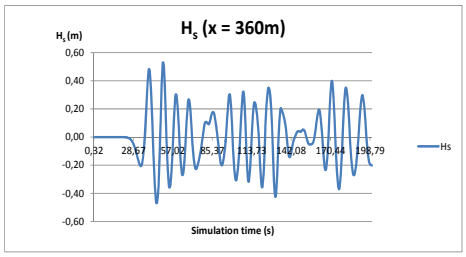

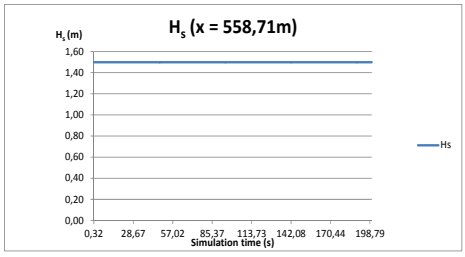

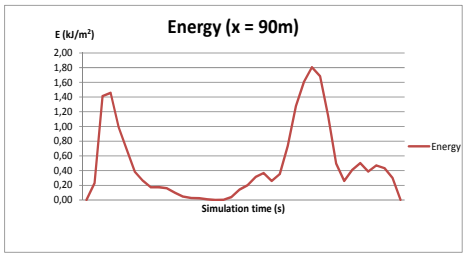

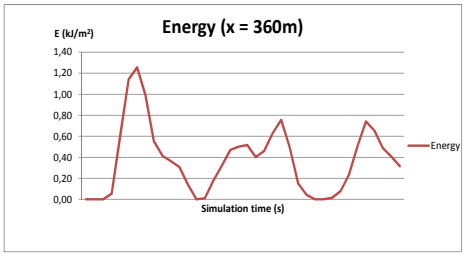

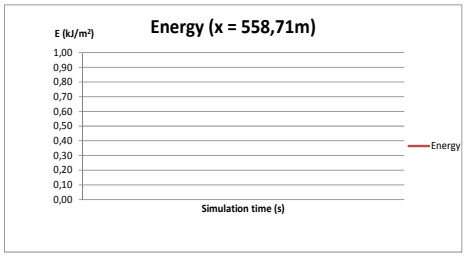

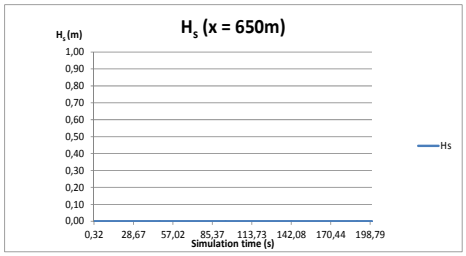

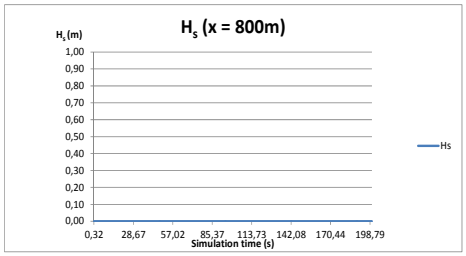

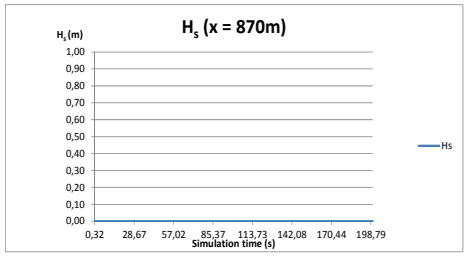

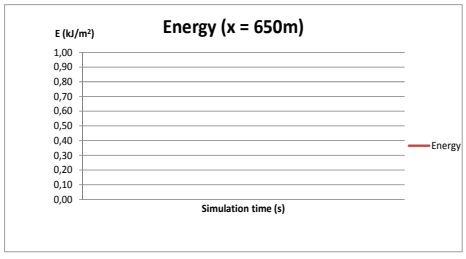

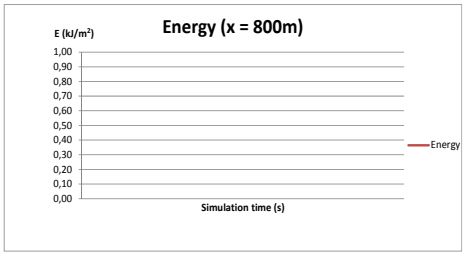

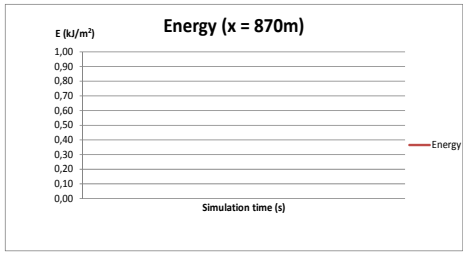

SC18	H_s (m)	T (s)	h_{cr} (m)	X (m)
	1,00	7,00	1,50	300,00

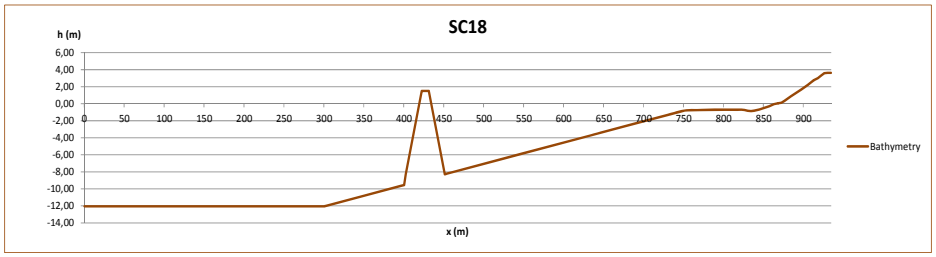

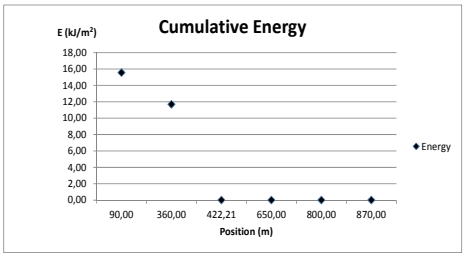

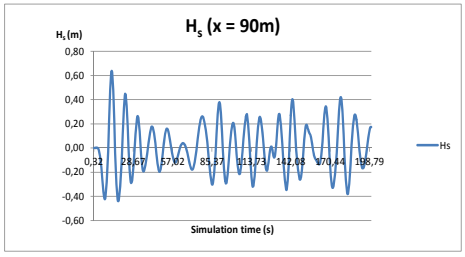

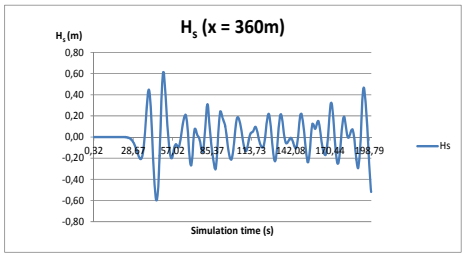

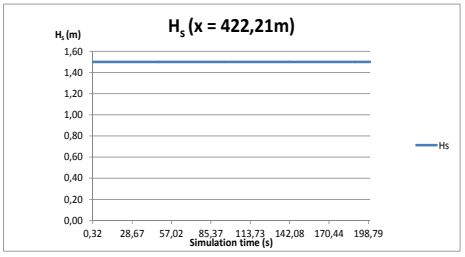

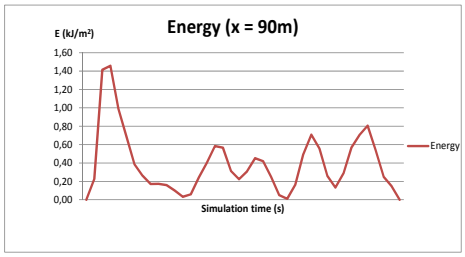

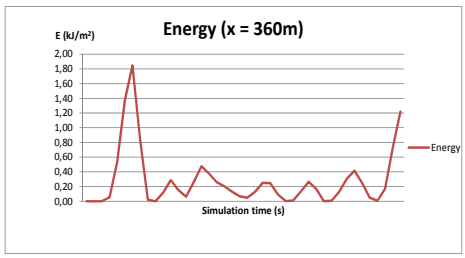

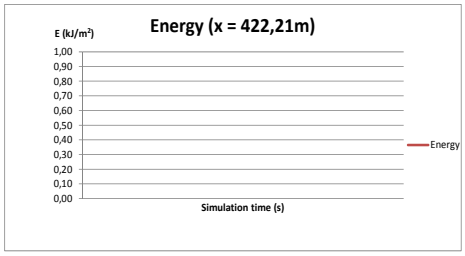

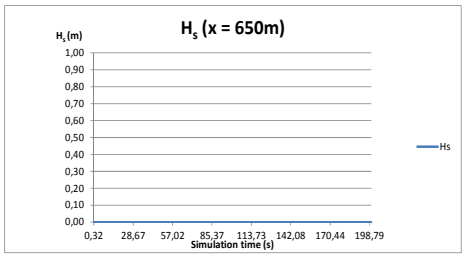

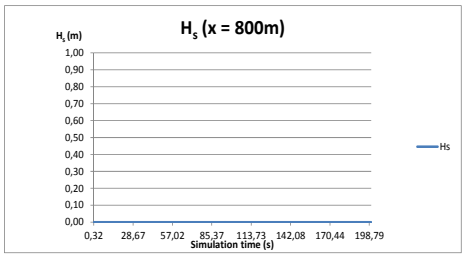

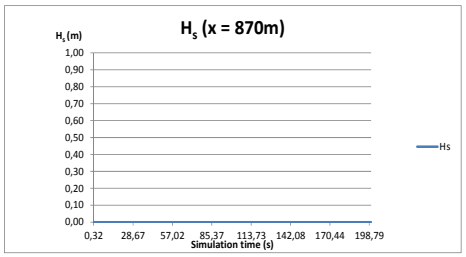

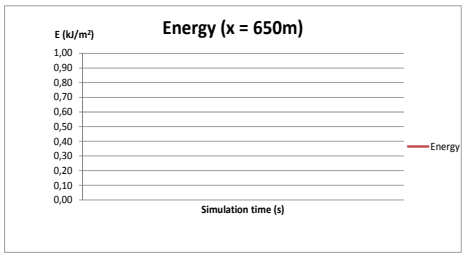

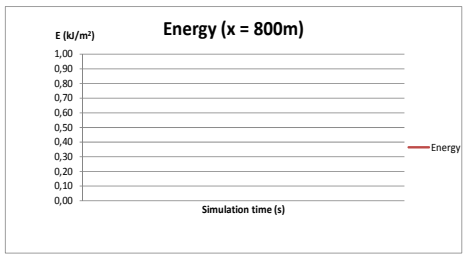

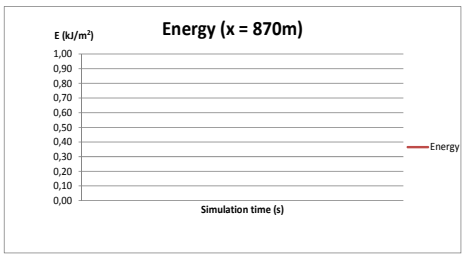

SC19	H_s (m)	T (s)	h_{cr} (m)	X (m)
	1,00	7,00	-1,50	235,00

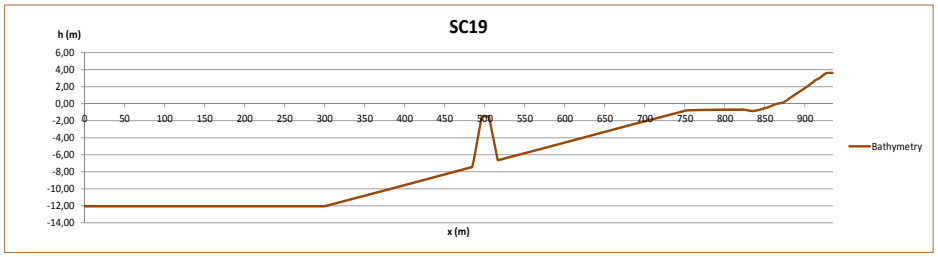

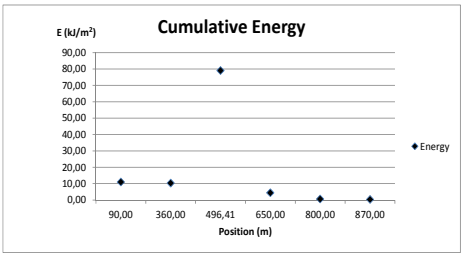

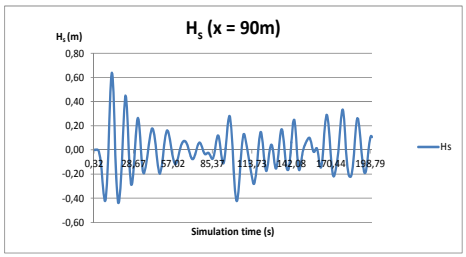

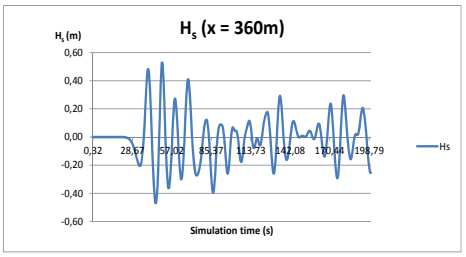

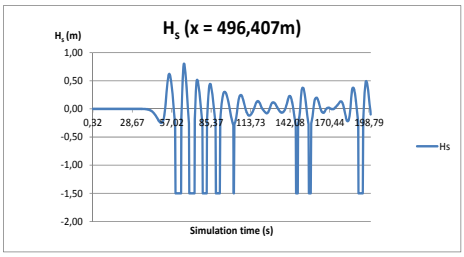

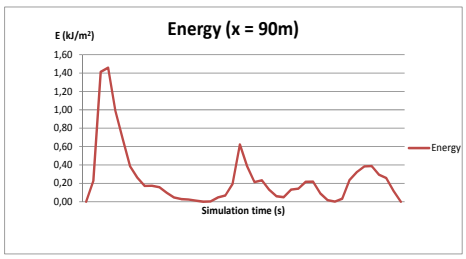

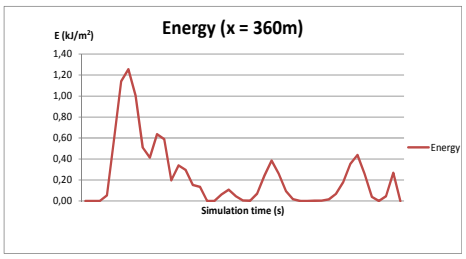

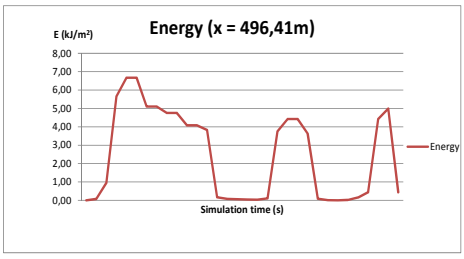

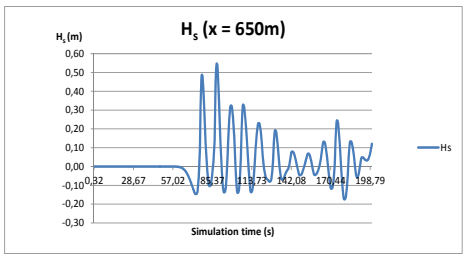

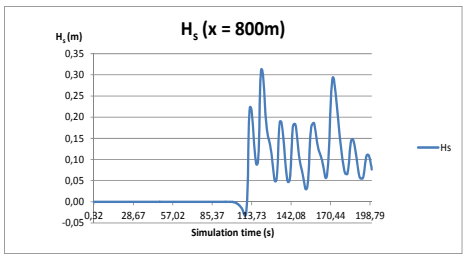

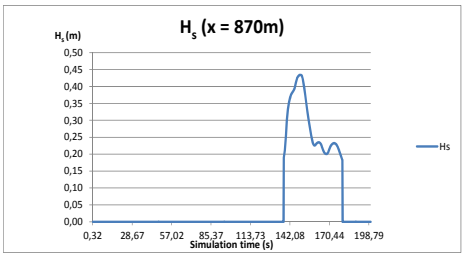

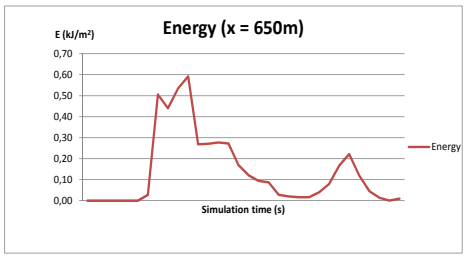

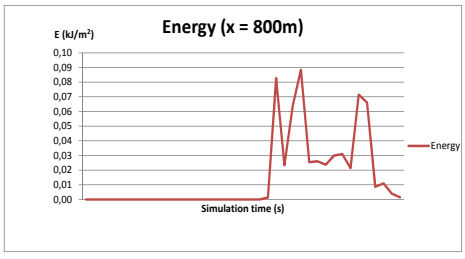

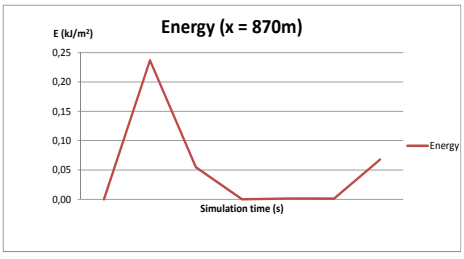

SC20	H_s (m)	T (s)	h_{cr} (m)	X (m)
	1,00	7,00	-1,50	170,00

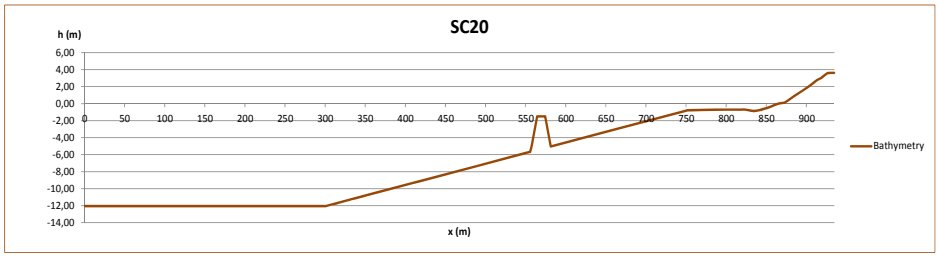

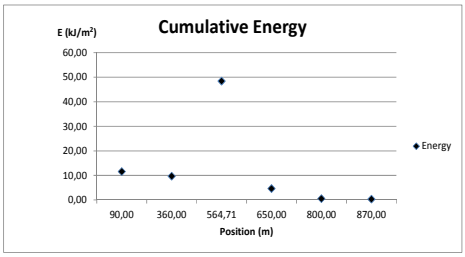

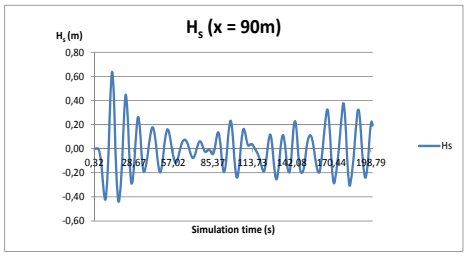

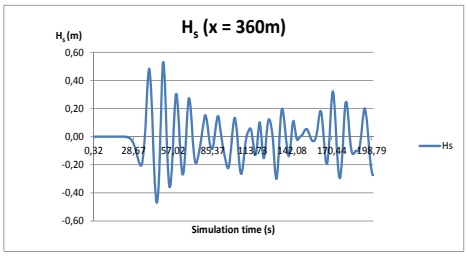

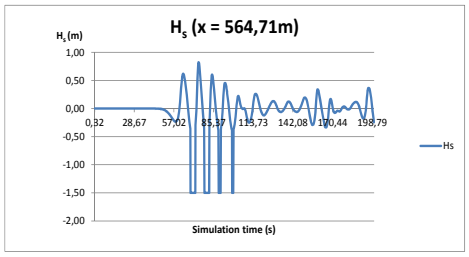

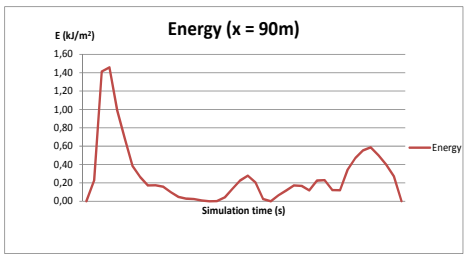

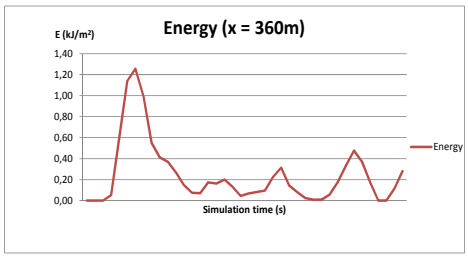

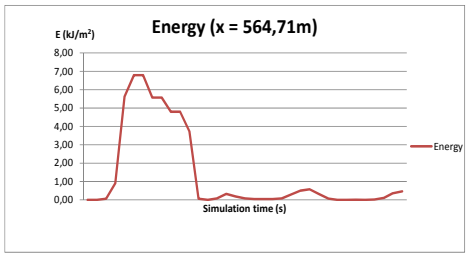

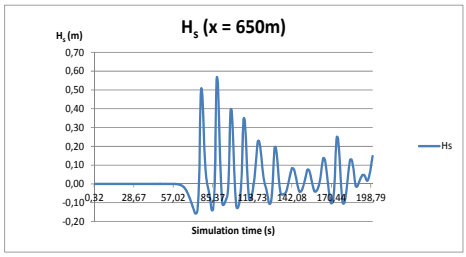

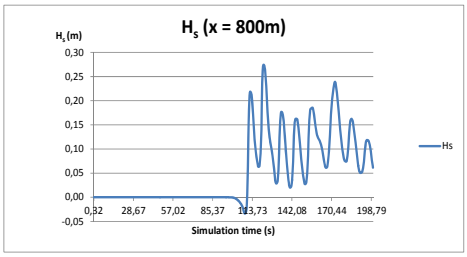

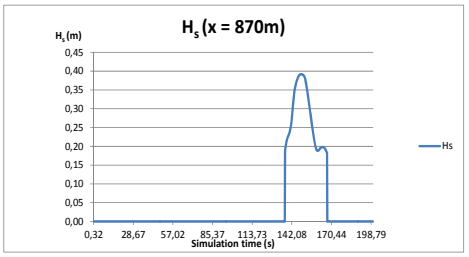

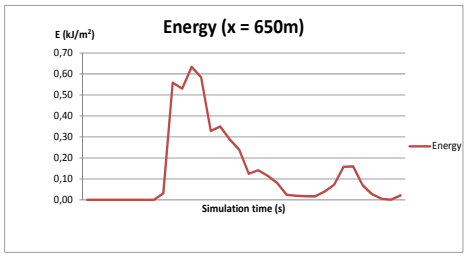

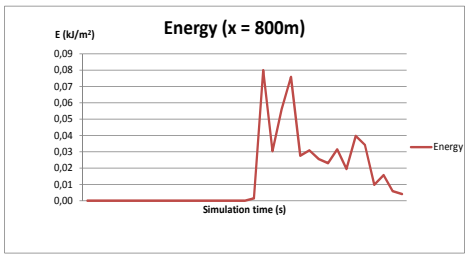

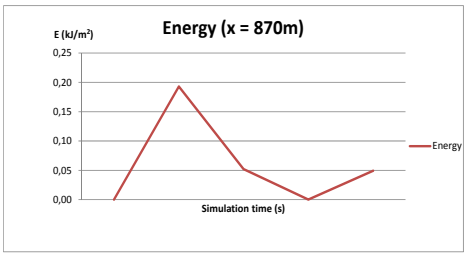

SC21	H_s (m)	T (s)	h_{cr} (m)	X (m)
	1,00	7,00	-1,50	300,00

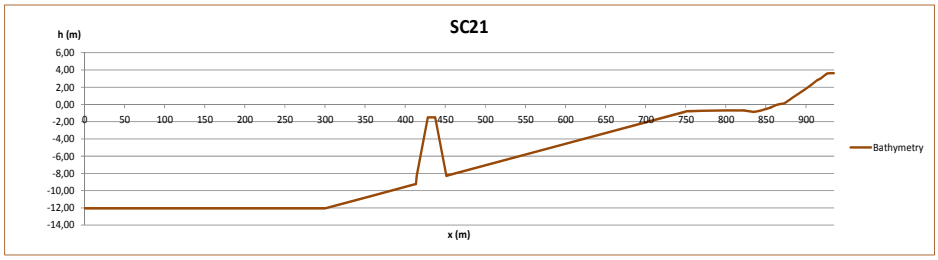

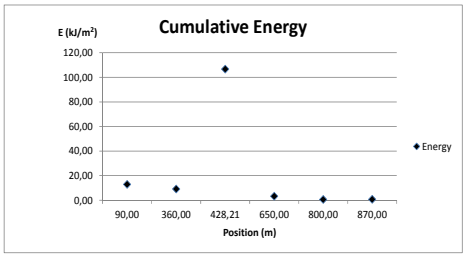

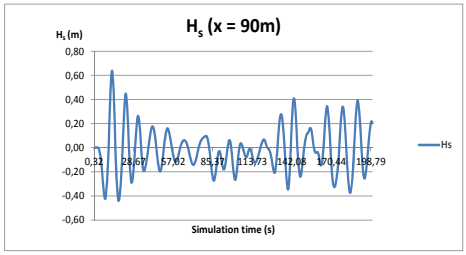

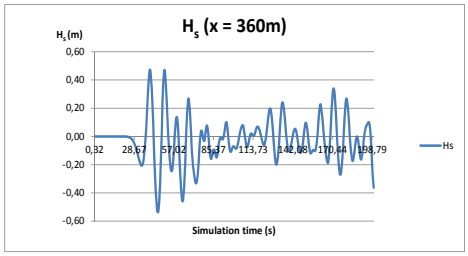

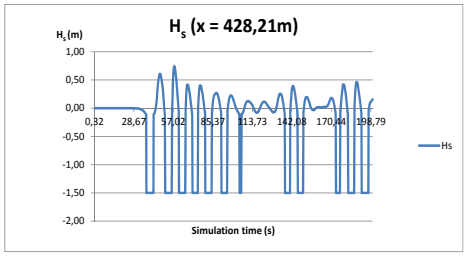

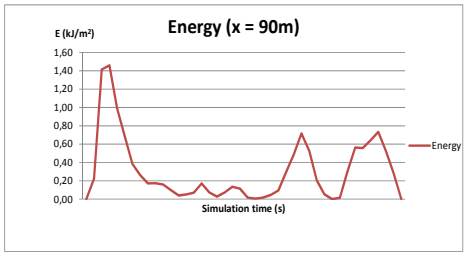

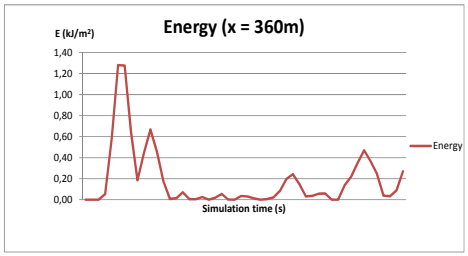

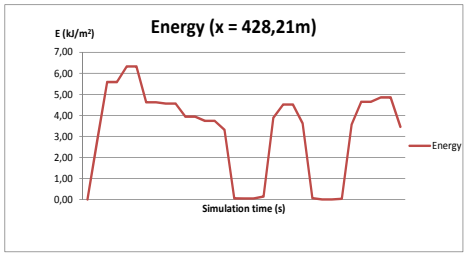

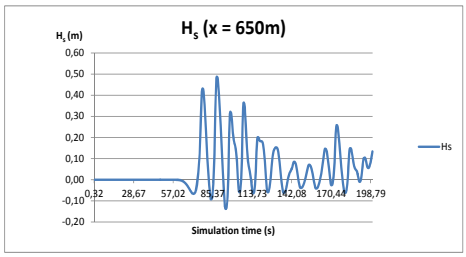

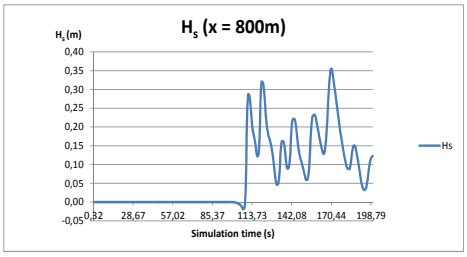

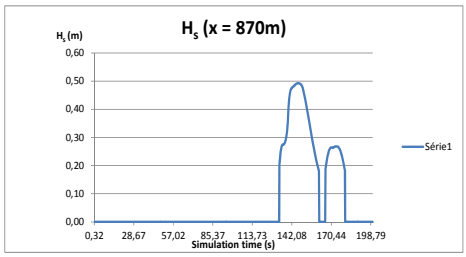

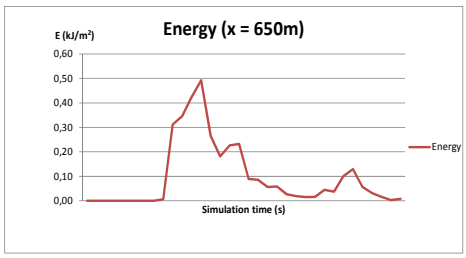

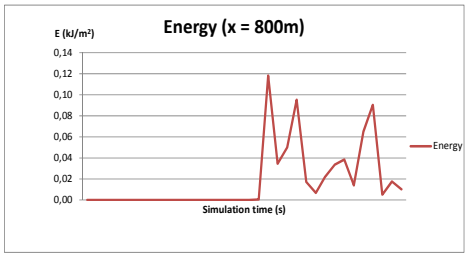

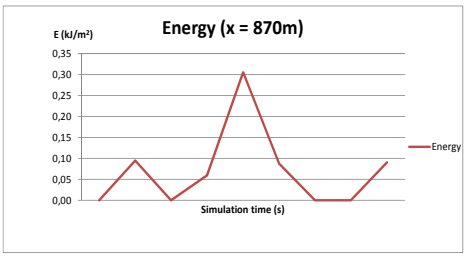

SC22	H_s (m)	T (s)	h_{cr} (m)	X (m)
	1,00	7,00	-0,50	235,00

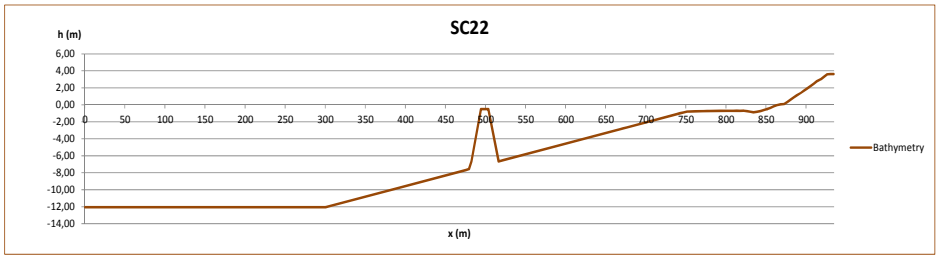

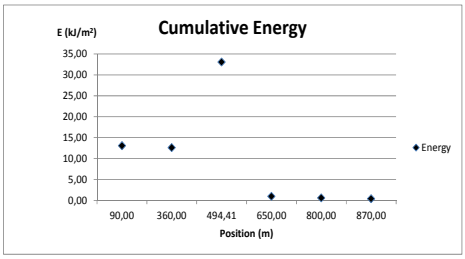

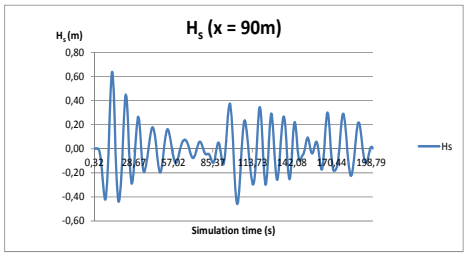

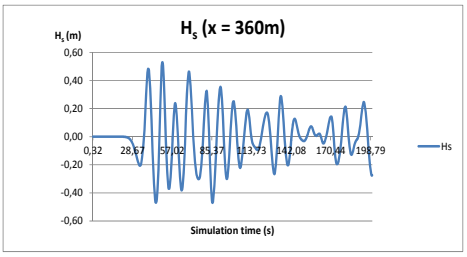

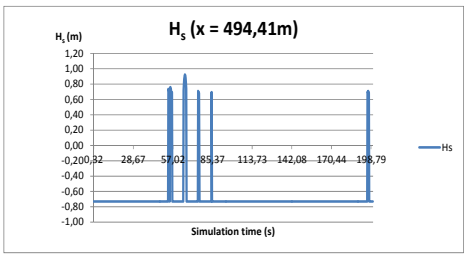

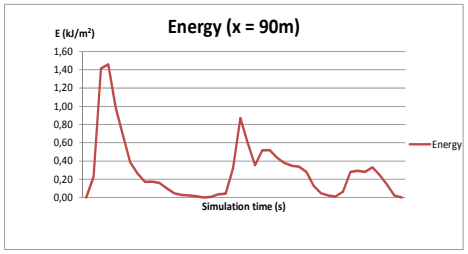

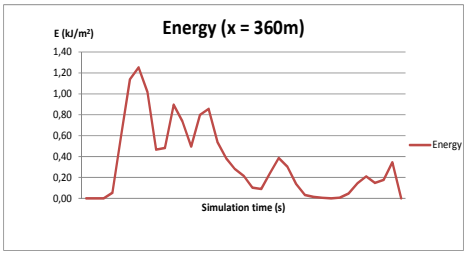

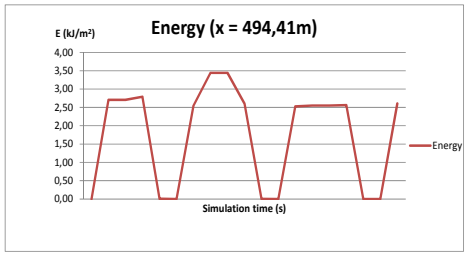

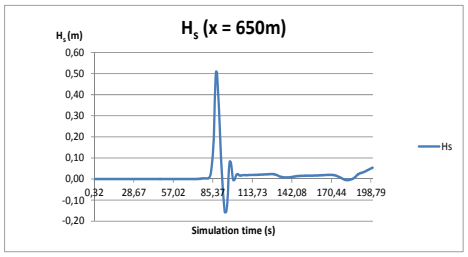

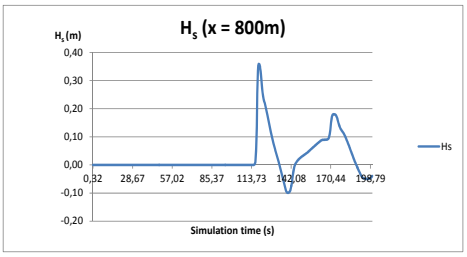

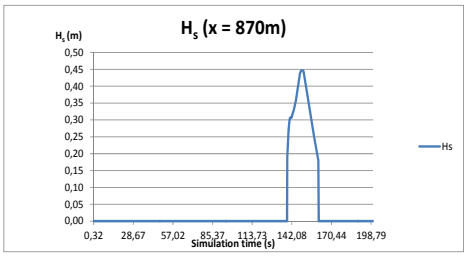

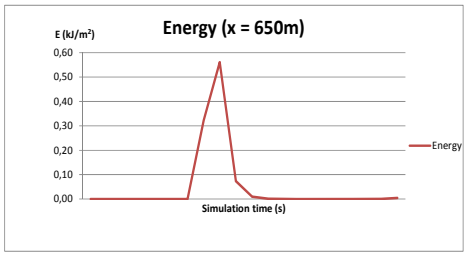

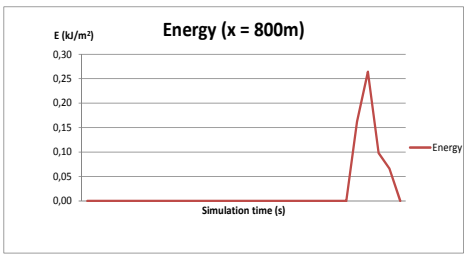

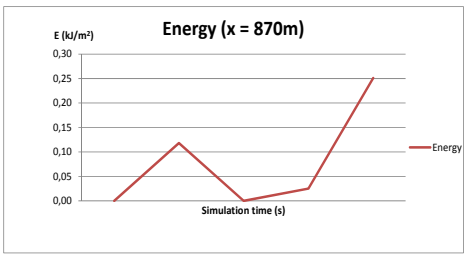

SC23	H_s (m)	T (s)	h_{cr} (m)	X (m)
	1,00	7,00	-0,50	170,00

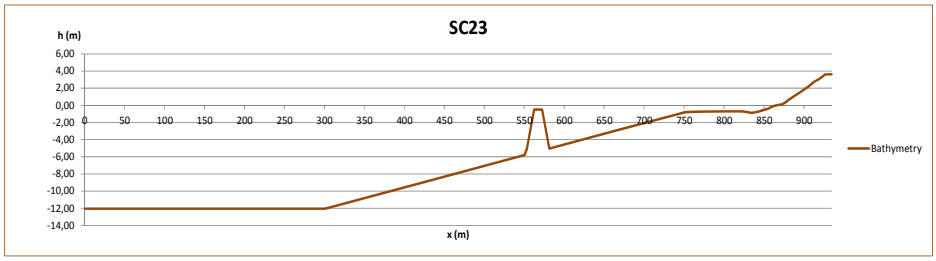

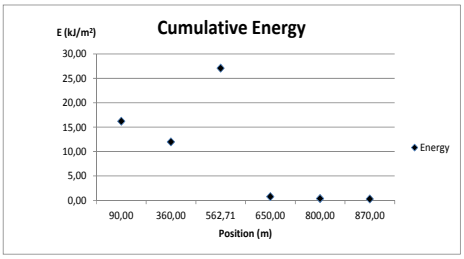

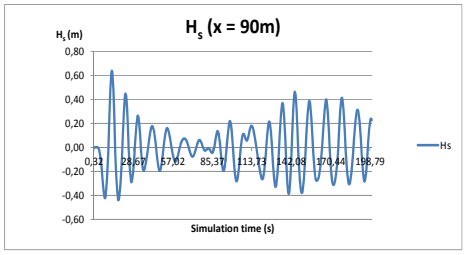

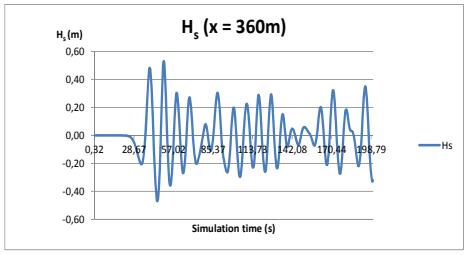

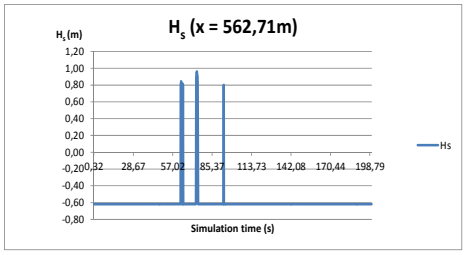

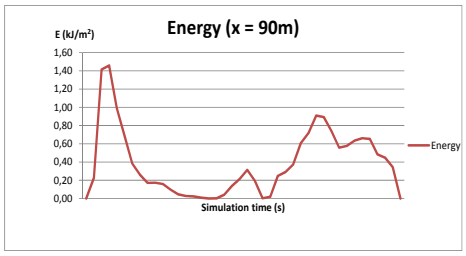

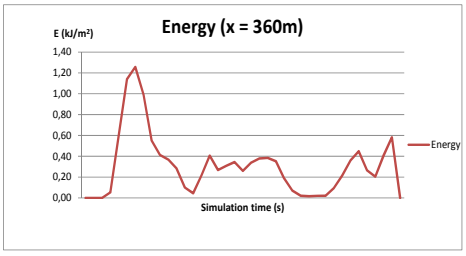

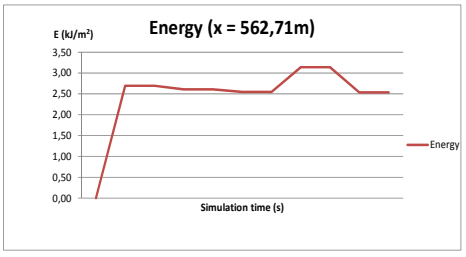

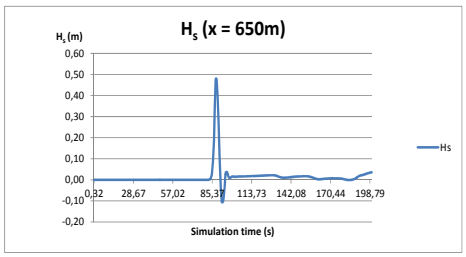

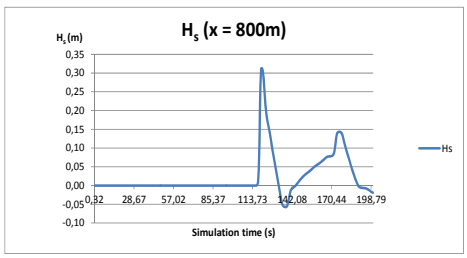

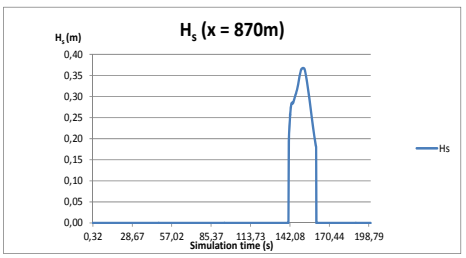

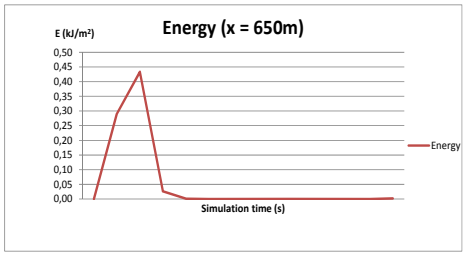

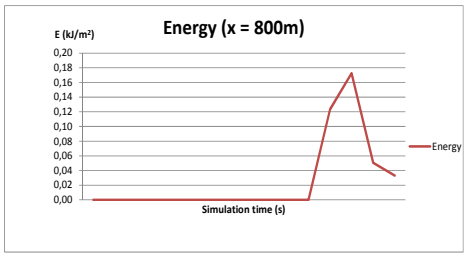

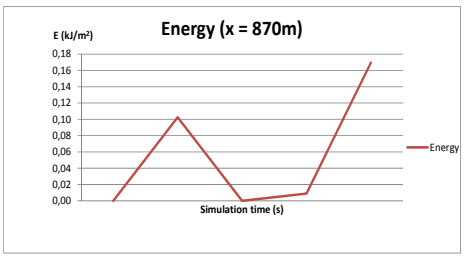

SC24	H_s (m)	T (s)	h_{cr} (m)	X (m)
	1,00	7,00	-0,50	300,00

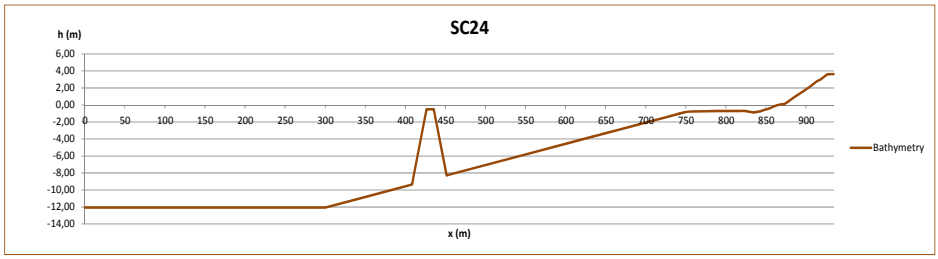

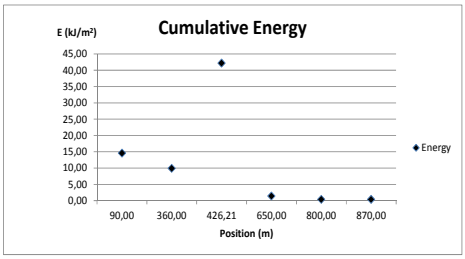

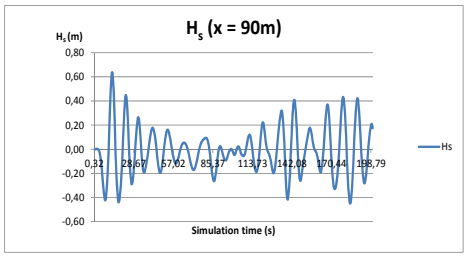

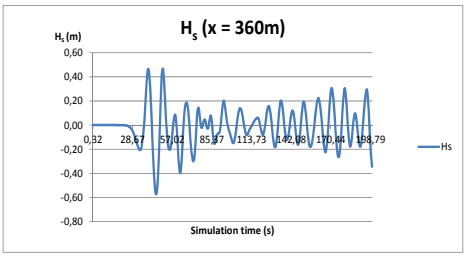

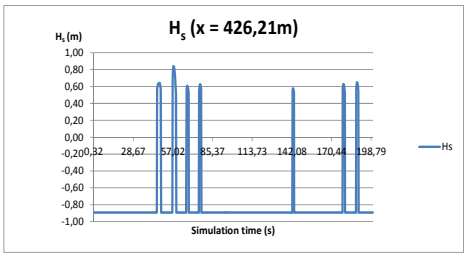

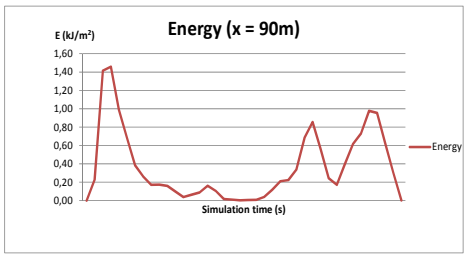

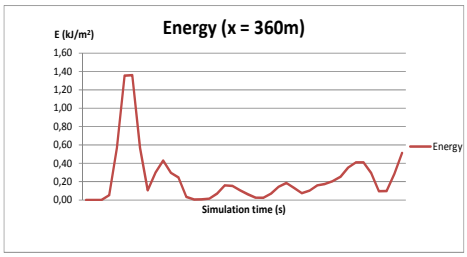

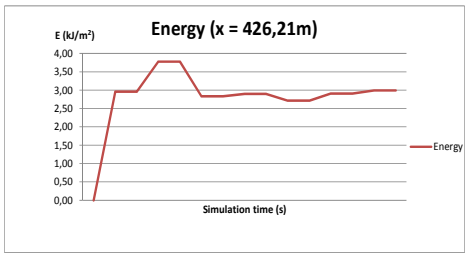

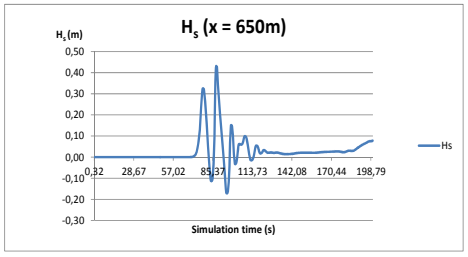

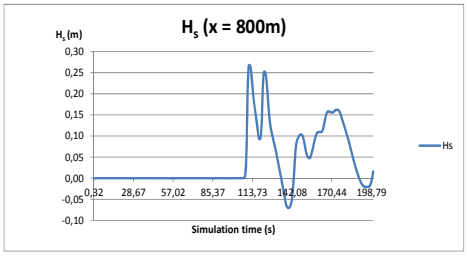

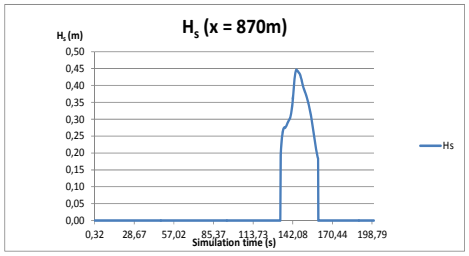

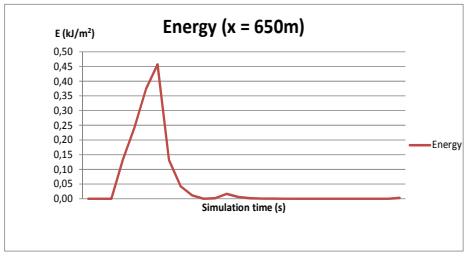

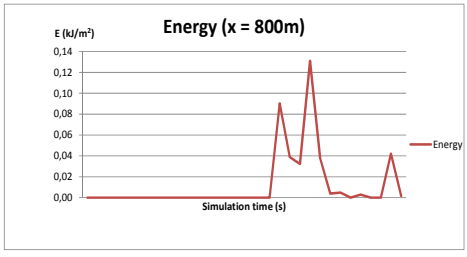

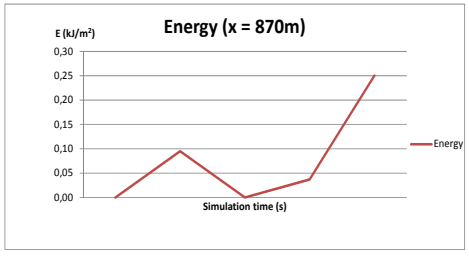

APPENDIX 4

COULWAVE.

Scenario Initial3

Scenarios 25 to 36

(Page intentionally left blank)

Scenarios Initial and scenarios with detached breakwater

Wave characteristics		Scenario
Hs (m)	T (s)	
6,64	9,30	**Initial1**
1,00	7,00	**Initial2**
2,00	7,00	**Initial3**
3,00	7,00	**Initial4**
4,00	11,00	**Initial5**

Wave characteristics		Breakwater characteristics		Scenario
H (m)	T (s)	hcr (m)	X (m)	
6,64	9,30	2,70	235,00	SC1
			170,00	SC2
			300,00	SC3
		1,50	235,00	SC4
			170,00	SC5
			300,00	SC6
		-1,50	235,00	SC7
			170,00	SC8
			300,00	SC9
		-0,50	235,00	SC10
			170,00	SC11
			300,00	SC12
1,00	7,00	2,70	235,00	SC13
			170,00	SC14
			300,00	SC15
		1,50	235,00	SC16
			170,00	SC17
			300,00	SC18
		-1,50	235,00	SC19
			170,00	SC20
			300,00	SC21
		-0,50	235,00	SC22
			170,00	SC23
			300,00	SC24
2,00	7,00	2,70	235,00	SC25
			170,00	SC26
			300,00	SC27
		1,50	235,00	SC28
			170,00	SC29
			300,00	SC30
		-1,50	235,00	SC31
			170,00	SC32
			300,00	SC33
		-0,50	235,00	SC34
			170,00	SC35
			300,00	SC36
3,00	7,00	2,70	235,00	SC37
			170,00	SC38
			300,00	SC39
		1,50	235,00	SC40
			170,00	SC41
			300,00	SC42
		-1,50	235,00	SC43
			170,00	SC44
			300,00	SC45
		-0,50	235,00	SC46
			170,00	SC47
			300,00	SC48
4,00	11,00	2,70	235,00	SC49
			170,00	SC50
			300,00	SC51
		1,50	235,00	SC52
			170,00	SC53
			300,00	SC54
		-1,50	235,00	SC55
			170,00	SC56
			300,00	SC57
		-0,50	235,00	SC58
			170,00	SC59
			300,00	SC60

Initial3	Hs (m)	T (s)
	2,00	7,00

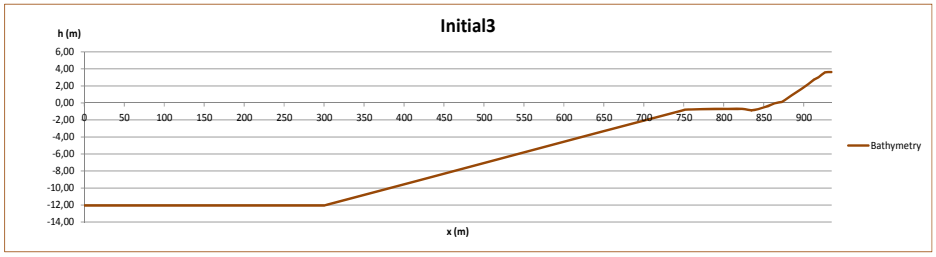

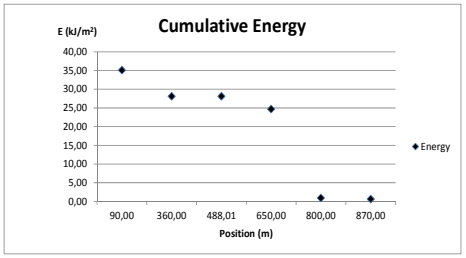

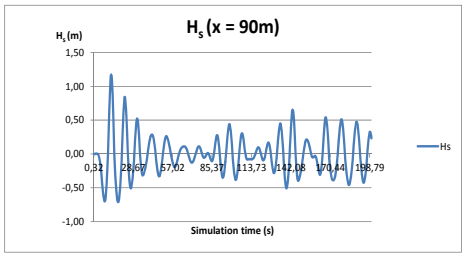

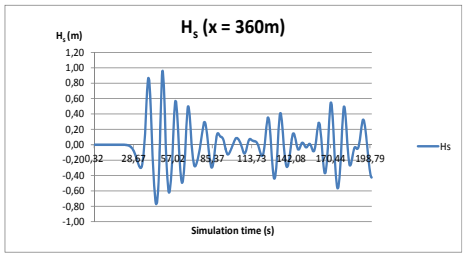

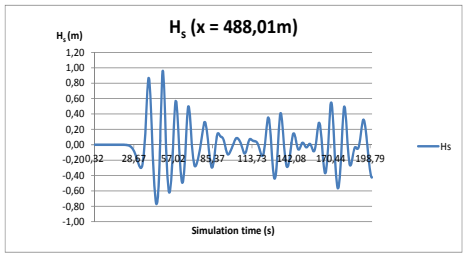

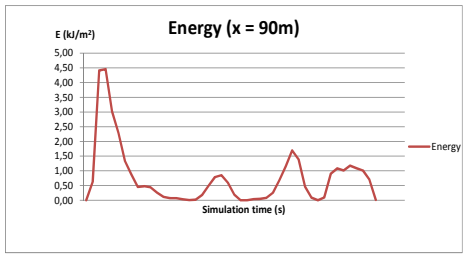

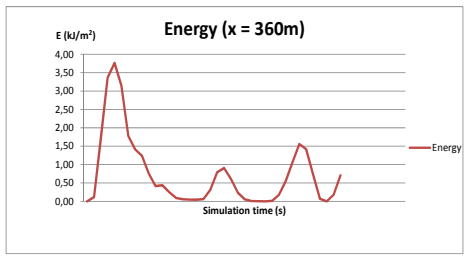

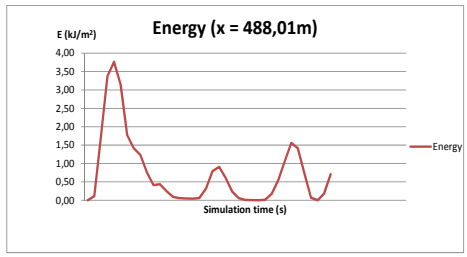

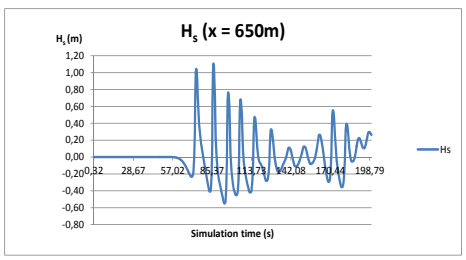

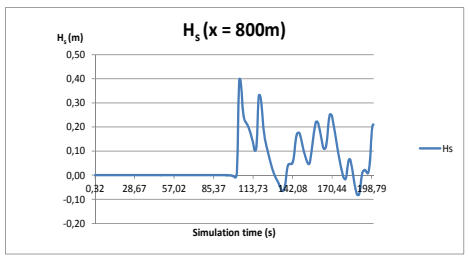

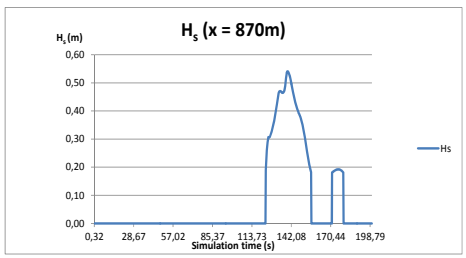

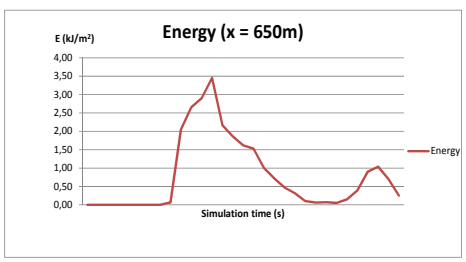

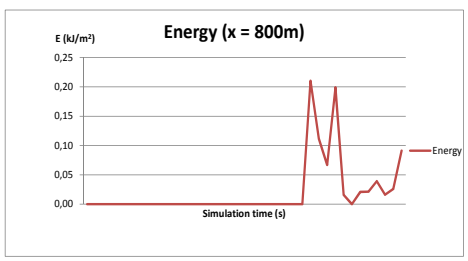

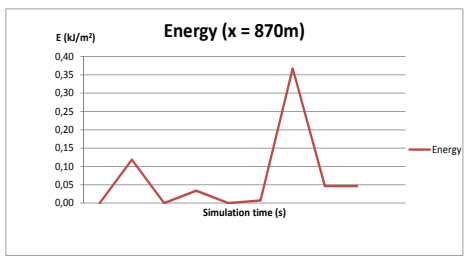

SC25	H_s (m)	T (s)	h_{cr} (m)	X (m)
	2,00	7,00	2,70	235,00

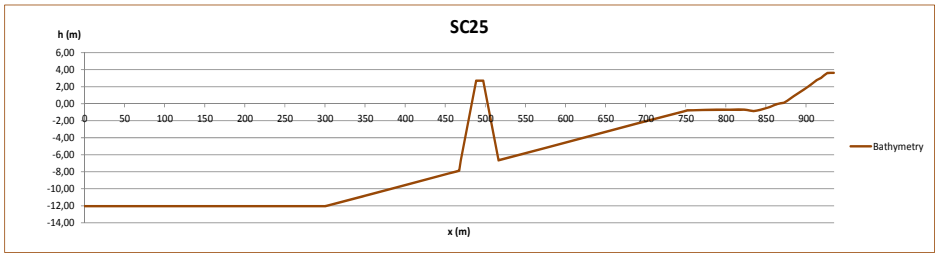

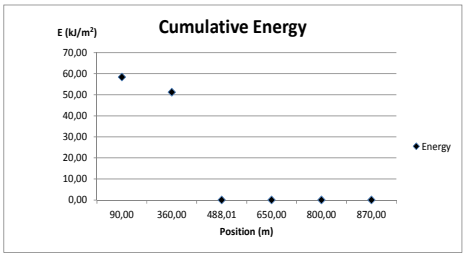

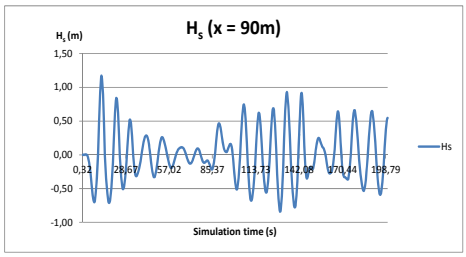

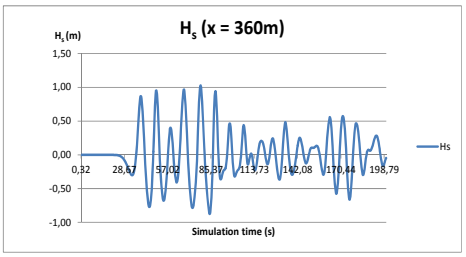

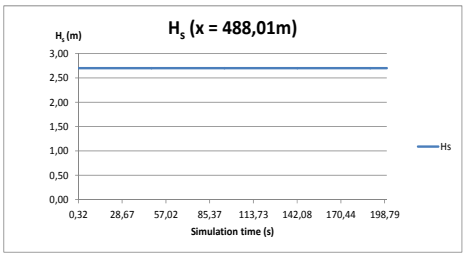

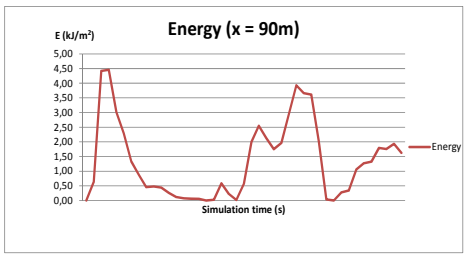

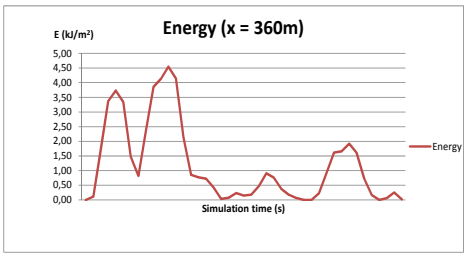

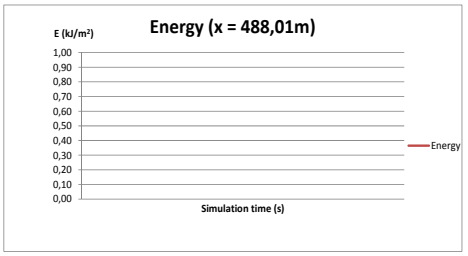

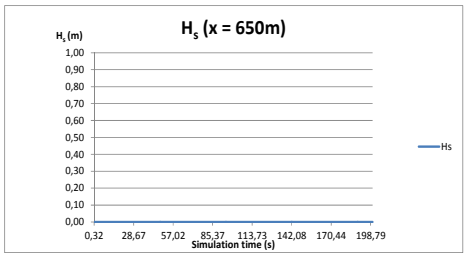

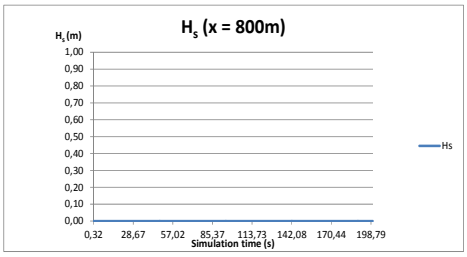

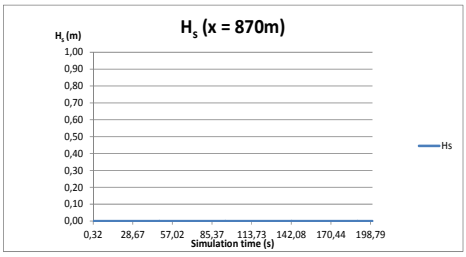

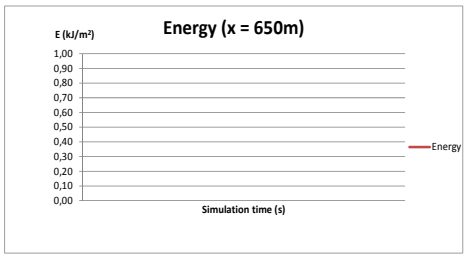

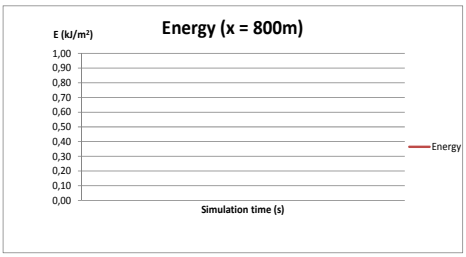

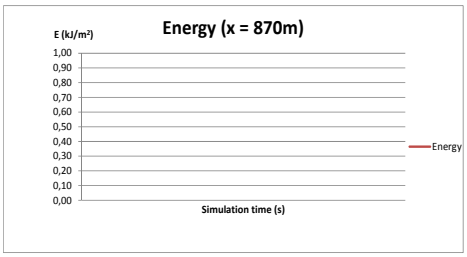

SC26	H_s (m)	T (s)	h_{cr} (m)	X (m)
	2,00	7,00	2,70	170,00

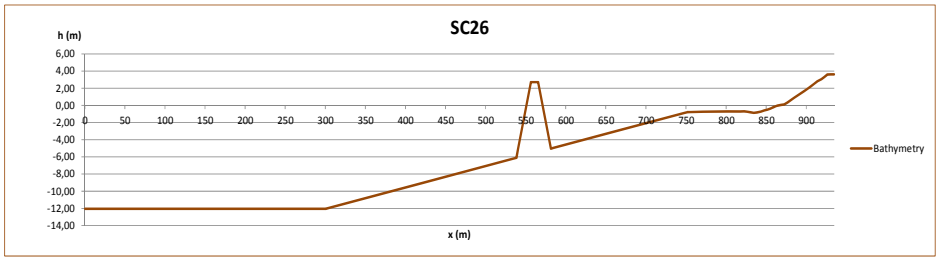

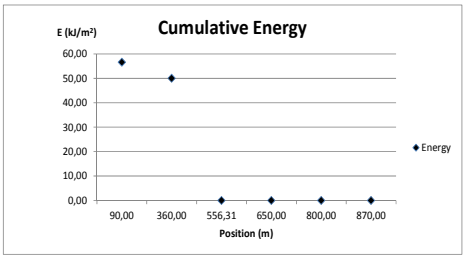

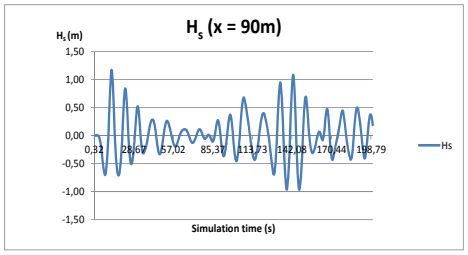

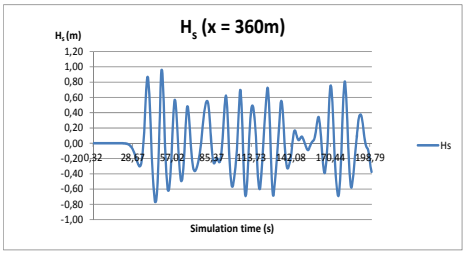

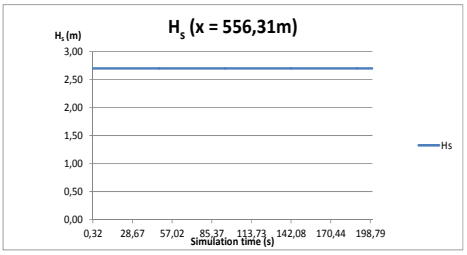

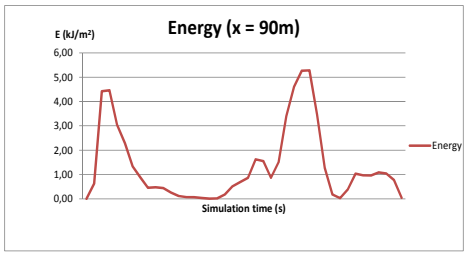

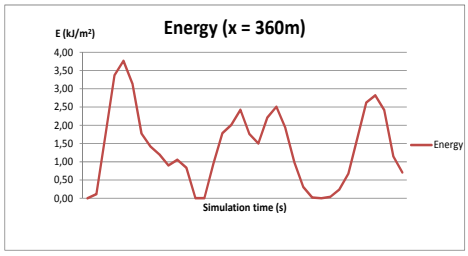

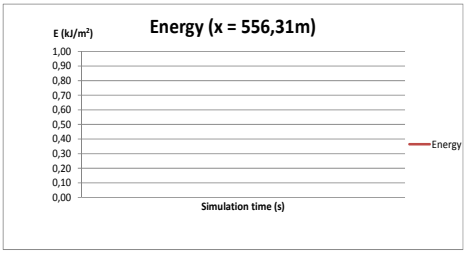

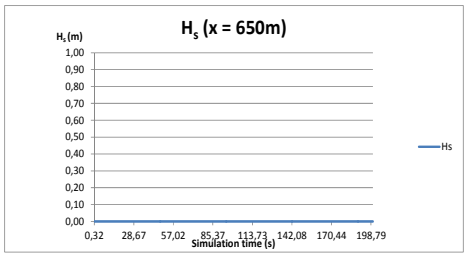

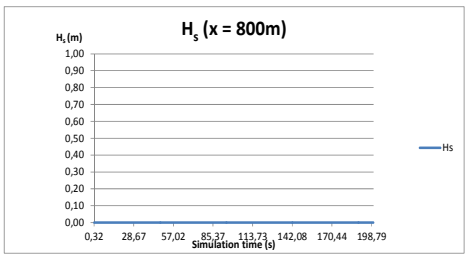

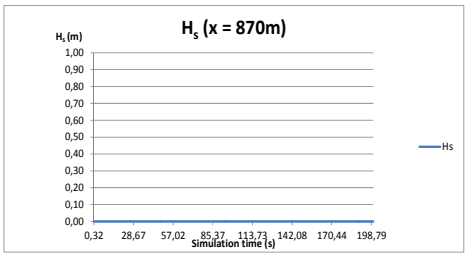

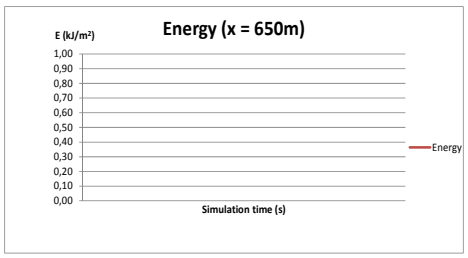

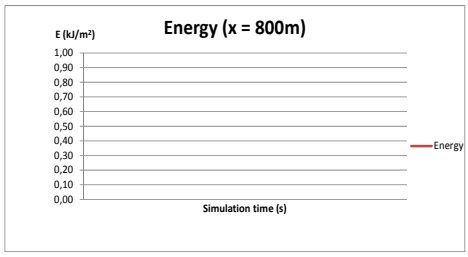

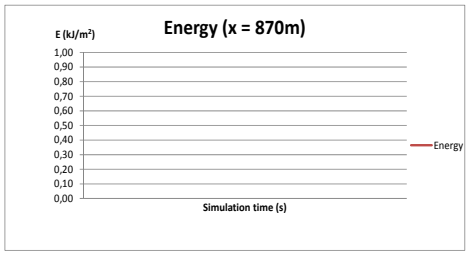

SC27	H_s (m)	T (s)	h_{cr} (m)	X (m)
	2,00	7,00	2,70	300,00

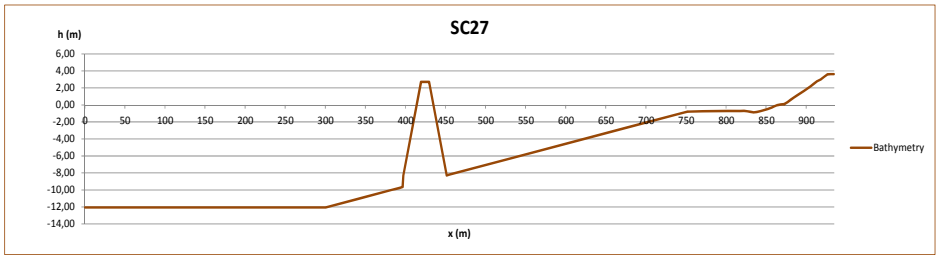

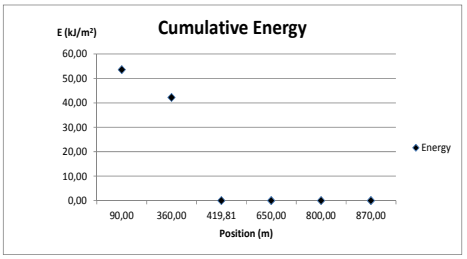

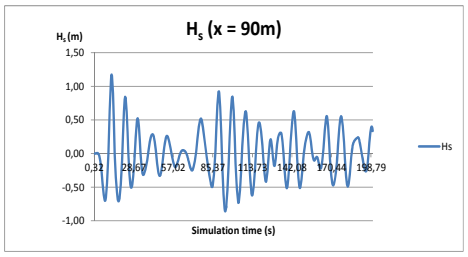

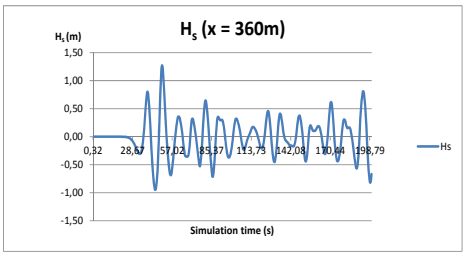

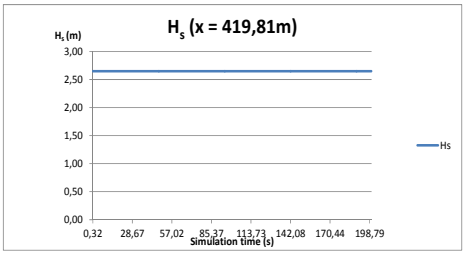

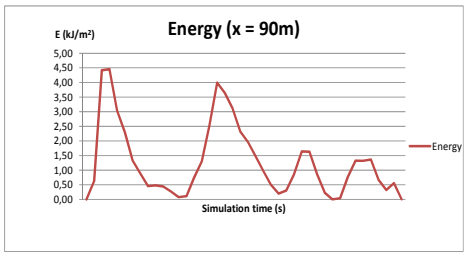

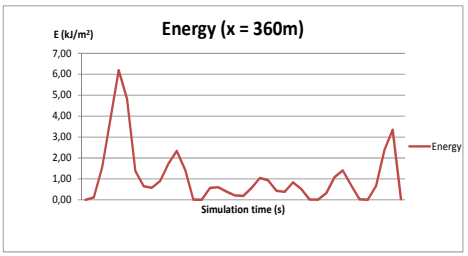

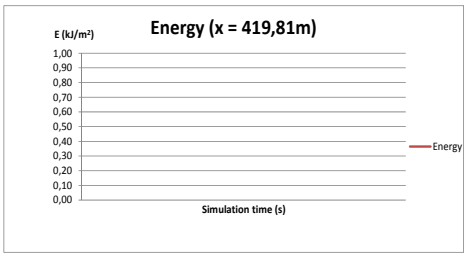

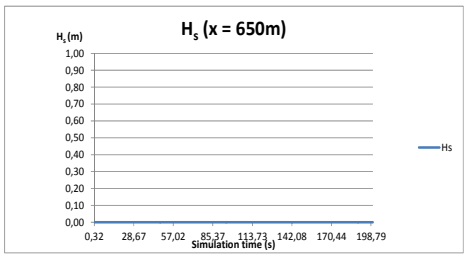

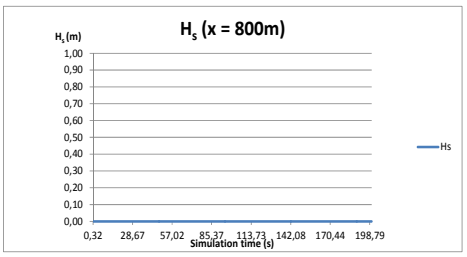

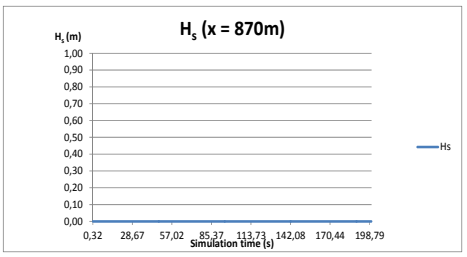

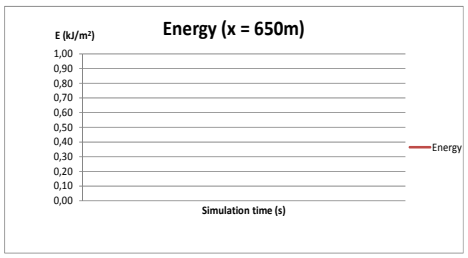

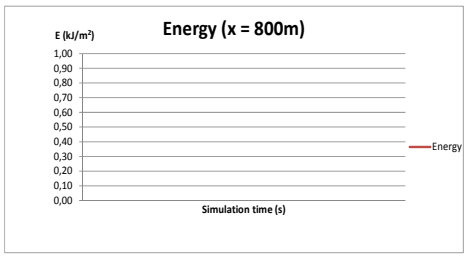

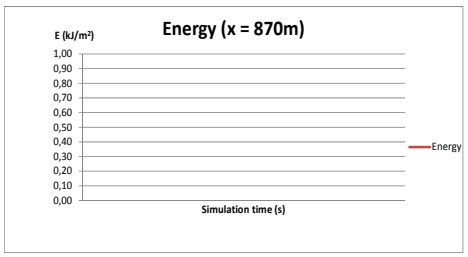

SC28	H_s (m)	T (s)	h_{cr} (m)	X (m)
	2,00	7,00	1,50	235,00

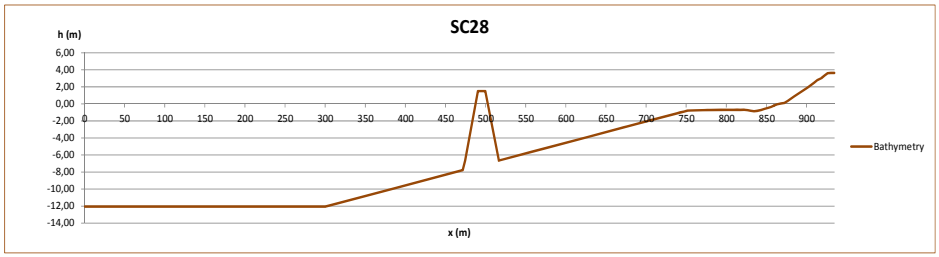

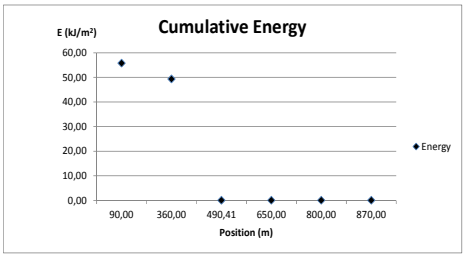

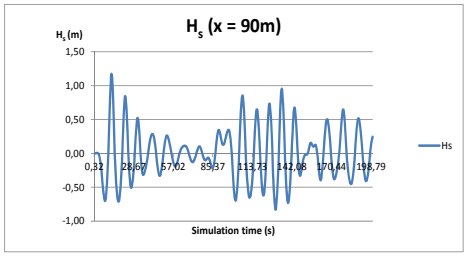

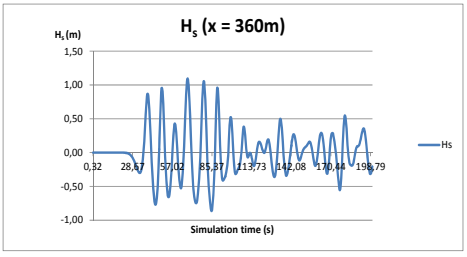

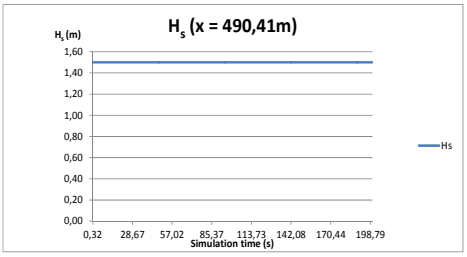

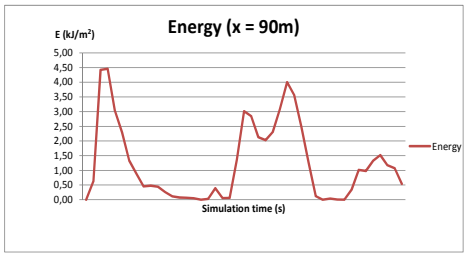

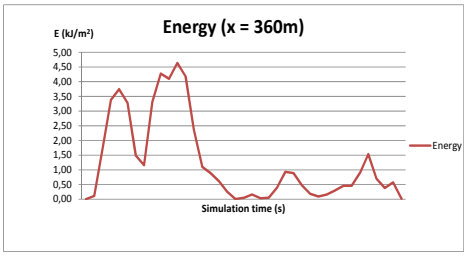

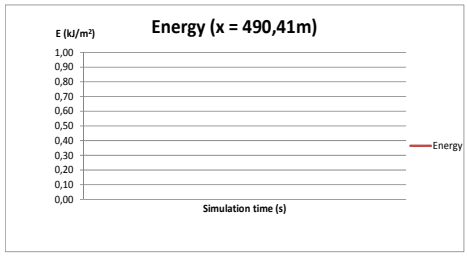

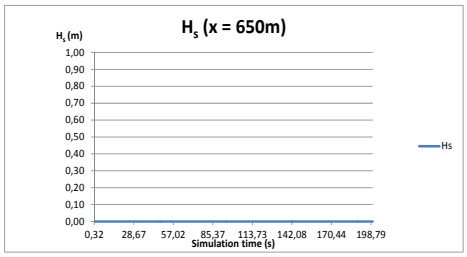

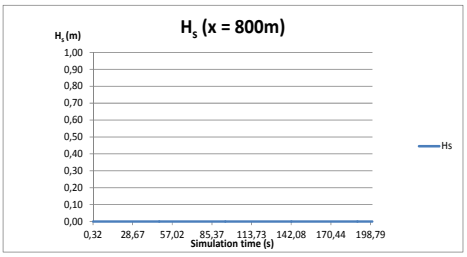

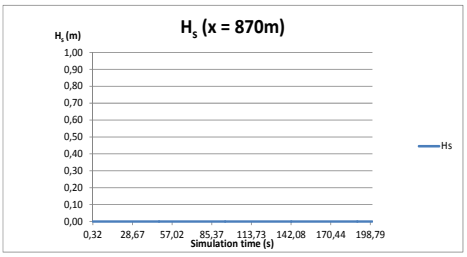

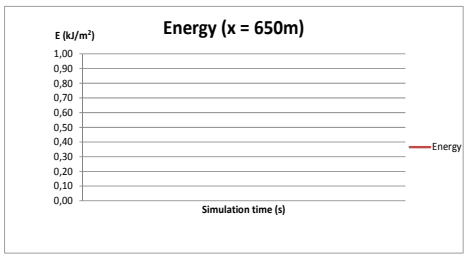

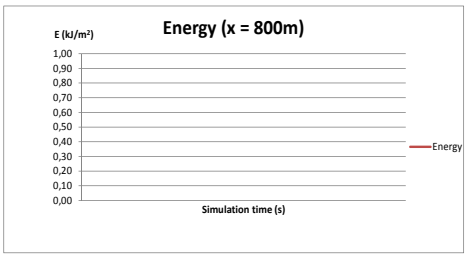

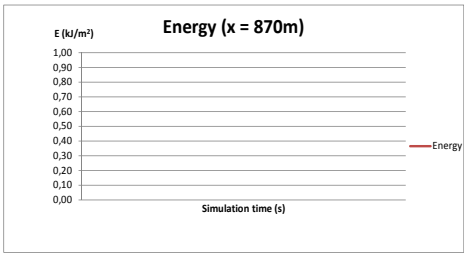

SC29	H_s (m)	T (s)	h_{cr} (m)	X (m)
	2,00	7,00	1,50	170,00

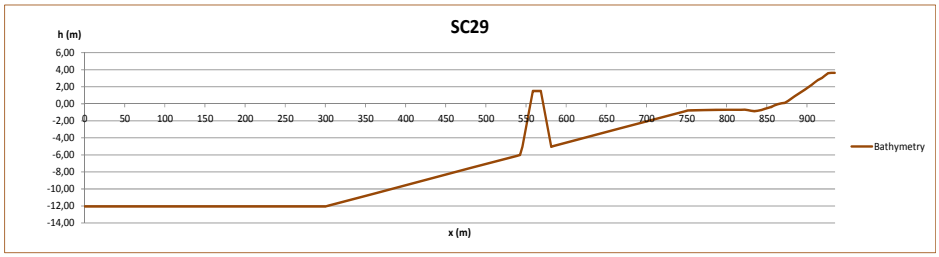

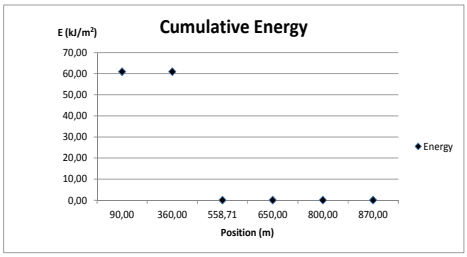

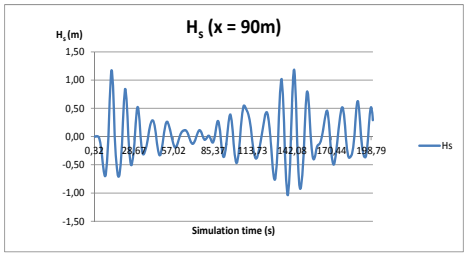

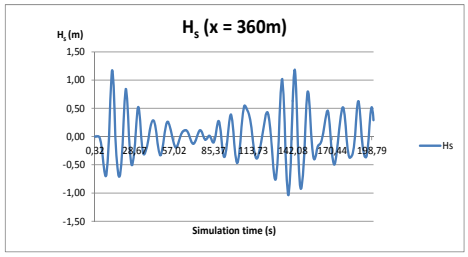

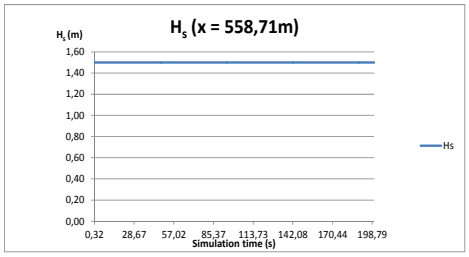

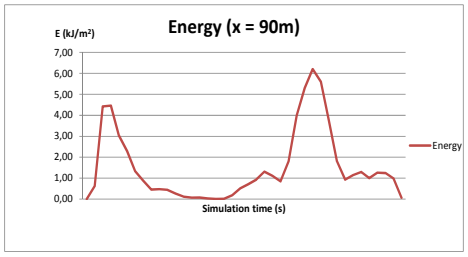

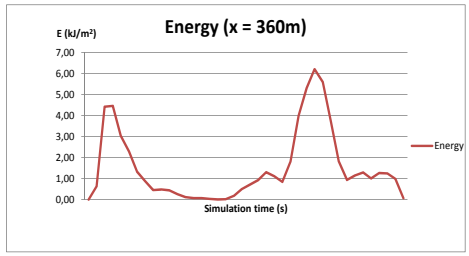

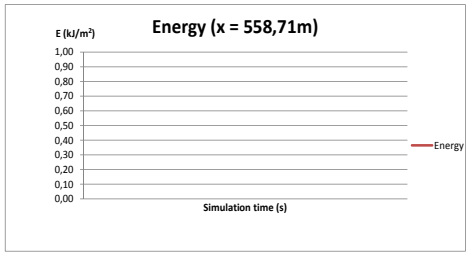

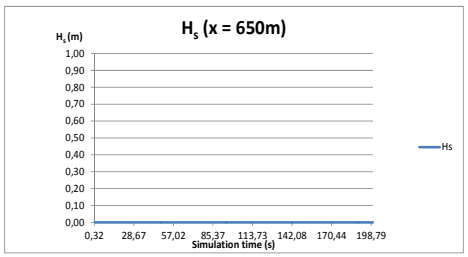

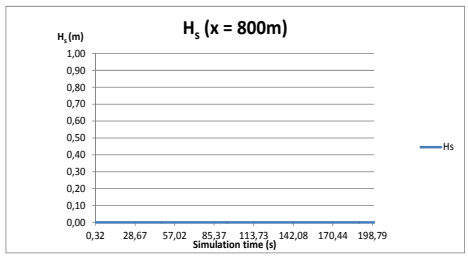

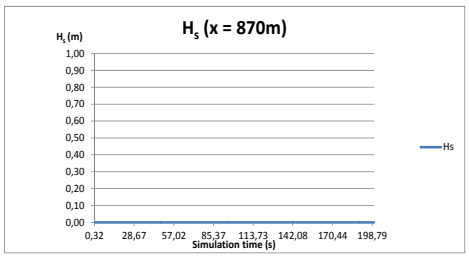

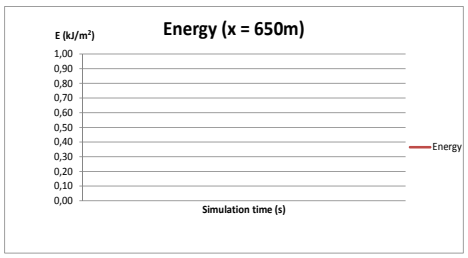

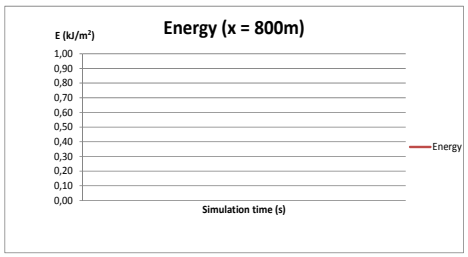

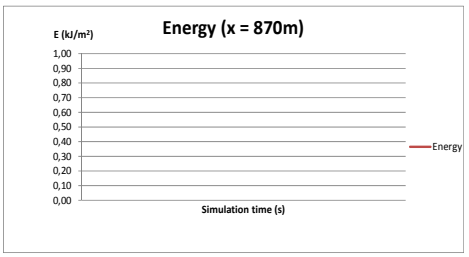

SC30	H_s (m)	T (s)	h_{cr} (m)	X (m)
	2,00	7,00	1,50	300,00

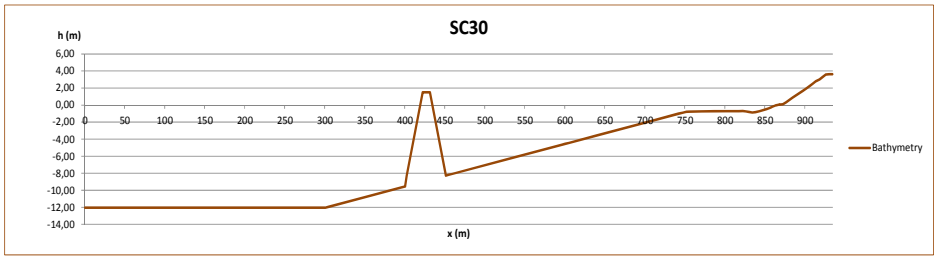

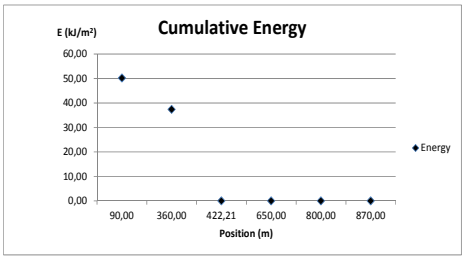

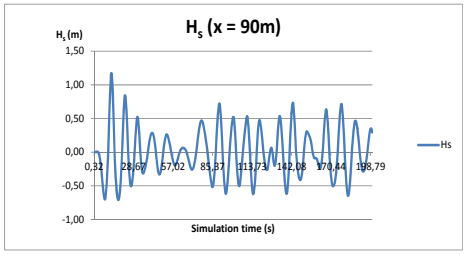

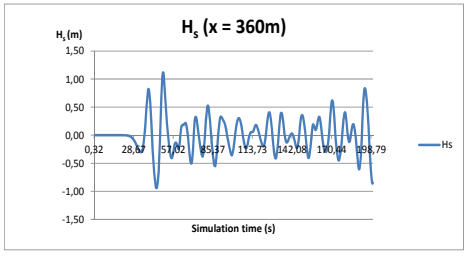

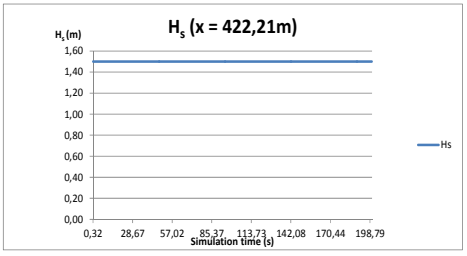

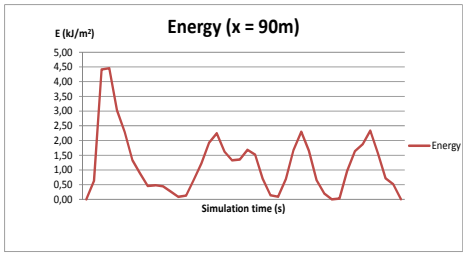

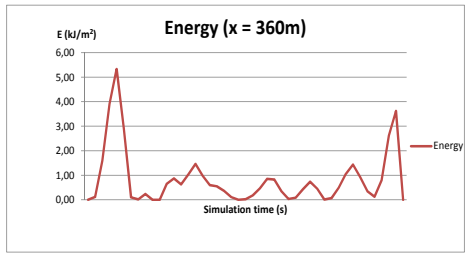

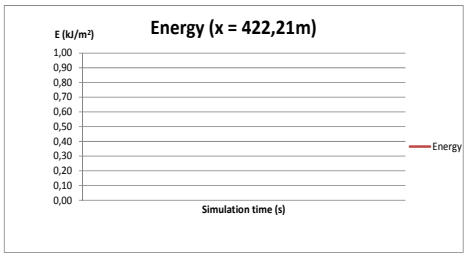

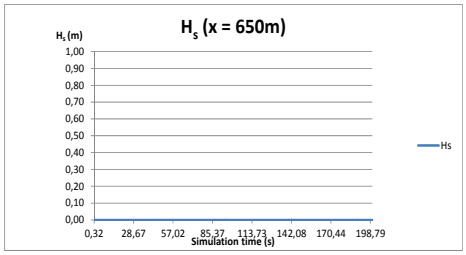

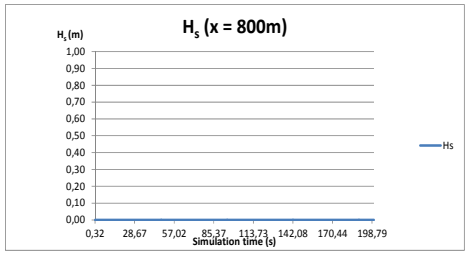

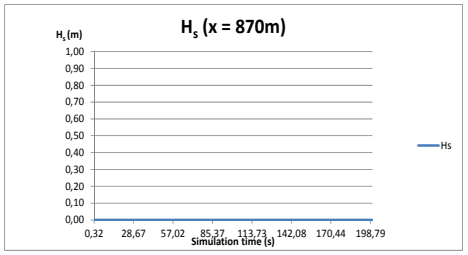

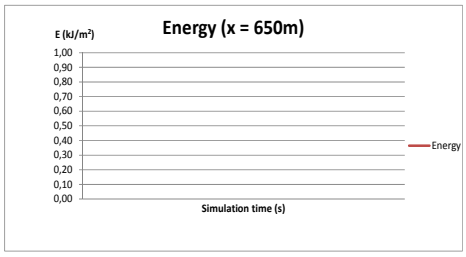

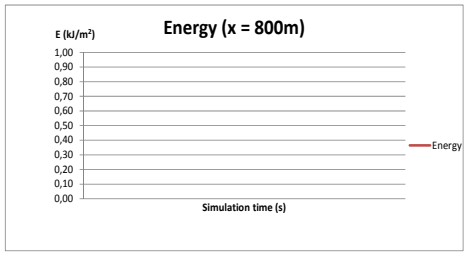

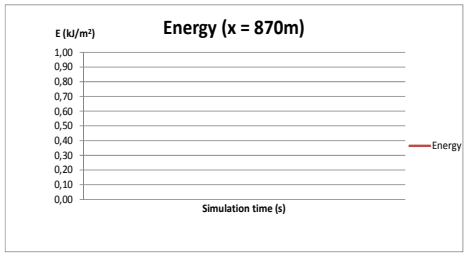

SC31	H_s (m)	T (s)	h_{cr} (m)	X (m)
	2,00	7,00	-1,50	235,00

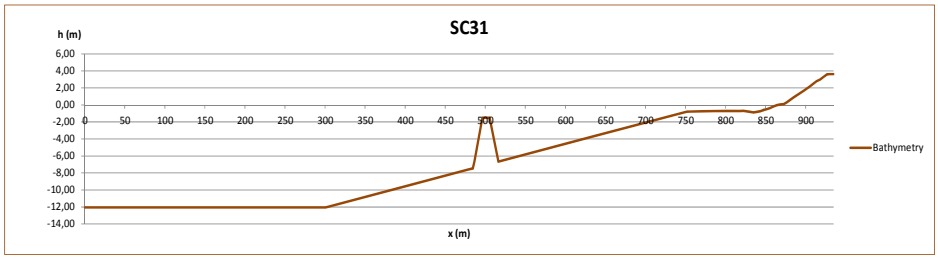

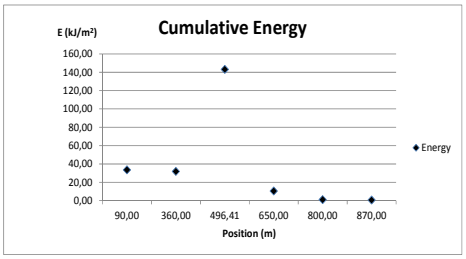

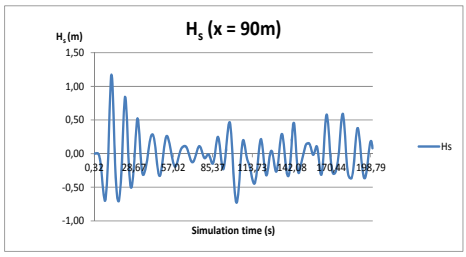

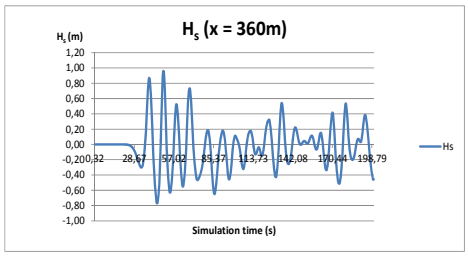

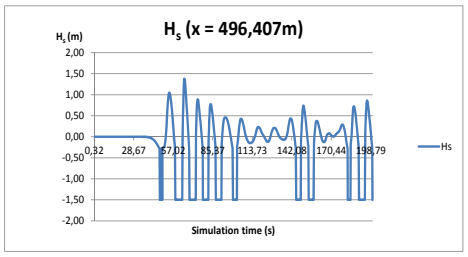

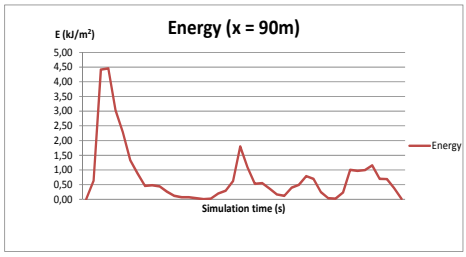

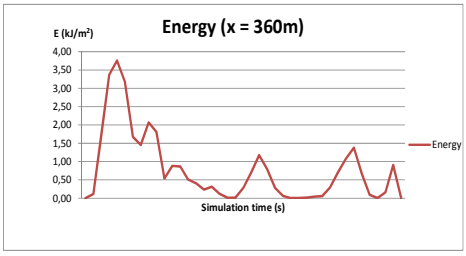

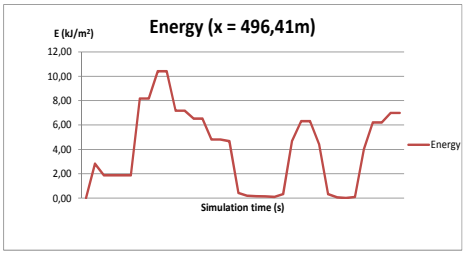

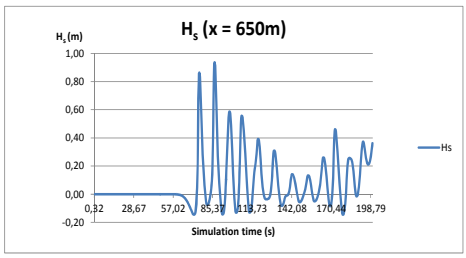

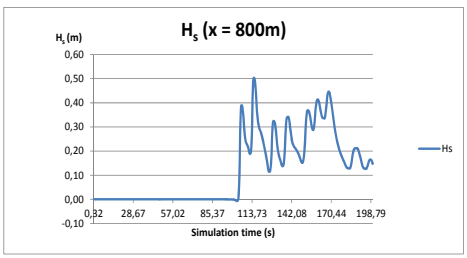

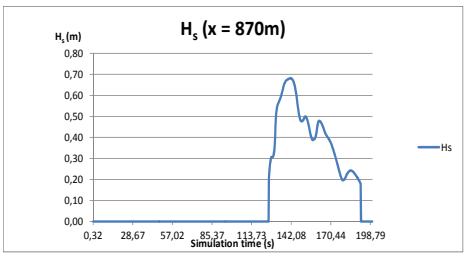

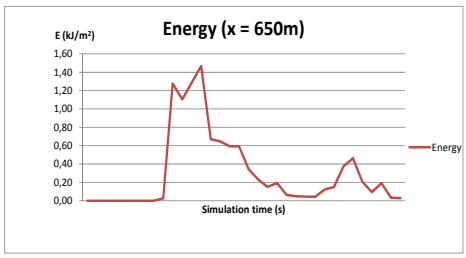

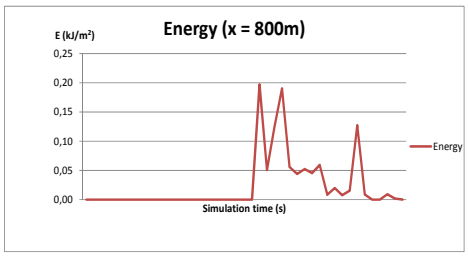

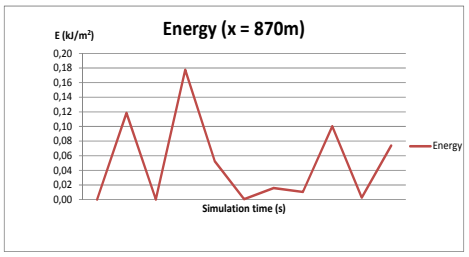

SC32	H_s (m)	T (s)	h_{cr} (m)	X (m)
	2,00	7,00	-1,50	170,00

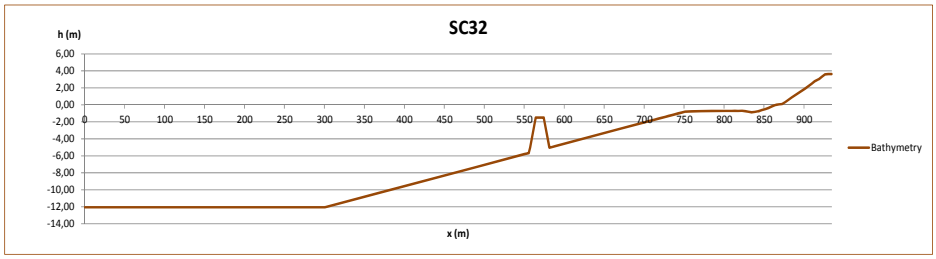

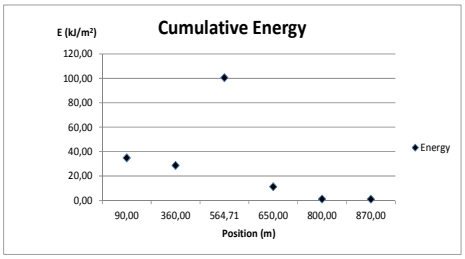

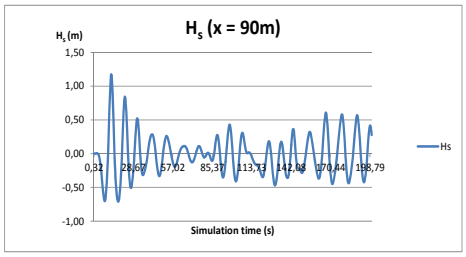

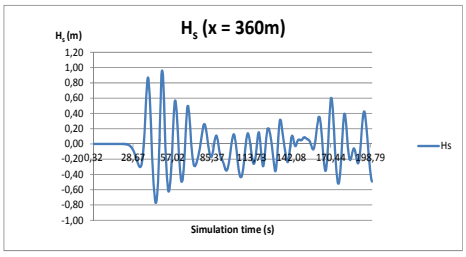

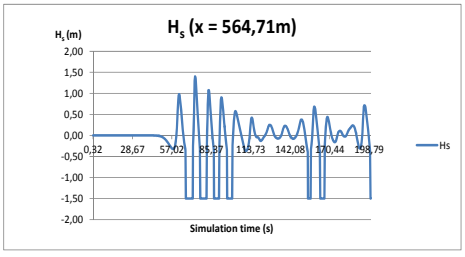

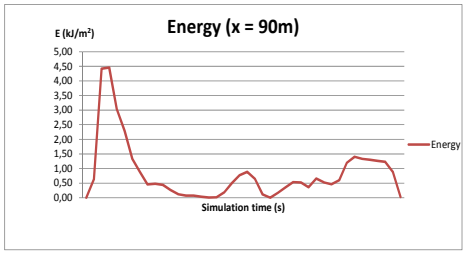

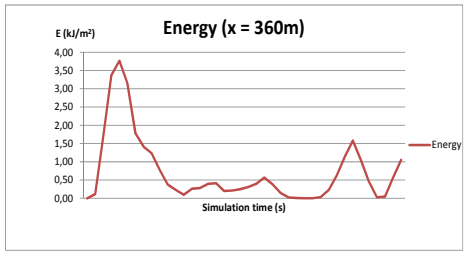

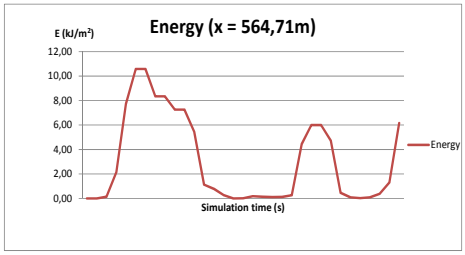

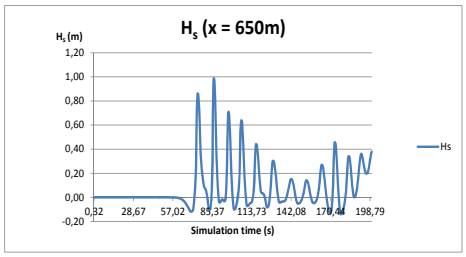

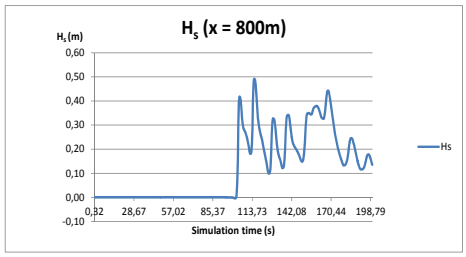

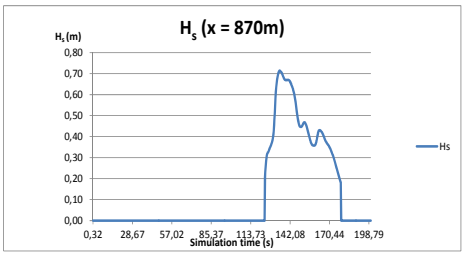

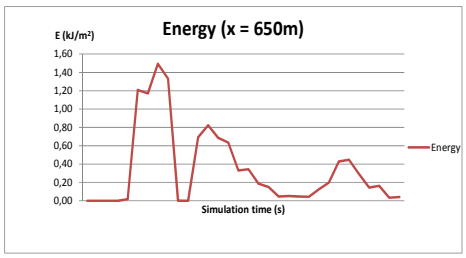

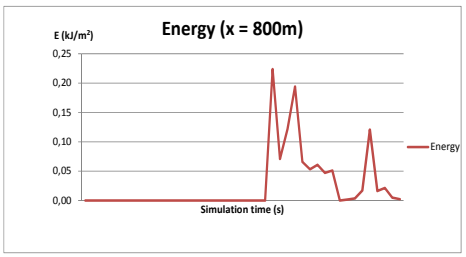

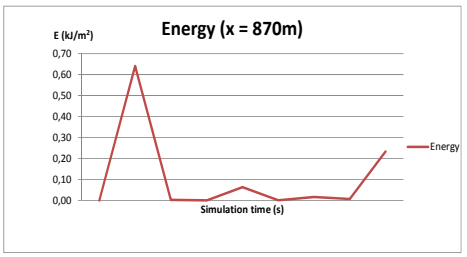

SC33	H_s (m)	T (s)	h_{cr} (m)	X (m)
	2,00	7,00	-1,50	300,00

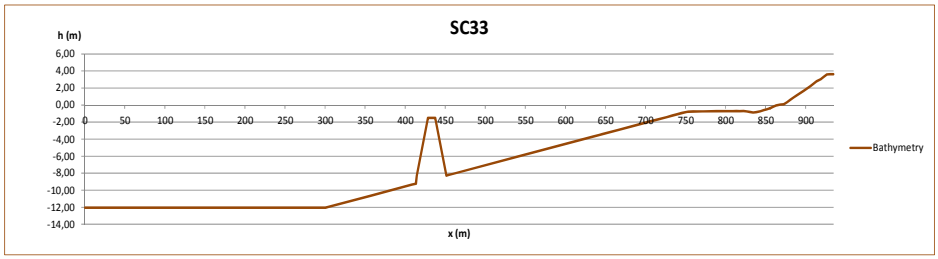

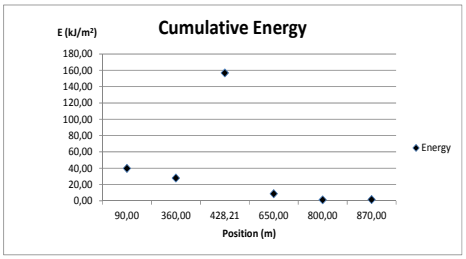

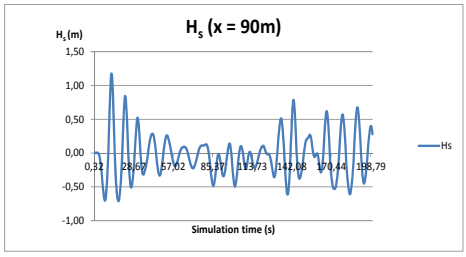

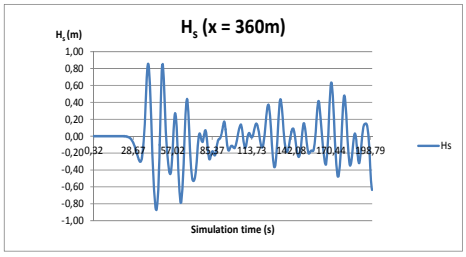

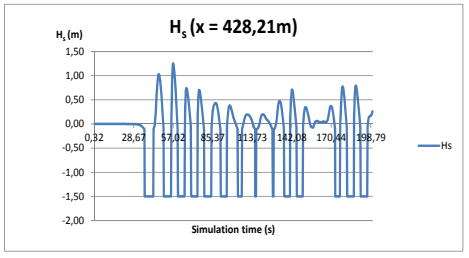

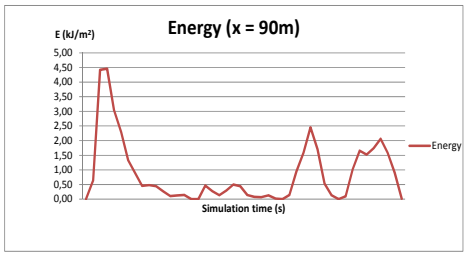

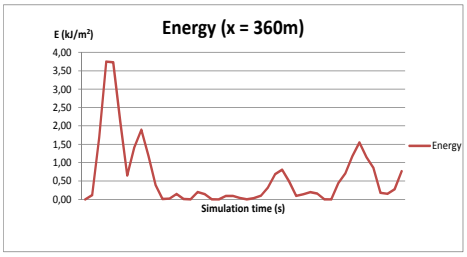

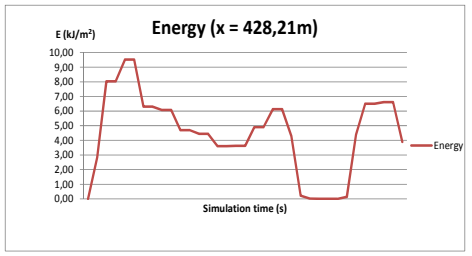

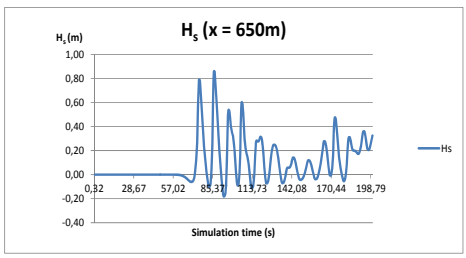

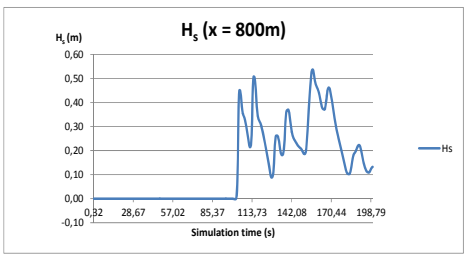

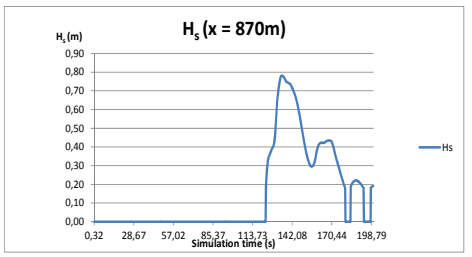

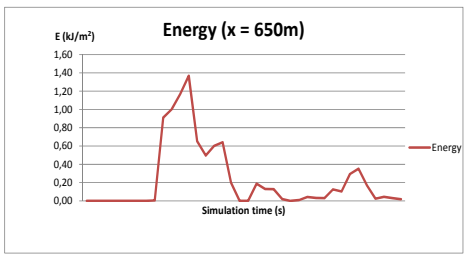

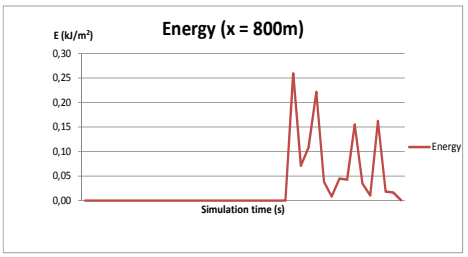

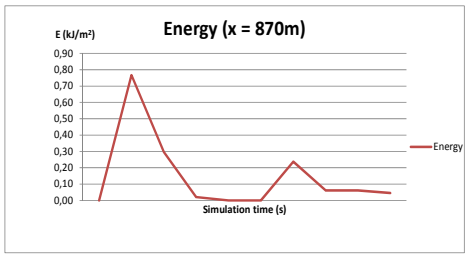

SC34	H_s (m)	T (s)	h_{cr} (m)	X (m)
	2,00	7,00	-0,50	235,00

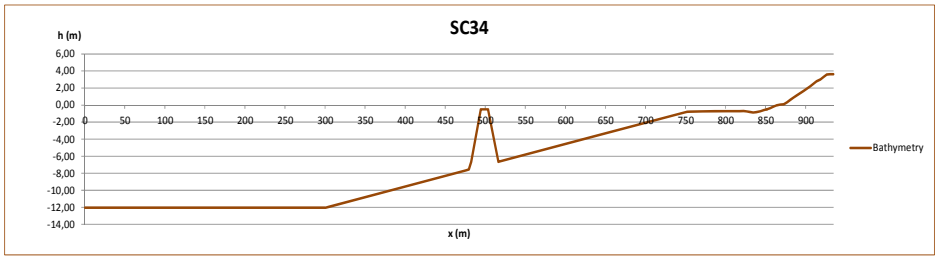

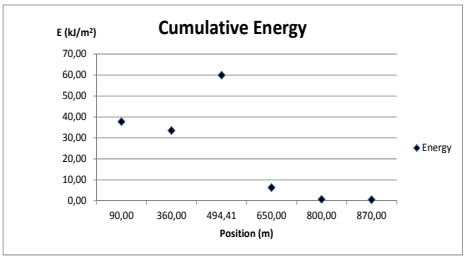

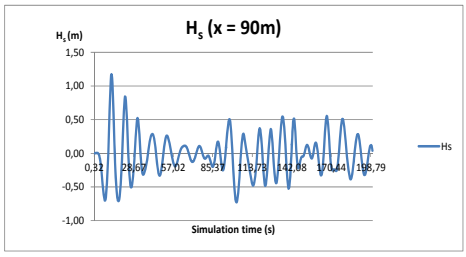

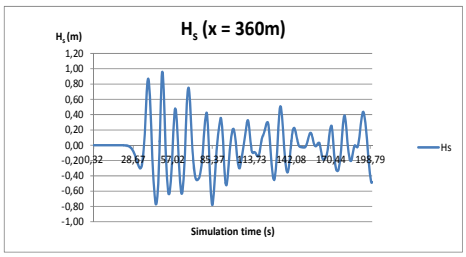

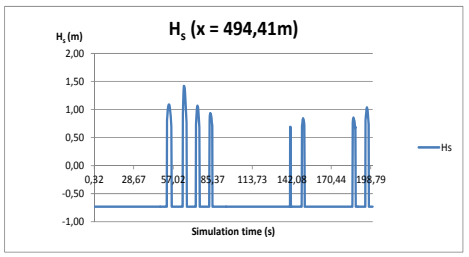

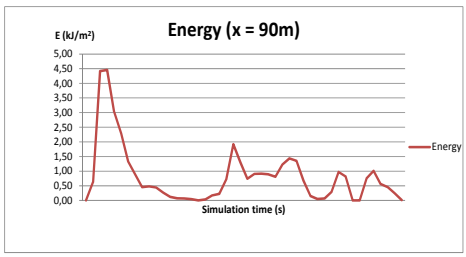

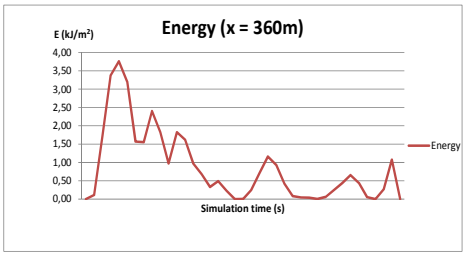

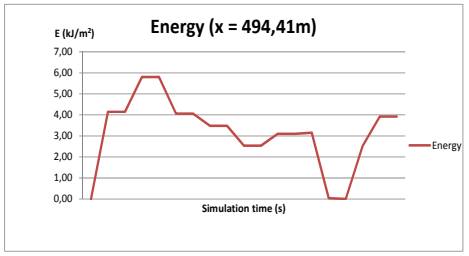

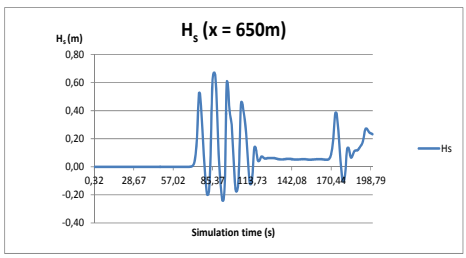

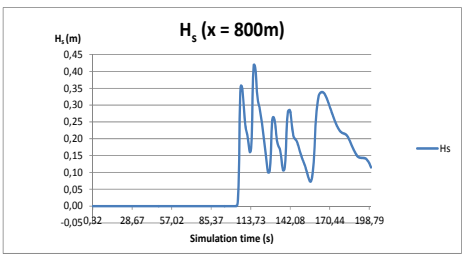

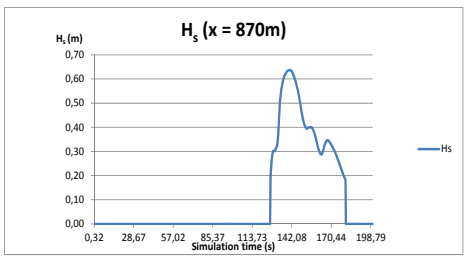

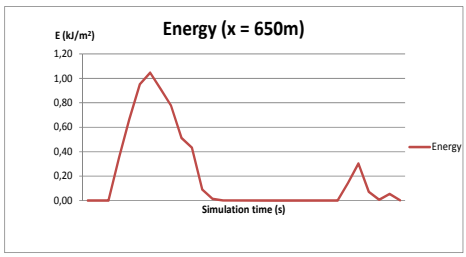

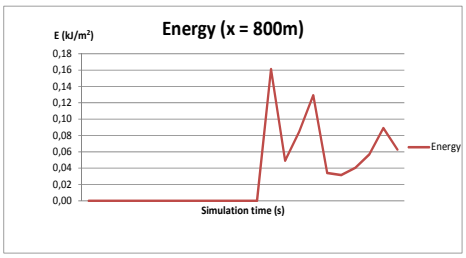

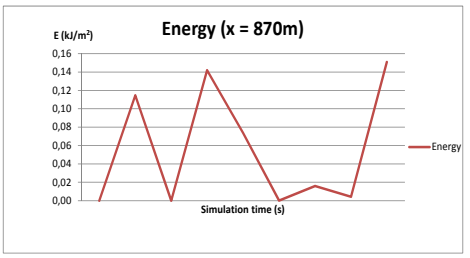

SC35	H_s (m)	T (s)	h_{cr} (m)	X (m)
	2,00	7,00	-0,50	170,00

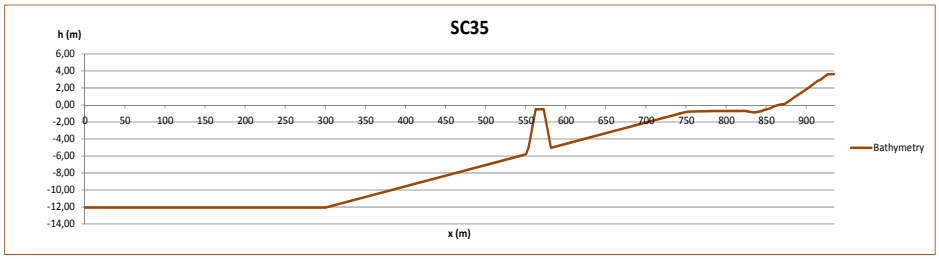

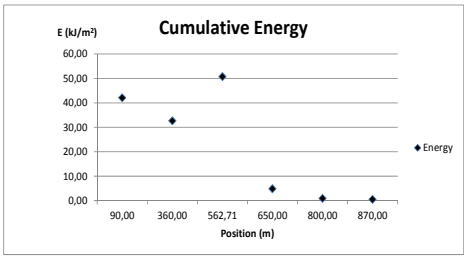

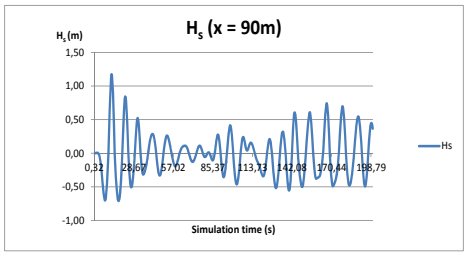

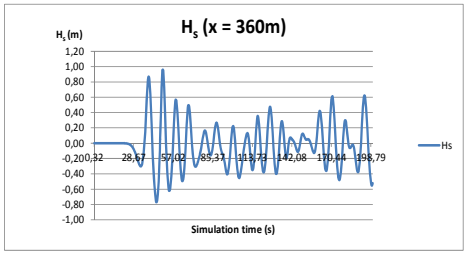

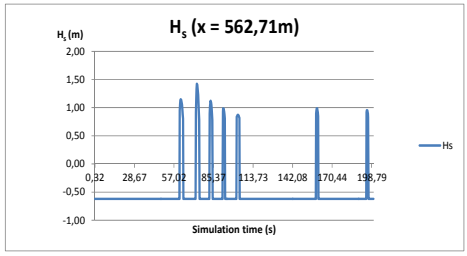

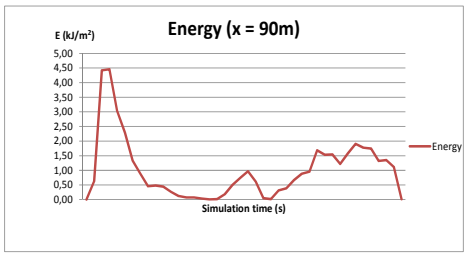

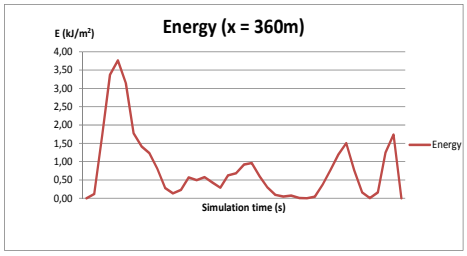

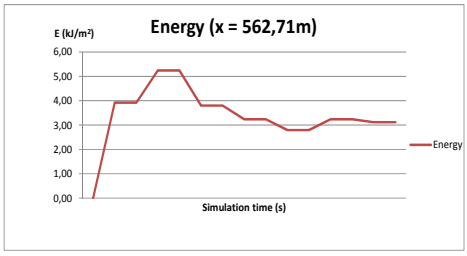

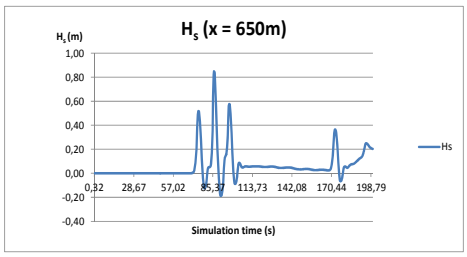

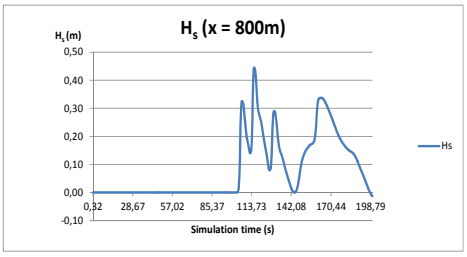

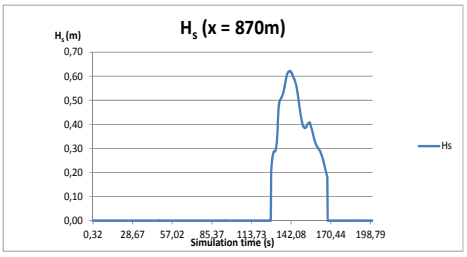

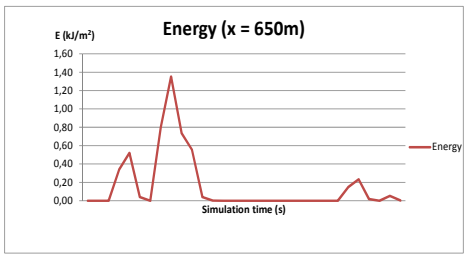

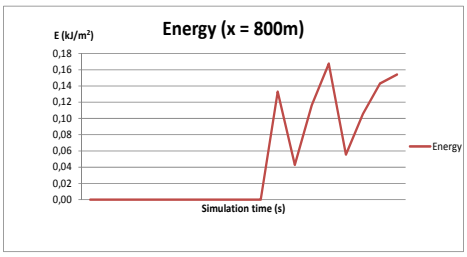

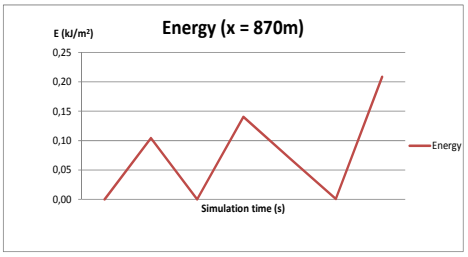

SC36	H_s (m)	T (s)	h_{cr} (m)	X (m)
	2,00	7,00	-0,50	300,00

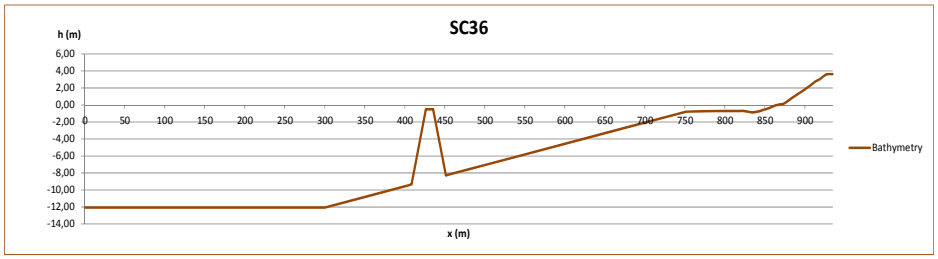

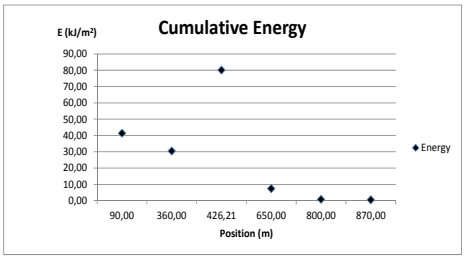

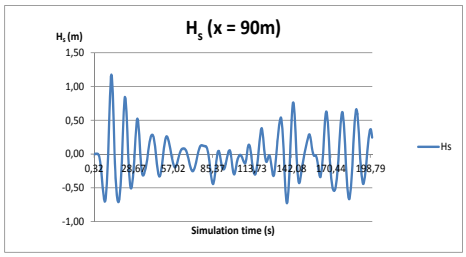

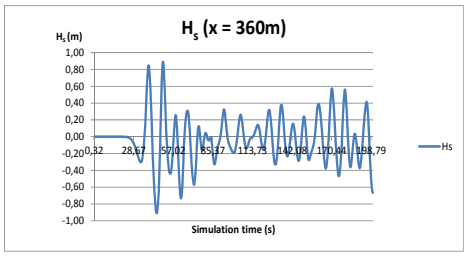

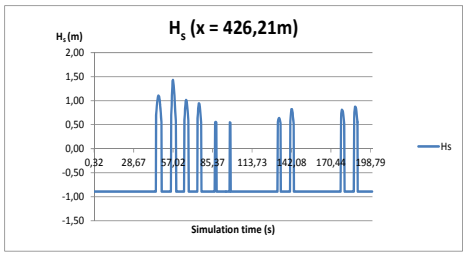

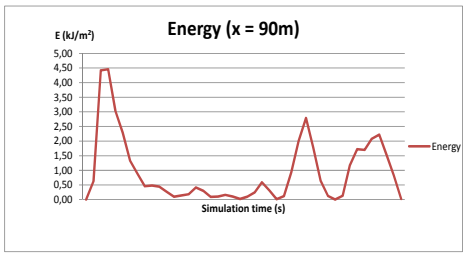

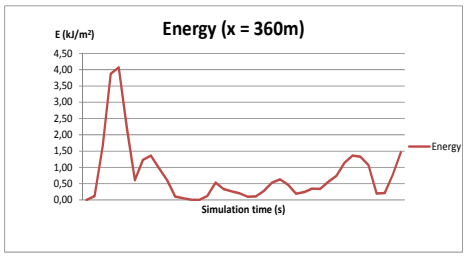

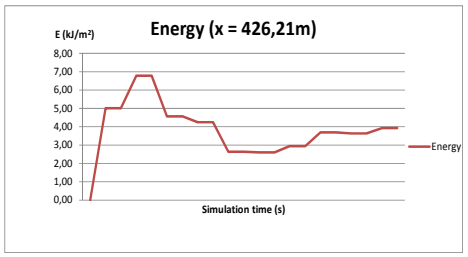

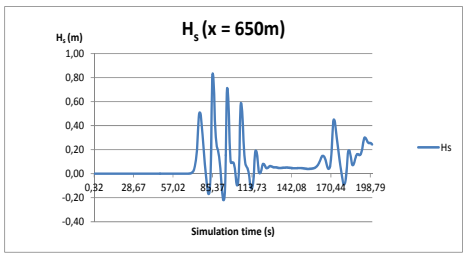

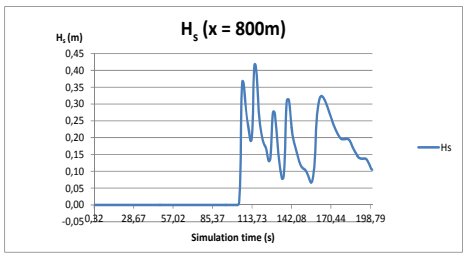

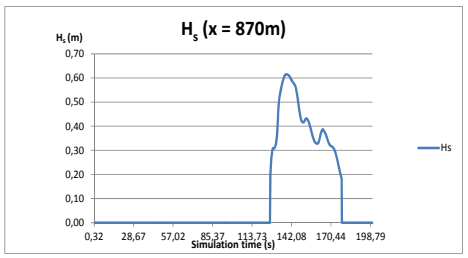

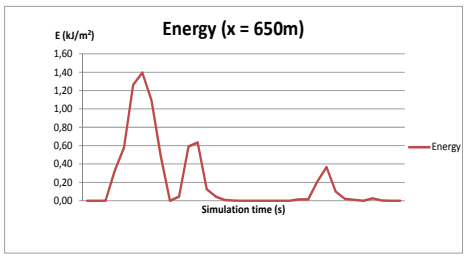

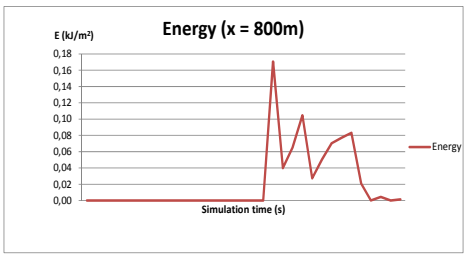

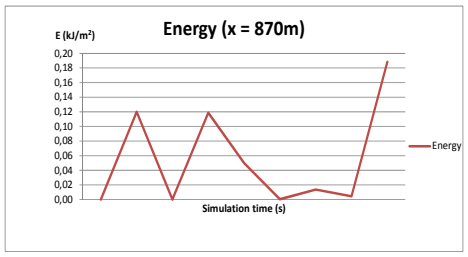

APPENDIX 5

COULWAVE.

Scenario Initial4

Scenarios 37 to 48

(Page intentionally left blank)

Scenarios Initial and scenarios with detached breakwater

Wave characteristics		Scenario
Hs (m)	T (s)	
6,64	9,30	**Initial1**
1,00	7,00	**Initial2**
2,00	7,00	**Initial3**
3,00	7,00	**Initial4**
4,00	11,00	**Initial5**

Wave characteristics		Breakwater characteristics		Scenario
H (m)	T (s)	hcr (m)	X (m)	
6,64	9,30	2,70	235,00	SC1
			170,00	SC2
			300,00	SC3
		1,50	235,00	SC4
			170,00	SC5
			300,00	SC6
		-1,50	235,00	SC7
			170,00	SC8
			300,00	SC9
		-0,50	235,00	SC10
			170,00	SC11
			300,00	SC12
1,00	7,00	2,70	235,00	SC13
			170,00	SC14
			300,00	SC15
		1,50	235,00	SC16
			170,00	SC17
			300,00	SC18
		-1,50	235,00	SC19
			170,00	SC20
			300,00	SC21
		-0,50	235,00	SC22
			170,00	SC23
			300,00	SC24
2,00	7,00	2,70	235,00	SC25
			170,00	SC26
			300,00	SC27
		1,50	235,00	SC28
			170,00	SC29
			300,00	SC30
		-1,50	235,00	SC31
			170,00	SC32
			300,00	SC33
		-0,50	235,00	SC34
			170,00	SC35
			300,00	SC36
3,00	7,00	2,70	235,00	SC37
			170,00	SC38
			300,00	SC39
		1,50	235,00	SC40
			170,00	SC41
			300,00	SC42
		-1,50	235,00	SC43
			170,00	SC44
			300,00	SC45
		-0,50	235,00	SC46
			170,00	SC47
			300,00	SC48
4,00	11,00	2,70	235,00	SC49
			170,00	SC50
			300,00	SC51
		1,50	235,00	SC52
			170,00	SC53
			300,00	SC54
		-1,50	235,00	SC55
			170,00	SC56
			300,00	SC57
		-0,50	235,00	SC58
			170,00	SC59
			300,00	SC60

Initial4	Hs (m)	T (s)
	3,00	7,00

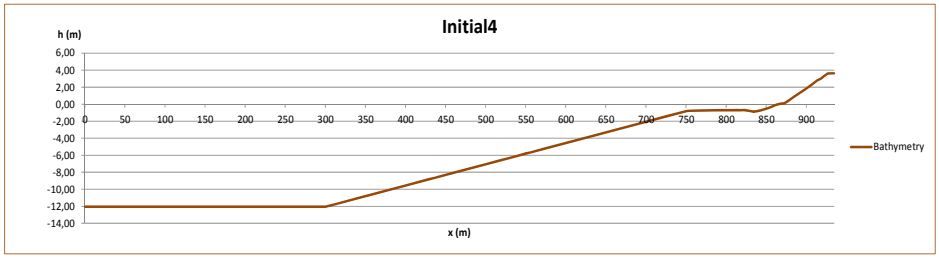

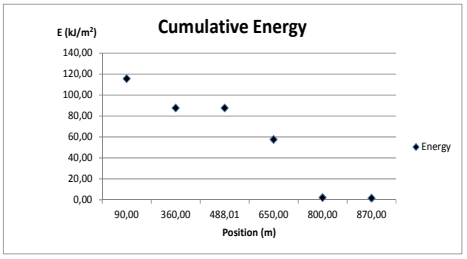

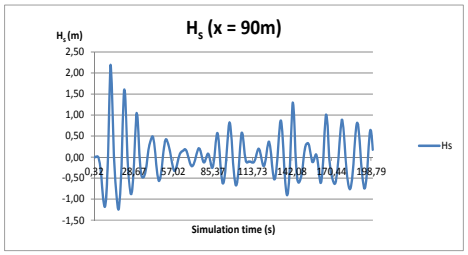

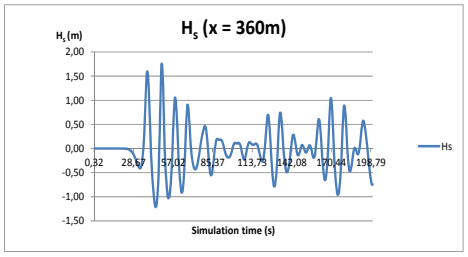

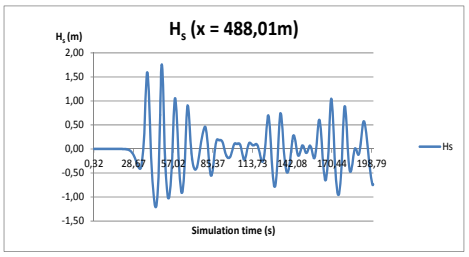

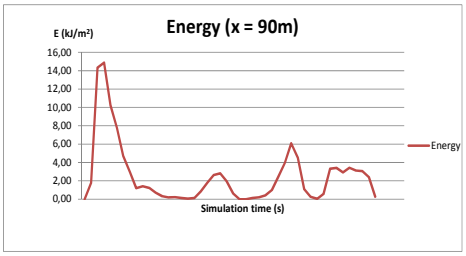

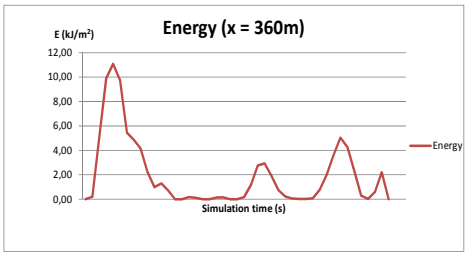

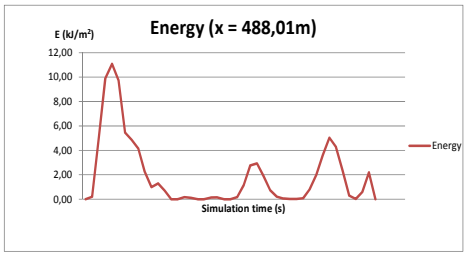

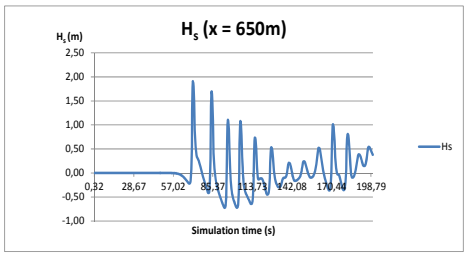

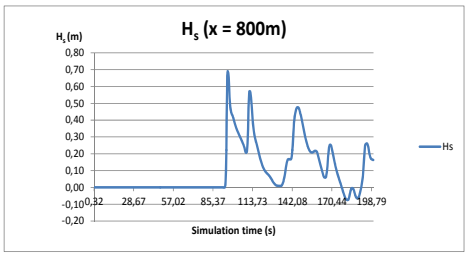

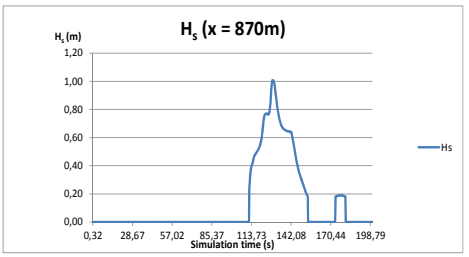

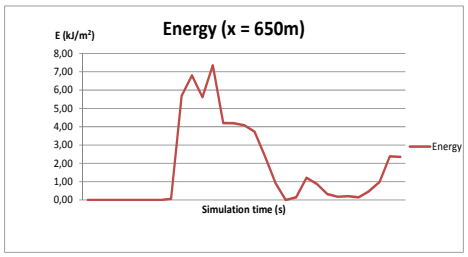

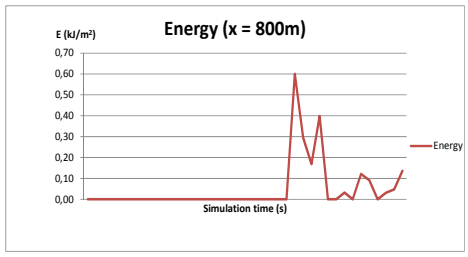

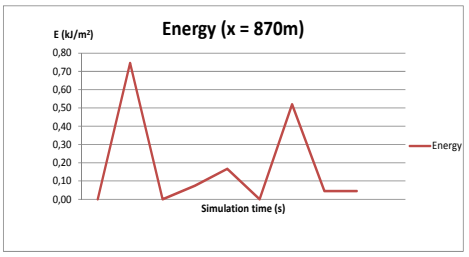

SC37	H_s (m)	T (s)	h_{cr} (m)	X (m)
	3,00	7,00	2,70	235,00

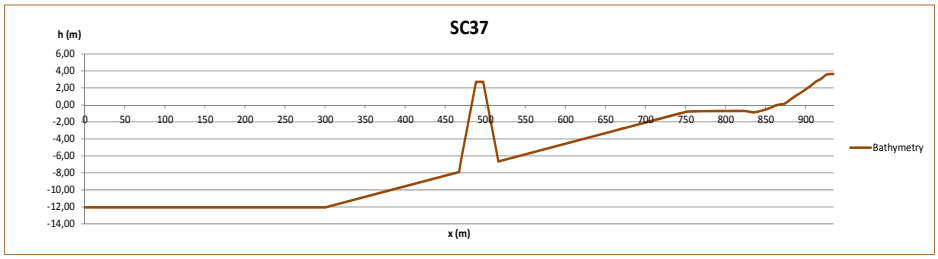

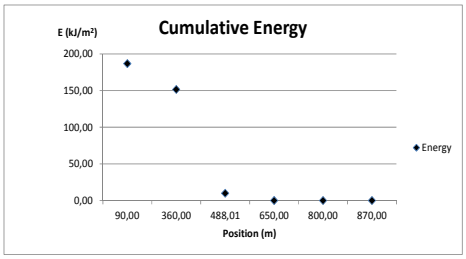

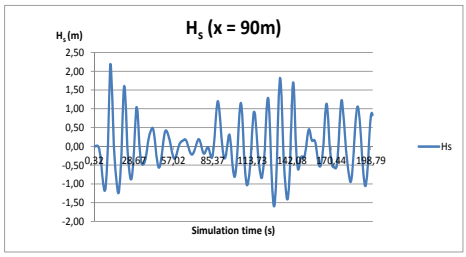

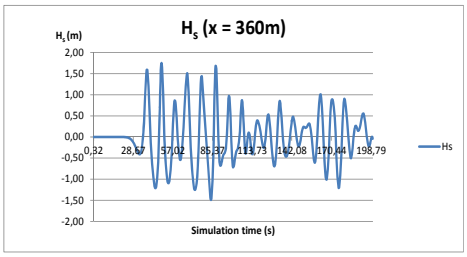

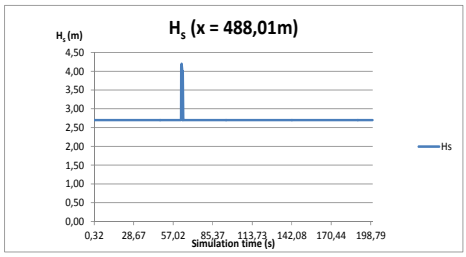

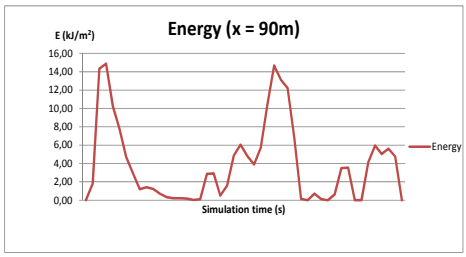

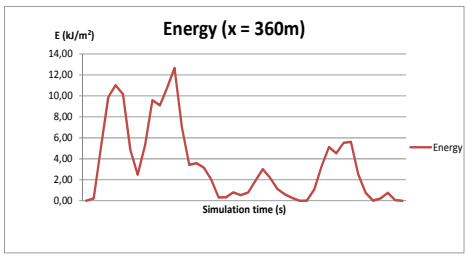

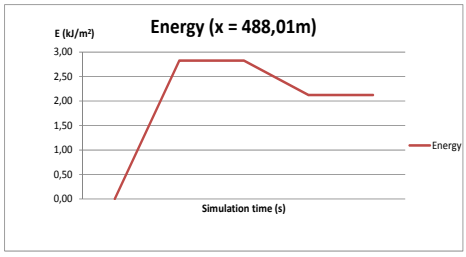

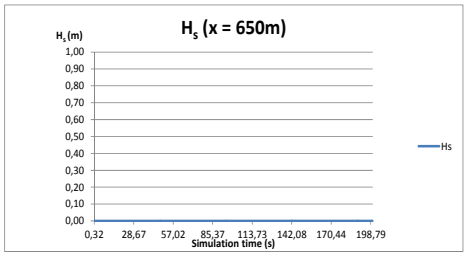

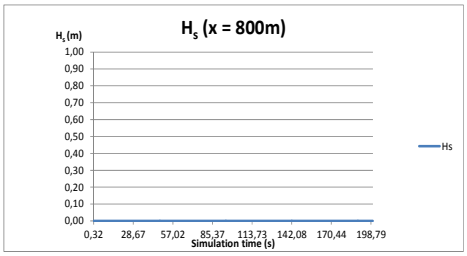

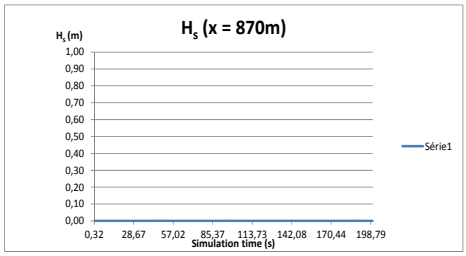

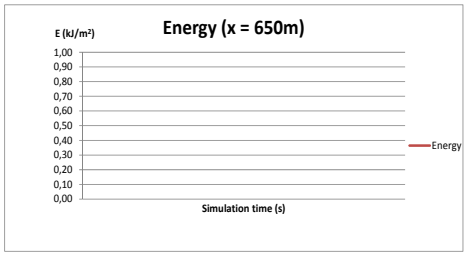

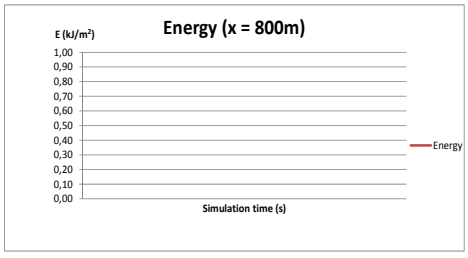

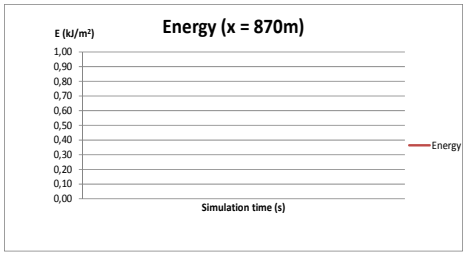

SC38	H_s (m)	T (s)	h_{cr} (m)	X (m)
	3,00	7,00	2,70	170,00

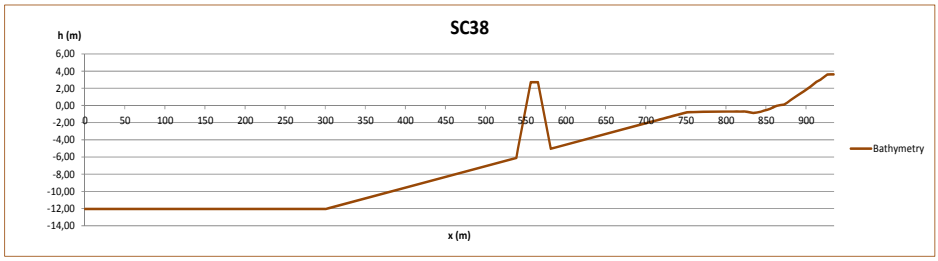

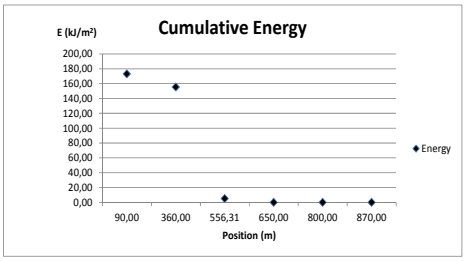

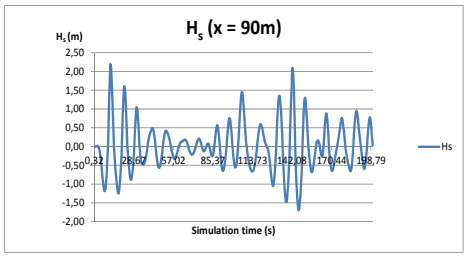

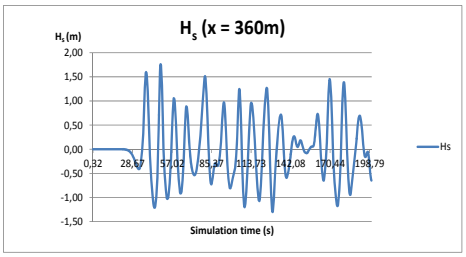

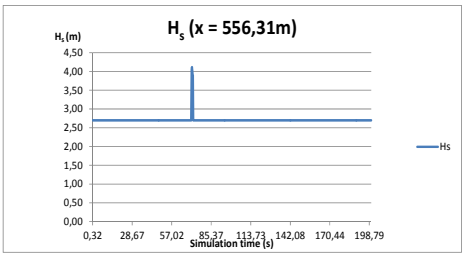

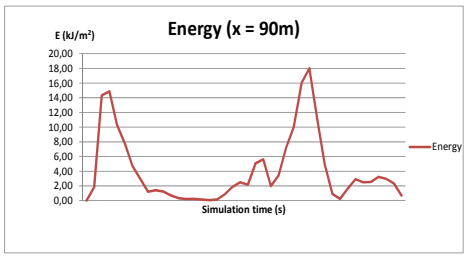

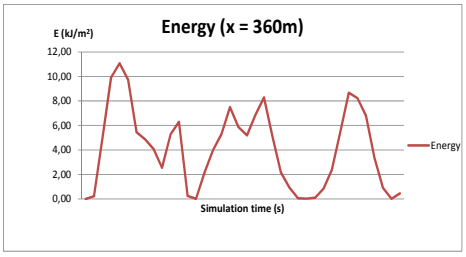

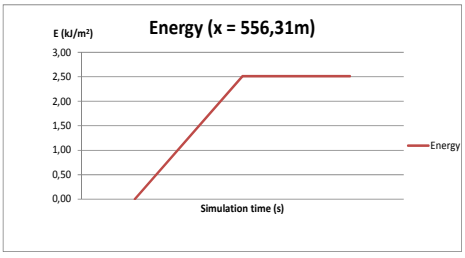

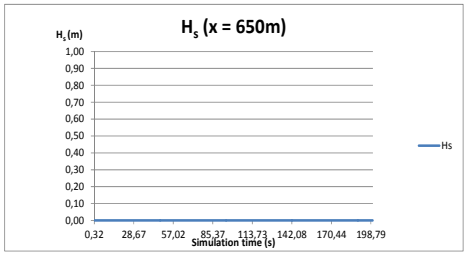

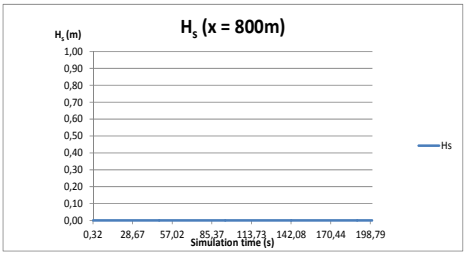

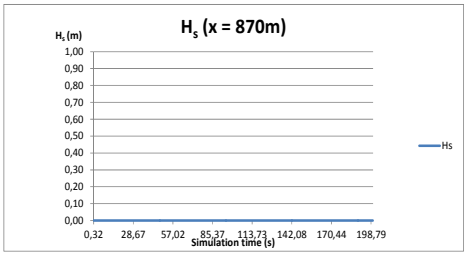

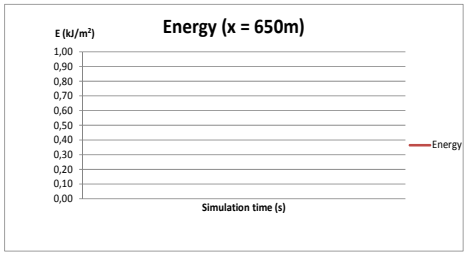

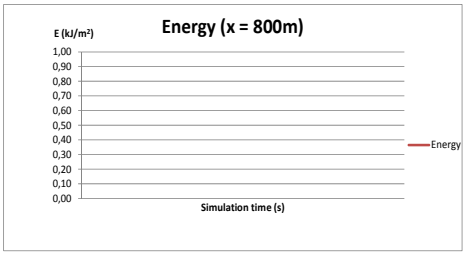

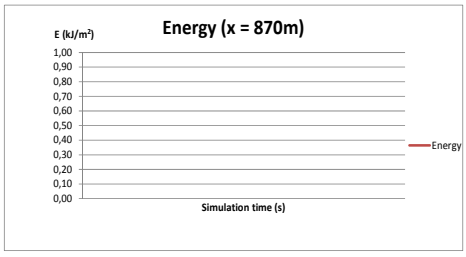

SC39	H_s (m)	T (s)	h_{cr} (m)	X (m)
	3,00	7,00	2,70	300,00

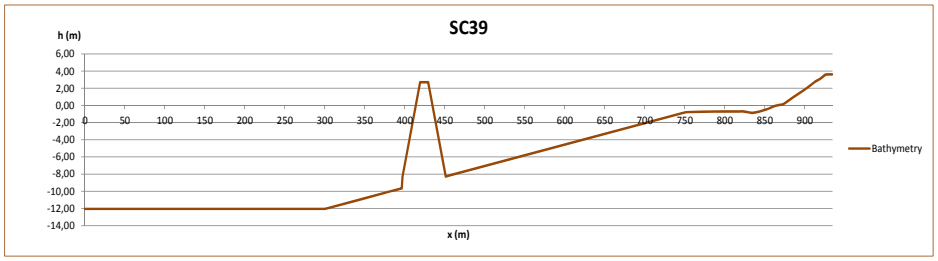

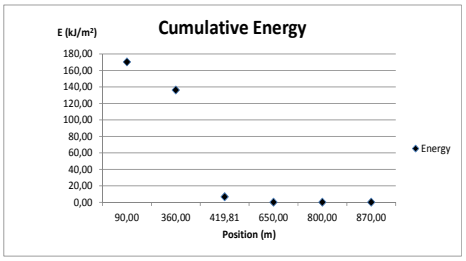

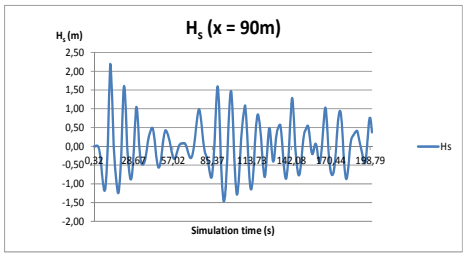

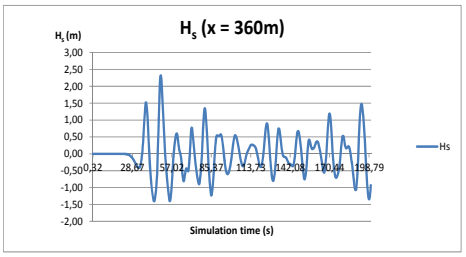

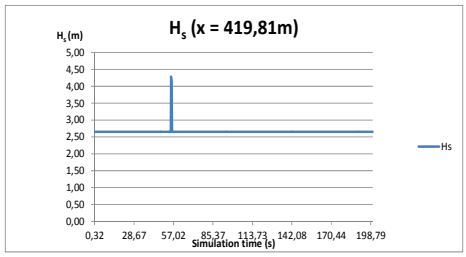

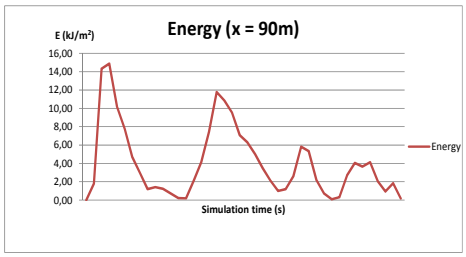

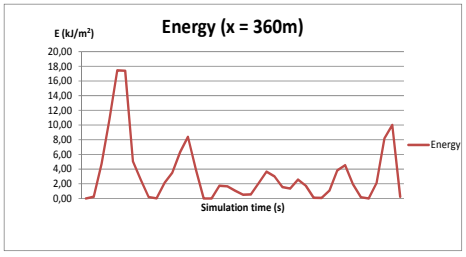

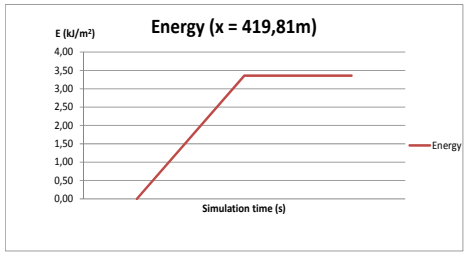

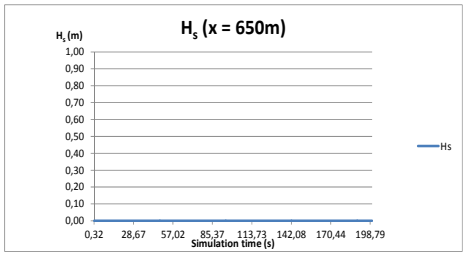

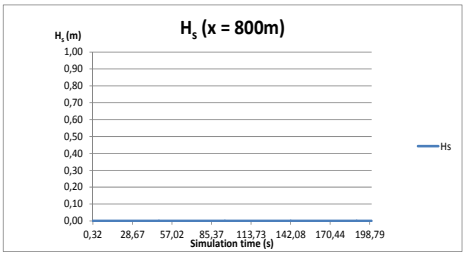

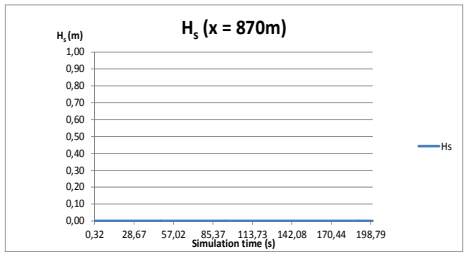

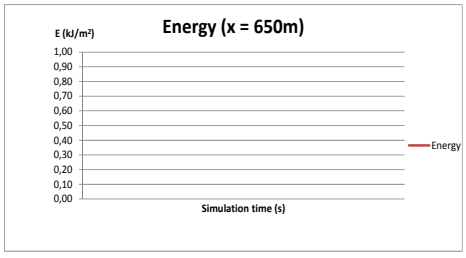

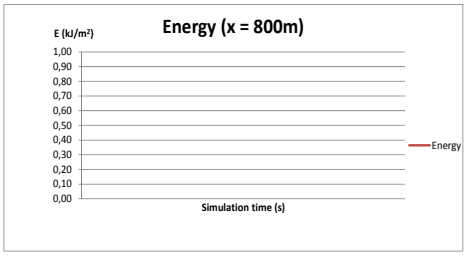

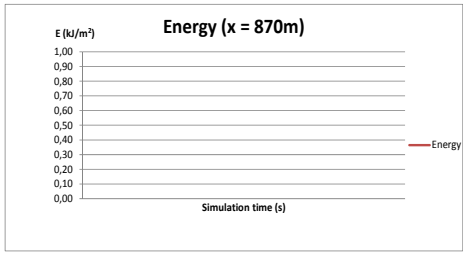

SC40	H_s (m)	T (s)	h_{cr} (m)	X (m)
	3,00	7,00	1,50	235,00

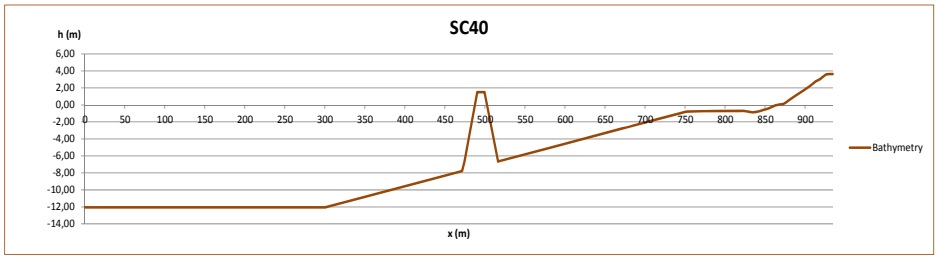

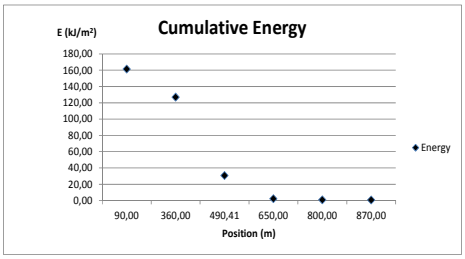

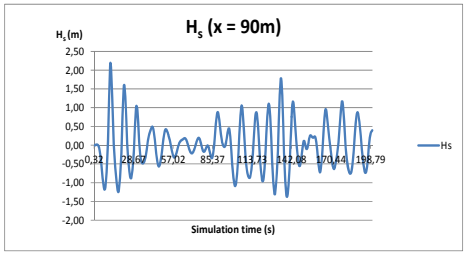

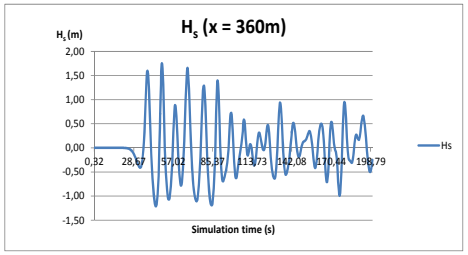

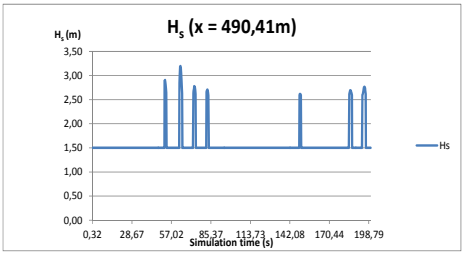

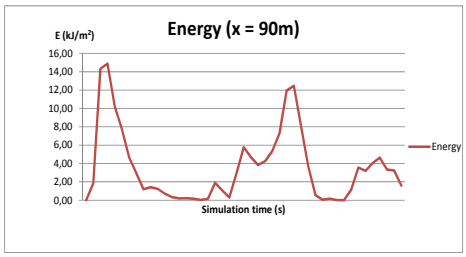

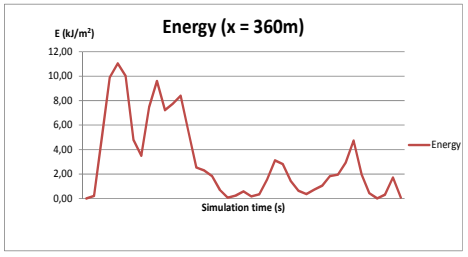

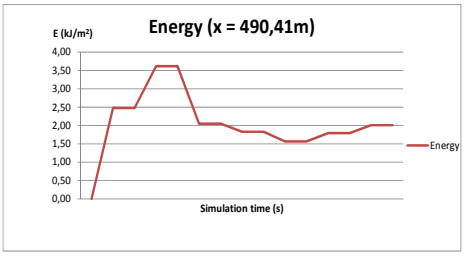

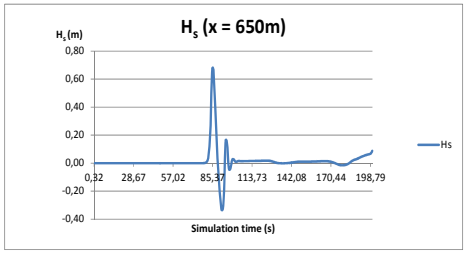

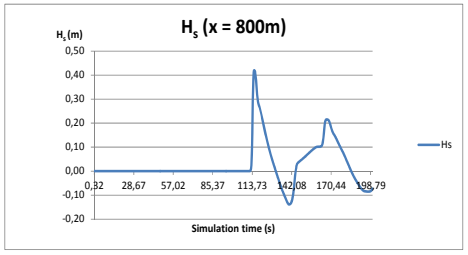

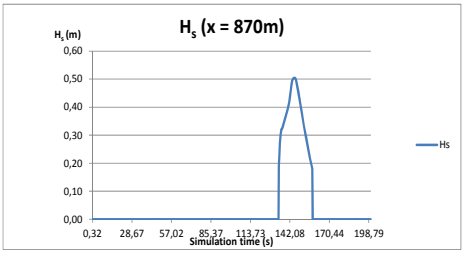

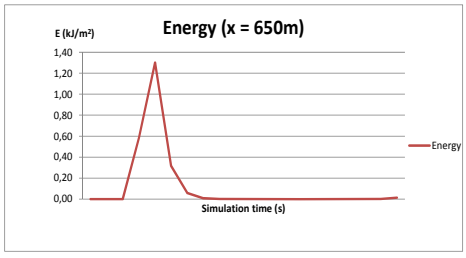

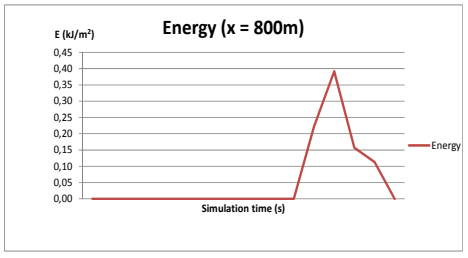

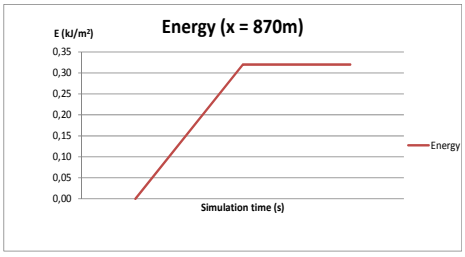

SC41	H_s (m)	T (s)	h_{cr} (m)	X (m)
	3,00	7,00	1,50	170,00

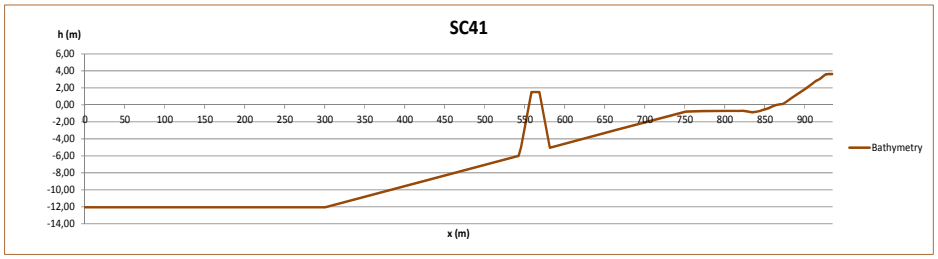

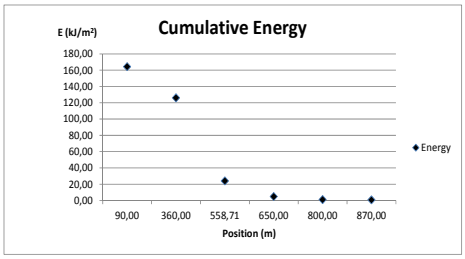

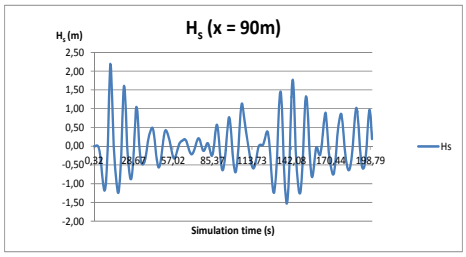

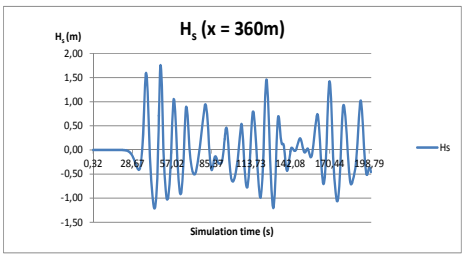

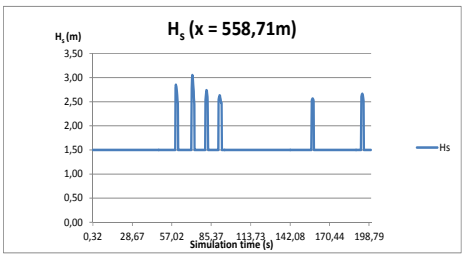

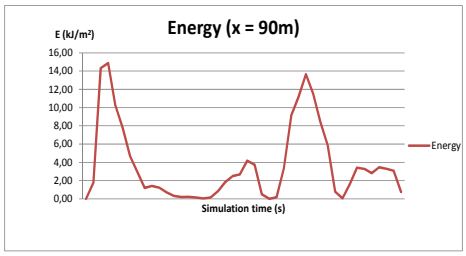

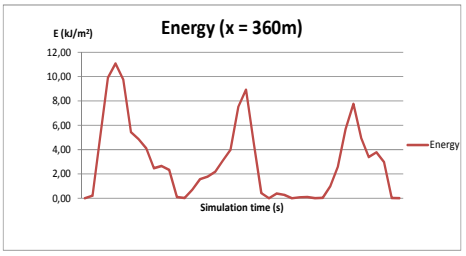

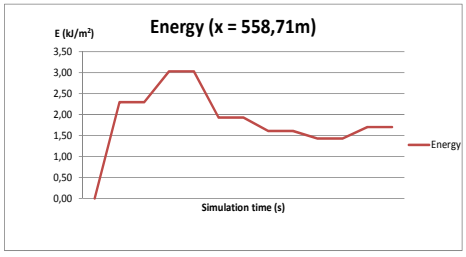

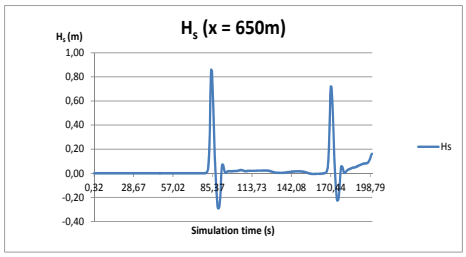

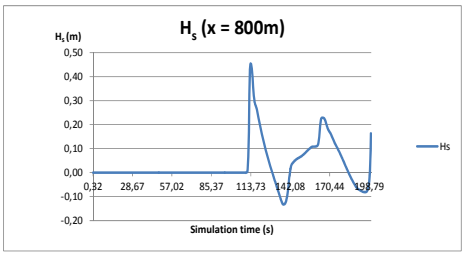

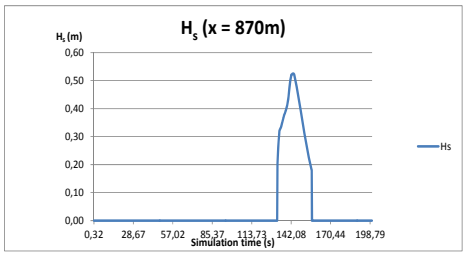

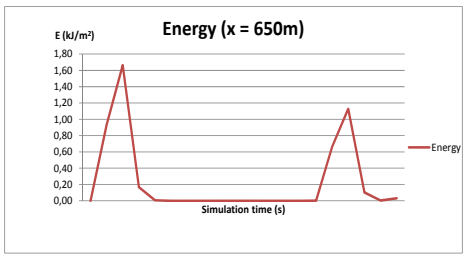

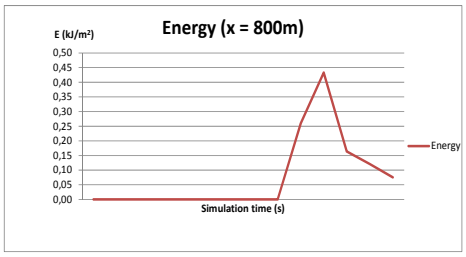

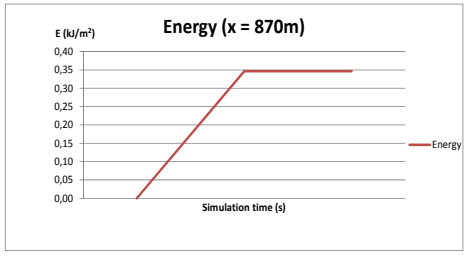

SC42	H_s (m)	T (s)	h_{cr} (m)	X (m)
	3,00	7,00	1,50	300,00

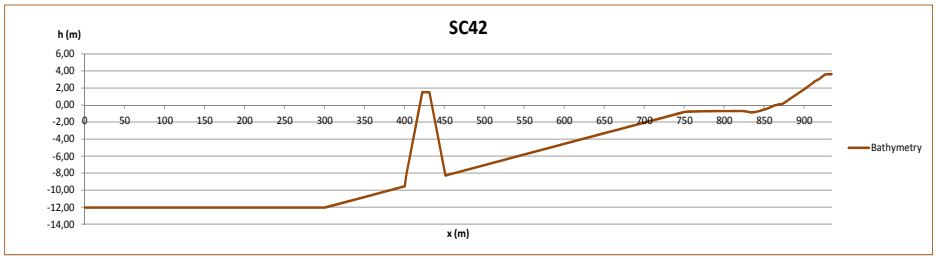

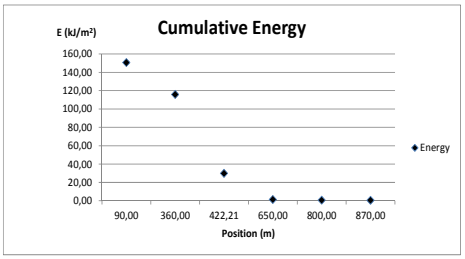

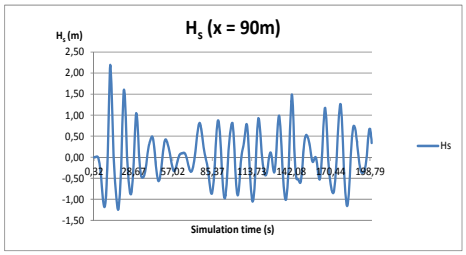

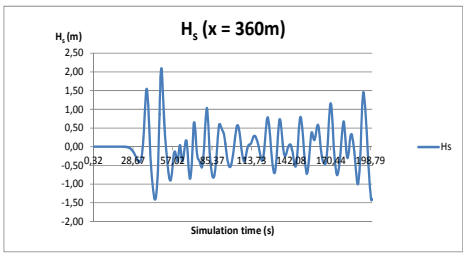

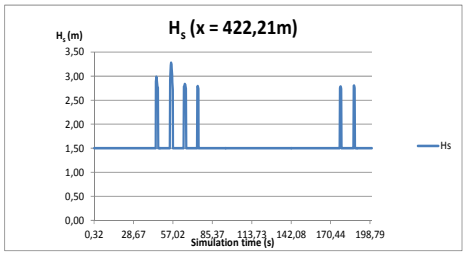

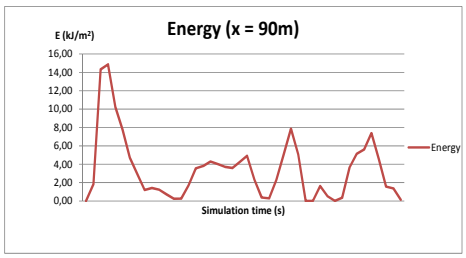

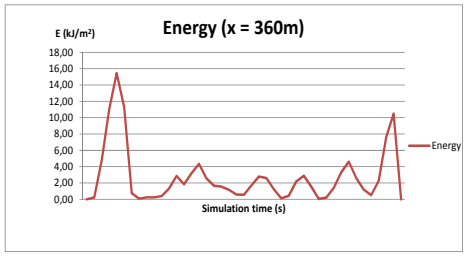

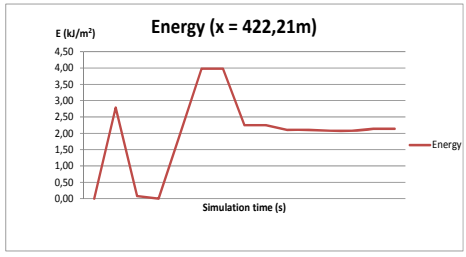

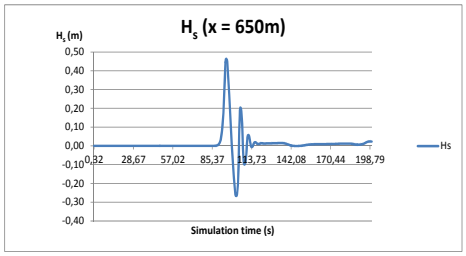

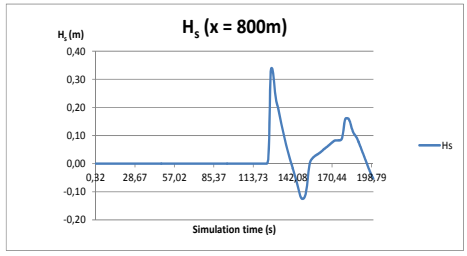

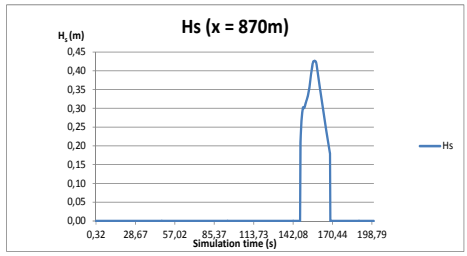

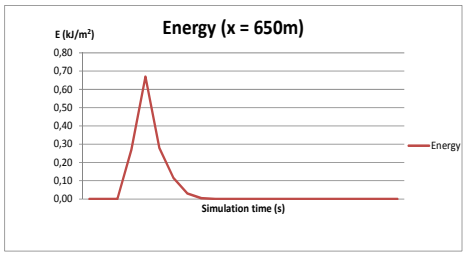

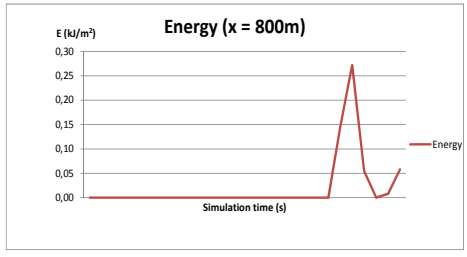

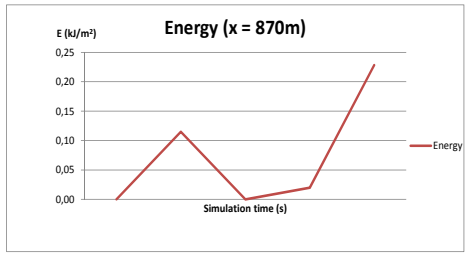

SC43	H_s (m)	T (s)	h_{cr} (m)	X (m)
	3,00	7,00	-1,50	235,00

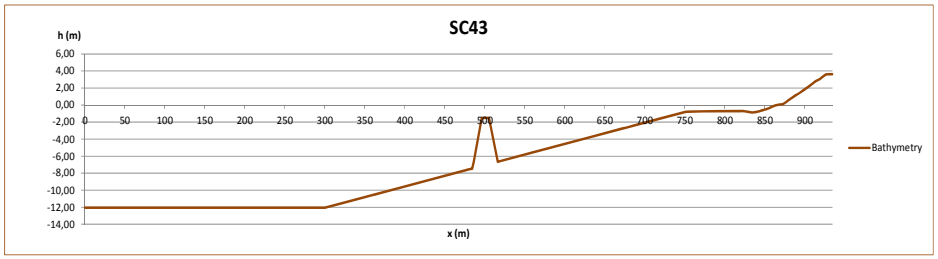

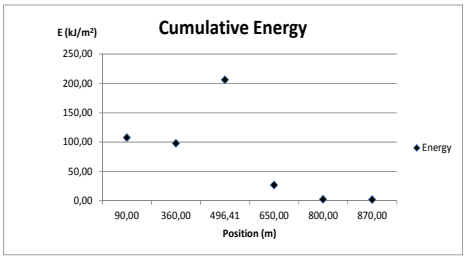

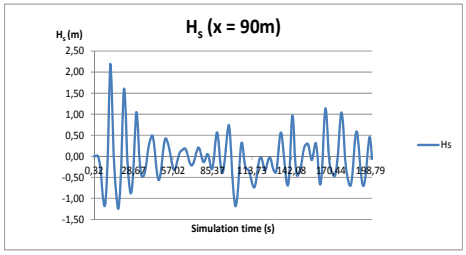

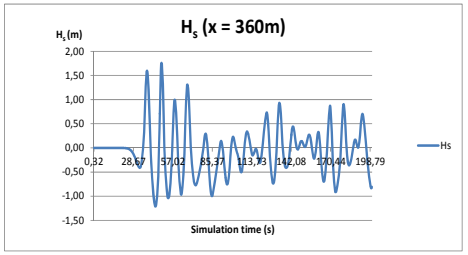

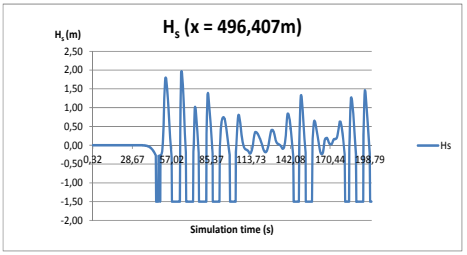

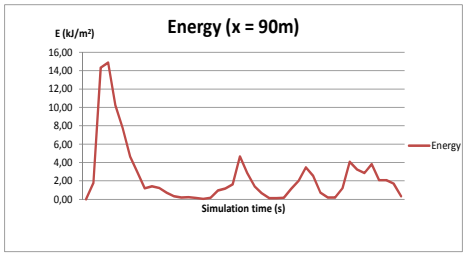

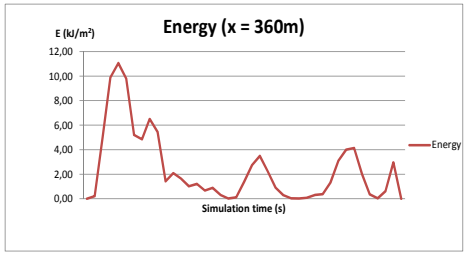

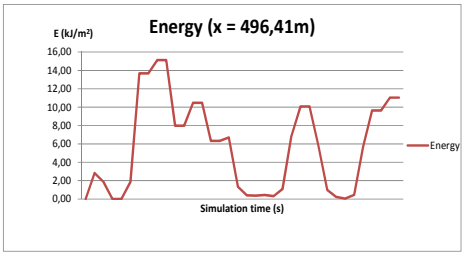

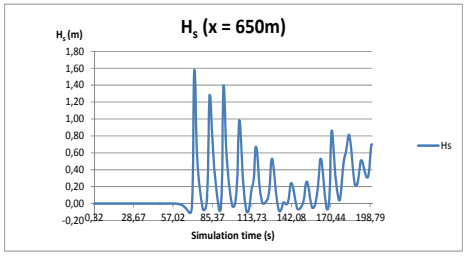

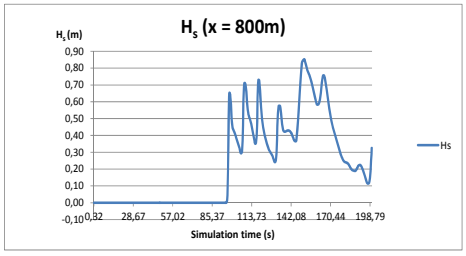

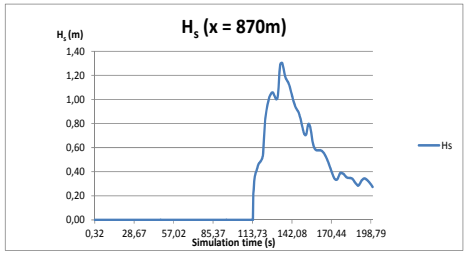

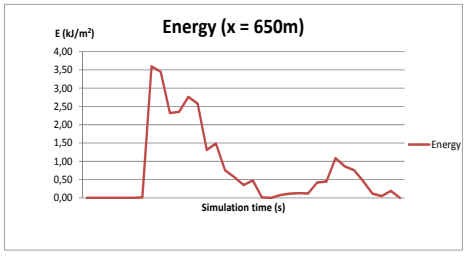

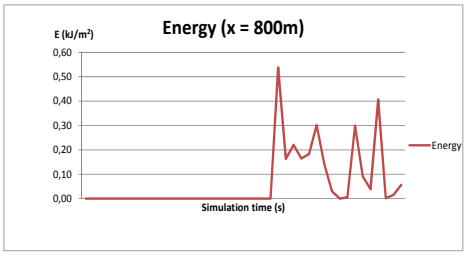

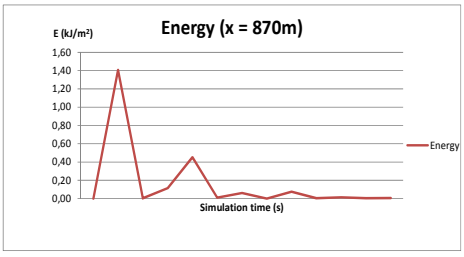

SC44	H_s (m)	T (s)	h_{cr} (m)	X (m)
	3,00	7,00	-1,50	170,00

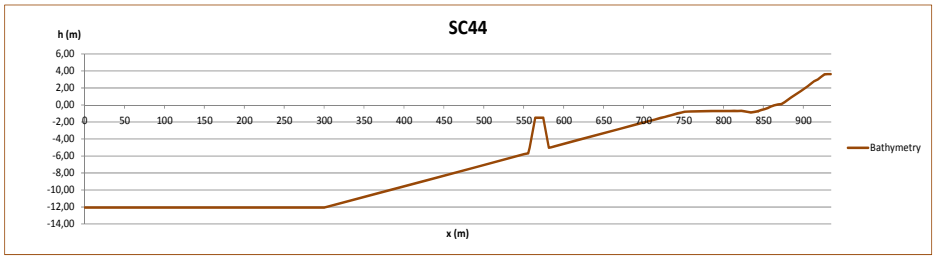

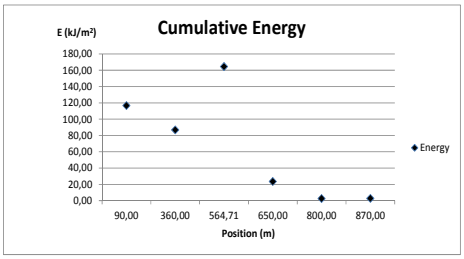

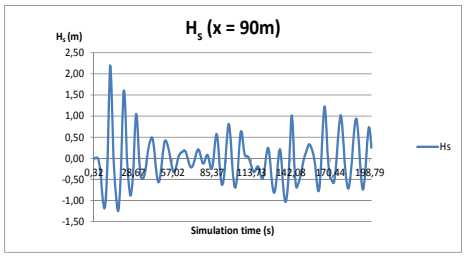

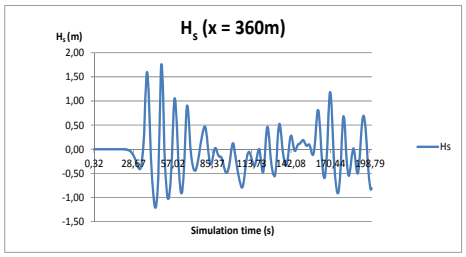

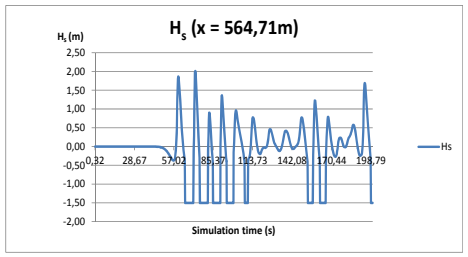

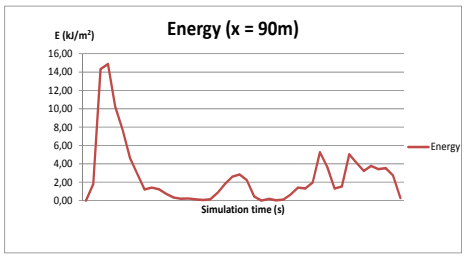

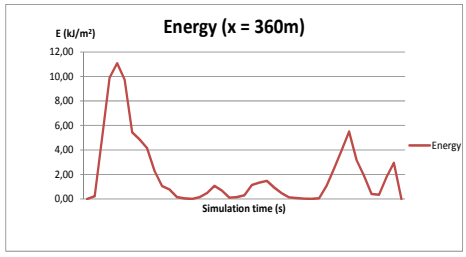

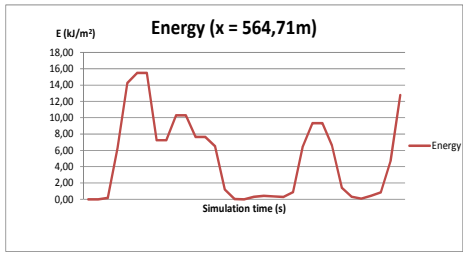

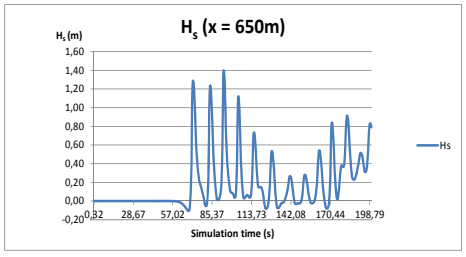

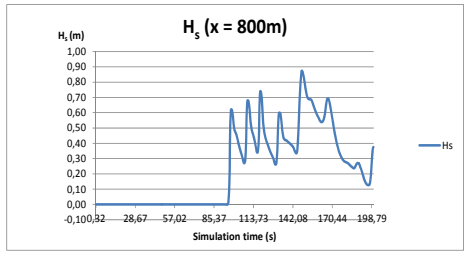

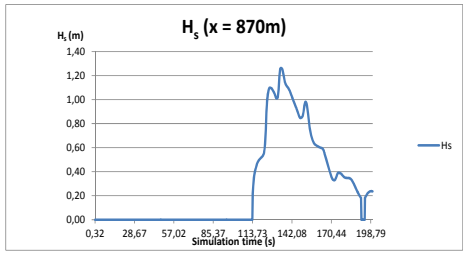

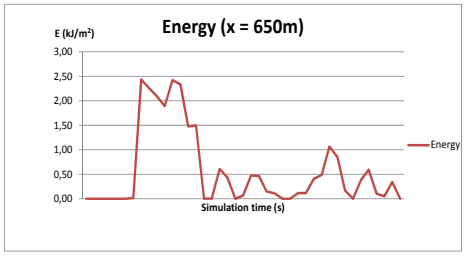

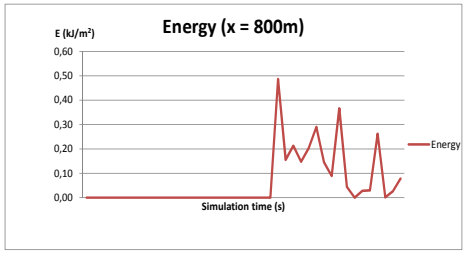

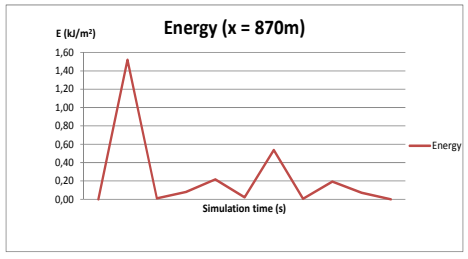

SC45	H_s (m)	T (s)	h_{cr} (m)	X (m)
	3,00	7,00	-1,50	300,00

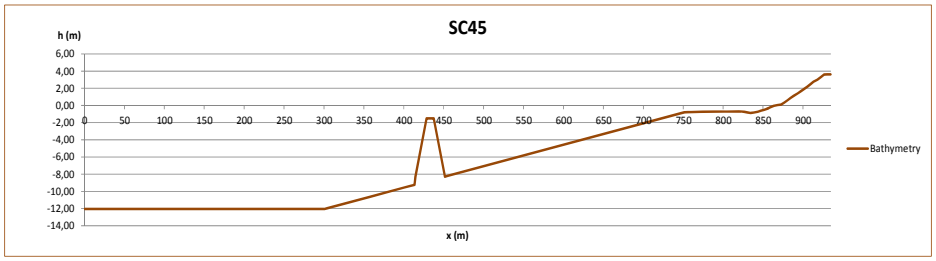

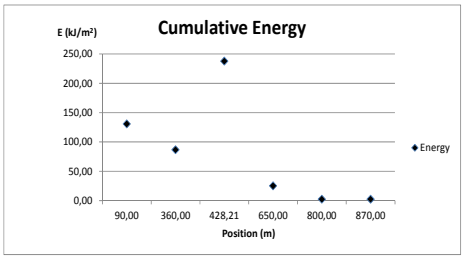

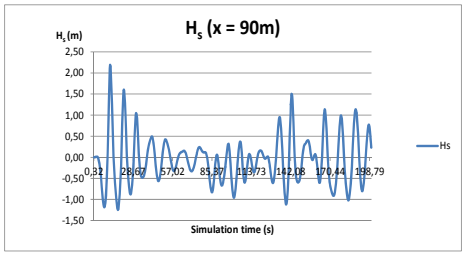

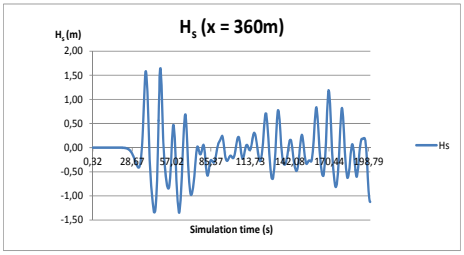

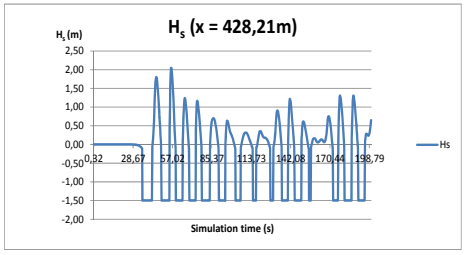

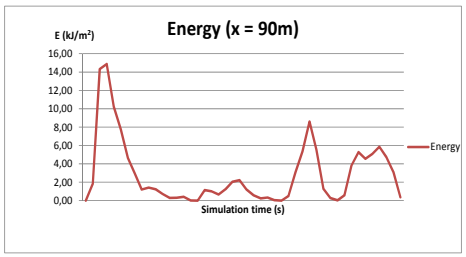

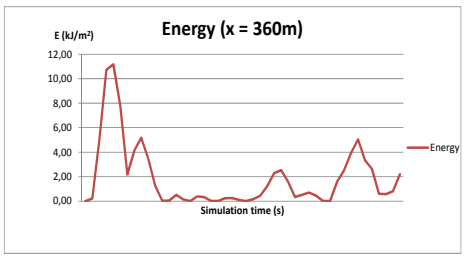

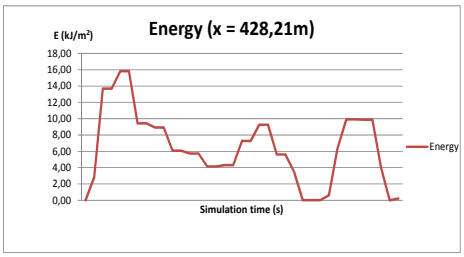

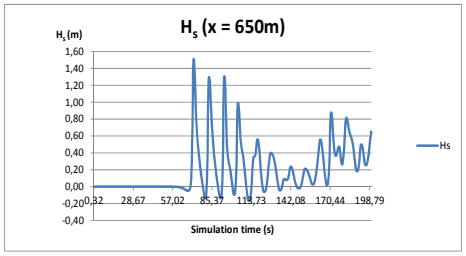

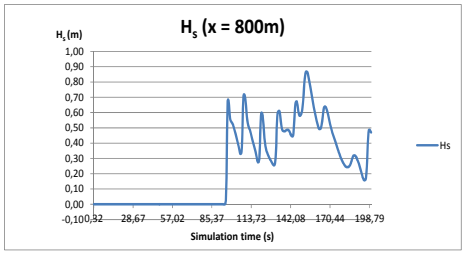

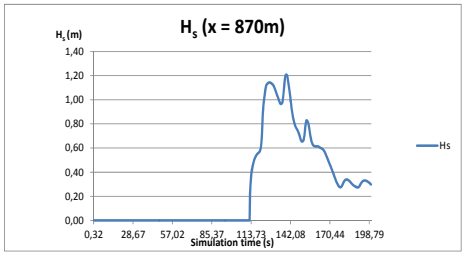

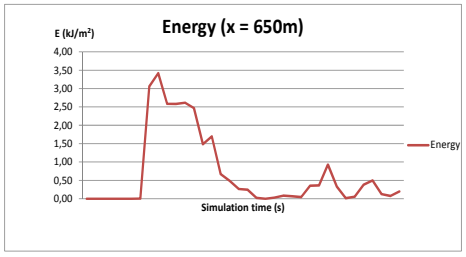

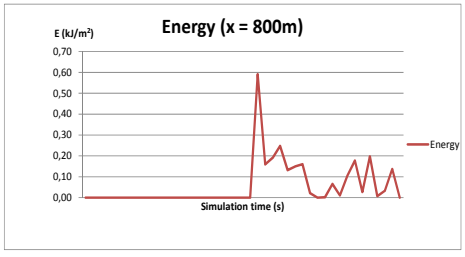

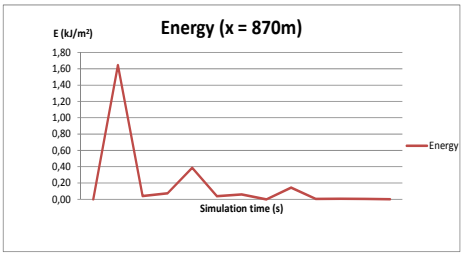

SC46	H_s (m)	T (s)	h_{cr} (m)	X (m)
	3,00	7,00	-0,50	235,00

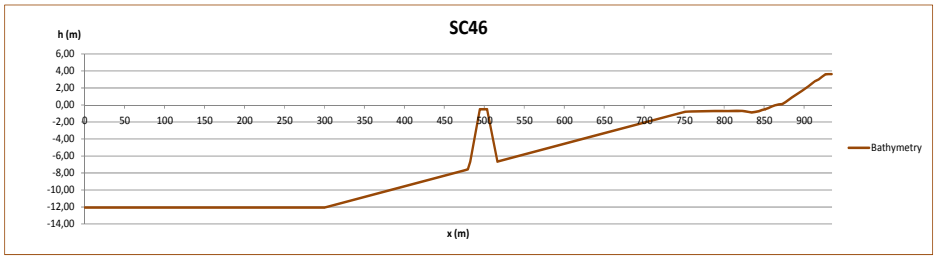

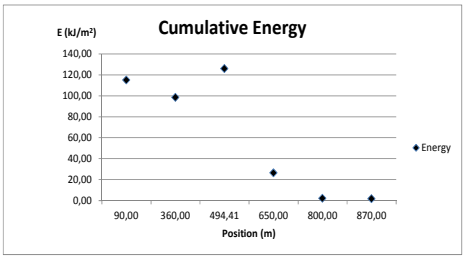

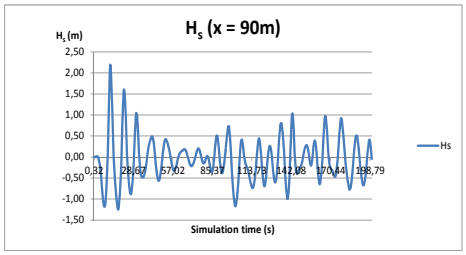

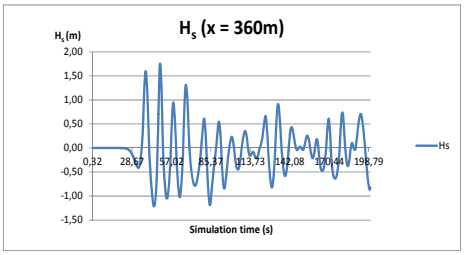

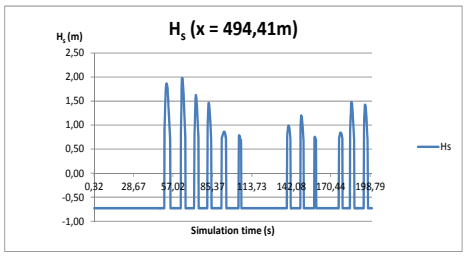

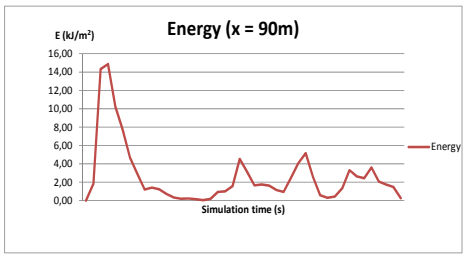

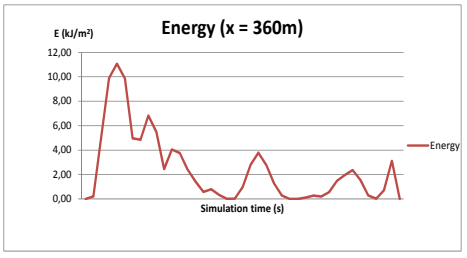

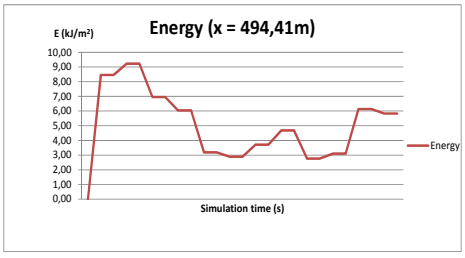

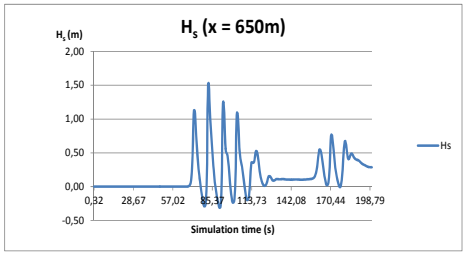

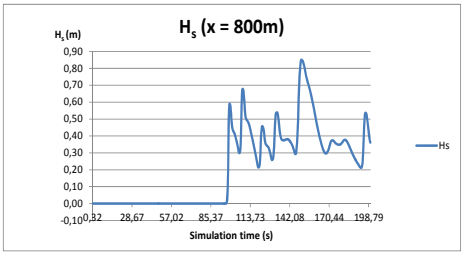

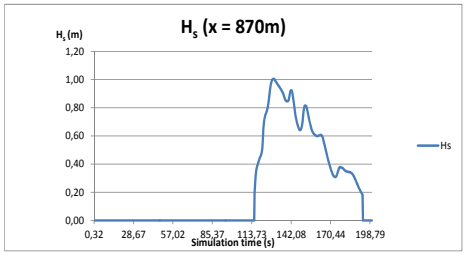

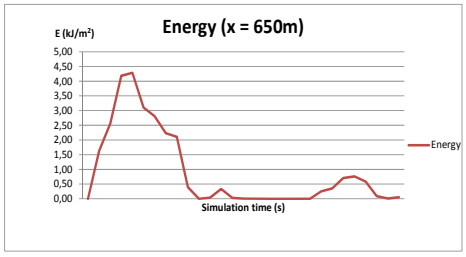

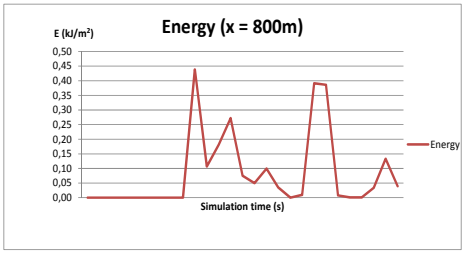

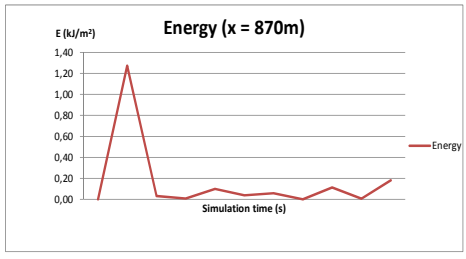

SC47	H_s (m)	T (s)	h_{cr} (m)	X (m)
	3,00	7,00	-0,50	170,00

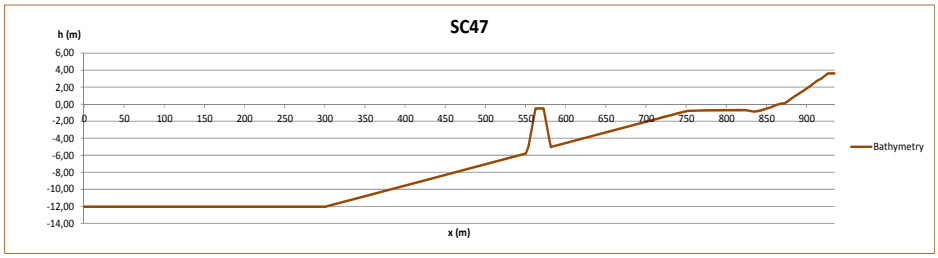

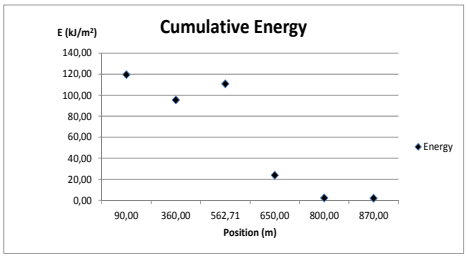

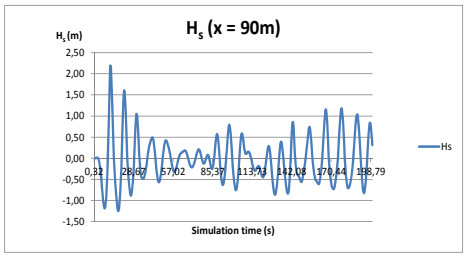

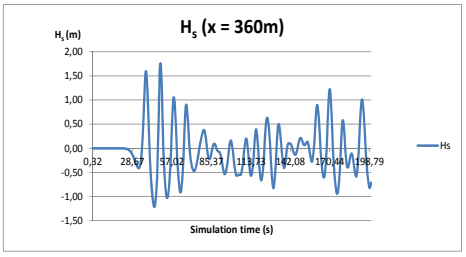

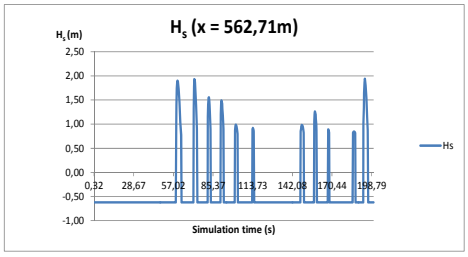

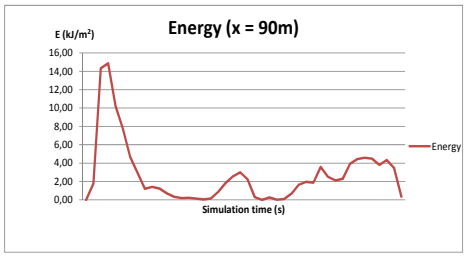

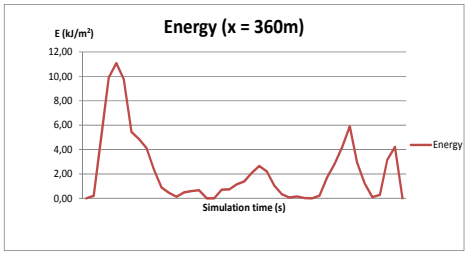

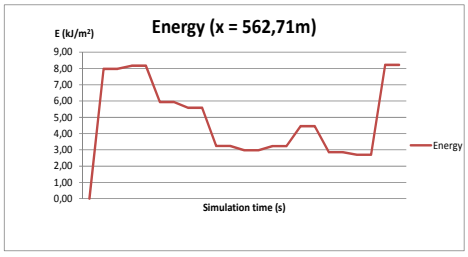

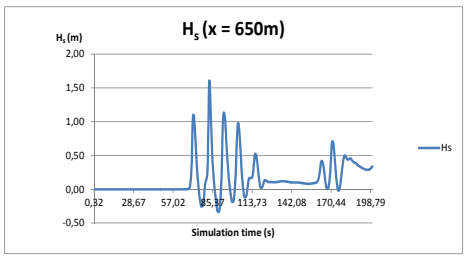

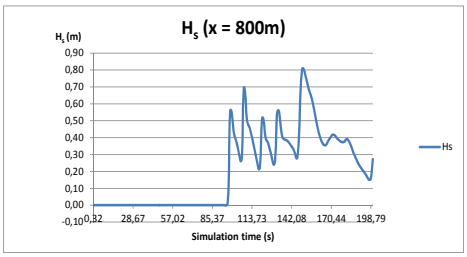

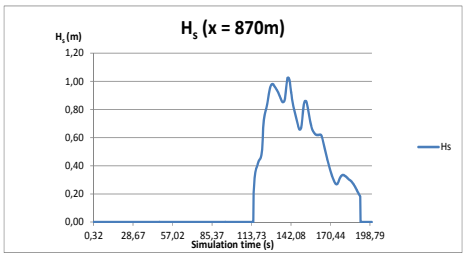

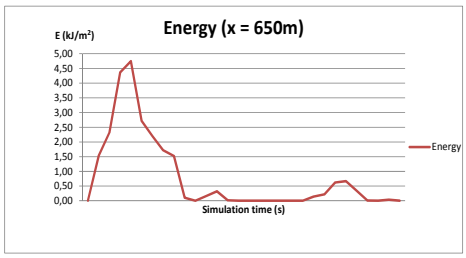

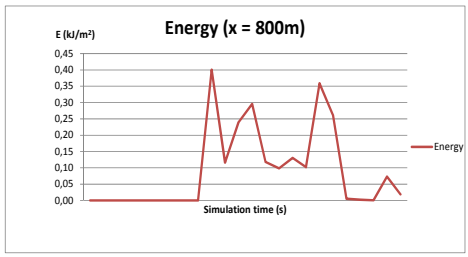

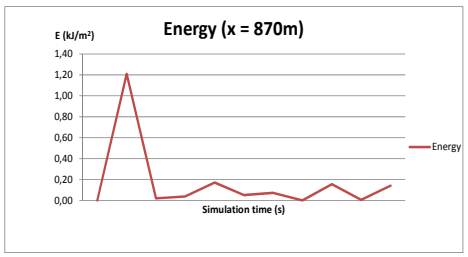

SC48	H_s (m)	T (s)	h_{cr} (m)	X (m)
	3,00	7,00	-0,50	300,00

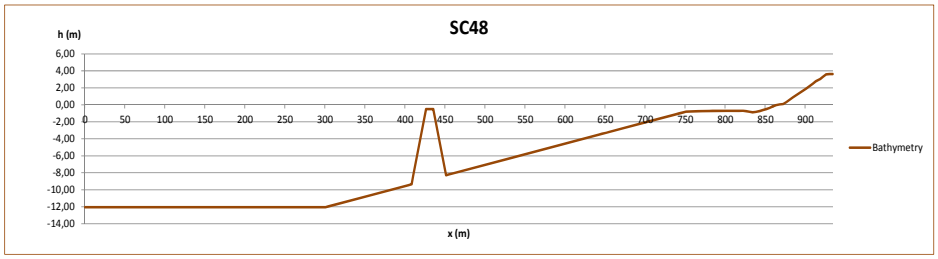

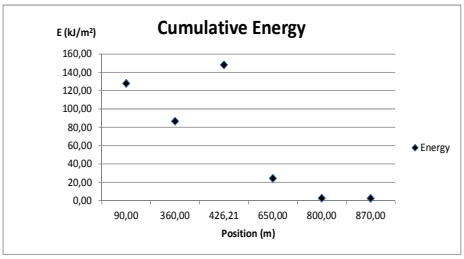

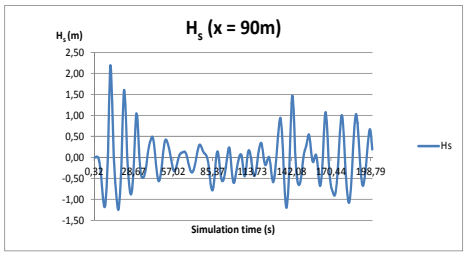

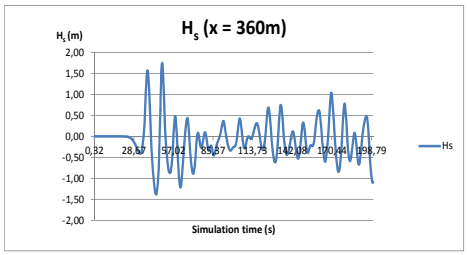

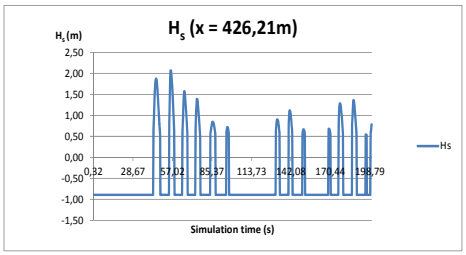

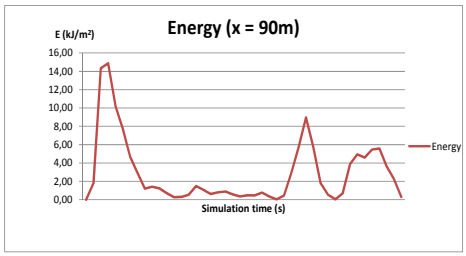

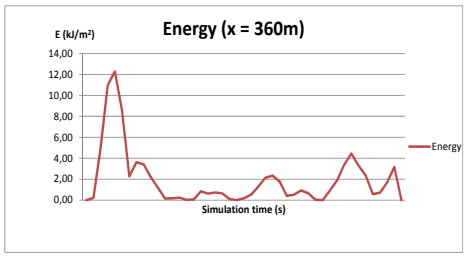

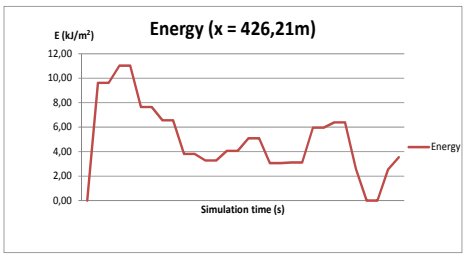

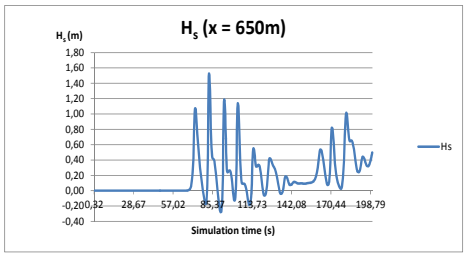

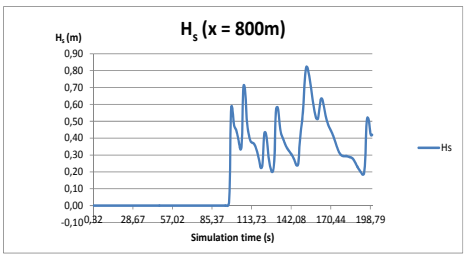

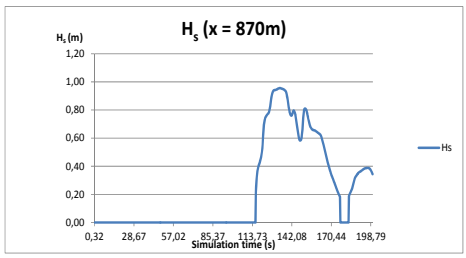

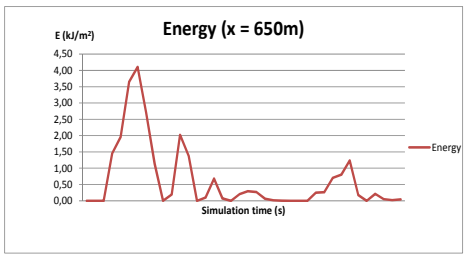

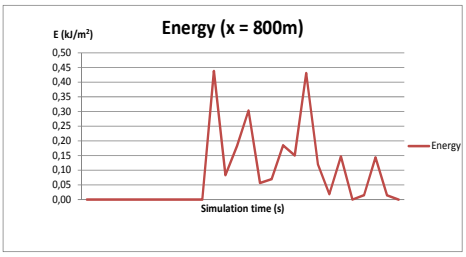

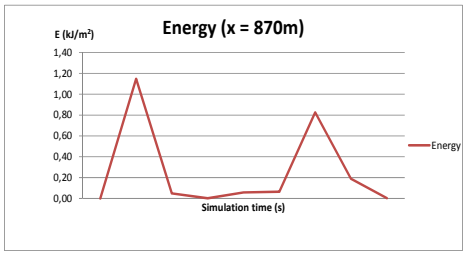

APPENDIX 6

COULWAVE.

Scenario Initial5

Scenarios 49 to 60

(Page intentionally left blank)

Scenarios Initial and scenarios with detached breakwater

Wave characteristics		Scenario
Hs (m)	T (s)	
6,64	9,30	**Initial1**
1,00	7,00	**Initial2**
2,00	7,00	**Initial3**
3,00	7,00	**Initial4**
4,00	11,00	**Initial5**

Wave characteristics		Breakwater characteristics		Scenario
H (m)	T (s)	hcr (m)	X (m)	
6,64	9,30	2,70	235,00	SC1
			170,00	SC2
			300,00	SC3
		1,50	235,00	SC4
			170,00	SC5
			300,00	SC6
		-1,50	235,00	SC7
			170,00	SC8
			300,00	SC9
		-0,50	235,00	SC10
			170,00	SC11
			300,00	SC12
1,00	7,00	2,70	235,00	SC13
			170,00	SC14
			300,00	SC15
		1,50	235,00	SC16
			170,00	SC17
			300,00	SC18
		-1,50	235,00	SC19
			170,00	SC20
			300,00	SC21
		-0,50	235,00	SC22
			170,00	SC23
			300,00	SC24
2,00	7,00	2,70	235,00	SC25
			170,00	SC26
			300,00	SC27
		1,50	235,00	SC28
			170,00	SC29
			300,00	SC30
		-1,50	235,00	SC31
			170,00	SC32
			300,00	SC33
		-0,50	235,00	SC34
			170,00	SC35
			300,00	SC36
3,00	7,00	2,70	235,00	SC37
			170,00	SC38
			300,00	SC39
		1,50	235,00	SC40
			170,00	SC41
			300,00	SC42
		-1,50	235,00	SC43
			170,00	SC44
			300,00	SC45
		-0,50	235,00	SC46
			170,00	SC47
			300,00	SC48
4,00	11,00	2,70	235,00	SC49
			170,00	SC50
			300,00	SC51
		1,50	235,00	SC52
			170,00	SC53
			300,00	SC54
		-1,50	235,00	SC55
			170,00	SC56
			300,00	SC57
		-0,50	235,00	SC58
			170,00	SC59
			300,00	SC60

Initial5	Hs (m)	T (s)
	4,00	11,00

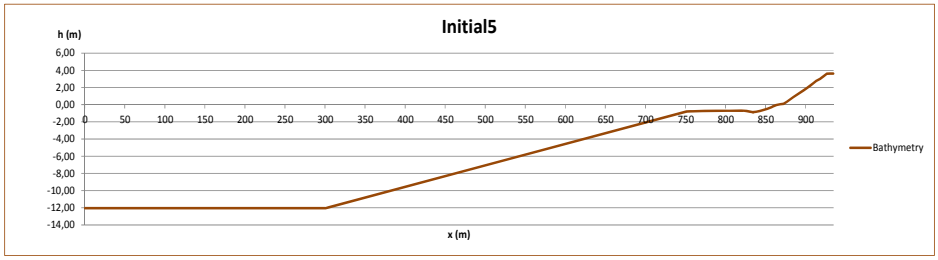

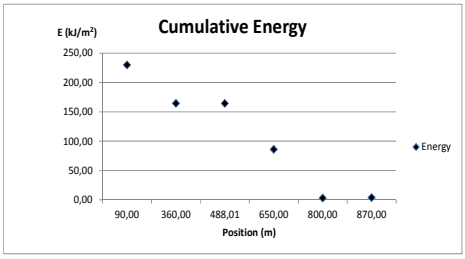

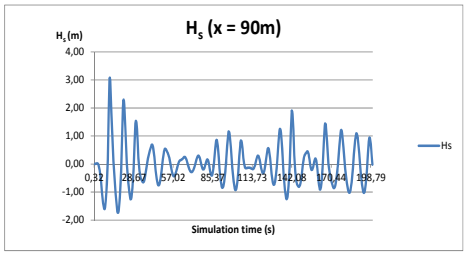

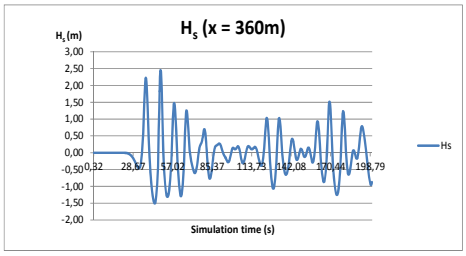

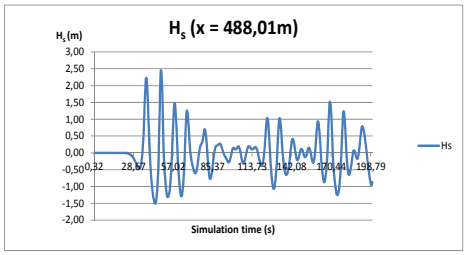

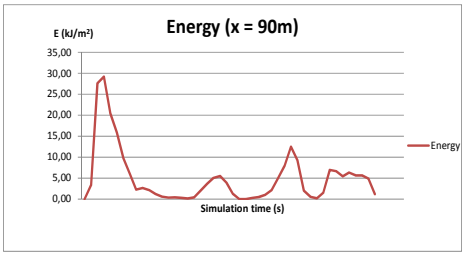

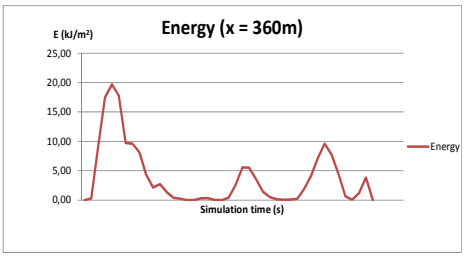

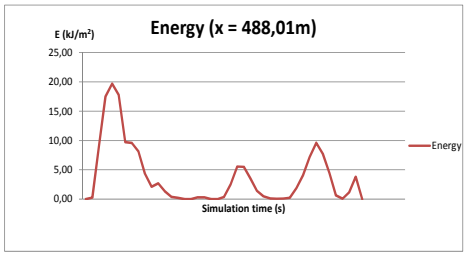

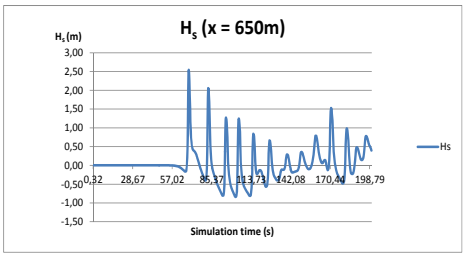

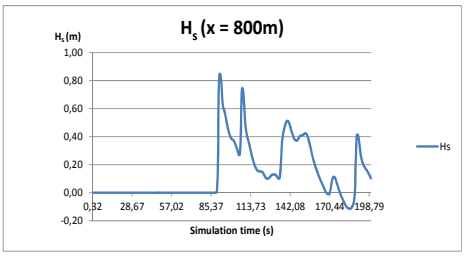

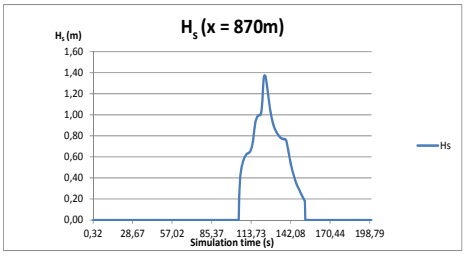

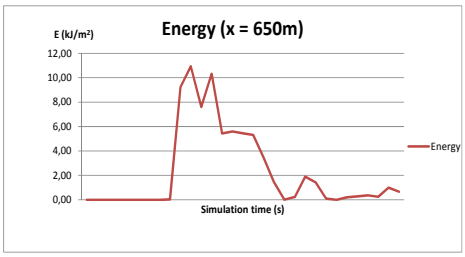

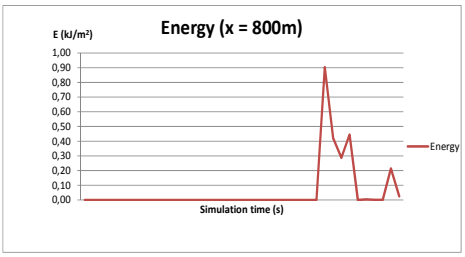

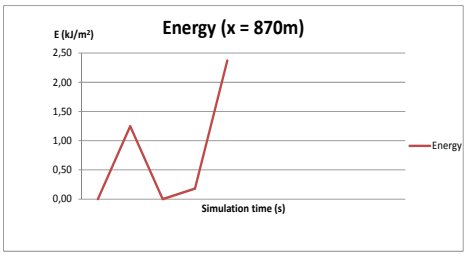

SC49	H_s (m)	T (s)	h_{cr} (m)	X (m)
	4,00	11,00	2,70	235,00

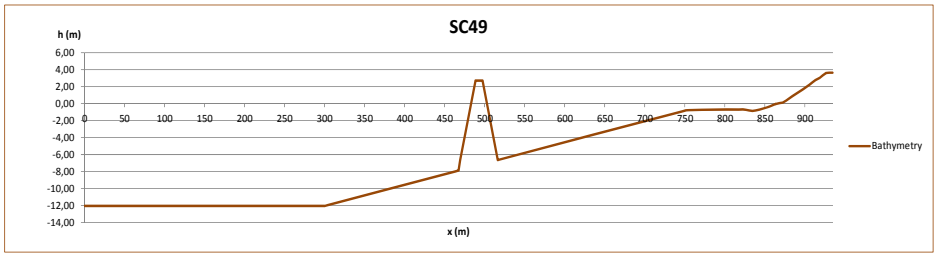

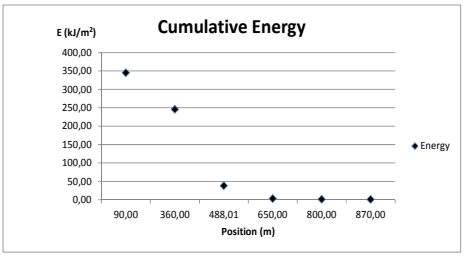

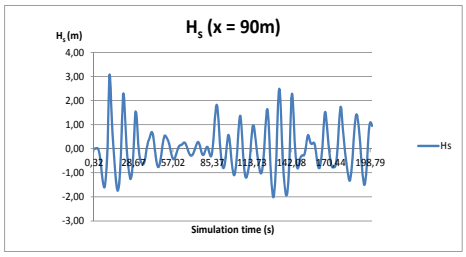

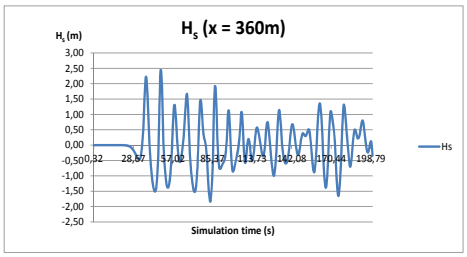

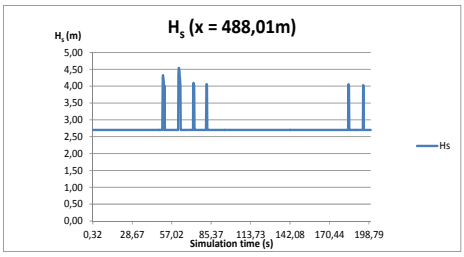

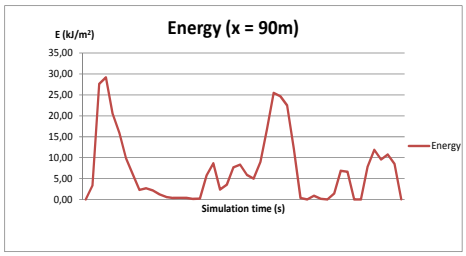

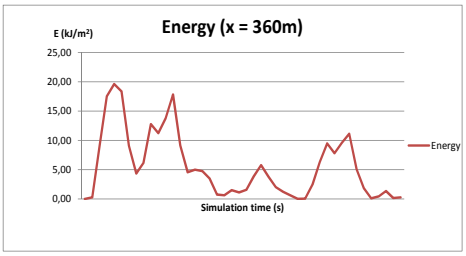

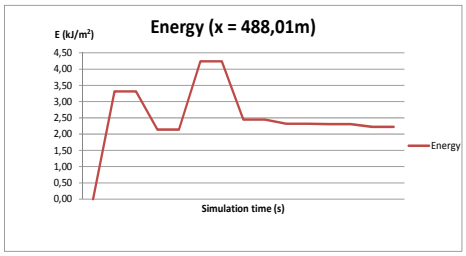

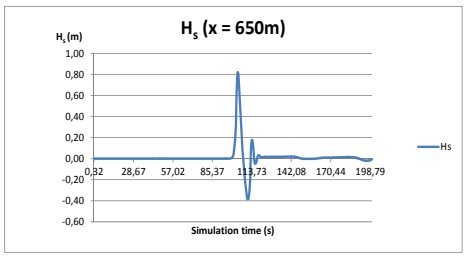

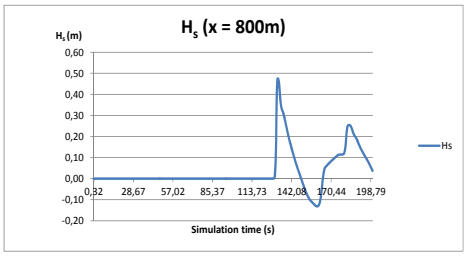

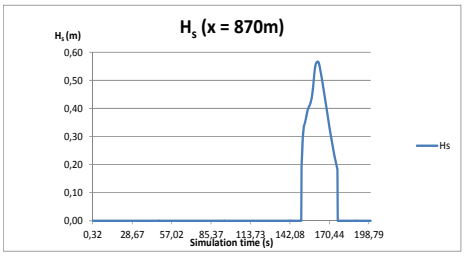

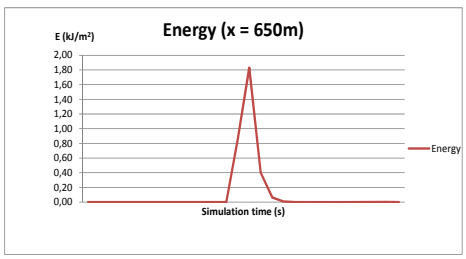

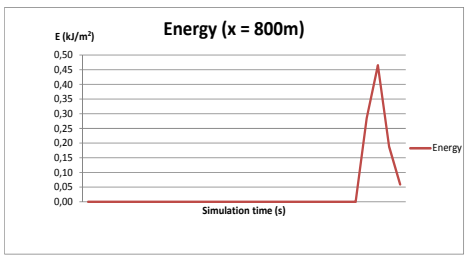

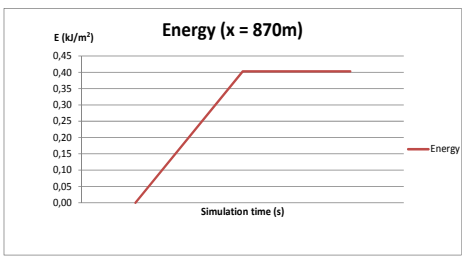

SC50	H_s (m)	T (s)	h_{cr} (m)	X (m)
	4,00	11,00	2,70	170,00

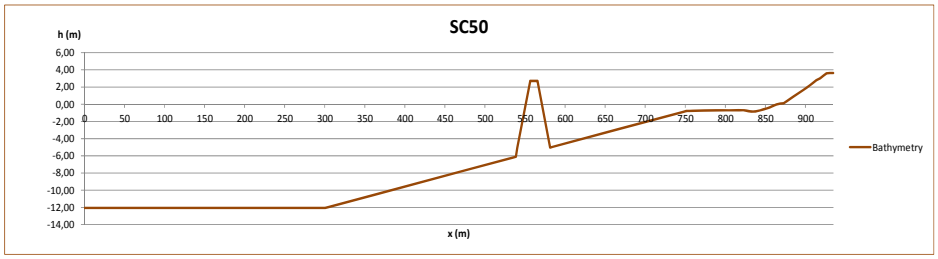

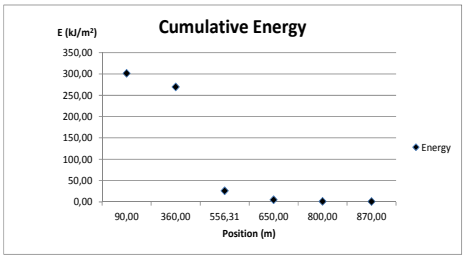

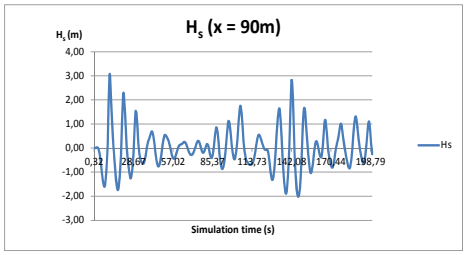

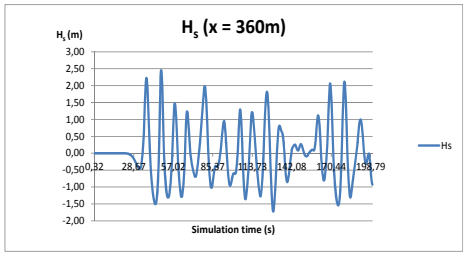

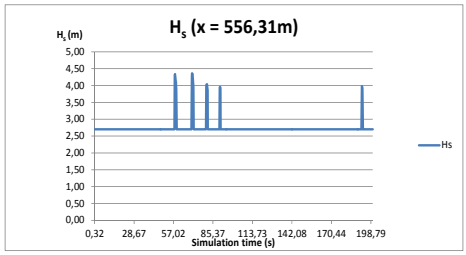

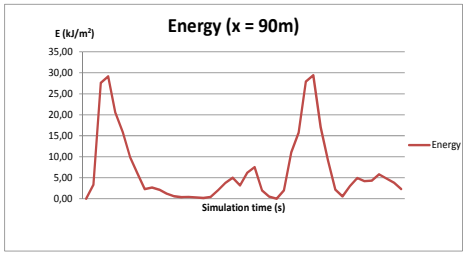

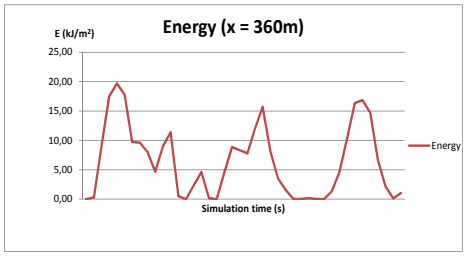

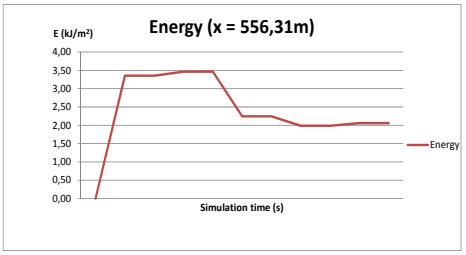

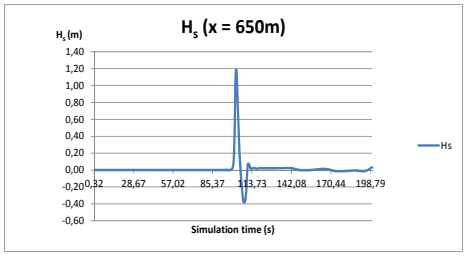

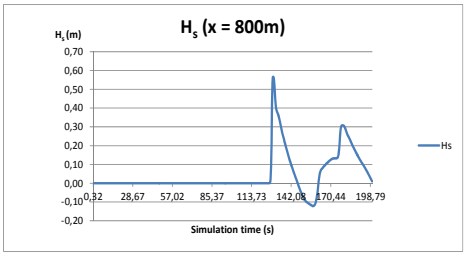

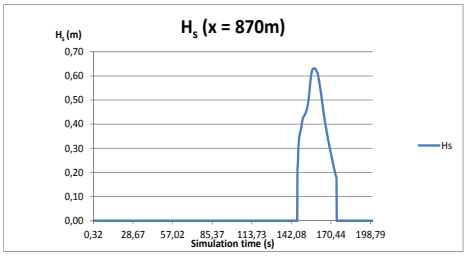

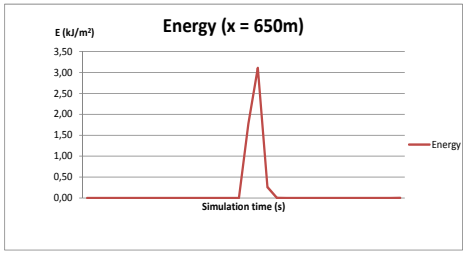

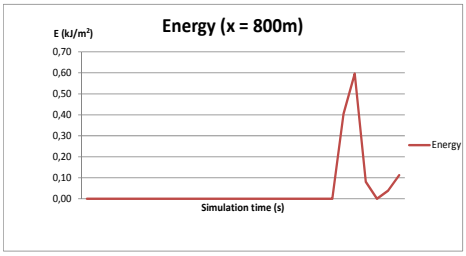

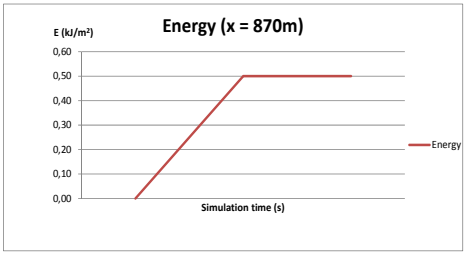

SC51	H_s (m)	T (s)	h_{cr} (m)	X (m)
	4,00	11,00	2,70	300,00

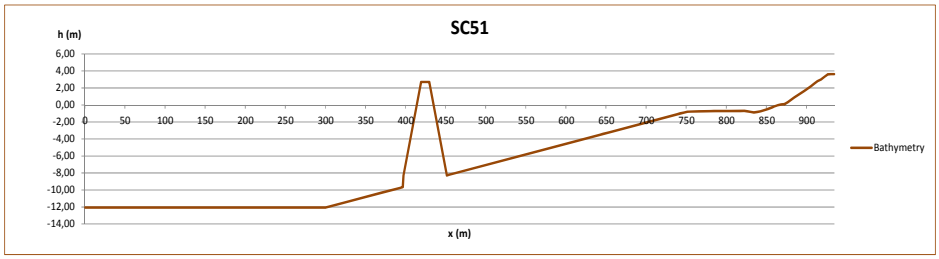

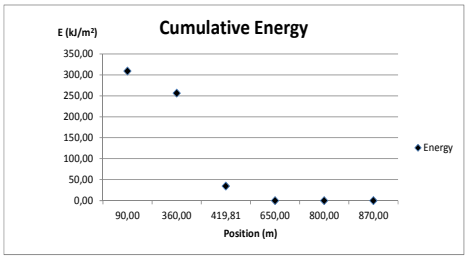

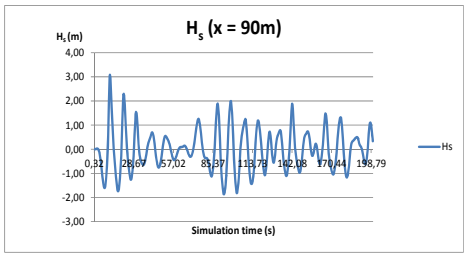

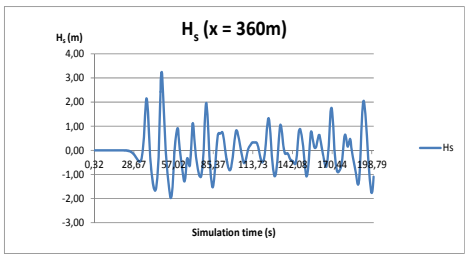

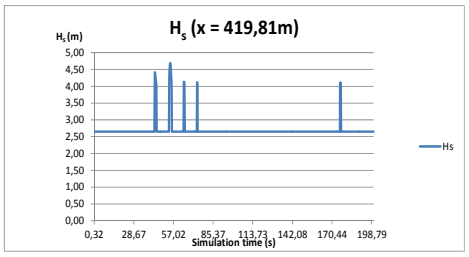

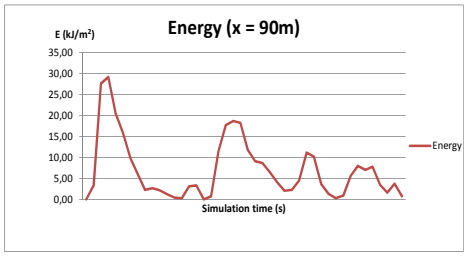

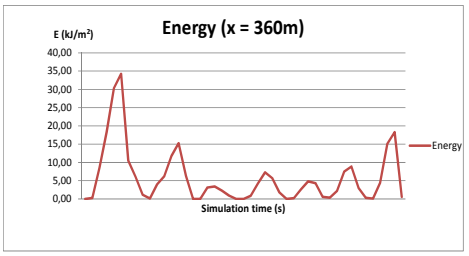

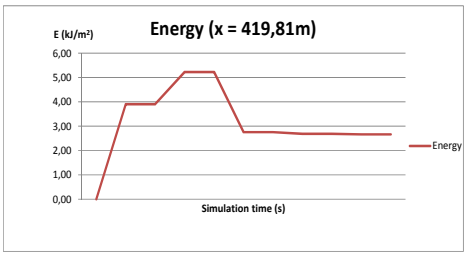

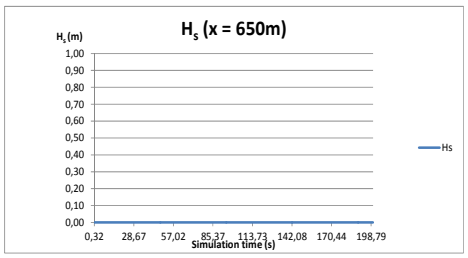

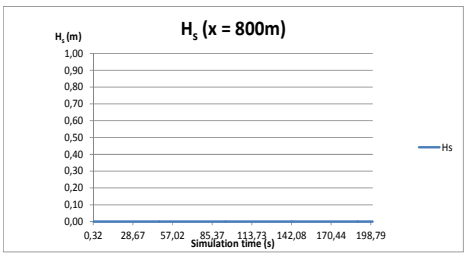

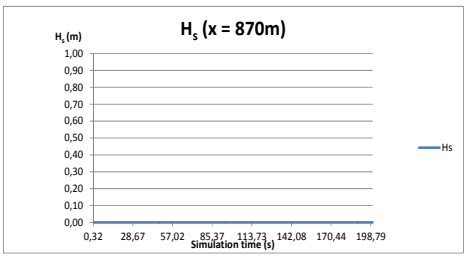

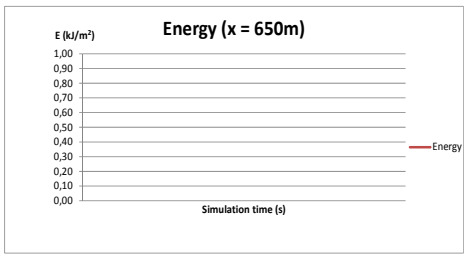

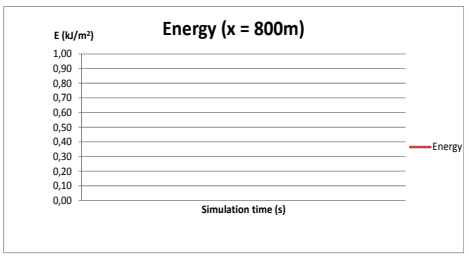

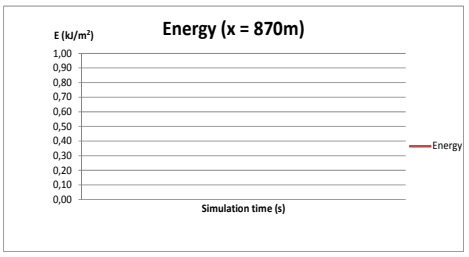

SC52	H_s (m)	T (s)	h_{cr} (m)	X (m)
	4,00	11,00	1,50	235,00

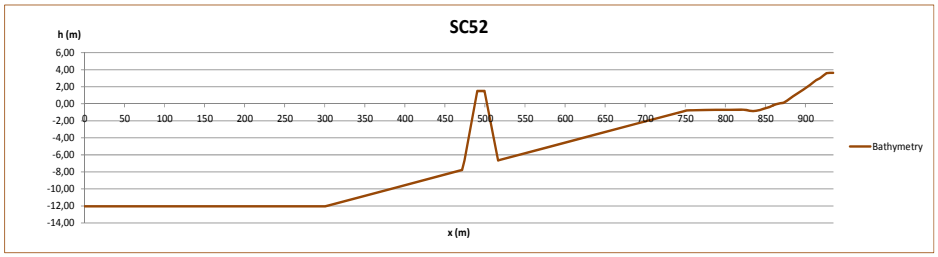

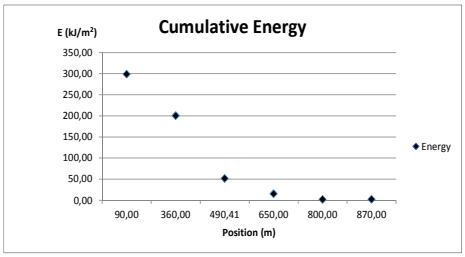

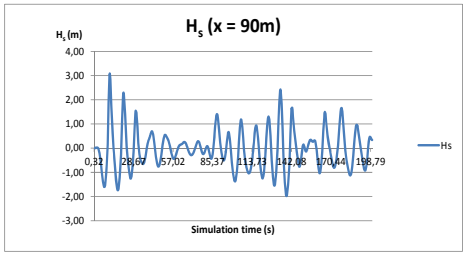

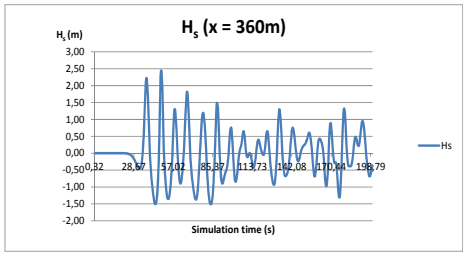

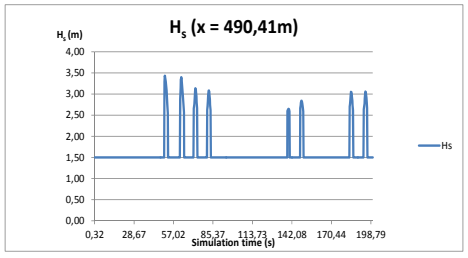

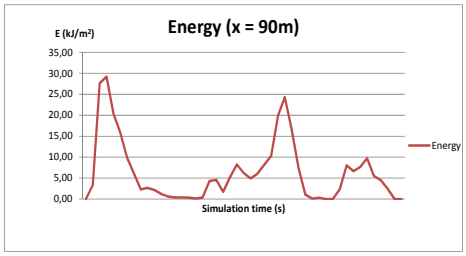

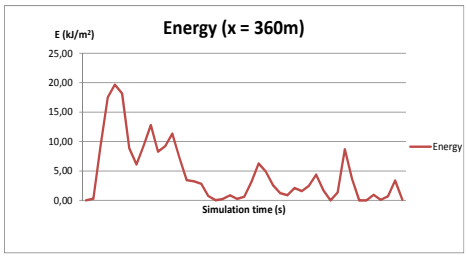

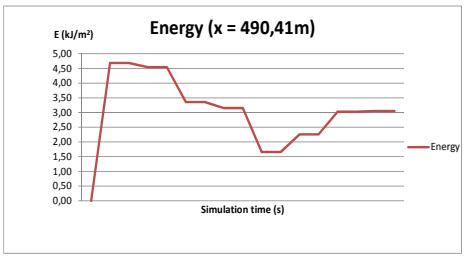

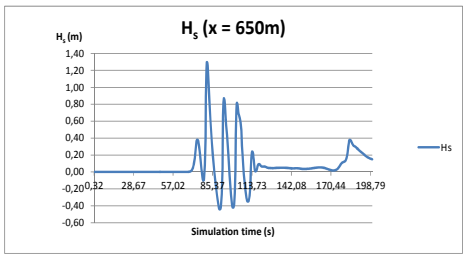

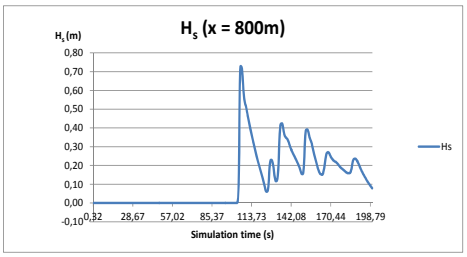

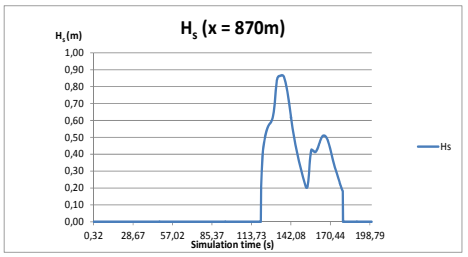

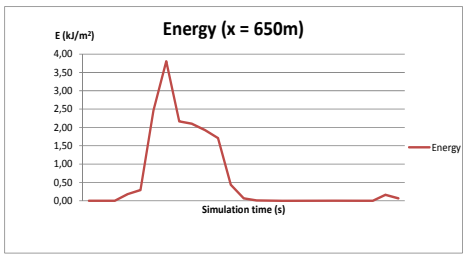

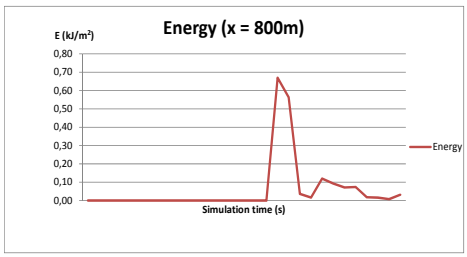

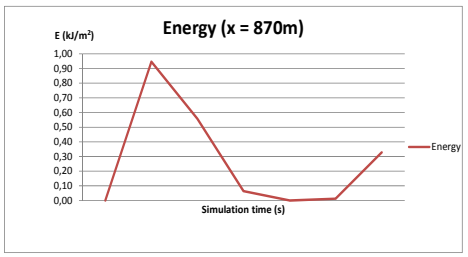

SC53	H_s (m)	T (s)	h_{cr} (m)	X (m)
	4,00	11,00	1,50	170,00

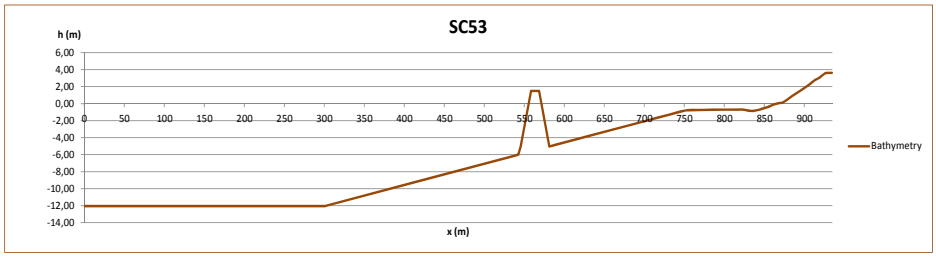

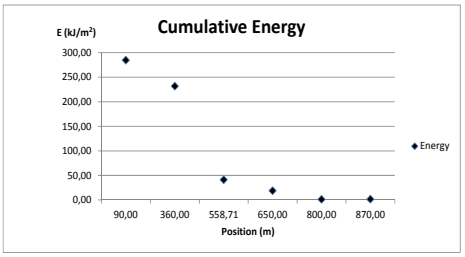

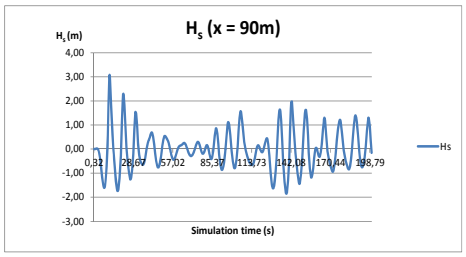

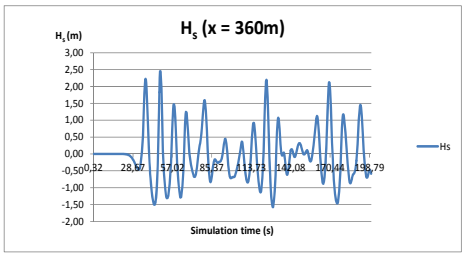

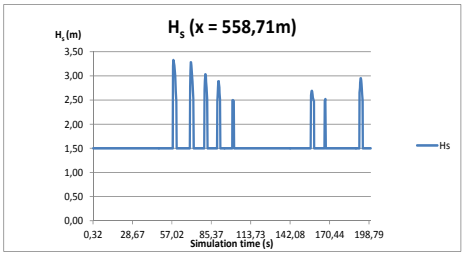

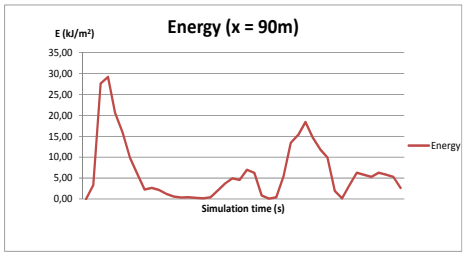

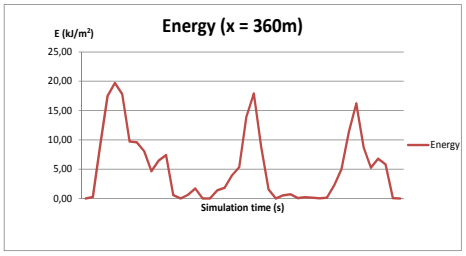

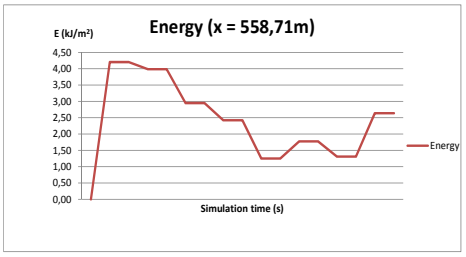

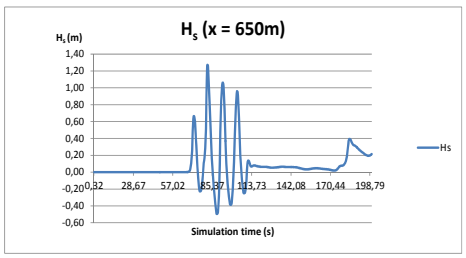

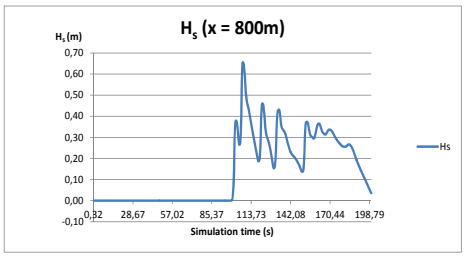

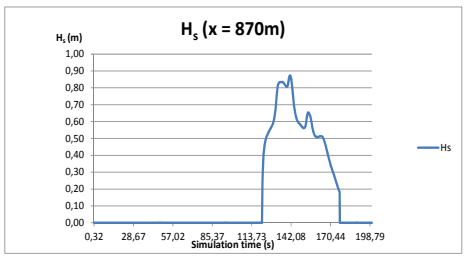

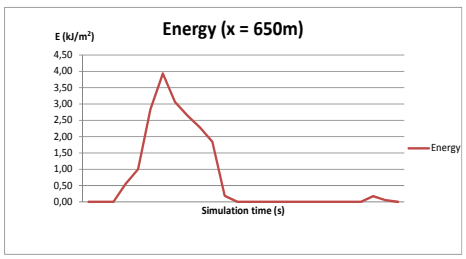

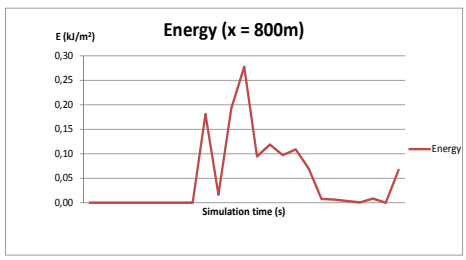

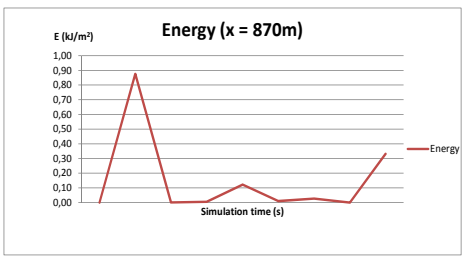

SC54	H_s (m)	T (s)	h_{cr} (m)	X (m)
	4,00	11,00	1,50	300,00

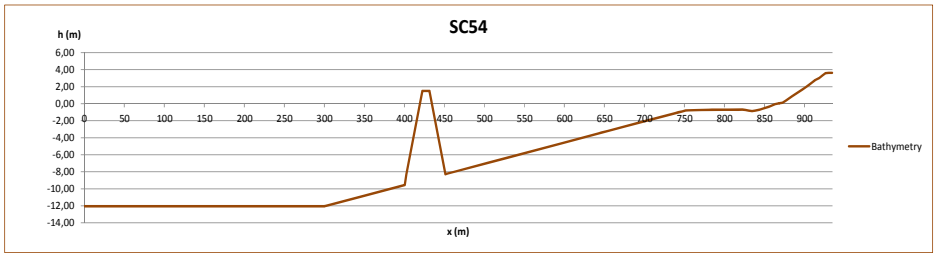

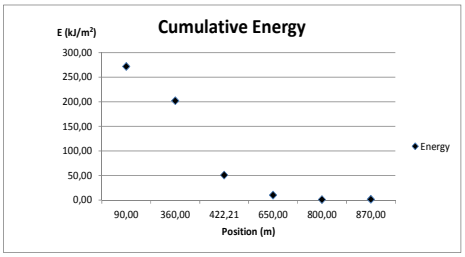

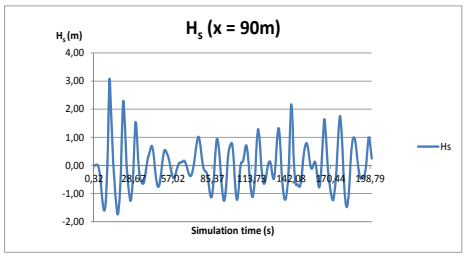

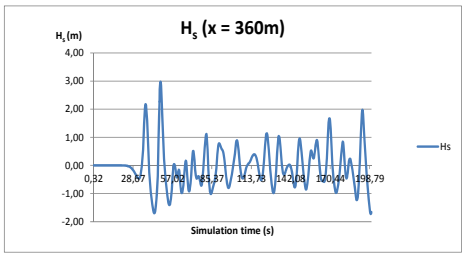

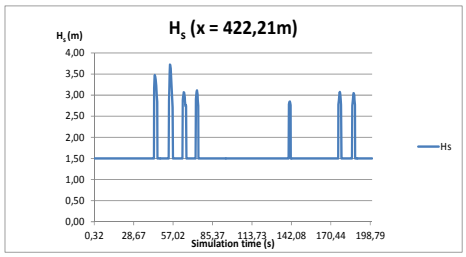

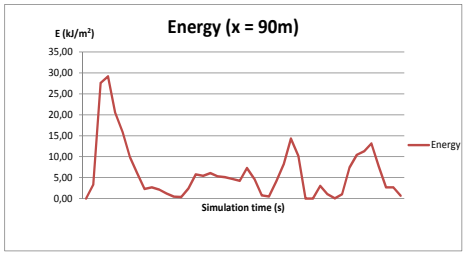

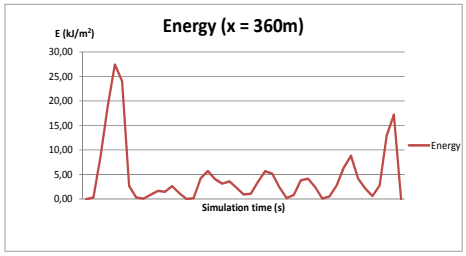

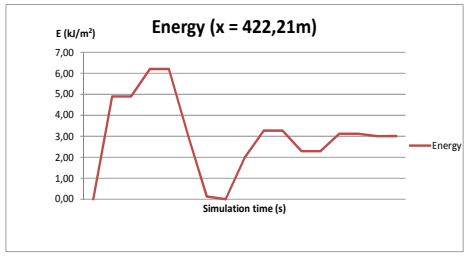

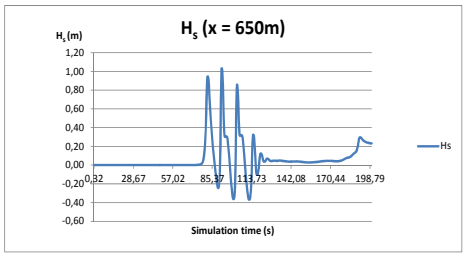

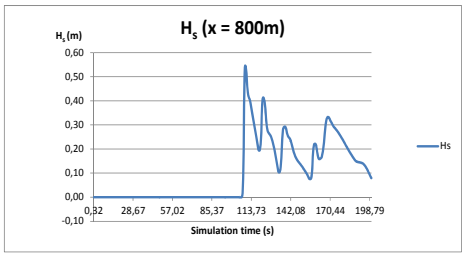

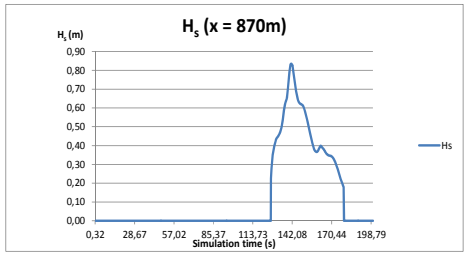

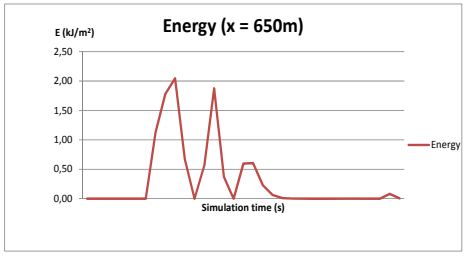

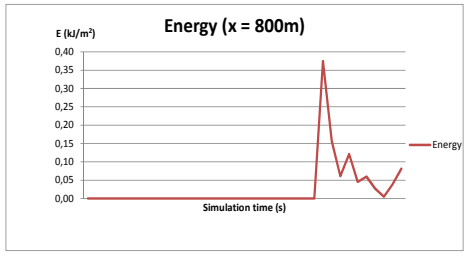

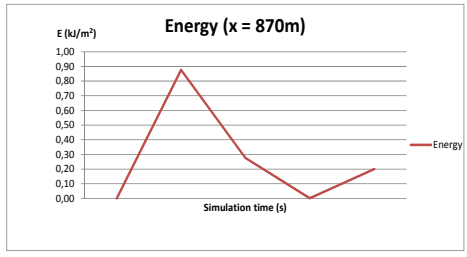

SC55	H_s (m)	T (s)	h_{cr} (m)	X (m)
	4,00	11,00	-1,50	235,00

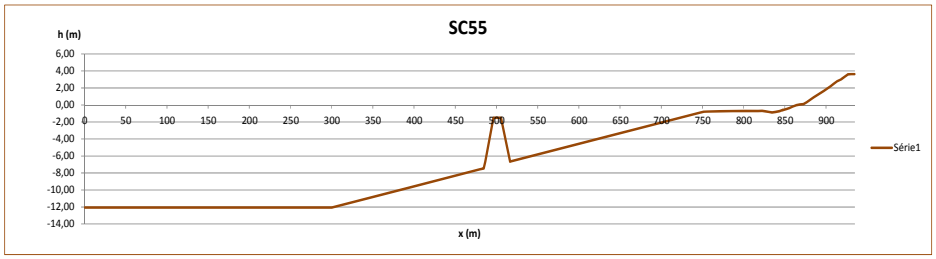

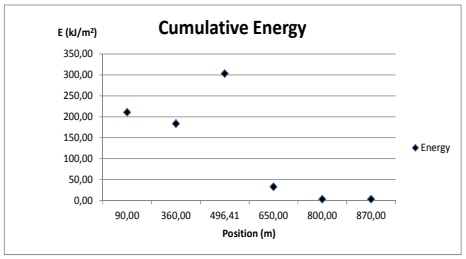

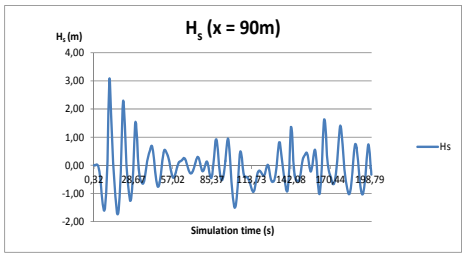

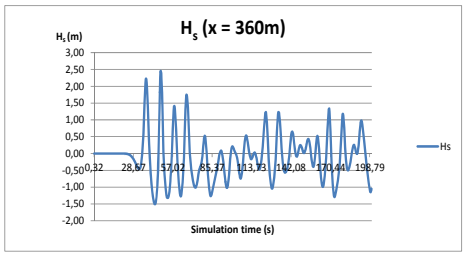

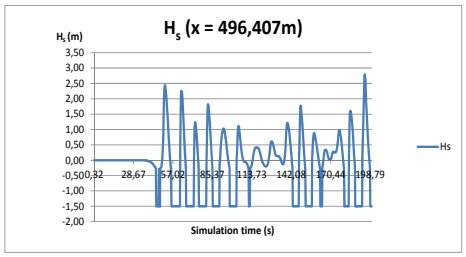

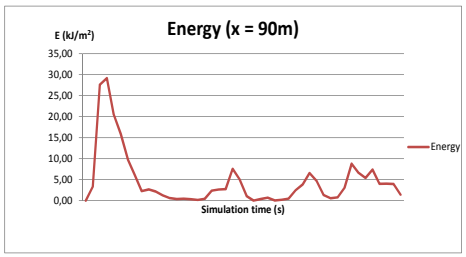

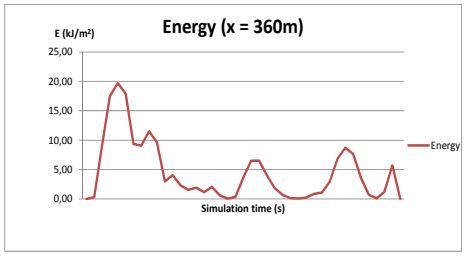

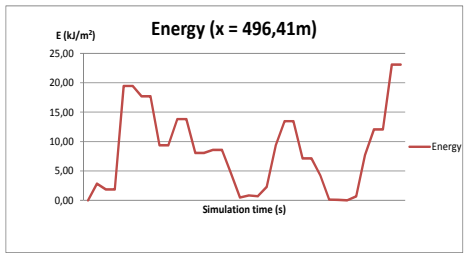

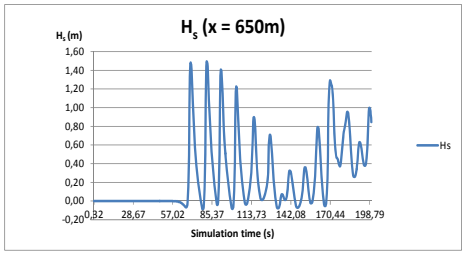

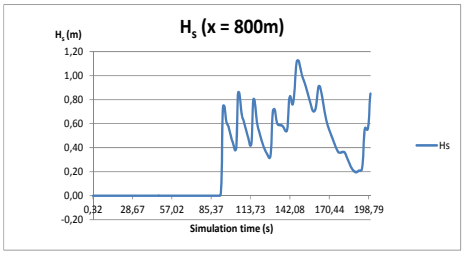

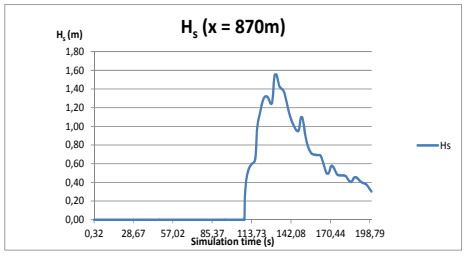

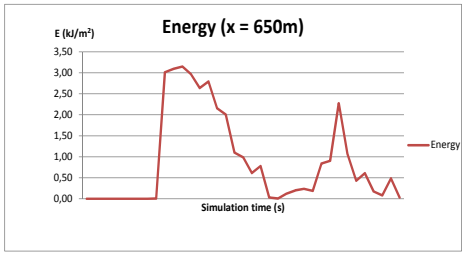

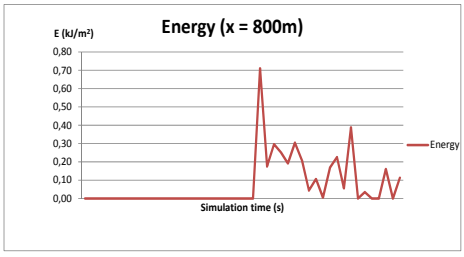

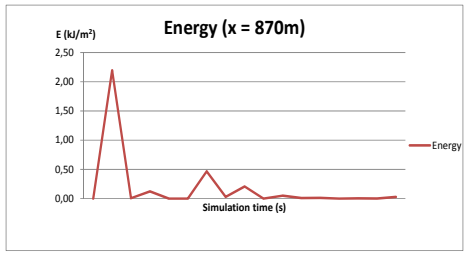

SC56	H_s (m)	T (s)	h_{cr} (m)	X (m)
	4,00	11,00	-1,50	170,00

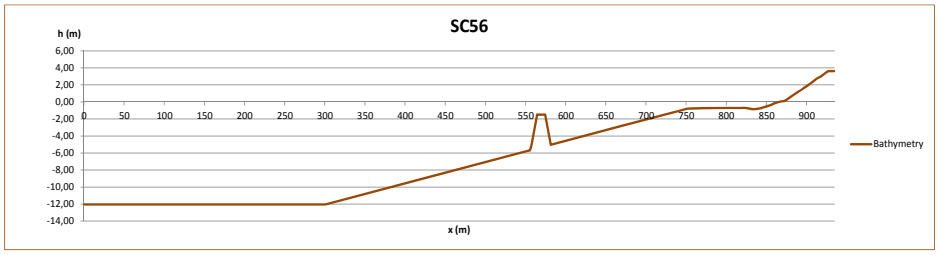

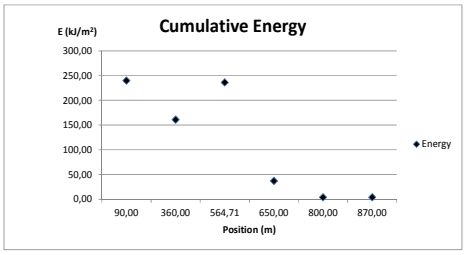

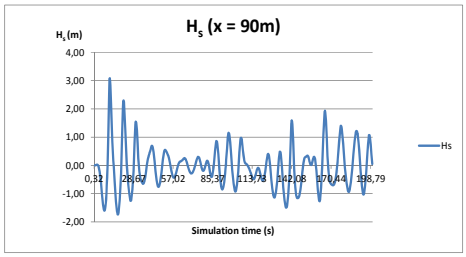

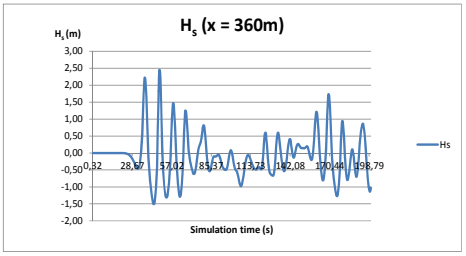

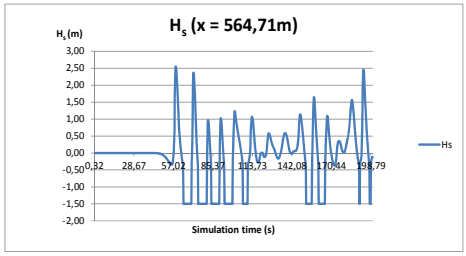

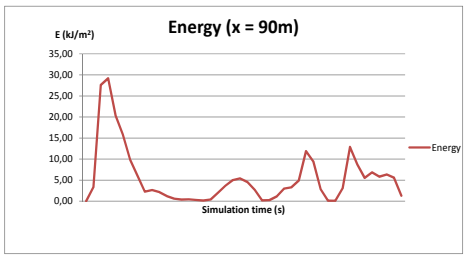

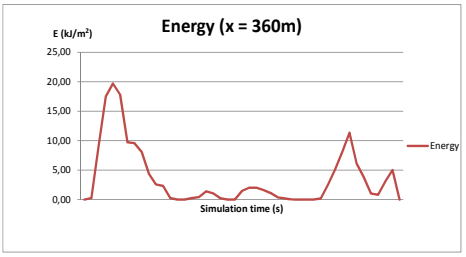

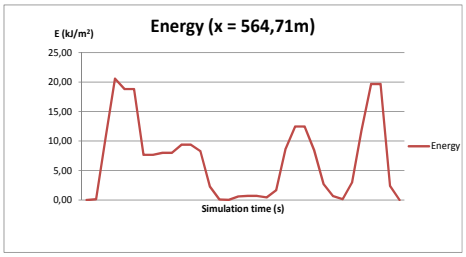

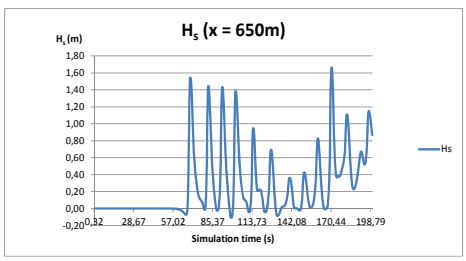

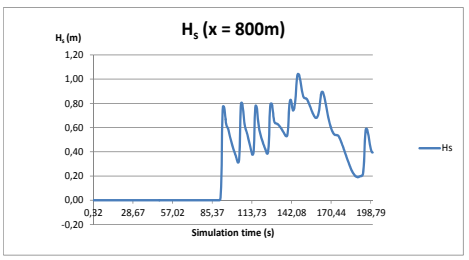

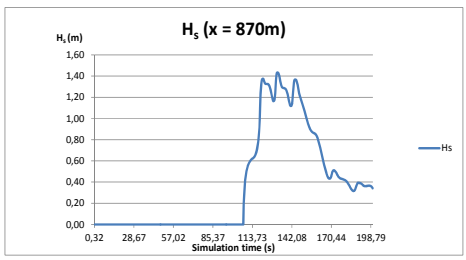

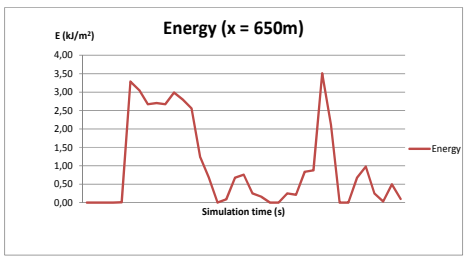

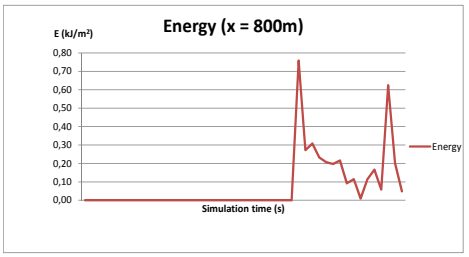

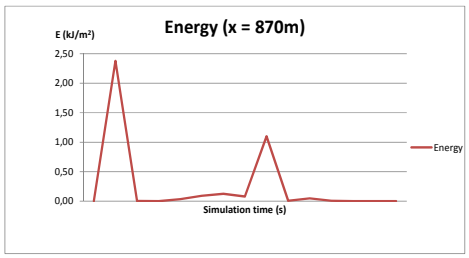

SC57	H_s (m)	T (s)	h_{cr} (m)	X (m)
	4,00	11,00	-1,50	300,00

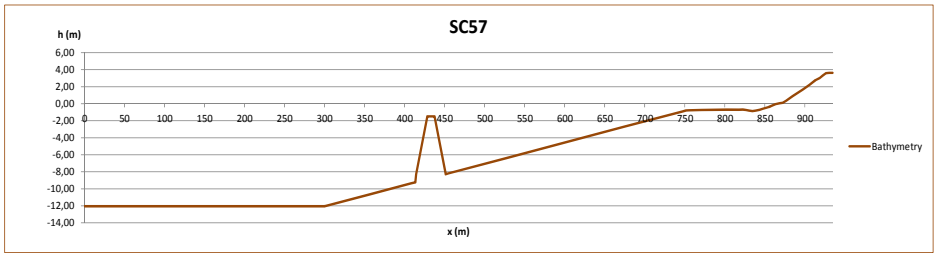

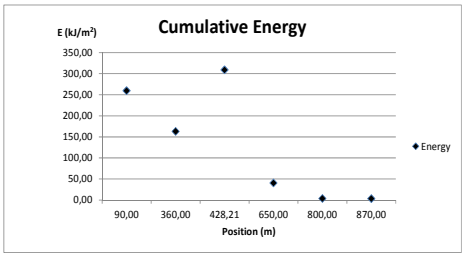

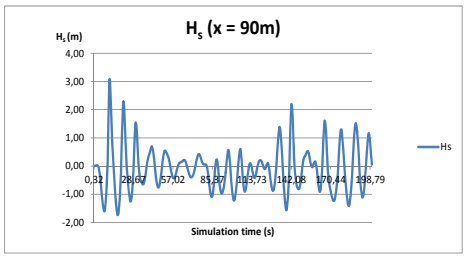

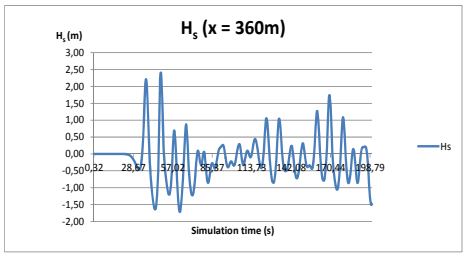

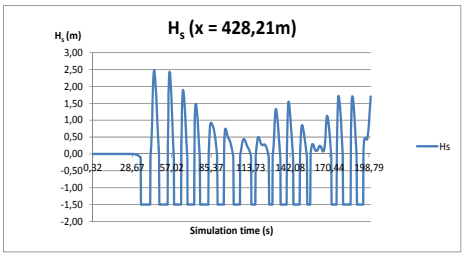

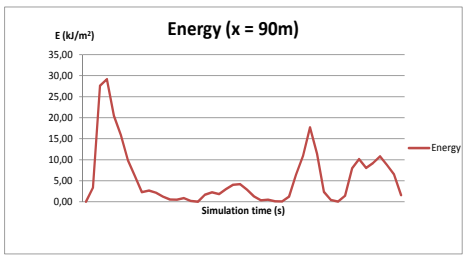

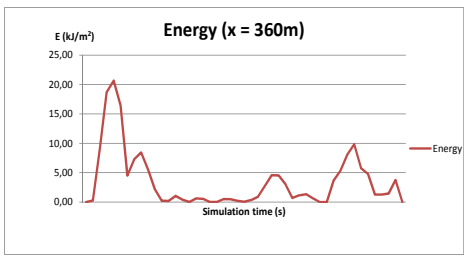

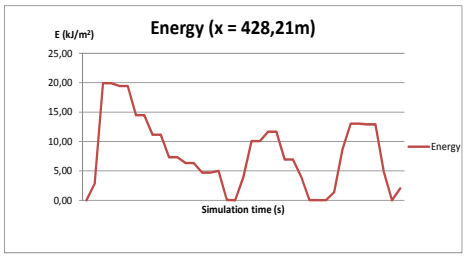

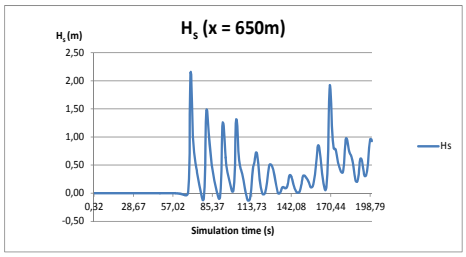

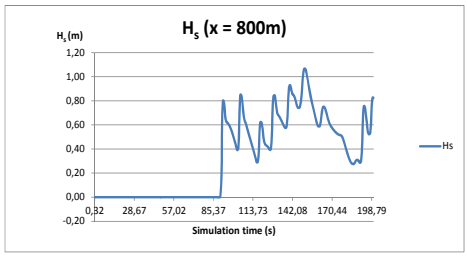

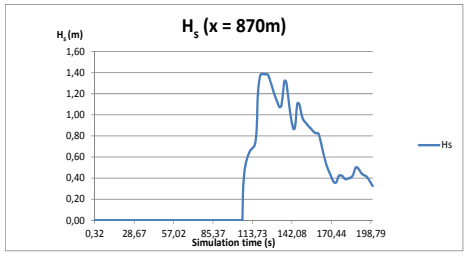

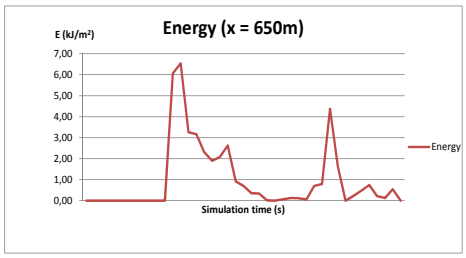

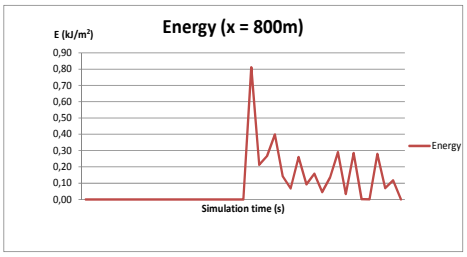

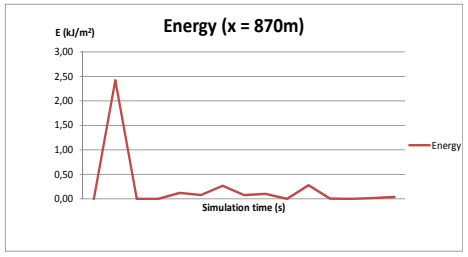

SC58	H_s (m)	T (s)	h_{cr} (m)	X (m)
	4,00	11,00	-0,50	235,00

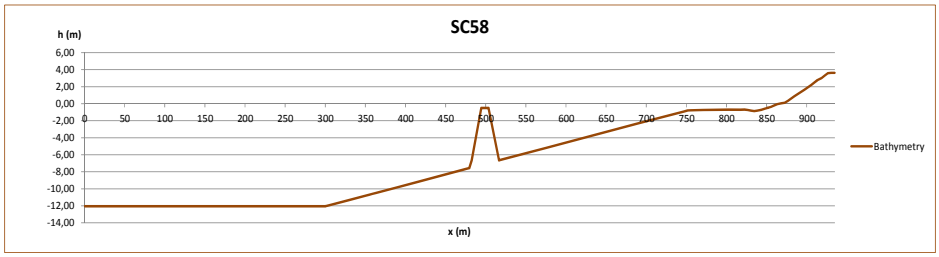

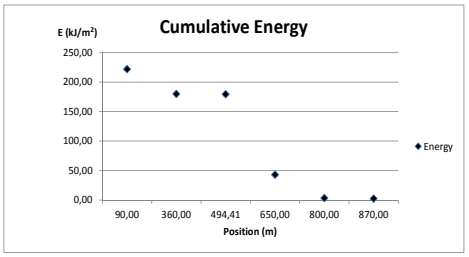

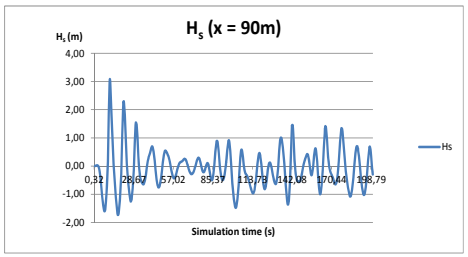

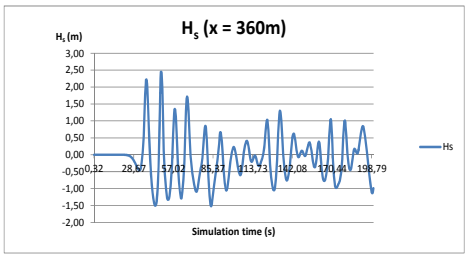

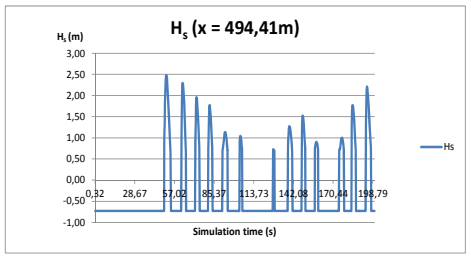

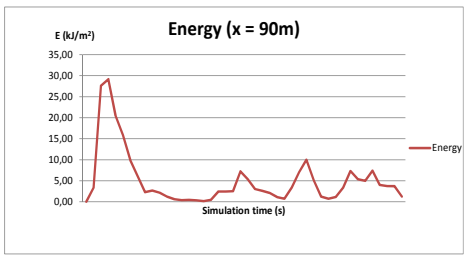

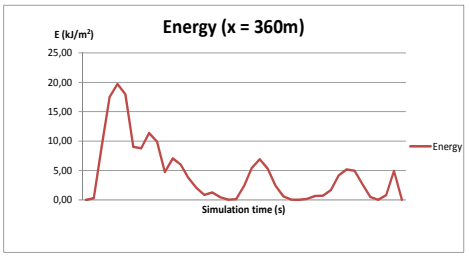

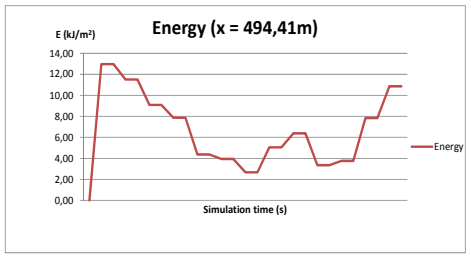

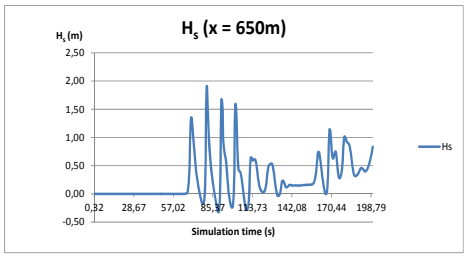

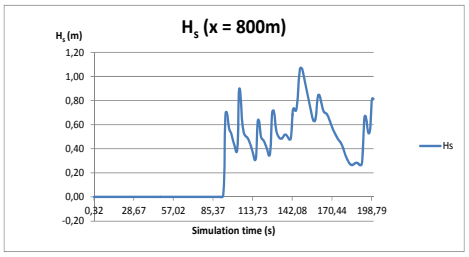

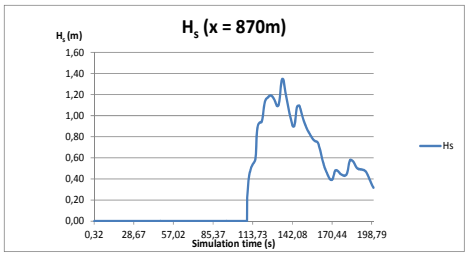

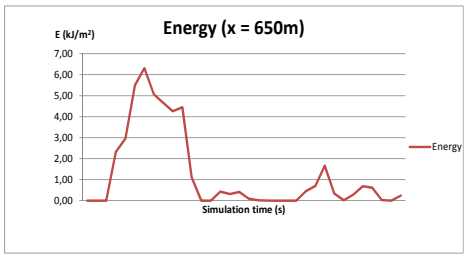

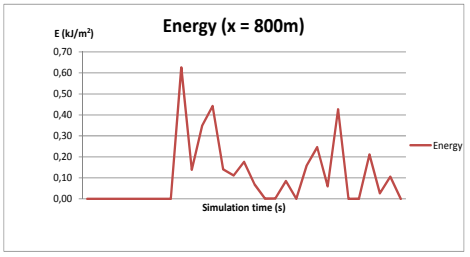

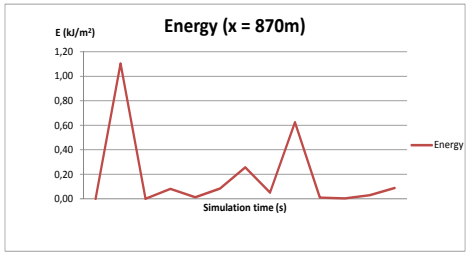

SC59	H_s (m)	T (s)	h_{cr} (m)	X (m)
	4,00	11,00	-0,50	170,00

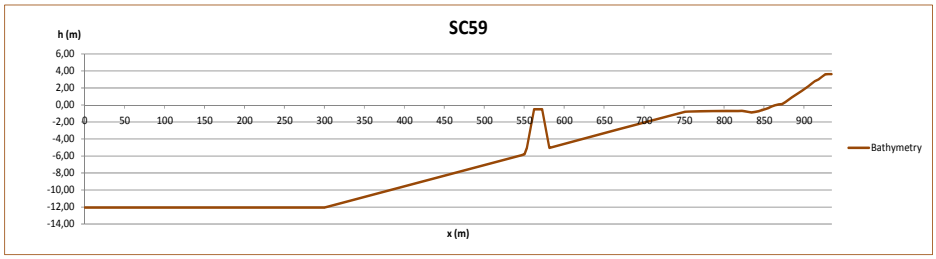

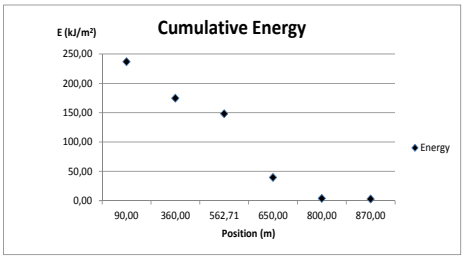

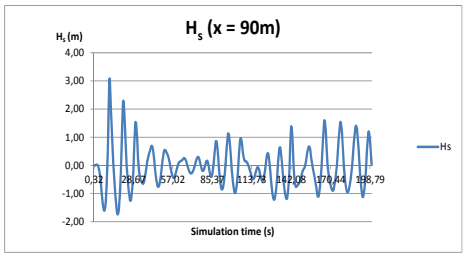

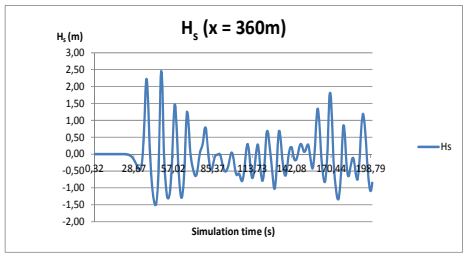

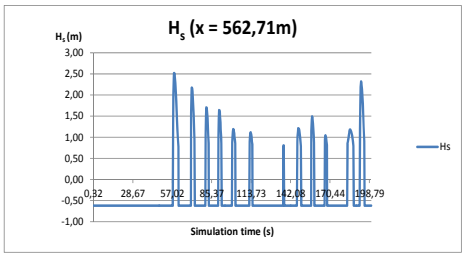

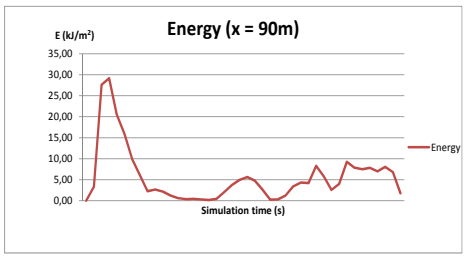

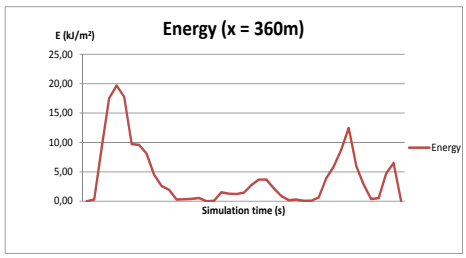

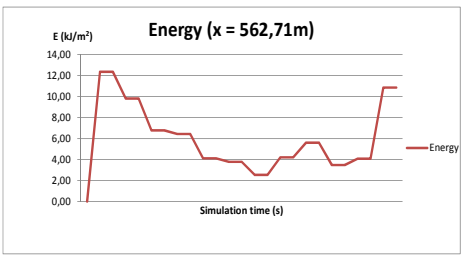

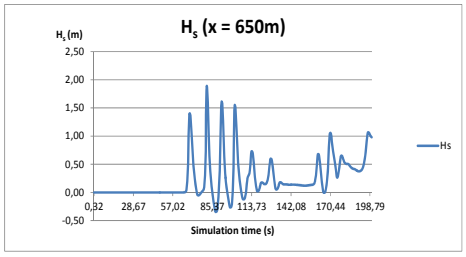

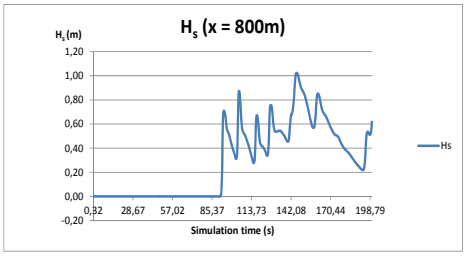

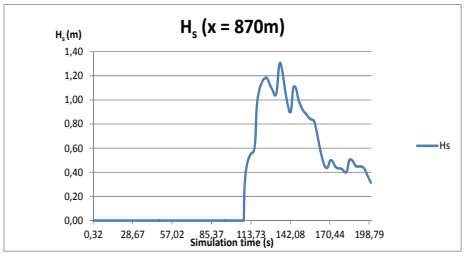

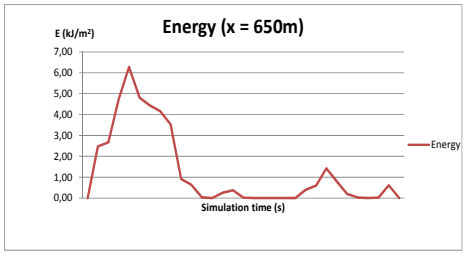

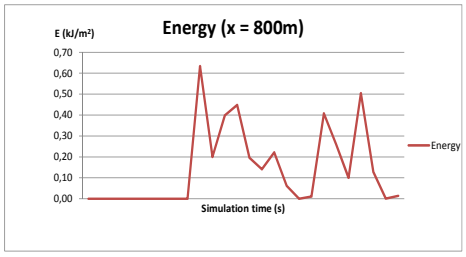

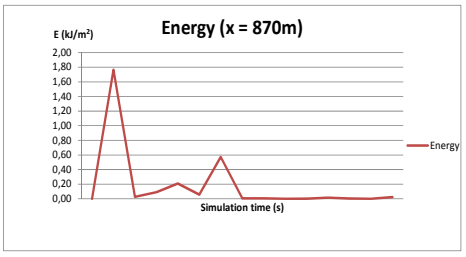

SC60	H_s (m)	T (s)	h_{cr} (m)	X (m)
	4,00	11,00	-0,50	300,00

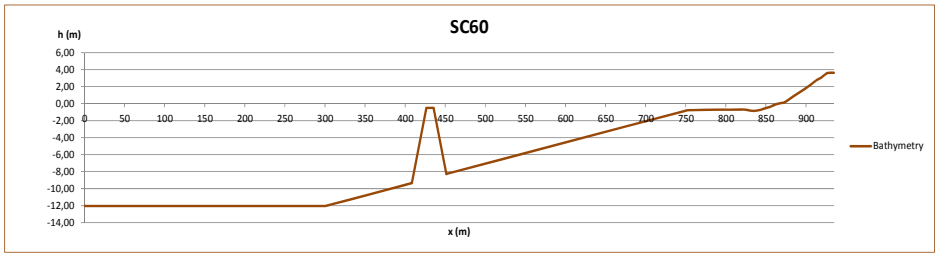

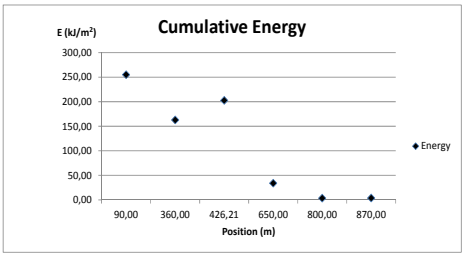

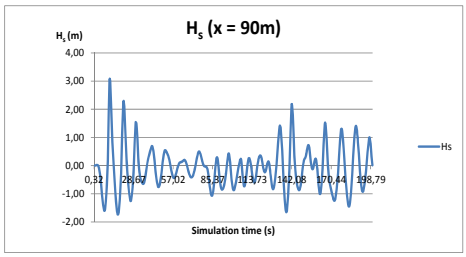

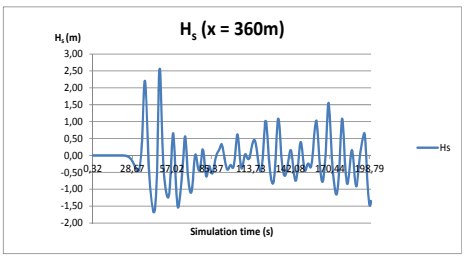

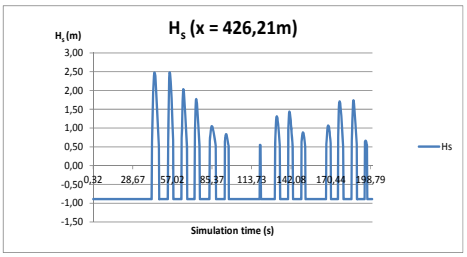

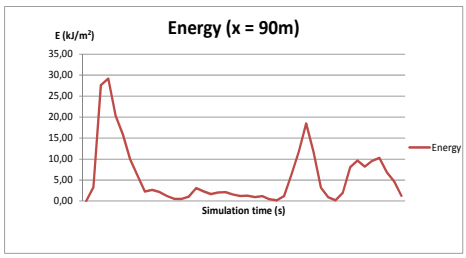

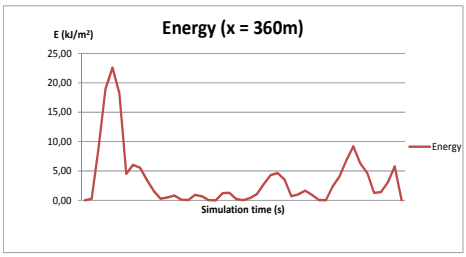

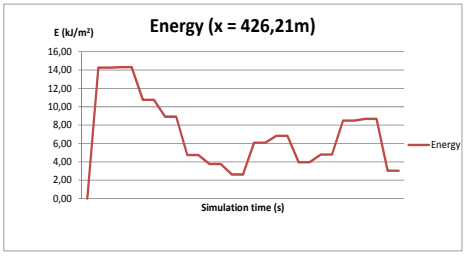

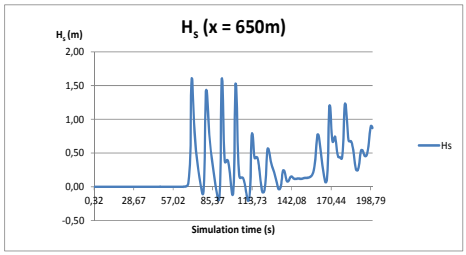

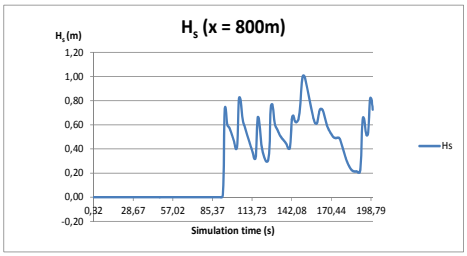

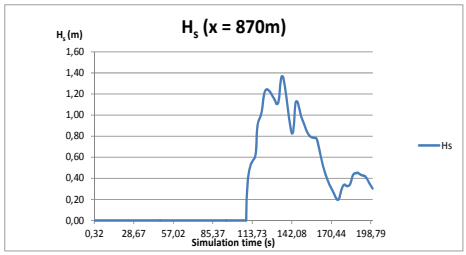

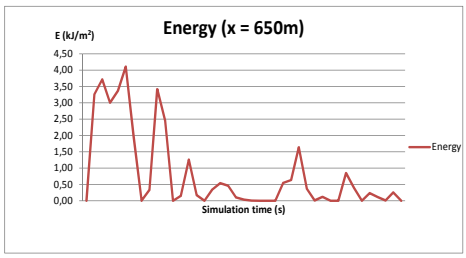

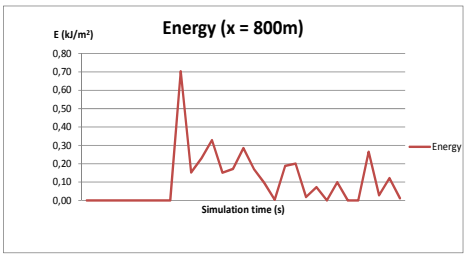

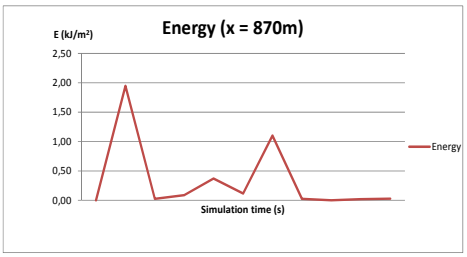

APPENDIX 7

COULWAVE.

VBA algorithm to compute wave energy

at each position of every scenario.

Example for scenario SC1

(Page intentionally left blank)

```
Sub energy()
Dim bUp As Boolean, rCell As Range, iLastRow As Integer, iCount As Integer

With ThisWorkbook.Worksheets("SC1") ' STARTS SELECTING WAVES EXTREME (MIN/MAX)
     .Range("E3") = .Range("B3")
     iLastRow = 4
     If .Range("B4") > .Range("B3") Then bUp = True Else bUp = False
     For Each rCell In .Range("B4:B848")
          If bUp = True Then
                    If rCell < rCell.Offset(-1, 0) Then
                         iLastRow = iLastRow + 1
                         bUp = False
                         End If
               Else
                    If rCell > rCell.Offset(-1, 0) Then
                         iLastRow = iLastRow + 1
                         bUp = True
                         End If
               End If
          .Range("E" & iLastRow) = rCell
          Next
     iLastRow = .Range("E" & .Rows.Count).End(xlUp).Row ' STARTS CALCULATING SINGULAR WAVE HEIGHTS
     For iCount = 3 To iLastRow - 1
          .Range("F" & iCount) = .Range("E" & iCount + 1) - .Range("E" & iCount)
          Next iCount
     End With
     LR = Cells(Rows.Count, "F").End(xlUp).Row ' STARTS CALCULATING WAVE ENERGY
For r = 3 To LR
  Cells(r, 7) = 1 / 8 * (1025 * 9.81 * Cells(r, 6) ^ 2) / 1000

  Next
Range("G849").Value = Application.Sum(Range("G3:G848")) ' STARTS CALCULATING ENERGY SUM
Range("H849").Value = Application.Max(Range("G3:G848")) 'IDENTIFIES THE MAXIMUM ENERGY VALUE


With ThisWorkbook.Worksheets("SC1") ' STARTS SELECTING WAVES EXTREME (MIN/MAX)
     .Range("M3") = .Range("J3")
     iLastRow = 4
     If .Range("J4") > .Range("J3") Then bUp = True Else bUp = False
     For Each rCell In .Range("J4:J848")
          If bUp = True Then
                    If rCell < rCell.Offset(-1, 0) Then
                         iLastRow = iLastRow + 1
                         bUp = False
                         End If
               Else
                    If rCell > rCell.Offset(-1, 0) Then
                         iLastRow = iLastRow + 1
                         bUp = True
                         End If
               End If
          .Range("M" & iLastRow) = rCell
          Next
     iLastRow = .Range("M" & .Rows.Count).End(xlUp).Row ' STARTS CALCULATING SINGULAR WAVE HEIGHTS
     For iCount = 3 To iLastRow - 1
          .Range("N" & iCount) = .Range("M" & iCount + 1) - .Range("M" & iCount)
          Next iCount
     End With
     LR = Cells(Rows.Count, "N").End(xlUp).Row ' STARTS CALCULATING WAVE ENERGY
For r = 3 To LR
  Cells(r, 15) = 1 / 8 * (1025 * 9.81 * Cells(r, 14) ^ 2) / 1000

  Next
Range("O849").Value = Application.Sum(Range("O3:O848")) ' STARTS CALCULATING ENERGY SUM
Range("P849").Value = Application.Max(Range("O3:O848")) 'IDENTIFIES THE MAXIMUM ENERGY VALUE


With ThisWorkbook.Worksheets("SC1") ' STARTS SELECTING WAVES EXTREME (MIN/MAX)
     .Range("U3") = .Range("R3")
     iLastRow = 4
     If .Range("R4") > .Range("R3") Then bUp = True Else bUp = False
     For Each rCell In .Range("R4:R848")
          If bUp = True Then
                    If rCell < rCell.Offset(-1, 0) Then
                         iLastRow = iLastRow + 1
                         bUp = False
                         End If
               Else
                    If rCell > rCell.Offset(-1, 0) Then
                         iLastRow = iLastRow + 1
                         bUp = True
                         End If
               End If
          .Range("U" & iLastRow) = rCell
          Next
     iLastRow = .Range("U" & .Rows.Count).End(xlUp).Row ' STARTS CALCULATING SINGULAR WAVE HEIGHTS
     For iCount = 3 To iLastRow - 1
          .Range("V" & iCount) = .Range("U" & iCount + 1) - .Range("U" & iCount)
```

```
          Next iCount
     End With
     LR = Cells(Rows.Count, "V").End(xlUp).Row ' STARTS CALCULATING WAVE ENERGY
For r = 3 To LR
  Cells(r, 23) = 1 / 8 * (1025 * 9.81 * Cells(r, 22) ^ 2) / 1000

  Next
Range("W849").Value = Application.Sum(Range("W3:W848")) ' STARTS CALCULATING ENERGY SUM
Range("X849").Value = Application.Max(Range("W3:W848")) 'IDENTIFIES THE MAXIMUM ENERGY VALUE


With ThisWorkbook.Worksheets("SC1") ' STARTS SELECTING WAVES EXTREME (MIN/MAX)
     .Range("AC3") = .Range("Z3")
     iLastRow = 4
     If .Range("Z4") > .Range("Z3") Then bUp = True Else bUp = False
     For Each rCell In .Range("Z4:Z848")
          If bUp = True Then
                    If rCell < rCell.Offset(-1, 0) Then
                         iLastRow = iLastRow + 1
                         bUp = False
                         End If
               Else
                    If rCell > rCell.Offset(-1, 0) Then
                         iLastRow = iLastRow + 1
                         bUp = True
                         End If
               End If
          .Range("AC" & iLastRow) = rCell
          Next
     iLastRow = .Range("AC" & .Rows.Count).End(xlUp).Row ' STARTS CALCULATING SINGULAR WAVE HEIGHTS
     For iCount = 3 To iLastRow - 1
          .Range("AD" & iCount) = .Range("AC" & iCount + 1) - .Range("AC" & iCount)
          Next iCount
     End With
     LR = Cells(Rows.Count, "AD").End(xlUp).Row ' STARTS CALCULATING WAVE ENERGY
For r = 3 To LR
  Cells(r, 31) = 1 / 8 * (1025 * 9.81 * Cells(r, 30) ^ 2) / 1000

  Next
Range("AE849").Value = Application.Sum(Range("AE3:AE848")) ' STARTS CALCULATING ENERGY SUM
Range("AF849").Value = Application.Max(Range("AE3:AE848")) 'IDENTIFIES THE MAXIMUM ENERGY VALUE


With ThisWorkbook.Worksheets("SC1") ' STARTS SELECTING WAVES EXTREME (MIN/MAX)
     .Range("AK3") = .Range("AH3")
     iLastRow = 4
     If .Range("AH4") > .Range("AH3") Then bUp = True Else bUp = False
     For Each rCell In .Range("AH4:AH848")
          If bUp = True Then
                    If rCell < rCell.Offset(-1, 0) Then
                         iLastRow = iLastRow + 1
                         bUp = False
                         End If
               Else
                    If rCell > rCell.Offset(-1, 0) Then
                         iLastRow = iLastRow + 1
                         bUp = True
                         End If
               End If
          .Range("AK" & iLastRow) = rCell
          Next
     iLastRow = .Range("AK" & .Rows.Count).End(xlUp).Row ' STARTS CALCULATING SINGULAR WAVE HEIGHTS
     For iCount = 3 To iLastRow - 1
          .Range("AL" & iCount) = .Range("AK" & iCount + 1) - .Range("AK" & iCount)
          Next iCount
     End With
     LR = Cells(Rows.Count, "AL").End(xlUp).Row ' STARTS CALCULATING WAVE ENERGY
For r = 3 To LR
  Cells(r, 39) = 1 / 8 * (1025 * 9.81 * Cells(r, 38) ^ 2) / 1000

  Next
Range("AM849").Value = Application.Sum(Range("AM3:AM848")) ' STARTS CALCULATING ENERGY SUM
Range("AN849").Value = Application.Max(Range("AM3:AM848")) 'IDENTIFIES THE MAXIMUM ENERGY VALUE


With ThisWorkbook.Worksheets("SC1") ' STARTS SELECTING WAVES EXTREME (MIN/MAX)
     .Range("AS3") = .Range("AP3")
     iLastRow = 4
     If .Range("AP4") > .Range("AP3") Then bUp = True Else bUp = False
     For Each rCell In .Range("AP4:AP848")
          If bUp = True Then
                    If rCell < rCell.Offset(-1, 0) Then
                         iLastRow = iLastRow + 1
                         bUp = False
                         End If
               Else
                    If rCell > rCell.Offset(-1, 0) Then
                         iLastRow = iLastRow + 1
```

```
                        bUp = True
                        End If
                End If
            .Range("AS" & iLastRow) = rCell
            Next
     iLastRow = .Range("AS" & .Rows.Count).End(xlUp).Row ' STARTS CALCULATING SINGULAR WAVE HEIGHTS
     For iCount = 3 To iLastRow - 1
            .Range("AT" & iCount) = .Range("AS" & iCount + 1) - .Range("AS" & iCount)
            Next iCount
     End With
     LR = Cells(Rows.Count, "AT").End(xlUp).Row ' STARTS CALCULATING WAVE ENERGY
For r = 3 To LR
  Cells(r, 47) = 1 / 8 * (1025 * 9.81 * Cells(r, 46) ^ 2) / 1000

  Next
Range("AU849").Value = Application.Sum(Range("AU3:AU848")) ' STARTS CALCULATING ENERGY SUM
Range("AV849").Value = Application.Max(Range("AU3:AU848")) 'IDENTIFIES THE MAXIMUM ENERGY VALUE
End Sub
```

(Page intentionally left blank)

APPENDIX 8

BOUSS-2D.

Residual velocity

(Page intentionally left blank)

Scenarios Initial and scenarios with detached breakwater

Wave characteristics					Scenario
H_s (m)	T (s)	X (m)	Direction (°)		
2,00	7,00	235,00	270,00	→	Initial1
			315,00	↘	Initial2
			225,00	↗	Initial3
6,64	9,30	235,00	270,00	→	Initial4
			315,00	↘	Initial5
			225,00	↗	Initial6

Wave characteristics				Breakwater characteristics					Scenario
H_s (m)	T (s)	Direction (°)		X (m)	h_{cr} (m)	Number	G (m)	L (m)	
2,00	7,00	270,00	→	235,00	2,70	1	---	470,00	SC1
						2	115,00	235,00	SC2
					-0,50	1	---	470,00	SC3
						2	115,00	235,00	SC4
		315,00	↘		2,70	1	---	470,00	SC5
						2	115,00	235,00	SC6
					-0,50	1	---	470,00	SC7
						2	115,00	235,00	SC8
		225,00	↗		2,70	1	---	470,00	SC9
						2	115,00	235,00	SC10
					-0,50	1	---	470,00	SC11
						2	115,00	235,00	SC12
6,64	9,30	270,00	→	235,00	2,70	1	---	470,00	SC13
						2	115,00	235,00	SC14
					-0,50	1	---	470,00	SC15
						2	115,00	235,00	SC16
		315,00	↘		2,70	1	---	470,00	SC17
						2	115,00	235,00	SC18
					-0,50	1	---	470,00	SC19
						2	115,00	235,00	SC20
		225,00	↗		2,70	1	---	470,00	SC21
						2	115,00	235,00	SC22
					-0,50	1	---	470,00	SC23
						2	115,00	235,00	SC24

Residual Velocity

Initial1

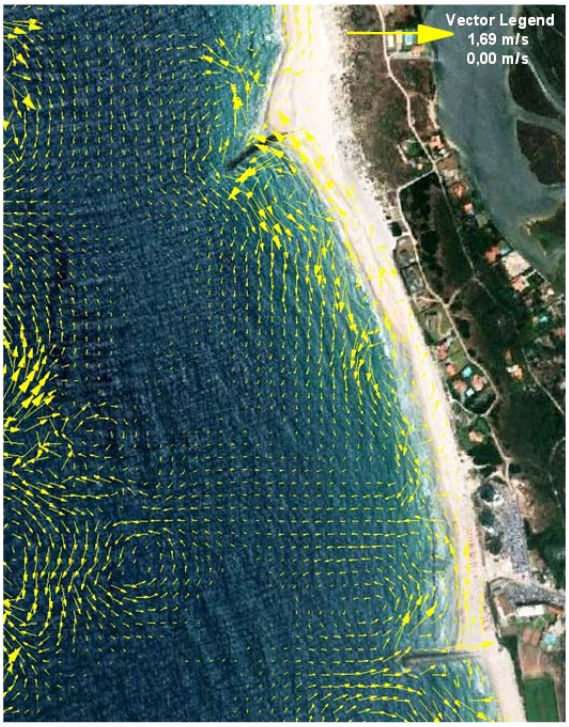

Initial2

Initial3

Initial4

Residual Velocity

Initial5

Initial6

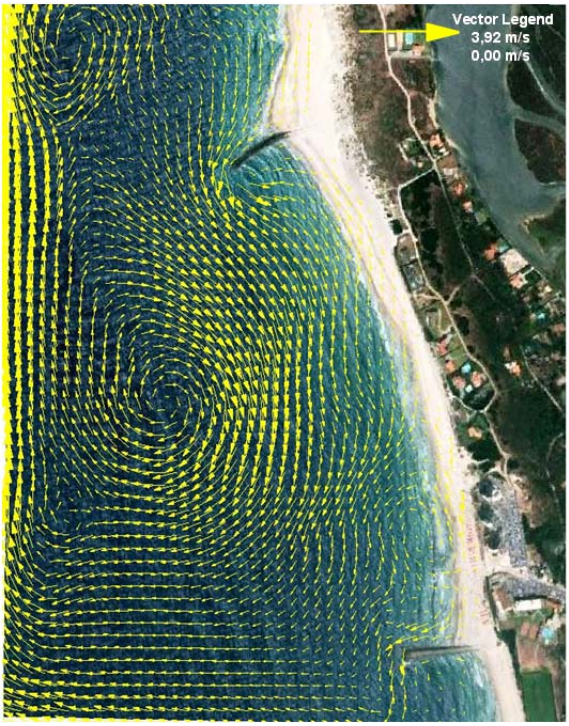

SC1

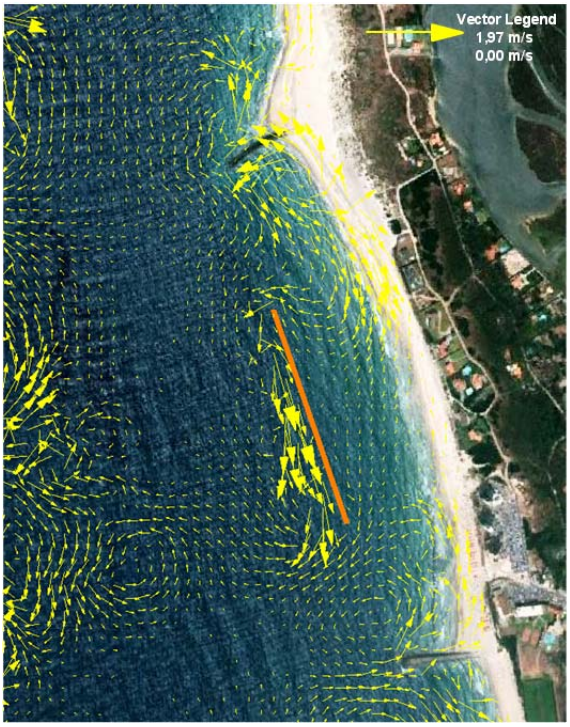

SC2

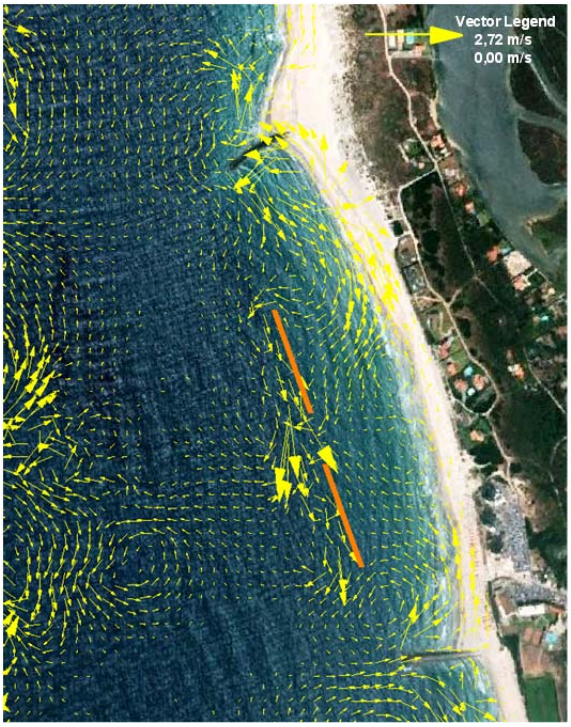

Residual Velocity

SC3

SC4

SC5

SC6

Residual Velocity

SC7

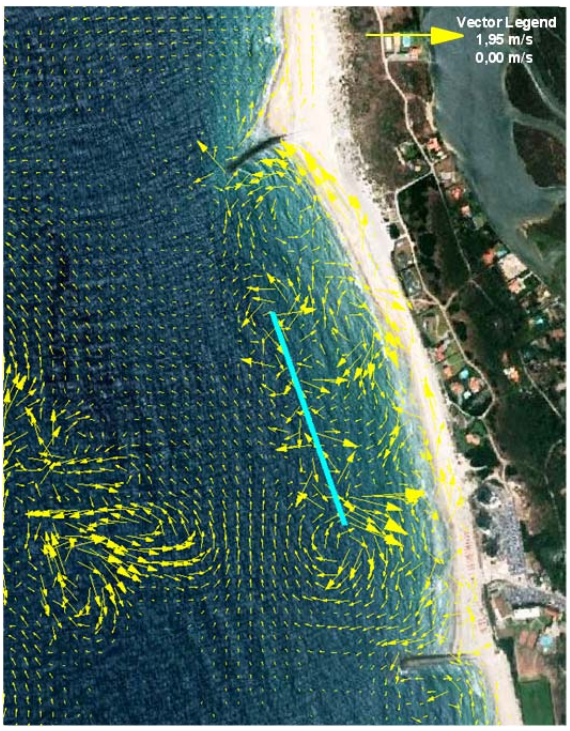

SC8

SC9

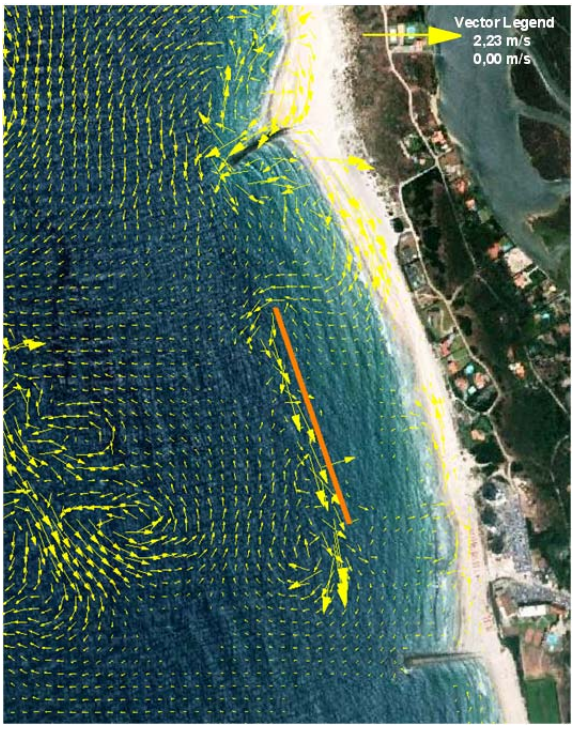

SC10

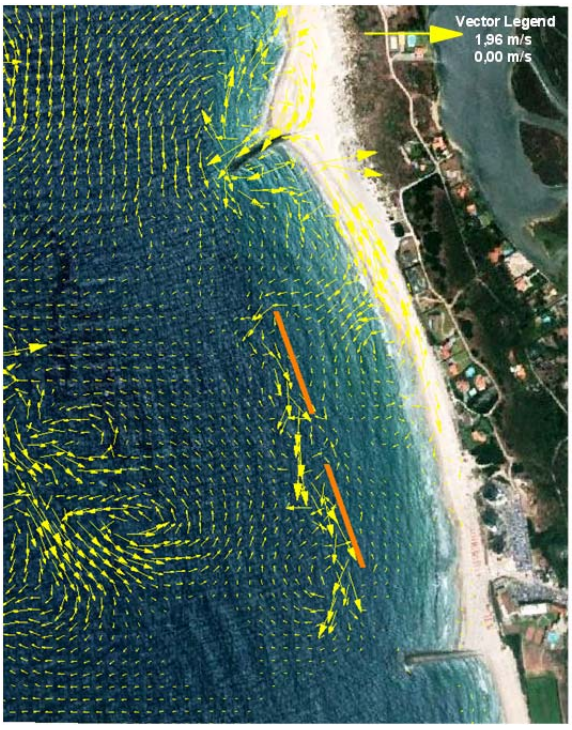

Residual Velocity

SC11

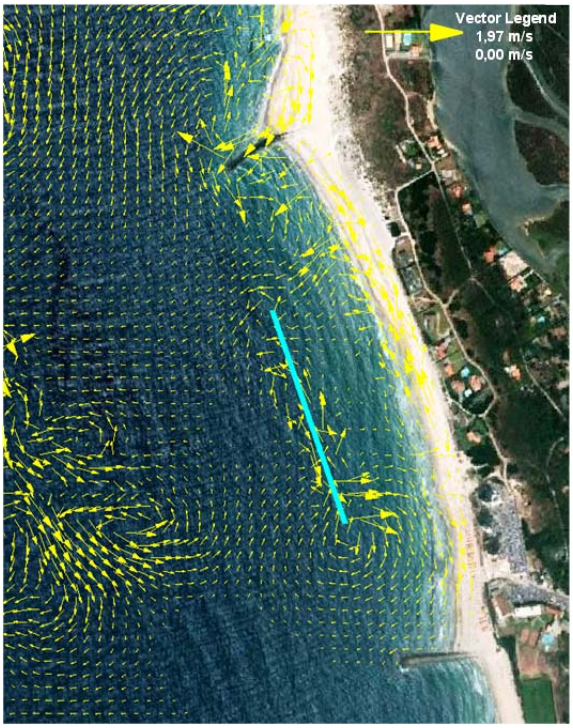

SC12

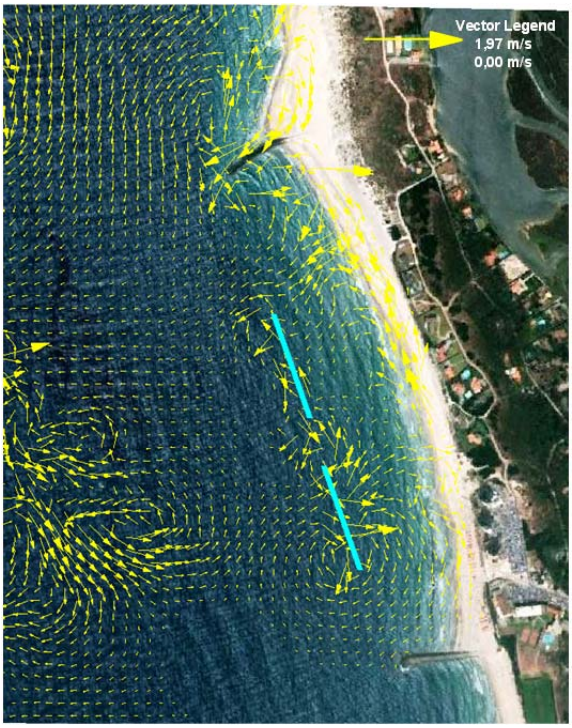

SC13

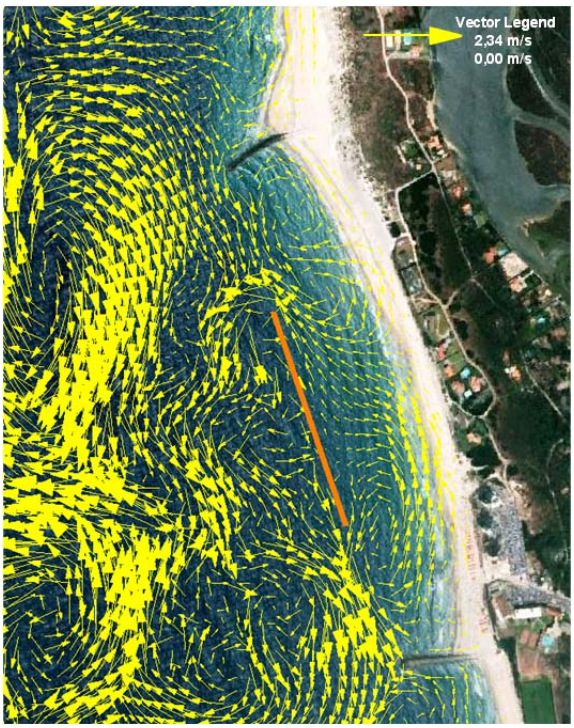

SC14

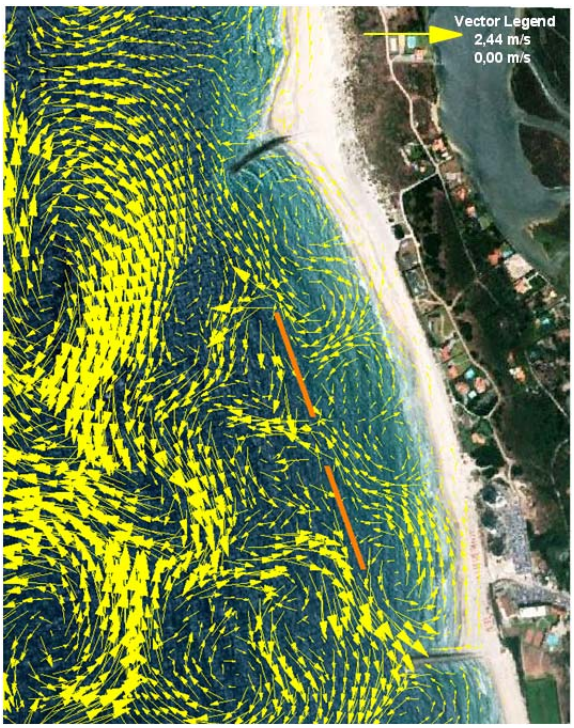

Residual Velocity

SC15

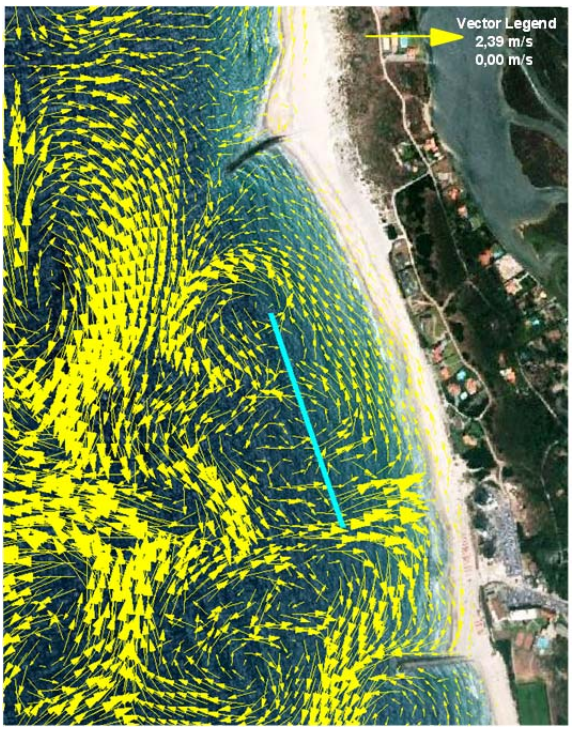

SC16

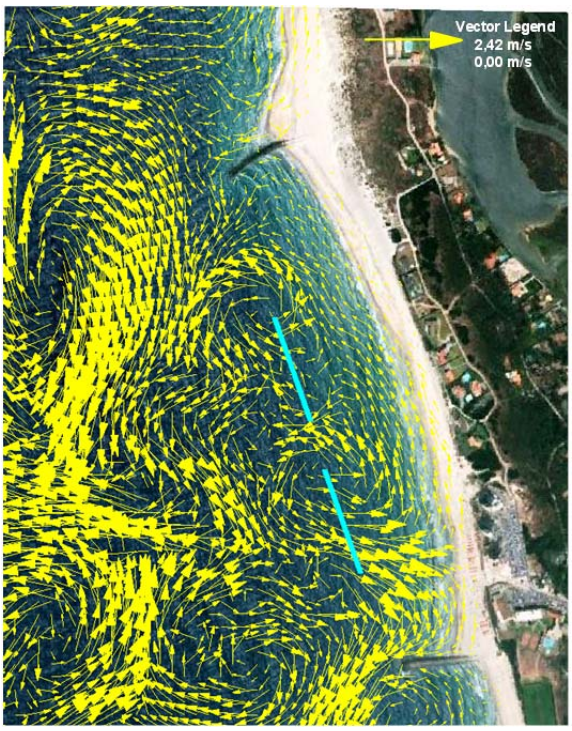

SC17

SC18

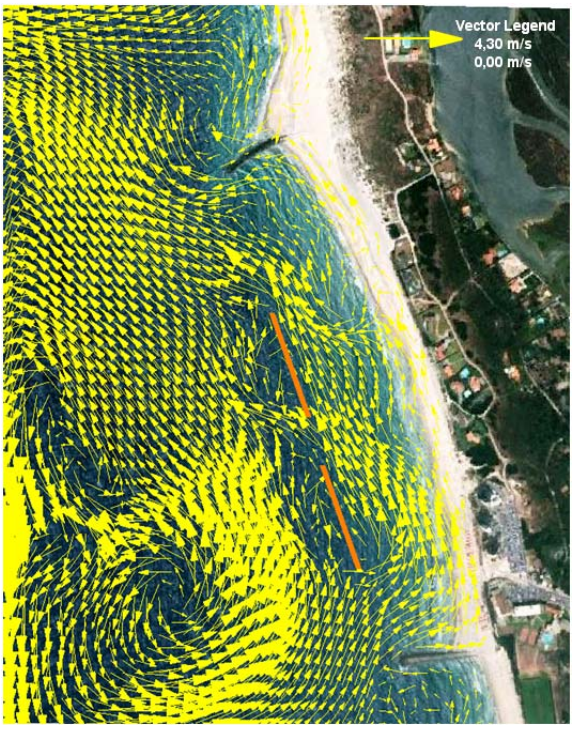

Residual Velocity

SC19

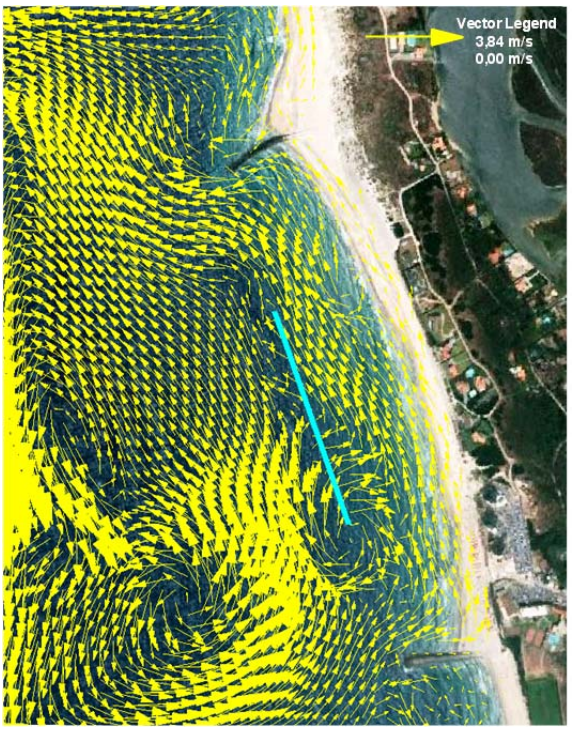

SC20

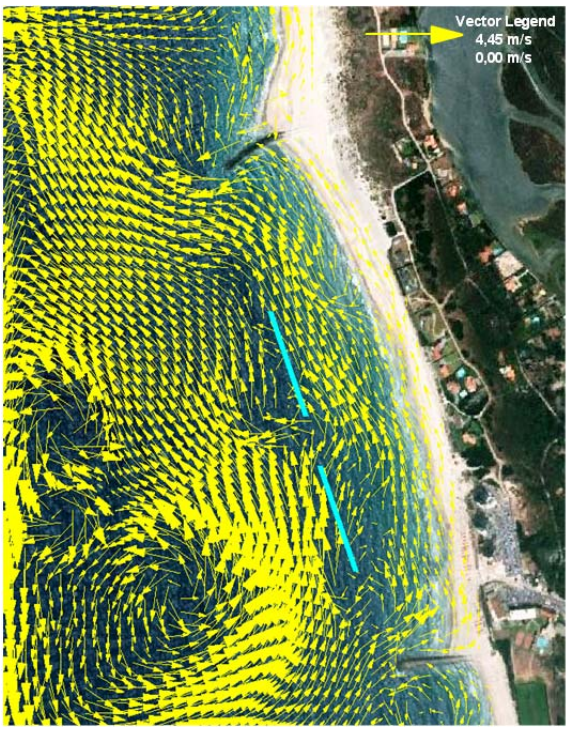

SC21

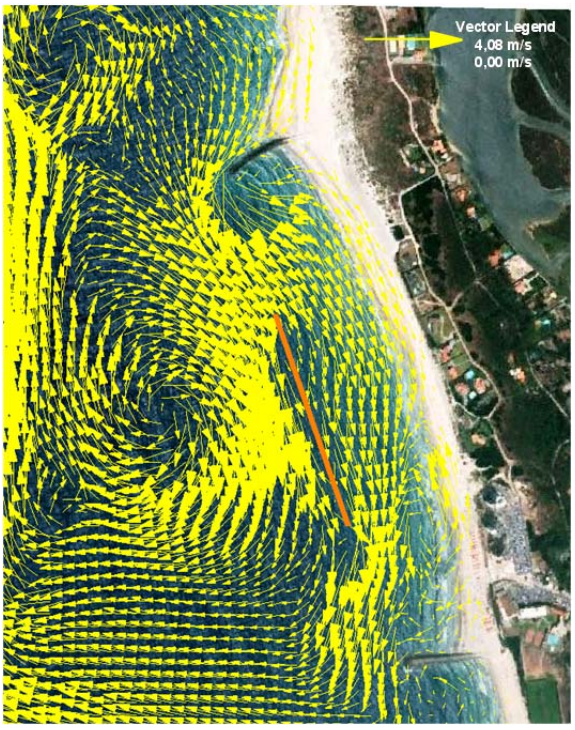

SC22

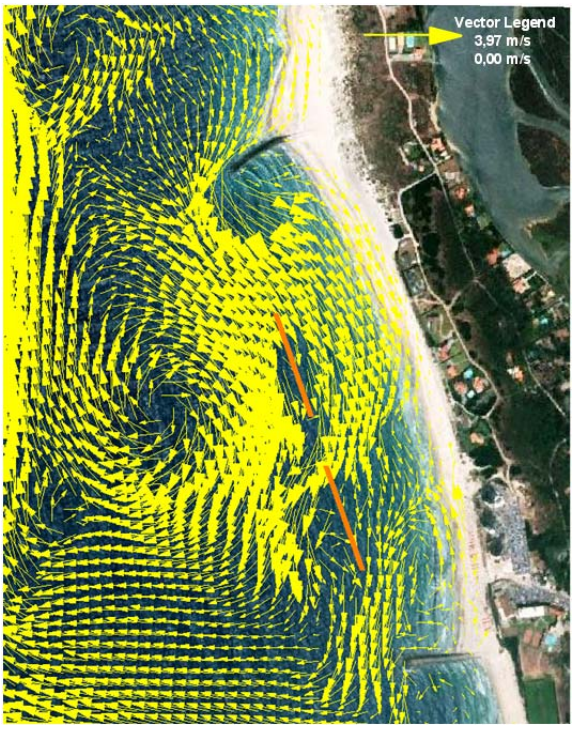

Residual Velocity

SC23

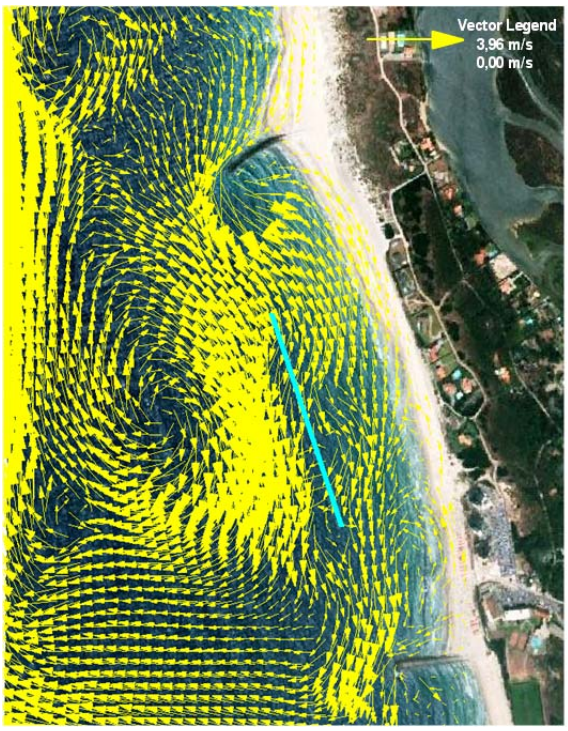

SC24

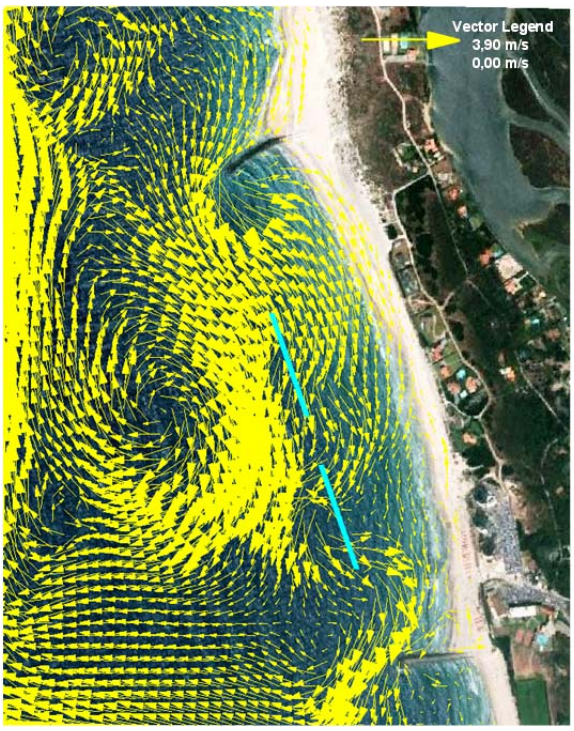

(Page intentionally left blank)

APPENDIX 9

BOUSS-2D.

Significant wave height: Initial – SC

(Page intentionally left blank)

Scenarios Initial and scenarios with detached breakwater

Wave characteristics					Scenario
H_s (m)	T (s)	X (m)	Direction (°)		
2,00	7,00	235,00	270,00	→	Initial1
			315,00	↘	Initial2
			225,00	↗	Initial3
6,64	9,30	235,00	270,00	→	Initial4
			315,00	↘	Initial5
			225,00	↗	Initial6

Wave characteristics				Breakwater characteristics					Scenario
H_s (m)	T (s)	Direction (°)		X (m)	h_{cr} (m)	Number	G (m)	L (m)	
2,00	7,00	270,00	→	235,00	2,70	1	---	470,00	SC1
						2	115,00	235,00	SC2
					-0,50	1	---	470,00	SC3
						2	115,00	235,00	SC4
		315,00	↘		2,70	1	---	470,00	SC5
						2	115,00	235,00	SC6
					-0,50	1	---	470,00	SC7
						2	115,00	235,00	SC8
		225,00	↗		2,70	1	---	470,00	SC9
						2	115,00	235,00	SC10
					-0,50	1	---	470,00	SC11
						2	115,00	235,00	SC12
6,64	9,30	270,00	→	235,00	2,70	1	---	470,00	SC13
						2	115,00	235,00	SC14
					-0,50	1	---	470,00	SC15
						2	115,00	235,00	SC16
		315,00	↘		2,70	1	---	470,00	SC17
						2	115,00	235,00	SC18
					-0,50	1	---	470,00	SC19
						2	115,00	235,00	SC20
		225,00	↗		2,70	1	---	470,00	SC21
						2	115,00	235,00	SC22
					-0,50	1	---	470,00	SC23
						2	115,00	235,00	SC24

Significant Wave Height: Initial – SC

Hi1-H1

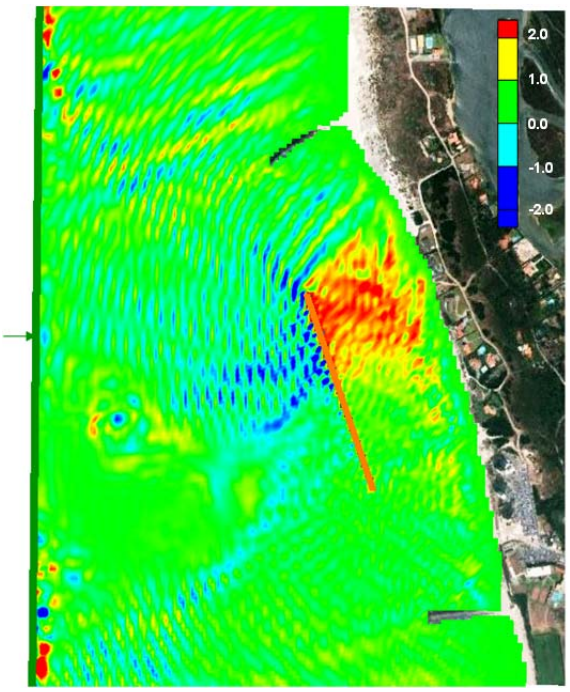

Hi1-H2

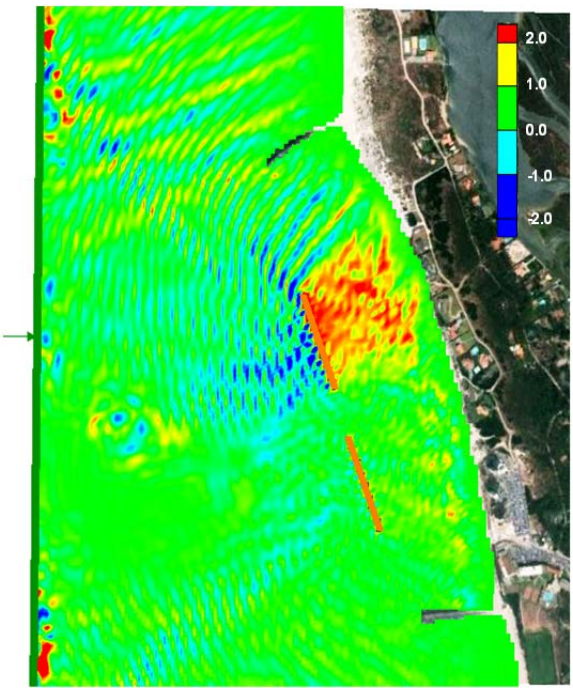

Hi1-H3

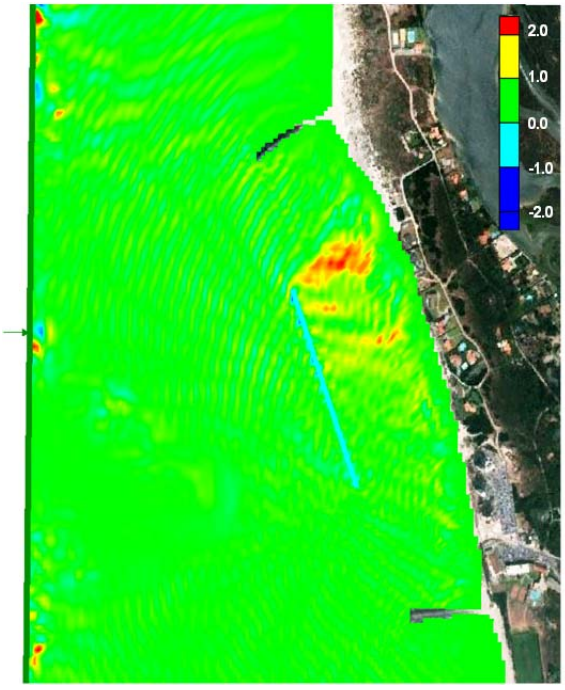

Hi1-H4

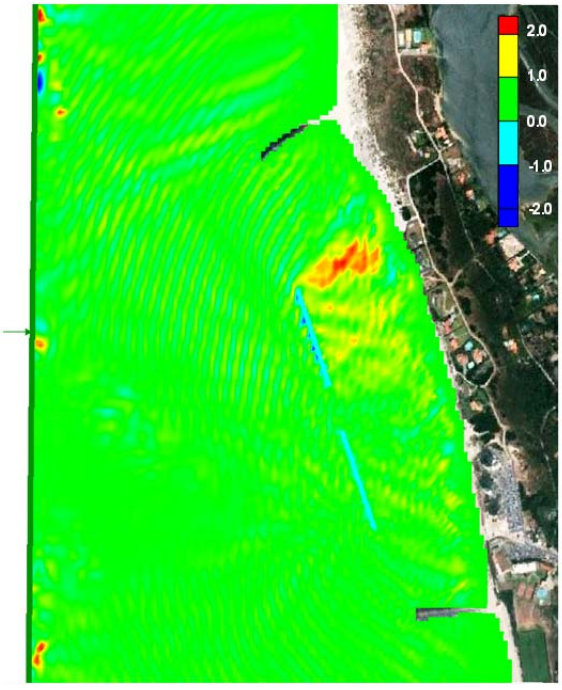

Significant Wave Height: Initial – SC

Hi2-H5

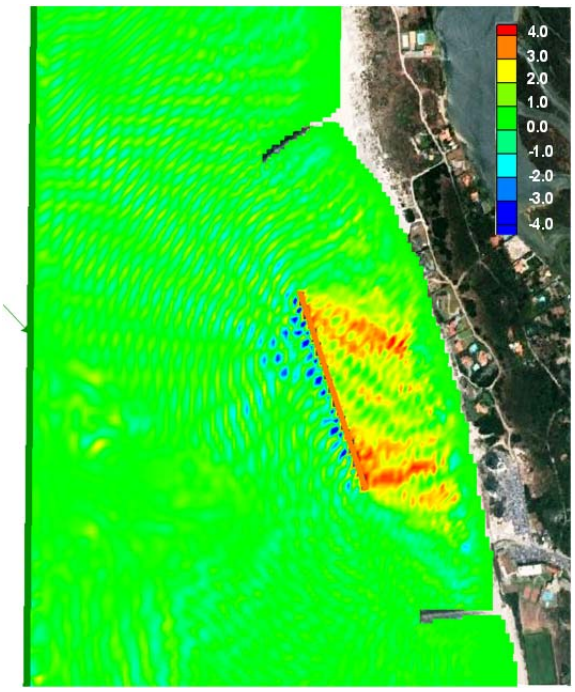

Hi2-H6

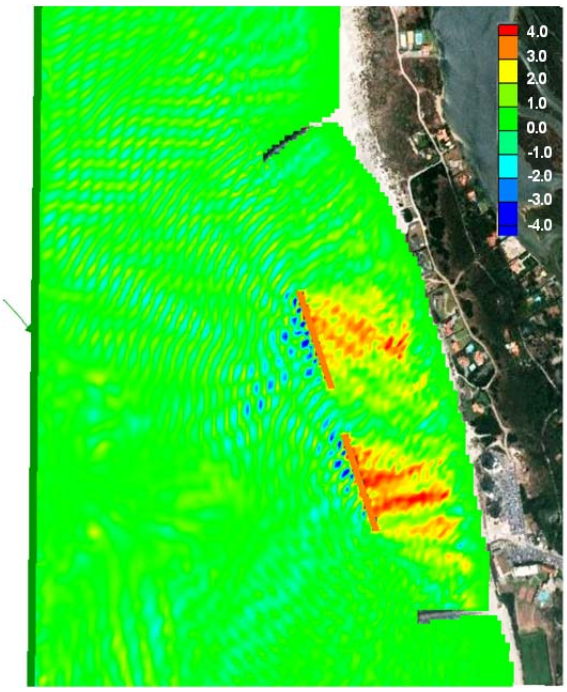

Hi2-H7

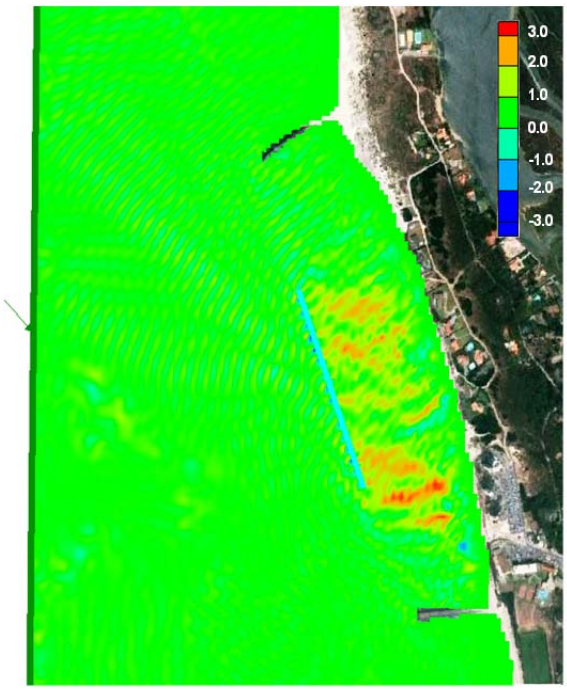

Hi2-H8

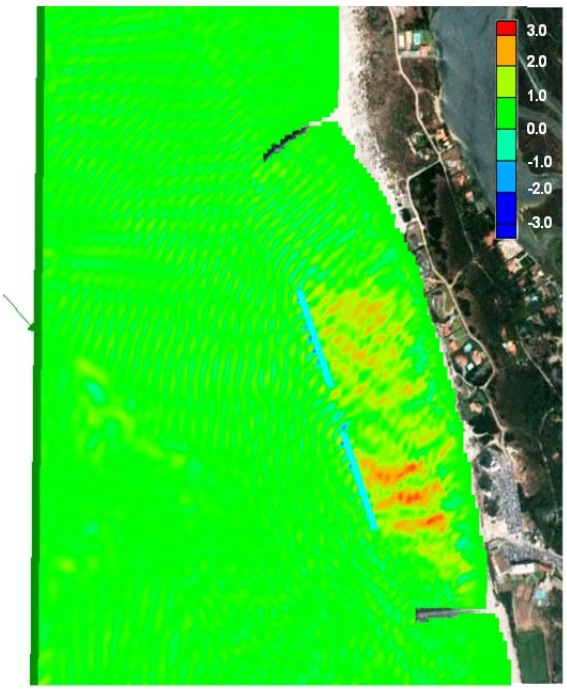

Significant Wave Height: Initial – SC

Hi3-H9

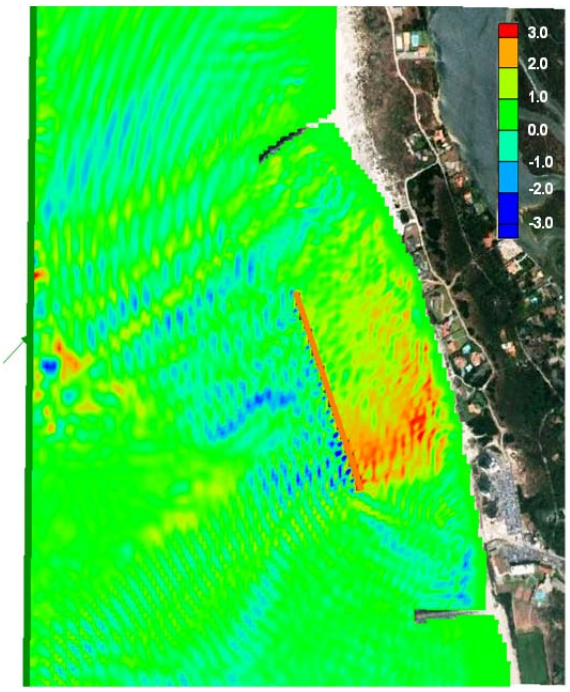

Hi3-H10

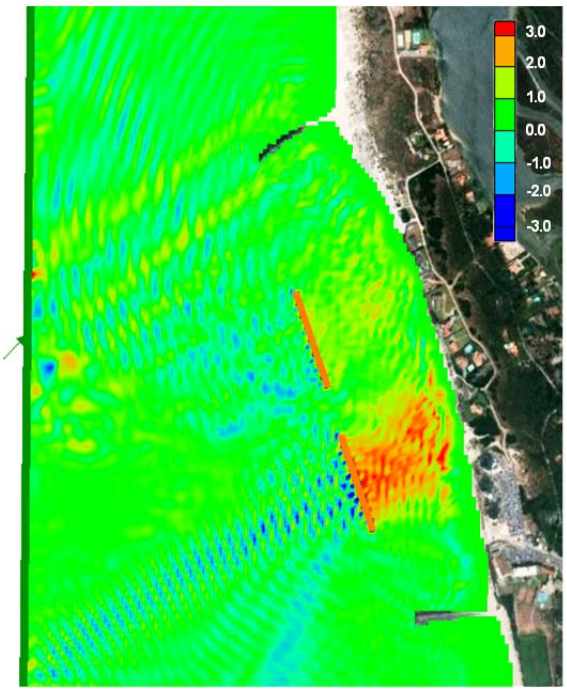

Hi3-H11

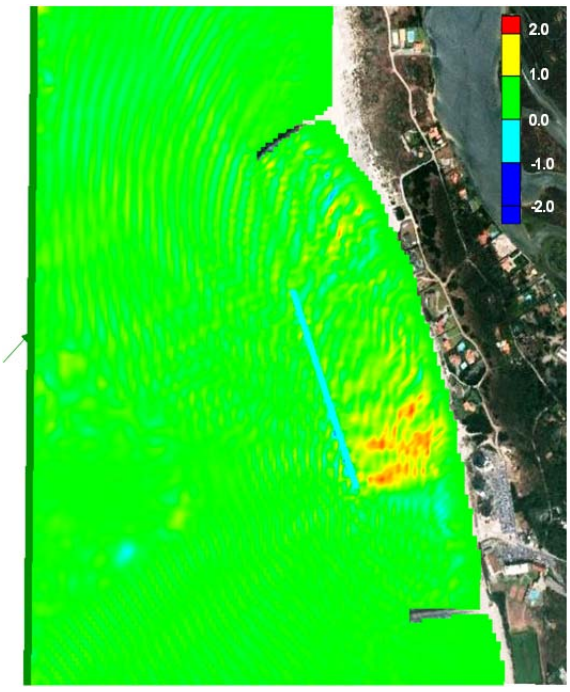

Hi3-H12

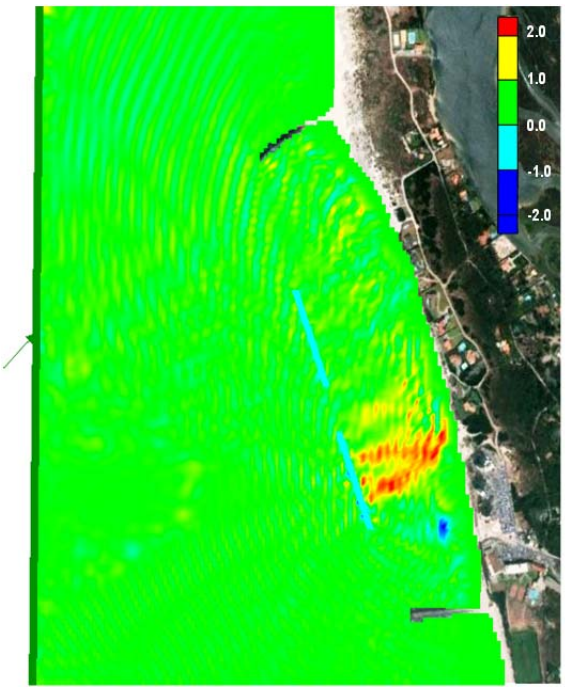

Significant Wave Height: Initial – SC

Hi4-H13

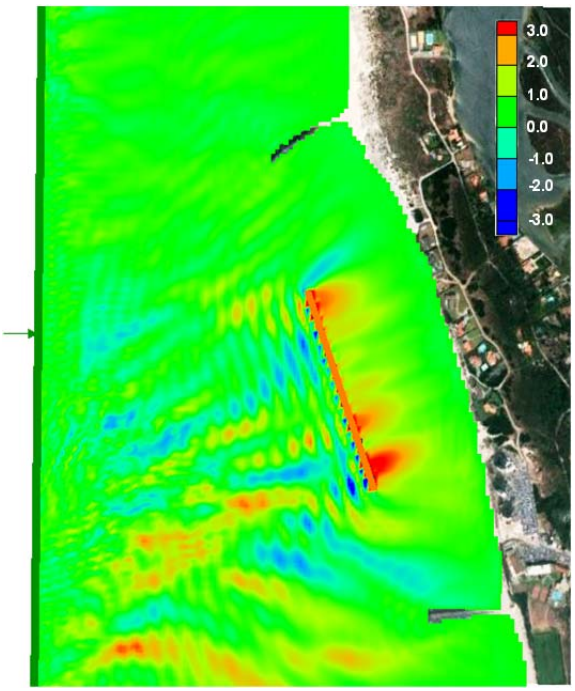

Hi4-H14

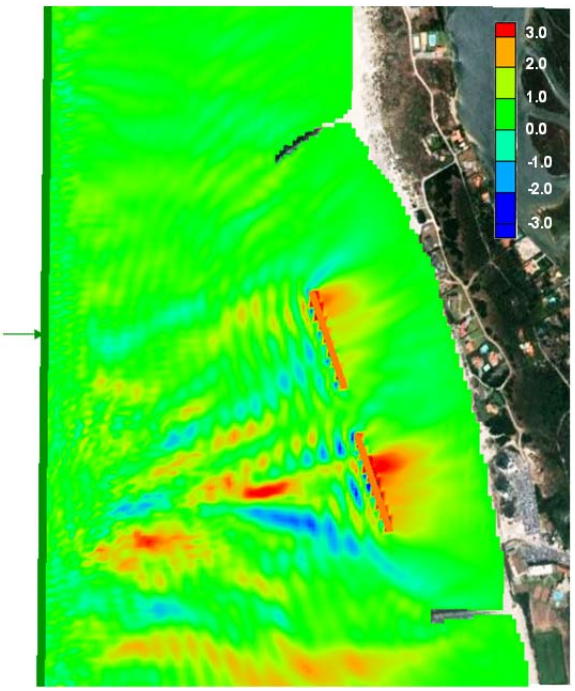

Hi4-H15

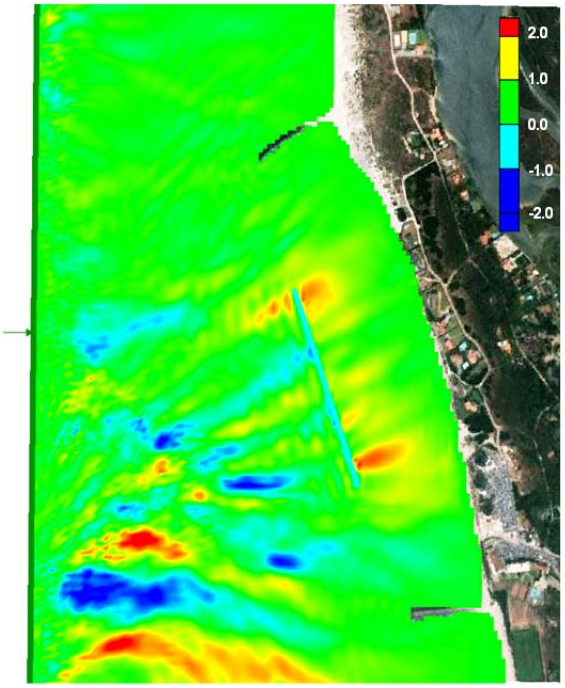

Hi4-H16

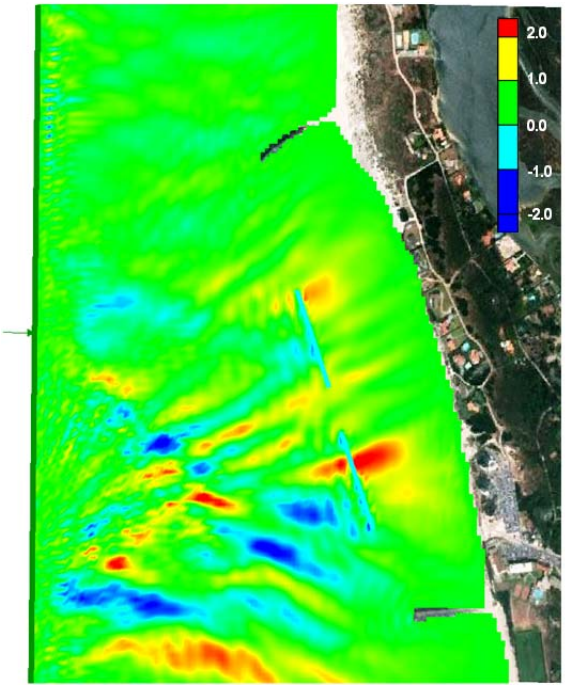

Significant Wave Height: Initial – SC

Hi5-H17

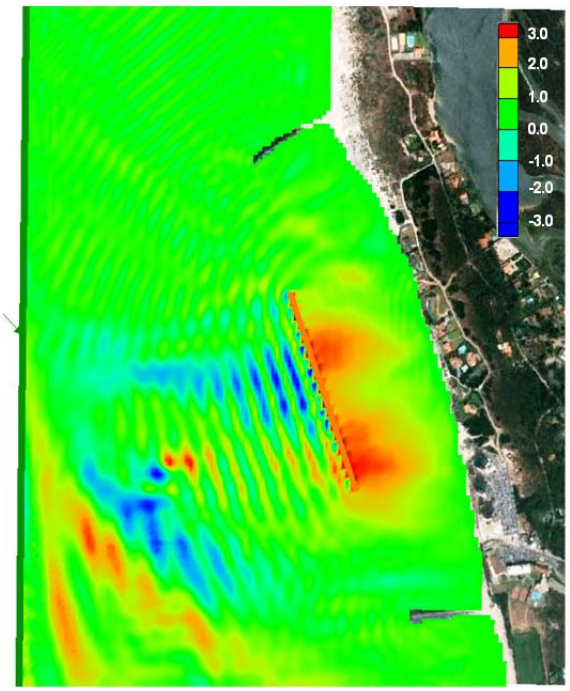

Hi5-H18

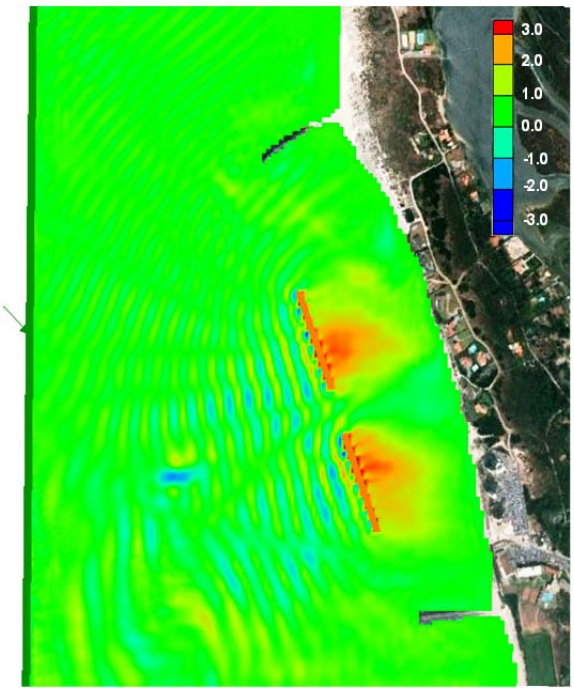

Hi5-H19

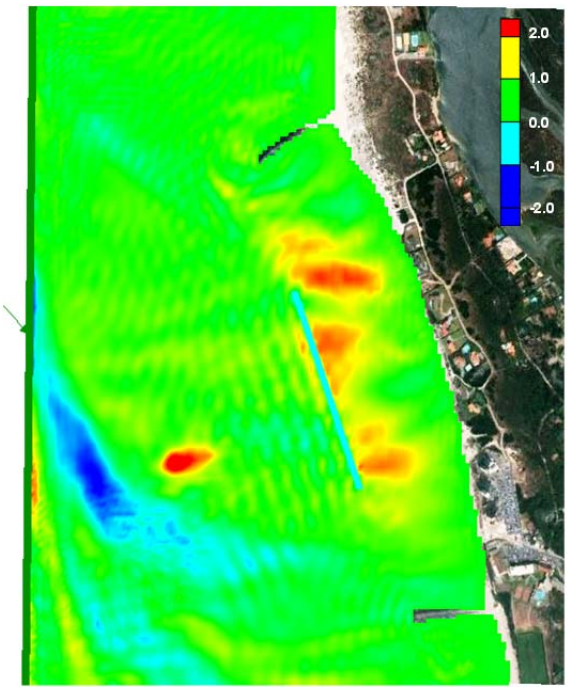

Hi5-H20

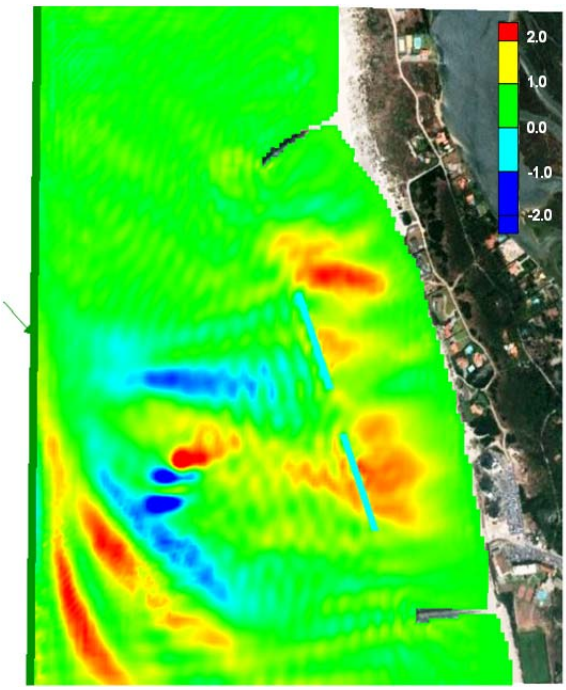

Significant Wave Height: Initial – SC

Hi6-H21

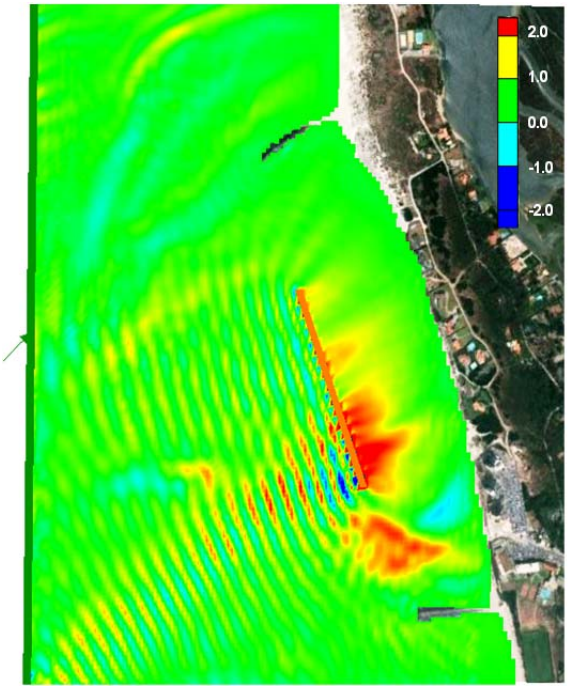

Hi6-H22

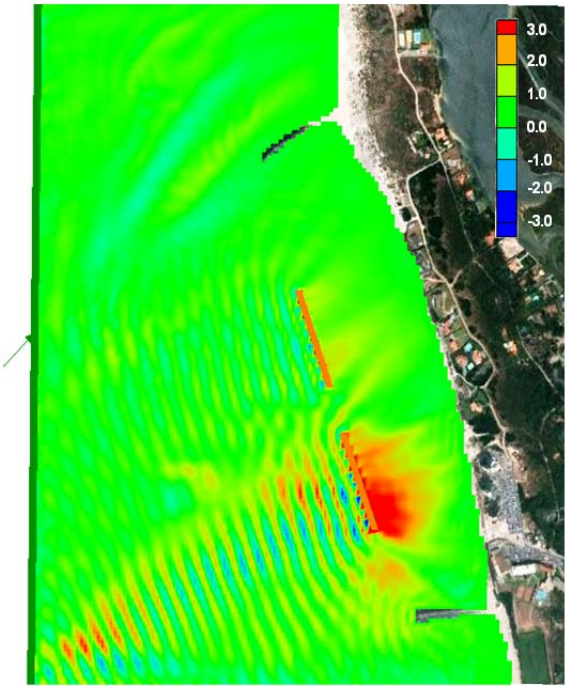

Hi6-H23

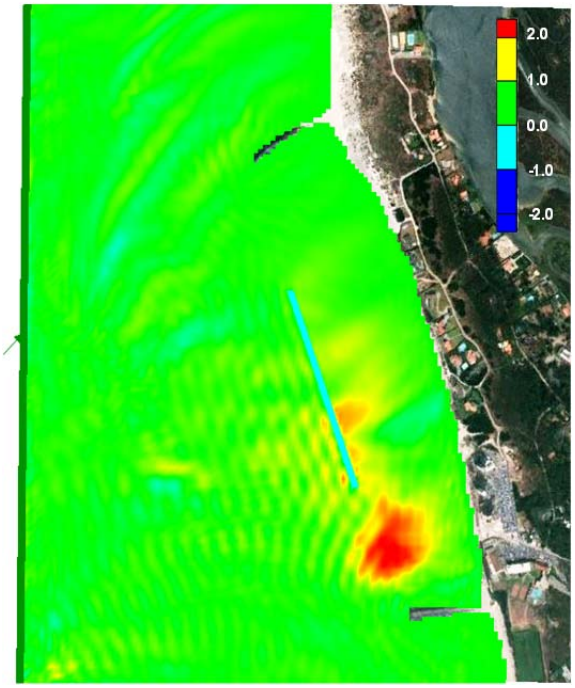

Hi6-H24

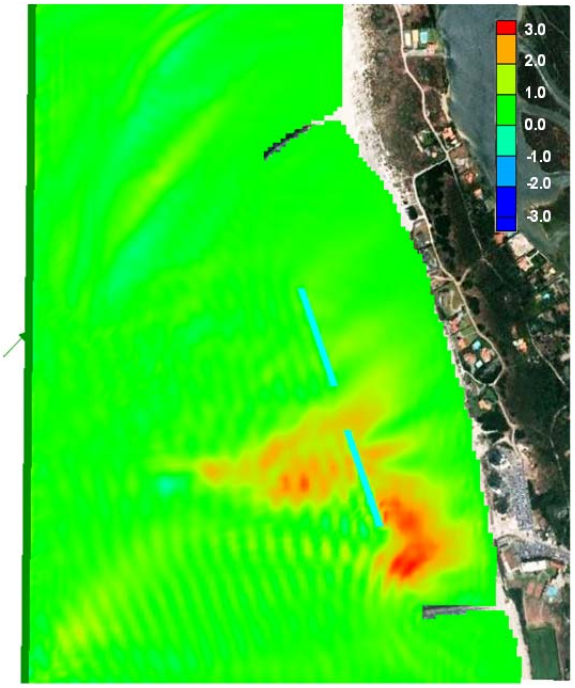

(Page intentionally left blank)

APPENDIX 10

BOUSS-2D.

Significant wave height: Submerged – Emerged

(Page intentionally left blank)

Scenarios Initial and scenarios with detached breakwater

Wave characteristics					Scenario
H_s (m)	T (s)	X (m)	Direction (°)		
2,00	7,00	235,00	270,00	→	Initial1
			315,00	↘	Initial2
			225,00	↗	Initial3
6,64	9,30	235,00	270,00	→	Initial4
			315,00	↘	Initial5
			225,00	↗	Initial6

Wave characteristics				Breakwater characteristics					Scenario
H_s (m)	T (s)	Direction (°)		X (m)	h_{cr} (m)	Number	G (m)	L (m)	
2,00	7,00	270,00	→	235,00	2,70	1	---	470,00	SC1
						2	115,00	235,00	SC2
					-0,50	1	---	470,00	SC3
						2	115,00	235,00	SC4
		315,00	↘		2,70	1	---	470,00	SC5
						2	115,00	235,00	SC6
					-0,50	1	---	470,00	SC7
						2	115,00	235,00	SC8
		225,00	↗		2,70	1	---	470,00	SC9
						2	115,00	235,00	SC10
					-0,50	1	---	470,00	SC11
						2	115,00	235,00	SC12
6,64	9,30	270,00	→	235,00	2,70	1	---	470,00	SC13
						2	115,00	235,00	SC14
					-0,50	1	---	470,00	SC15
						2	115,00	235,00	SC16
		315,00	↘		2,70	1	---	470,00	SC17
						2	115,00	235,00	SC18
					-0,50	1	---	470,00	SC19
						2	115,00	235,00	SC20
		225,00	↗		2,70	1	---	470,00	SC21
						2	115,00	235,00	SC22
					-0,50	1	---	470,00	SC23
						2	115,00	235,00	SC24

Significant Wave Height: Submerged – Emerged

H3-H1

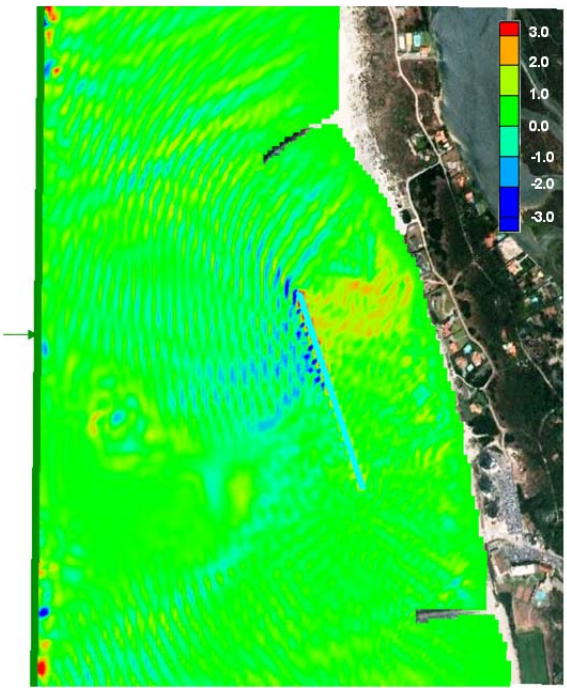

H4-H2

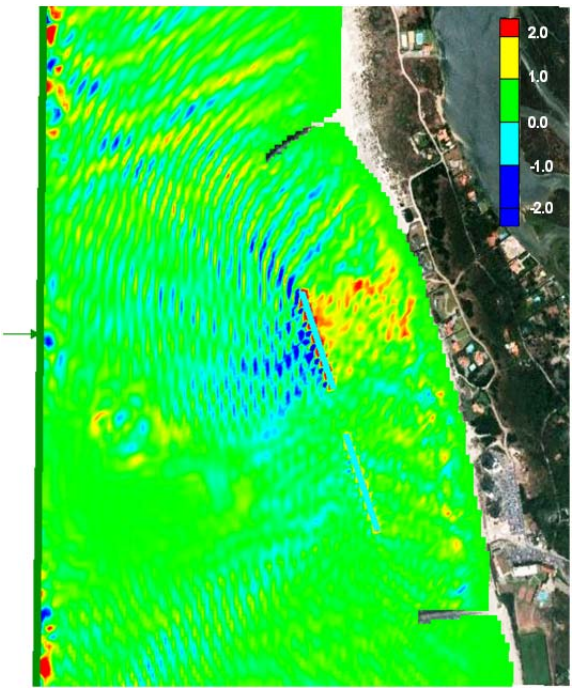

H7-H5

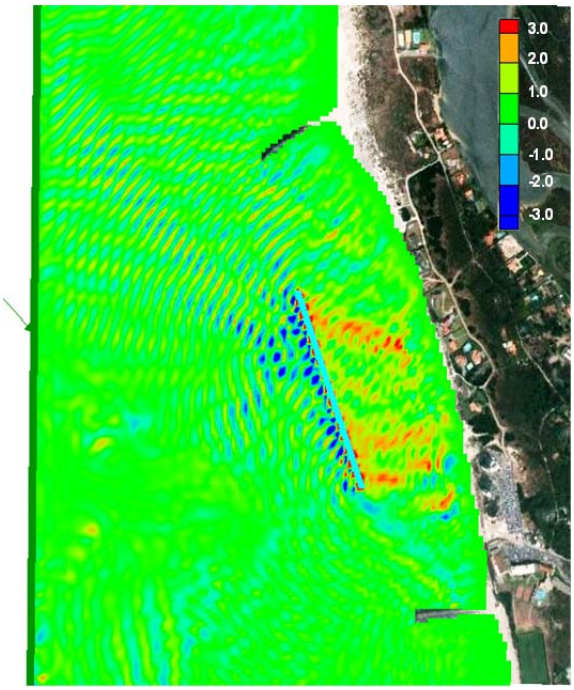

H8-H6

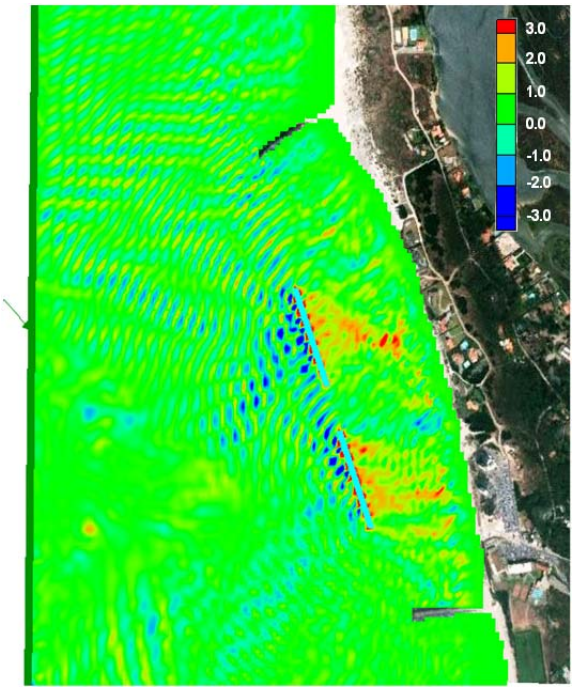

Significant Wave Height: Submerged – Emerged

H11-H9

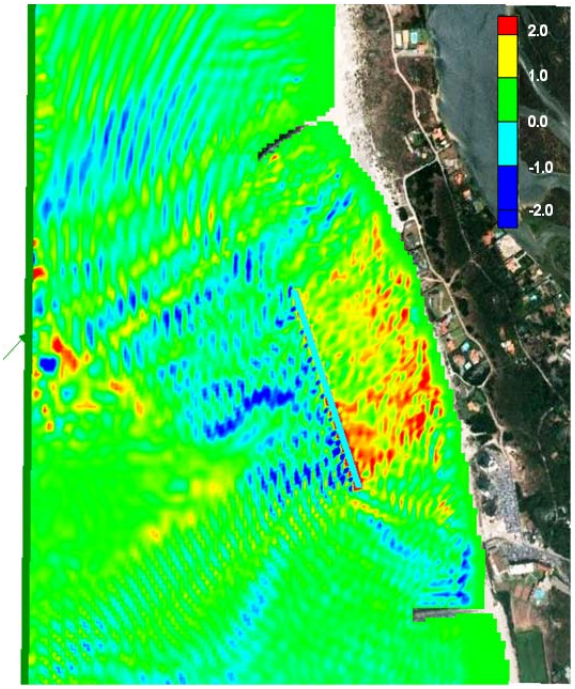

H12-H10

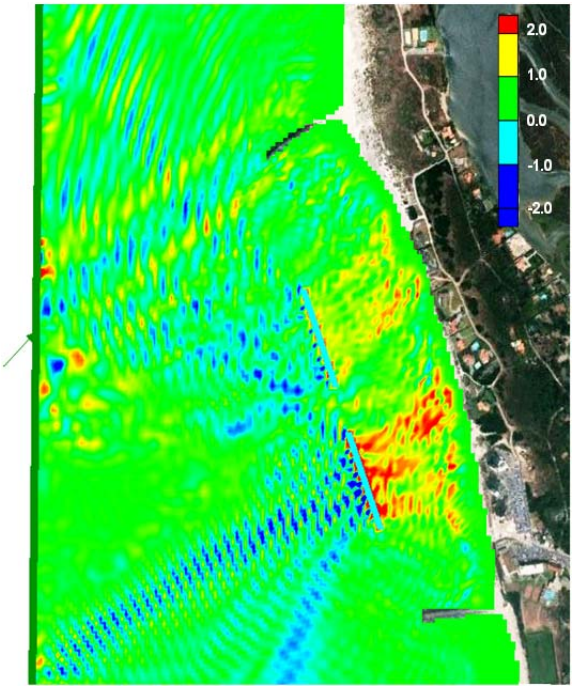

H15-H13

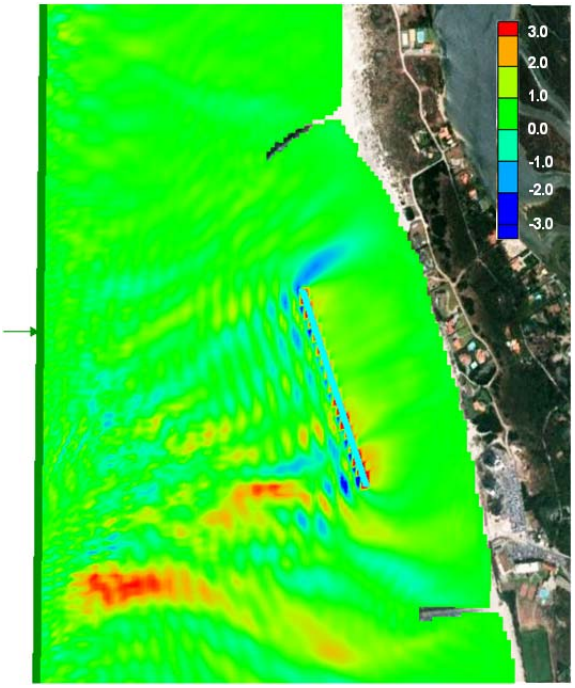

H16-H14

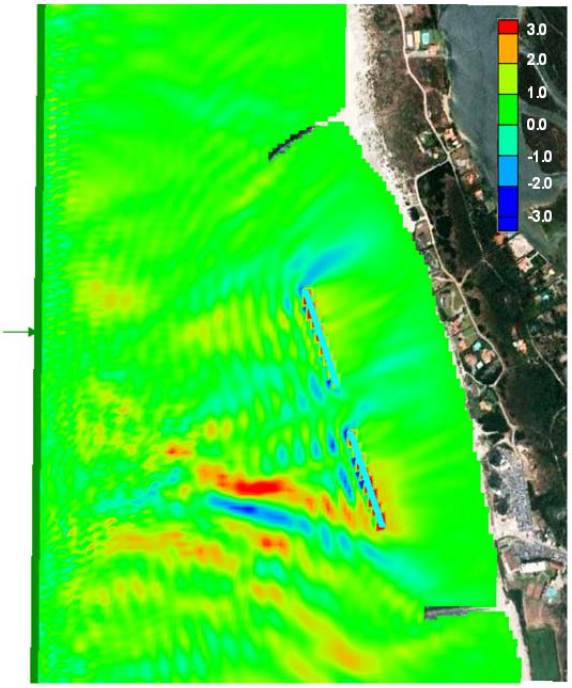

Significant Wave Height: Submerged – Emerged

H19-H17

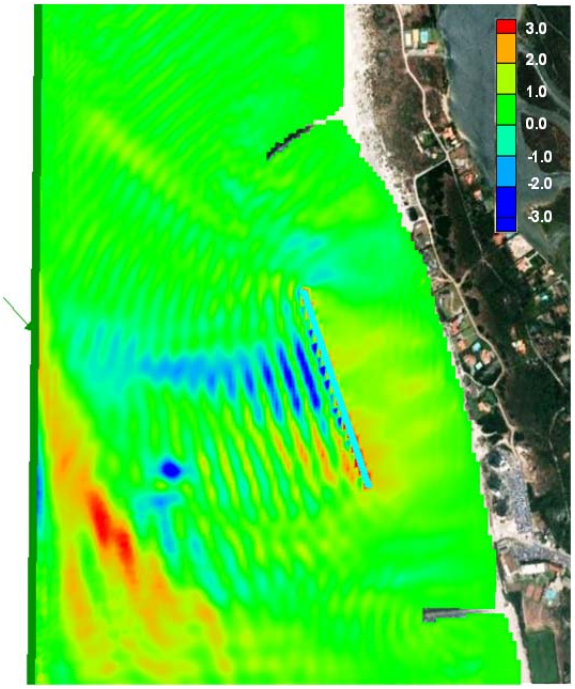

H20-H18

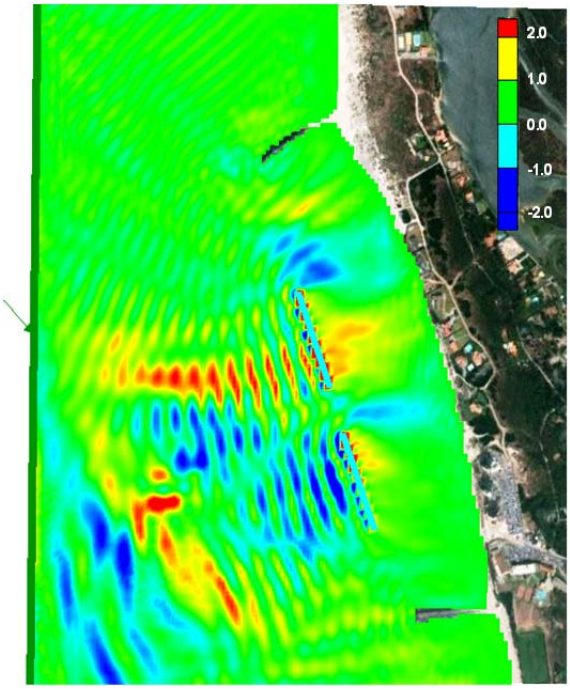

H23-H21

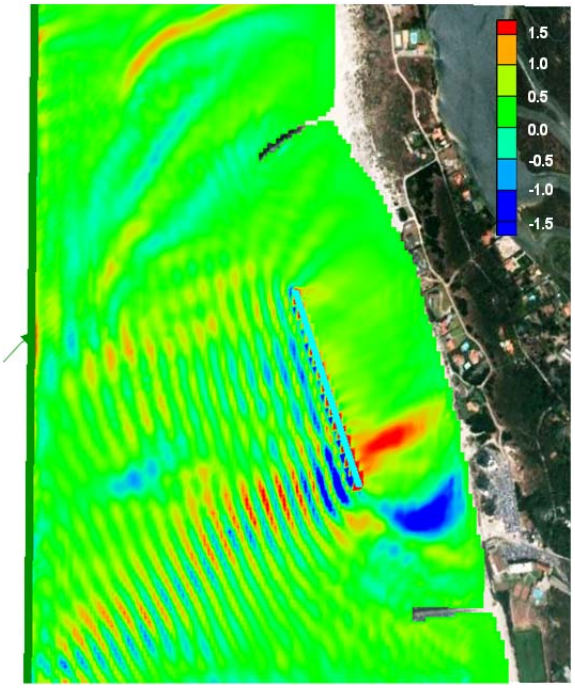

H24-H22

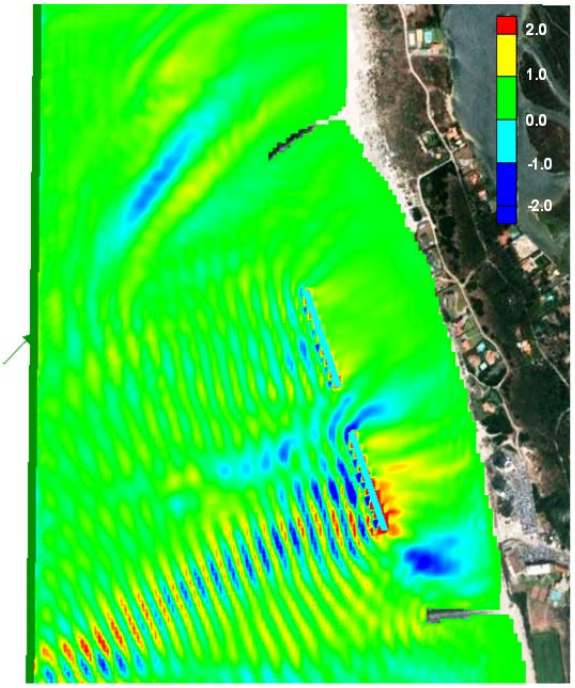

APPENDIX 11

BOUSS-2D.

Significant wave height: Duo breakwater – Solo breakwater

(Page intentionally left blank)

Scenarios Initial and scenarios with detached breakwater

Wave characteristics					Scenario
H_s (m)	T (s)	X (m)	Direction (°)		
2,00	7,00	235,00	270,00	→	Initial1
			315,00	↘	Initial2
			225,00	↗	Initial3
6,64	9,30	235,00	270,00	→	Initial4
			315,00	↘	Initial5
			225,00	↗	Initial6

Wave characteristics				Breakwater characteristics					Scenario
H_s (m)	T (s)	Direction (°)		X (m)	h_{cr} (m)	Number	G (m)	L (m)	
2,00	7,00	270,00	→	235,00	2,70	1	---	470,00	SC1
						2	115,00	235,00	SC2
					-0,50	1	---	470,00	SC3
						2	115,00	235,00	SC4
		315,00	↘		2,70	1	---	470,00	SC5
						2	115,00	235,00	SC6
					-0,50	1	---	470,00	SC7
						2	115,00	235,00	SC8
		225,00	↗		2,70	1	---	470,00	SC9
						2	115,00	235,00	SC10
					-0,50	1	---	470,00	SC11
						2	115,00	235,00	SC12
6,64	9,30	270,00	→	235,00	2,70	1	---	470,00	SC13
						2	115,00	235,00	SC14
					-0,50	1	---	470,00	SC15
						2	115,00	235,00	SC16
		315,00	↘		2,70	1	---	470,00	SC17
						2	115,00	235,00	SC18
					-0,50	1	---	470,00	SC19
						2	115,00	235,00	SC20
		225,00	↗		2,70	1	---	470,00	SC21
						2	115,00	235,00	SC22
					-0,50	1	---	470,00	SC23
						2	115,00	235,00	SC24

Significant Wave Height: Duo Breakwater – Solo Breakwater

H2-H1

H4-H3

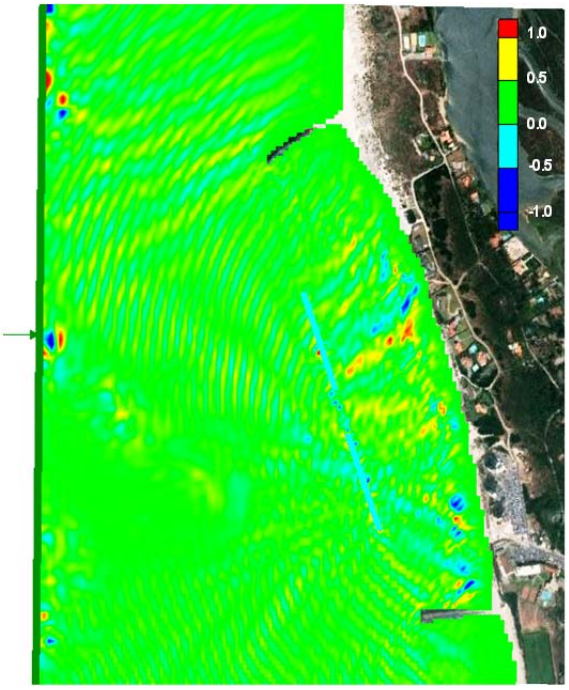

H6-H5

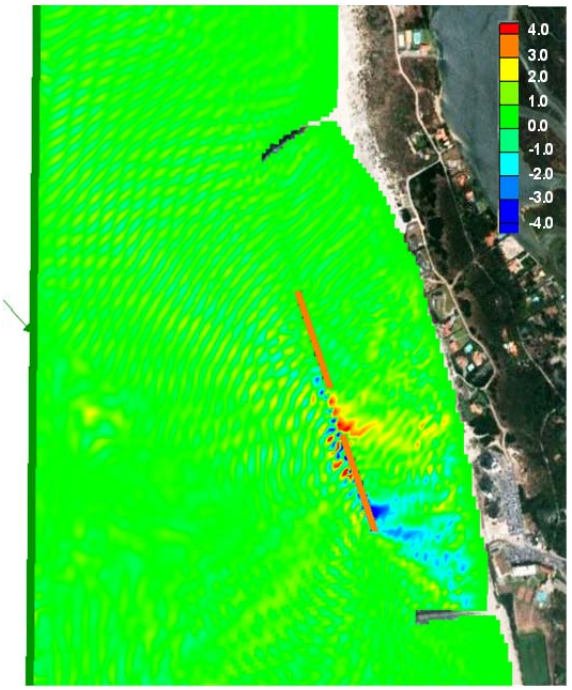

H8-H7

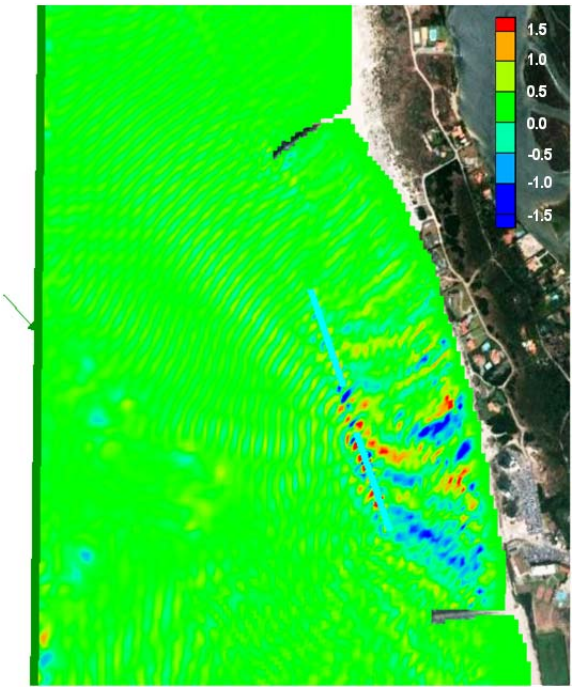

Significant Wave Height: Duo Breakwater – Solo Breakwater

H10-H9

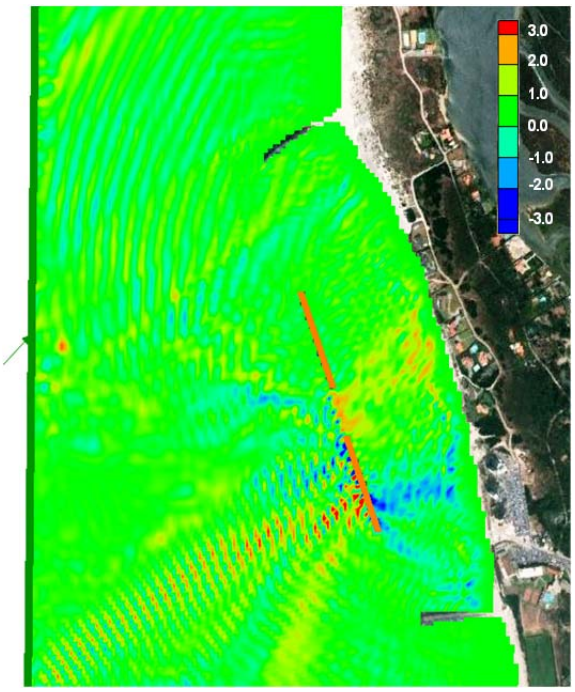

H12-H11

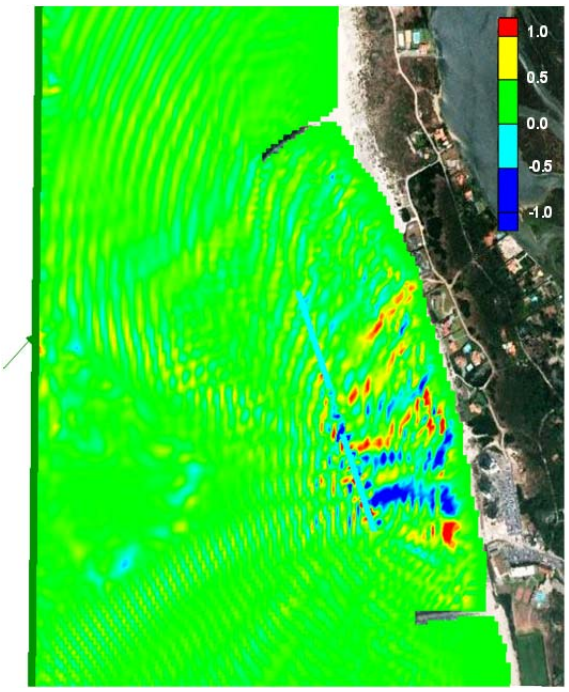

H14-H13

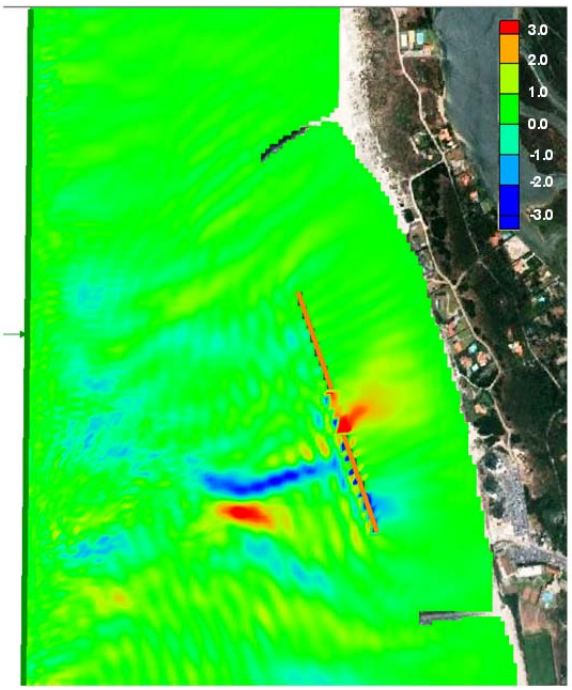

H16-H15

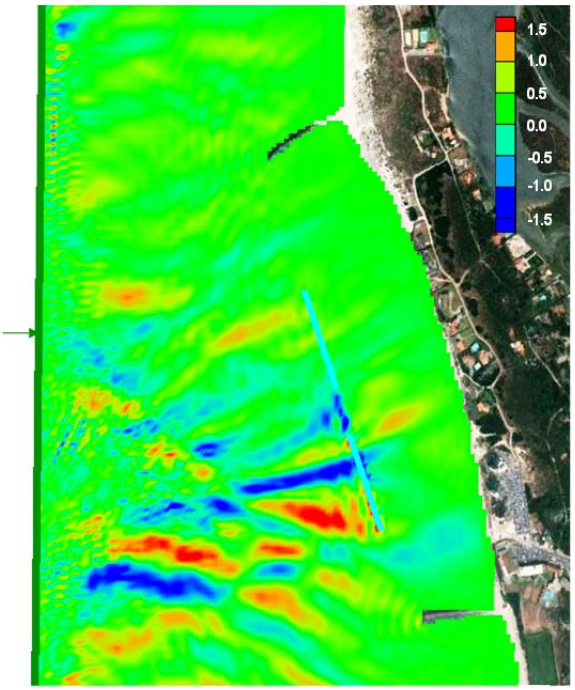

Significant Wave Height: Duo Breakwater – Solo Breakwater

H18-H17

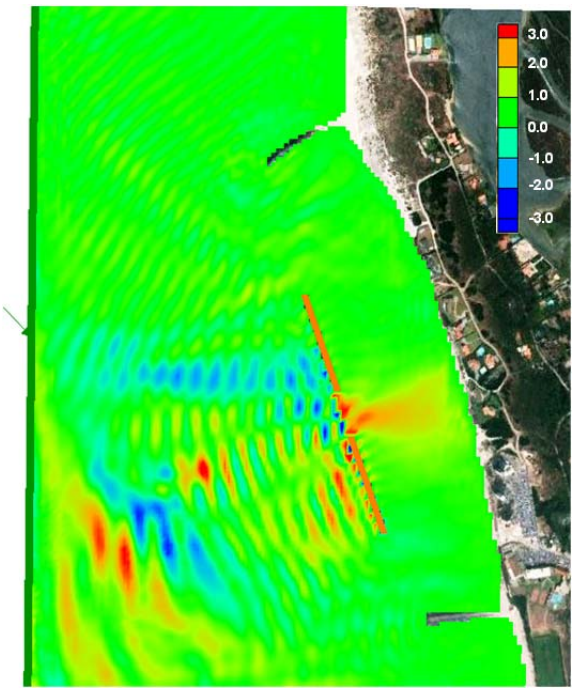

H20-H19

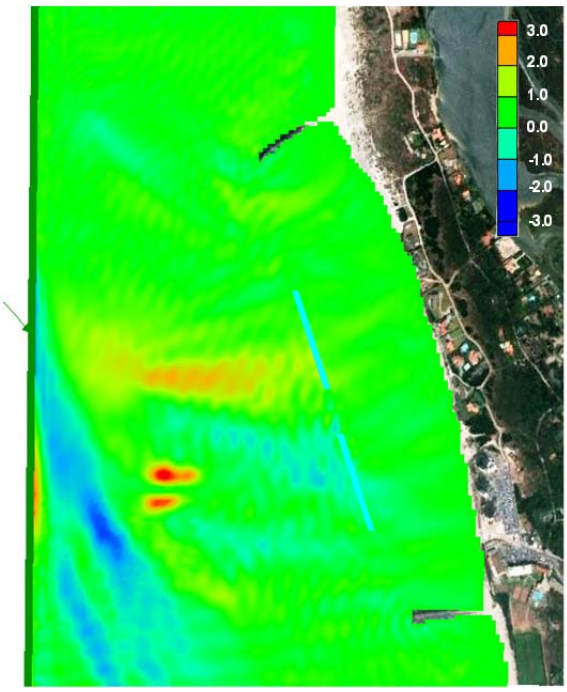

H22-H21

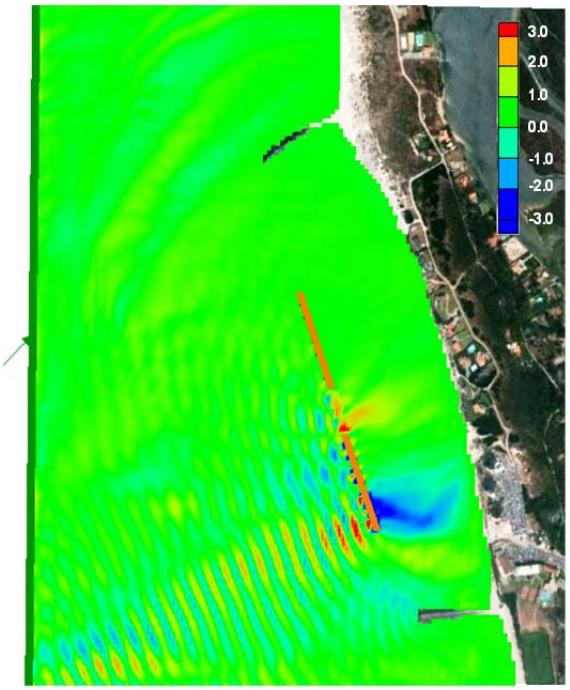

H24-H23